TAMPEREEN TEKNILLINEN YLIOPISTO
TAMPERE UNIVERSITY OF TECHNOLOGY

Juho Kerttula

Large-Mode-Volume Fiber Devices for High-Power and High-Energy Applications

Julkaisu 1140 • Publication 1140

Tampere 2013

Tampereen teknillinen yliopisto. Julkaisu 1140
Tampere University of Technology. Publication 1140

Juho Kerttula

Large-Mode-Volume Fiber Devices for High-Power and High-Energy Applications

Thesis for the degree of Doctor of Science in Technology to be presented with due permission for public examination and criticism in Tietotalo Building, Auditorium TB109, at Tampere University of Technology, on the 14th of June 2013, at 12 noon.

Tampereen teknillinen yliopisto - Tampere University of Technology
Tampere 2013

ISBN 978-952-15-3085-2 (printed)
ISBN 978-952-15-3093-7 (PDF)
ISSN 1459-2045

Abstract

This thesis explores a new type of gain medium for fiber lasers and amplifiers, active tapered double-clad fibers (TDCF), and describes their distinct properties, design, and applications. The TDCF technology is based on fabrication of axially non-uniform active optical fibers, with the aim to provide highly practical and cost-effective alternatives to the widely used fiber devices of today. While retaining all the flexibility associated to present-day double-clad fiber (DCF) instruments, these fibers offer the added benefits of low-brightness end pumping combined with high output brightness, a robust method for mode area scaling, and mitigation of certain deleterious optical effects.

The TDCF technology was first established as a proof of concept during this dissertation work, followed by gradual power scaling to near-kW range in the continuous-wave (CW) regime, and to multi-mJ energies in pulsed operation. Given the preceding, practically nonexistent, high-power fiber laser (HPFL) research at the home university, this progress required substantial developments in thermal management, pumping techniques, and fiber design. The characteristics of the asymmetric and non-reciprocal active fiber waveguides were found to be very distinct from regular, cylindrical fibers. Their special features have been thoroughly studied within this work.

The ytterbium-doped flared active DCFs studied in this dissertation work were applied as gain fibers in several types of laser cavities, as amplifiers in master oscillator – power amplifier (MOPA) configurations, and as pump sources for nonlinear processes. The appended publications demonstrate all these applications, and the related TDCF characteristics are discussed in the thesis. Given the directly-applicable wavelength versatility provided by manifold rare-earth dopants, the established technological platform appears particularly feasible for realization of compact MOPA systems for mid-power materials processing at 1 μm, as well as light detection and ranging (LIDAR) and medical applications at 1.5 μm.

Acknowledgements

This research has mostly been carried out at the Optoelectronics Research Centre (ORC) of Tampere University of Technology during 2008 – 2012. The work has been supported in part by the Graduate School in Electronics, Telecommunications and Automation, the Finnish Foundation for Technology Promotion, the Tampere University of Technology Support Foundation, the Ulla Tuominen Foundation, the Finnish Support Foundation for Economic and Technical Sciences, the Oskar Öflund Foundation, the HPY Research Foundation, and the Walter Ahlström Foundation.

I gratefully acknowledge the head of UIO group Prof. Oleg Okhotnikov, the former director of ORC Prof. (emeritus) Markus Pessa, and the director of ORC Dr. Pekka Savolainen for their supervision, leadership, and management, respectively. I would like to thank my thesis pre-examiners, Dr. Andrei Fotiadi and Dr. Daniel Soh for their valuable insights. I am most indebted to my co-authors in Moscow, especially Prof. Yuri Chamorovskiy, Prof. Konstantin Golant, and Mr. Vasily Ustimchik for their expertise in various respects.

My deepest gratitude goes to Dr. Valery Filippov for his fishing stories, tiger hunting tips, and endlessly patient mentoring over the past few years. Big thanks to Prof. Mircea Guina for all the help especially during my early years at ORC. Needless to say, I would like to thank all the past and present co-workers at ORC for making the everyday existential crisis bearable from time to time. Special thanks to former and current fine fellows of the UIO group, particularly Antti H., Lasse, Tommi, Samuli, Esa, Jussi, Regina, Jari, Alexander, and Antti R. Good times.

Finally, I would like to thank my parents, relatives, friends, my dear wife Milka, and the little Crawler for everything.

Tampere, May 2013
Juho Kerttula

Contents

Abstract i

Acknowledgements ii

Contents iii

List of Publications v

List of Abbreviations and Symbols vii

Symbols, Greek Alphabet ix

Symbols, Other ix

1 Introduction 1

1.1 Incentives 4

1.2 Outline of the Thesis 5

2 Theoretical Model of Tapered Double-Clad Fiber 7

2.1 Ray-Optic Modeling 7

2.2 Rate-Equation Modeling 10

2.3 Mode Coupling 14

2.4 Geometric Limitations 17

3 Experimental Study of Tapered Double-Clad Fiber 21

3.1 Pump Conversion Efficiency 22

3.2 Mode Coupling 23

3.3 Fundamental Mode Evolution 26

4 Continuous-Wave Fiber Lasers and Amplifiers **28**
4.1 Diode Pumping 28
4.1.1 Pump Source Brightness 29
4.1.2 Pumping Methods 30
4.2 Power Scaling Considerations 32
4.2.1 Thermal and Material Limitations 33
4.2.2 Fiber Nonlinearities 35
4.2.3 Other Limitations 37
4.2.4 Auxiliary Scaling Methods 38
4.3 Practical High-Power Devices 40

5 Pulsed Fiber Lasers and Amplifiers **46**
5.1 Pulse Generation Methods 46
5.2 Pulse Energy and Peak Power Scaling 48
5.2.1 Fiber Damage 49
5.2.2 Fiber Nonlinearities 50
5.2.3 Amplified Spontaneous Emission 51
5.2.4 Master Oscillator — Power Amplifier 52
5.3 Applications 53
5.3.1 Supercontinuum Generation 54

6 Conclusions **56**

References **58**

List of Publications

This work is a compendium and contains some unpublished material; however, the thesis is largely based on the following appended publications that will be referred to in the text as [P1–P9].

[P1] V. Filippov, Y. Chamorovskii, J. Kerttula, K. Golant, M. Pessa, and O. G. Okhotnikov, "Double clad tapered fiber for high power applications", *Optics Express*, vol. 16, no. 3, pp. 1929–1944, 2008.

[P2] J. Kerttula, V. Filippov, Y. Chamorovskii, V. Ustimchik, K. Golant, and O. G. Okhotnikov, "Principles and Performance of Tapered Fiber Lasers: from Uniform to Flared Geometry", *Applied Optics*, vol. 51, no. 29, pp. 7025–7038, 2012.

[P3] J. Kerttula, V. Filippov, Y. Chamorovskii, V. Ustimchik, and O. G. Okhotnikov, "Mode Evolution in Long Tapered Fibers with High Tapering Ratio", *Optics Express*, vol. 20, no. 23, pp. 25461-25470, 2012.

[P4] V. Filippov, Y. Chamorovskii, J. Kerttula, A. Kholodkov, and O. G. Okhotnikov, "Single-mode 212 W tapered fiber laser pumped by a low-brightness source", *Optics Letters*, vol. 33, no. 13, pp. 1416–1418, 2008.

[P5] V. Filippov, Y. Chamorovskii, J. Kerttula, A. Kholodkov, and O. G. Okhotnikov, "600 W power scalable single transverse mode tapered double-clad fiber laser", *Optics Express*, vol. 17, no. 3, pp. 1203–1214, 2009.

[P6] V. Filippov, Y. Chamorovskii, J. Kerttula, A. Kholodkov, and O. G. Okhotnikov, "Highly efficient 750 W tapered double-clad ytterbium fiber laser", *Optics Express*, vol. 18, no. 12, pp. 12499–12512, 2010.

[P7] J. Kerttula, V. Filippov, Y. Chamorovskii, V. Ustimchik, K. Golant, and O. G. Okhotnikov, "Tapered fiber amplifier with high gain and output power", *Laser Physics*, vol. 22, no. 11, pp. 1734-1738, 2012.

[P8] J. Kerttula, V. Filippov, Y. Chamorovskii, K. Golant, and O. G. Okhotnikov, "Actively Q-switched 1.6-mJ tapered double-clad ytterbium-doped fiber laser", *Optics Express*, vol. 18, no. 18, pp. 18543–18549, 2010.

[P9] J. Kerttula, V. Filippov, Y. Chamorovskii, K. Golant, and O. G. Okhotnikov, "250 μJ Broadband Supercontinuum Generated Using a Q-switched Tapered Fiber Laser", *IEEE Photonics Technology Letters*, vol. 29, no. 6, pp. 380–382, 2011.

Author's contribution

The work presented in this dissertation is a result of teamwork. The author had a major role in experimental work on all publications, and in preparation of the manuscript in publications [P2–P3, P7–P9]. However, the author benefited substantially from the work of all co-authors, particularly for fiber fabrication in all publications.

List of Abbreviations and Symbols

AOM	Acousto-optic modulator
AR	Anti-reflection
ASE	Amplified spontaneous emission
BPP	Beam parameter product
CCC	Chirally-coupled core
CPA	Chirped pulse amplification
CMS	Cladding mode stripper
COD	Catastrophic optical damage
CVD	Chemical vapor deposition
CW	Continuous-wave
DCF	Double-clad fiber
DFB	Distributed feedback
DPSSL	Diode-pumped solid state laser
EDFA	Erbium-doped fiber amplifier
EOM	Electro-optic modulator
FBG	Fiber Bragg grating
FWM	Four-wave mixing
HOM	High-order mode
HPFL	High-power fiber laser
HR	High-reflection
LCF	Leakage-channel fiber
LIDAR	Light detection and ranging

LMA	Large mode area
LR	Low-reflection
MCF	Multicore fiber
MFD	Mode field diameter
MM	Multi-mode
MOPA	Master oscillator – power amplifier
NA	Numerical aperture
ORC	Optoelectronics research centre
PCE	Pump Conversion Efficiency
PCF	Photonic crystal fiber
RE	Rare-earth
SBS	Stimulated Brillouin scattering
SC	Supercontinuum
SM	Single-mode
SMF	Single-mode fiber
SPCVD	Surface-plasma chemical vapor deposition
SPM	Self-phase modulation
SRS	Stimulated Raman scattering
SSL	Solid-state laser
SSP	Sustained self-pulsing
TDCF	Tapered double-clad fiber
TIR	Total internal reflection
TW	Traveling-wave
XPM	Cross-phase modulation

Symbols, Greek Alphabet

α	Propagation angle
α_p	Pump loss coefficient
α_s	Signal loss coefficient
ε	Mode field function
γ	Absorption coefficient
Γ	Confinement factor
λ	Wavelength
τ	Excited state lifetime
τ_{mn}	Intermodal group delay
τ_p	Pulse duration
θ	Taper angle
θ_d	Divergence
Ω	Mode coupling coefficient
ϕ	Azimuthal coordinate
ψ	Rotation angle
σ	Absorption/emission cross section
φ	Local normal mode function

Symbols, Other

A	Area
b	Parabolic shape factor
BPP	Beam parameter product
c	Speed of light; expansion coefficient
C	Beam contrast
D	Diameter
F	Fill factor
h	Planck constant

J	Bessel function
k	Vacuum wavenumber
K	Launch efficiency
L	Length
M^2	Beam quality factor
n	Refractive index
N	Ion concentration
NA	Numerical aperture
P	Optical (pump) power
R	Reflectivity
r	Radius; radial coordinate
S	Optical (signal) power
T	Tapering ratio
V	Volume; normalized frequency
w_0	Beam waist radius
z	Distance; axial coordinate

Chapter 1

Introduction

Where there is much light, the shadow is deep. – J.W. von Goethe

Soon after the first laser was realized by Maiman in 1960 [1], the concept became known as a solution in search of a problem. Countless suitable problems have presented themselves ever since, and in the modern society lasers have become ubiquitous, finding applications from Blu-Ray players to anti-missile systems [2] and ranging in size from single atoms [3] to football fields [4]. High-power lasers are particularly useful for applications including materials processing, remote sensing, medicine, military, and display technology, to name a few. The technical challenges associated with the high power levels include thermal management, material damage, nonlinear optical effects, delivery of high pump energy, and economic feasibility. In addition to fiber devices discussed here, the most common approaches to tackle such problems include diode bars or stacks, bulk solid-state diode- or lamp-pumped slab and thin-disk lasers, and CO_2 or excimer gas lasers. The fundamental inherent benefits of the fiber medium with respect to high power are the high surface-to-volume ratio enabling facile thermal management and the waveguiding nature that allows avoiding thermal lensing even under substantial heat loads.

Fiber lasers were demonstrated shortly after Maiman's discovery [5]; however, they remained a niche application for a while. General interest in fiber devices began to rise in the 1970s with strong investment in fiber-optic communication technology, leading to the now-legendary erbium-doped fiber amplifier (EDFA) at the 1.5 μm telecom wavelength [6]. The advent of DCFs in the late 1980s [7] finally allowed fiber laser output power scaling beyond approximately 1 W, due to the significantly relaxed requirements

for pump diode brightness. In these fibers, the signal light is guided in the small core as in single-mode fibers (SMF); however, the pump light is confined in a much larger cladding surrounding the core (Figure 1.1a). The DCF breakthrough was accompanied by tremendous progress in pump diode technology, and soon allowed output powers to rise to the 100-W level. Since the early days of the double-clad fiber, DCF devices have often been referred to as *brightness converters*, converting the low-brightness diode pump light into more useful high-brightness output light with high efficiency.

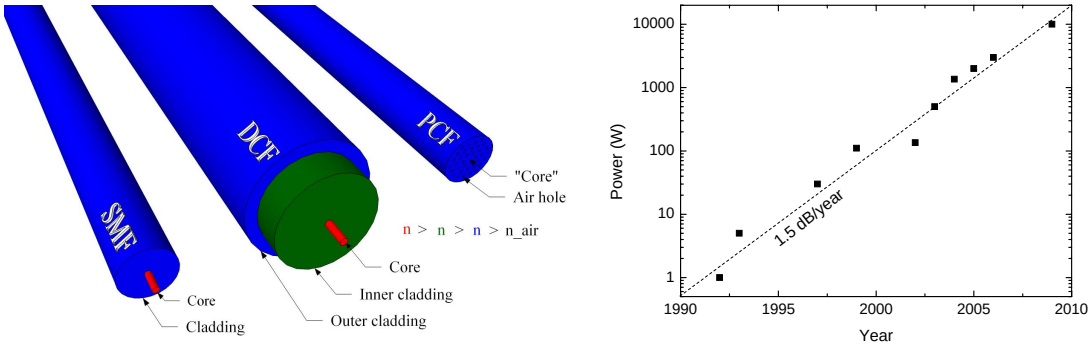

(a) (b)

Figure 1.1: (a) Schematic examples of a standard single-mode fiber, a double-clad fiber, and a photonic crystal fiber. (b) Highest reported continuous-wave, near-diffraction-limited fiber laser power by year [8–18].

However, further power scaling with the small, strictly single-transverse-mode fiber cores used for early DCFs were soon found to be limited by nonlinear optical effects due to high in-core intensities and long interaction lengths. The problem of nonlinearity could be alleviated by fibers with increased (effective) core sizes that later became known as large-mode-area (LMA) fibers [19, 20]. Goethe's shadow, however, lurks within the LMA concept, as a larger core generally leads to degraded output beam quality, and the increased power may be of little use due to decreased brightness. Nevertheless, LMA fibers form the basis of present-day high-power and high-energy fiber devices, now capable of handling kW-level continuous-wave (CW) in-core powers and multi-mJ pulse energies with high output beam quality.

Typically, the increase in core size of an LMA fiber must be accompanied by a decrease in the numerical aperture (NA) of the core to maintain output brightness. The NA is determined by the (effective) refractive index difference between the core and

cladding, i.e. $NA = \sqrt{n_{core}^2 - n_{clad}^2}$ for a step-index fiber, and is limited by fabrication technology to approximately 0.04–0.06. Due to this limitation, alternative methods to realize large mode areas without loss of brightness remain an active field of study [21]. Proposed approaches include selective mode excitation [22–24], dopant profiling [25], index profiling [26], bending-induced mode selection [27], and tapering-induced mode selection [P1]. Furthermore, various methods based on structural fiber modification have been demonstrated, including several types of microstructured photonic crystal fibers (PCF) [28–32] (Figure 1.1a), leakage-channel fibers (LCF) [33, 34], chirally-coupled core (CCC) fibers [35], multicore fibers (MCF) [36, 37], gain-guiding index-antiguiding fibers [38], and higher-order mode (HOM) fibers [39]. Progress in the field has been rapid, as illustrated by the development of highest CW fiber laser (amplifier) output powers achieved since mid-1990s (Figure 1.1b), a reasonable benchmark for the overall progress. In devices utilizing short pulses or narrow emission bandwidth, the scaling limits are different and often more stringent; however, the general direction of development remains unchanged.

All the proposed approaches have their specific downsides. Depending on the target application, the optimal solution is a compromise between several factors, such as brightness, robustness, size, simplicity, and cost. The TDCF technology discussed here enables the construction of bright, small-footprint, potentially monolithic fiber devices pumped by low-brightness and low-cost diode bars. Although numerous low-power fiber laser applications exists, especially in the ultrafast regime, this thesis is mostly concerned with industrial-scale mid- and high-power fiber lasers and amplifiers. In this application sector, the total available market is expected to reach $2.5 billion in 2013, out of which the share of fiber lasers nearly $500 million [40]. Along with direct diode lasers, fiber lasers are expected to be the fastest growing segment in the near future. More than 60 % of the fiber laser revenue consists of materials processing applications, whereas the medical sector holds roughly one quarter. The fiber laser market is currently dominated by IPG Photonics with more than a 70 % revenue share. Other major manufacturers include Trumpf group (SPI Lasers) and Rofin group (Nufern), the latter recently having announced a strong focus shift towards HPFLs [41], despite having traditionally been associated with other laser types.

Finally, nearly all HPFLs utilize rare-earth (RE) ion doping of the active medium. This thesis mainly focuses on ytterbium-doped silica devices (emitting at 0.98 μm – 1.11 μm), the common choice for materials processing applications due to pump wave-

length flexibility, low quantum defect, and the absence of certain adverse effects often encountered with other RE fibers. The two latter qualities provide a solid basis for all high power results achieved with Yb-doped fibers. Other common RE dopants for silica fibers include (typical emission wavelength in μm in parentheses) neodymium (1.06, 1.3), praseodymium (1.3), erbium (1.53 – 1.62), thulium (1.7 – 2.1), and holmium (1.9 – 2.2) [42,43]. In addition to Yb, 100-W CW level has been demonstrated with Er (Er/Yb, 297 W [44]), Tm (1 kW [45]), and Ho (140 W [46]). The TDCFs studied within this thesis are exclusively Yb-doped; however, changing the RE dopant would allow for flexible wavelength variation with little loss of generality for the results presented here.

1.1 Incentives

As outlined above, the market penetration of high-power fiber devices continues to grow. The main reasons for this are the well-known advantages of fibers in industrial applications, including high brightness, high wall-plug efficiency, facile beam delivery, and low maintenance. The main obstacle for further large-scale implementation in industrial applications at present is the relatively high cost. In general, the cost of a fiber laser is dominated by the pump diode costs; the exact cost breakdown depends on technical details and the utilized pumping approach (Section 4.1.2). This applies to both single-emitter and bar (or stack) pumping, whereas the advantages offered by the two alternatives are different and outlined in Section 4.1.1. The level of commercially available output power is currently in the 10-W order per single-emitter and in the 100-W order per bar; however, multi-emitter or multi-bar assemblies are often used to couple higher power into a single delivery fiber. As a common factor for both pumping schemes, the pump cost generally increases with increasing brightness of the source.

The core size of DCFs is limited by beam quality requirements. This in turn limits the inner cladding (pump core) size, as the pump absorption is determined by the core/cladding area ratio. Finally, the pump power that could be coupled through the fiber end face for a given pump brightness is limited by the cross-sectional area of the DCF cladding. While this limitation can be circumvented by side-pumping techniques, such a pumping scheme can lead to significant increase in device complexity and cost due to the large number of pump units required. However, the TDCF is naturally suited for low-brightness end-pumping due to the large end face in one of the active fiber ends, while retaining a high output brightness. Thus, in economic terms, the concept would

seem an interesting candidate for replacing existing mid- and high-power systems up to kW-range.

Furthermore, the non-uniform axial fiber shape has been shown to mitigate stimulated Brillouin scattering (SBS) in fiber lasers [47]. This advantage can be utilized together with previously demonstrated methods for increasing SBS threshold (cf. Section 4.2.2) in single-frequency devices. Akin to SBS mitigation, the recently popular topic of thermal mode instability (stimulated thermal Rayleigh scattering) appears interesting with respect to tapered devices; longitudinally varying effective mode area could be useful for mitigation of this effect as well. In addition, the tapered fiber shape enhances pump absorption due to the mode mixing effect in the pump propagation direction resulting from gradually decreasing diameter, and for the same reason, it can act as a filter for wide-to-narrow propagating amplified spontaneous emission (ASE). Finally, as noted in the previous section, fiber tapering is a feasible method for mode area scaling to cope with the high power levels. The main benefits gained by utilizing TDCF fibers can be summarized as follows:

- Mode area can be scaled substantially to mitigate fiber nonlinearities without significant beam quality degradation.
- Low-brightness pumping is possible due to the large cladding diameter at the pump end of the tapered fiber without significant absorption degradation.
- Mitigation of certain unwanted effects occurs due to the longitudinally varying core diameter.

1.2 Outline of the Thesis

As mentioned above, this thesis mostly deals with Yb-doped mid- and high-power silica fiber devices. In Chapter 2, the theoretical background of TDCF concept is introduced, and the distinct properties arising from the non-uniform waveguide are examined in detail for co- and counterpropagating laser configurations. In Chapter 3, the tapered geometry is discussed in terms of pump conversion efficiency (PCE) optimization. In addition, mode coupling and fundamental mode propagation in a TDCF are experimentally studied. Chapter 4 is focused on high-power CW fiber lasers and amplifiers with

emphasis on pumping methodology and power limitations in these devices. Practical devices utilizing TDCF technology are discussed. Pulse generation and energy scaling are analyzed in Chapter 5. The associated limits to device performance resulting from high peak power and narrow linewidth, somewhat distinct from the CW case, are discussed. Finally, conclusions and main achievements are presented in Chapter 6.

Chapter 2

Theoretical Model of Tapered Double-Clad Fiber

The TDCF concept, based on active DCFs adiabatically tapered along the entire fiber length, was first reported in 2008 [P1], with the aim to develop low-brightness-pumped, high-brightness fiber devices with additional benefits including increased SBS threshold [48]. During the course of this work, this proprietary [49] technology has been established at ORC, gradually power scaled, and implemented in various CW and pulsed laser and amplifier configurations. In this chapter, theoretical modeling of TDCFs is presented and the distinct properties of the non-uniform gain medium are discussed.

2.1 Ray-Optic Modeling

Within this work, two numeric models have been used to support the experimental studies and fiber design. First, ray-optic analysis was used to estimate the effect of pump *vignetting*, i.e. the (unabsorbed) pump light leakage out of the waveguide via the side of the fiber due to a violation of the total internal reflection (TIR) condition. Second, a rate equation model was developed to comparatively study the properties arising from the tapered waveguide shape in different fiber laser configurations.

Launching and propagation of highly multi-mode (MM) pump light can be considered in terms of ray optics. Figure 2.1a schematically illustrates the propagation of a meridional pump ray launched into the TDCF at an angle α_{in}. Assuming a linearly tapered fiber of length L, the propagation angle increases at each reflection by a constant,

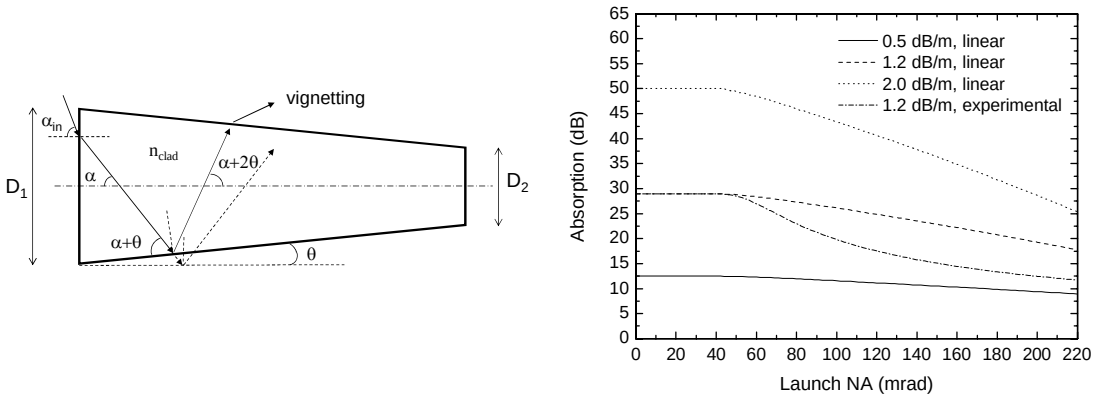

(a) (b)

Figure 2.1: (a) Schematic pump ray propagation in a tapered MM waveguide. (b) Simulated illustration of the dependence of double-clad absorption on the launch NA for three linearly tapered fibers with different paraxial absorption and one experimental taper [P5] with suboptimal shape.

equal to twice the tapering angle $2\theta = (D_1 - D_2)/L$, where D_1 and D_2 are the wide and narrow end cladding diameters, respectively. Because the taper angle in TDCFs is small, typically 10^{-6} to 10^{-5} radians, an infinitesimal section of the fiber can be approximated as a cylinder. With this approximation, the propagation angle at distance z can be shown to be [P5]

$$\alpha(z) = \arcsin \frac{D_1 \sin(\alpha_{in}/n_{clad})}{D_1 - 2\theta z}, \tag{2.1}$$

where n_{clad} is the refractive index of the cladding. The ray propagates without vignetting as long as $n_{clad} \sin(\alpha(z)) < NA_{clad}$,where NA_{clad} is the NA of the cladding, and through the entire taper without vignetting if

$$\sin \frac{\alpha_{in}}{n_{clad}} < \frac{NA_{clad}}{T n_{clad}}, \tag{2.2}$$

where $T = D_1/D_2$ is the tapering ratio, or for paraxial rays (small α_{in})

$$\alpha_{in} \lesssim \frac{NA_{clad}}{T}. \tag{2.3}$$

The double-clad absorption for such small-angle pump rays that do not experience vignetting is independent of the longitudinal taper diameter profile, and will be referred to as *paraxial ray absorption* γ_p.

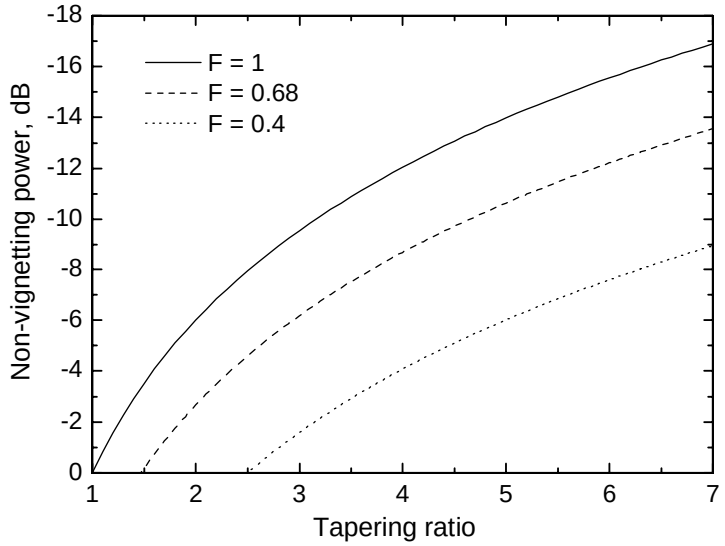

(a)

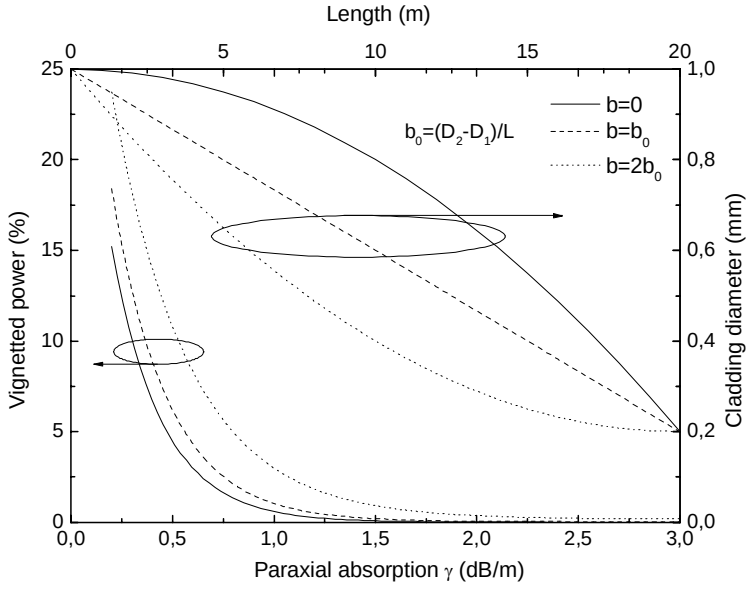

(b)

Figure 2.2: (a) The near-paraxial (vignetting-free) fraction of pump power as a function of tapering ratio for three different fill factors F. $F = 0.68$ corresponds to typical experimental values used in this study for all-glass fibers ($NA_{launch} = 0.15$, $NA_{clad} = 0.22$). (b) The dependence of vignetted power on paraxial absorption (bottom-left axes) for three different parabolic taper shapes, and the corresponding axial taper profiles (top-right axes) of the form $D(z) = (b_0 - b)/L \cdot z^2 + b \cdot z + D_1$.

However, the actual double-clad absorption is determined not only by paraxial absorption, but also by the taper geometry and the angular distribution of the pump beam. Typically, the critical paraxial angle is smaller than practical launch NAs, indicating that a large fraction of the incident pump power would eventually be lost due to vignetting in a tapered cladding. However, it has been shown in several studies that with proper fiber design, the effect of vignetting can be made negligible, and the total vignetted power is typically in the range of 1% – 2% [P6]. The reason for this is the high active volume in the large-diameter section of the TDCF, that results in absorption of most of the power for a given pump ray before vignetting would occur. Increasing the paraxial absorption e.g. by increasing the dopant concentration, further reduces the effect of vignetting (Figure 2.1b). In addition, assuming a Lorentzian power distribution of the pump beam, the large-angle rays that are vignetted first only contain a small fraction of the total power.

Nevertheless, to avoid a decrease in efficiency due to pump vignetting, the pump beam should underfill the cladding NA of the TDCF to an extent. The effect of the fill factor $F = NA_{launch}/NA_{clad}$ describing the launching condition is illustrated in Figure 2.2a. Furthermore, the fraction of vignetted power depends on paraxial absorption and the axial taper shape, as shown in Figure 2.2b. Despite the underfill launch condition, brightness enhancement in a properly designed TDCF laser remains several times higher than in a regular DCF laser, and will be discussed further in Section 2.4.

2.2 Rate-Equation Modeling

To simulate the signal generation in a TDCF laser, a conventional rate-equation model was used, as outlined e.g. in [50]. In addition to the TDCF design, the simulations were performed for a regular cylindrical fiber with diameter similar to that of the narrow end diameter of the TDCF, i.e. with approximately similar output beam quality. Furthermore, two different fiber laser configurations were simulated: one with *co-propagating* signal and pump, and the other with the opposite (*counter-propagating*) directions.

The schematic energy level diagram of the Yb^{3+} ion and the simulated laser configurations are illustrated in Figure 2.3a and b, respectively. The configurations were modeled by solving the coupled-wave equations in adiabatic approximation [50]

$$\begin{cases} \pm\frac{dS^{\pm}}{dz} = \Gamma_S((\sigma_{es}+\sigma_{as})N_2 - \sigma_{as}N)S^{\pm} - \alpha_s S^{\pm} \\ \pm\frac{dP^{\pm}}{dz} = -\Gamma_P(\sigma_{ap}N - (\sigma_{ap}+\sigma_{ep})N_2)P^{\pm} - \alpha_p P^{\pm} \end{cases}, \tag{2.4}$$

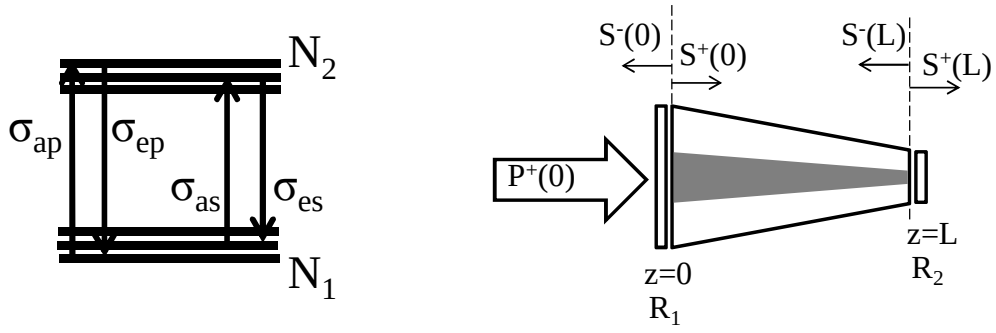

(a) (b)

Figure 2.3: (a) Simplified energy level diagram of the Yb^{3+} ion. (b) A schematic of the simulated laser cavity. Co- and counter-propagating configurations correspond to mirror pairs with reflectivities $R_1 = 100\%$, $R_2 = 4\%$ and $R_1 = 4\%$, $R_2 = 100\%$, respectively.

where $S^{\pm}$ and $P^{\pm}$ are the signal and pump powers, respectively, propagating to the right (+) and left (-) in Figure 2.3b. N is the total Yb^{3+} concentration in the core, σ_{as} and σ_{es} are the signal absorption and emission cross-sections, respectively, and σ_{ap} and σ_{ep} are the pump absorption and emission cross-sections, respectively. α_s and α_p are the scattering loss coefficients for signal and pump, respectively, and Γ_S and Γ_P are the confinement (fill) factors for signal and pump, respectively. Finally, the excited state concentration N_2 was found from the steady state rate equations to yield [51]

$$N_2(z) = \frac{N(z)(\Gamma_P\sigma_{ap}\lambda_P(P^+ + P^-) + \Gamma_S\sigma_{as}\lambda_S(S^+ + S^-))}{Ahc/\tau + \Gamma_P\lambda_P(\sigma_{ap} + \sigma_{ep})(P^+ + P^-) + \Gamma_S\lambda_S(\sigma_{as} + \sigma_{es})(S^+ + S^-)}, \quad (2.5)$$

where λ_S and λ_P are the wavelengths of signal and pump, respectively, A is the core area, h is the Planck constant, c is the speed of light, and τ is the excited state lifetime.

Equation 2.4 was solved subject to boundary conditions

$$\begin{cases} P^+(0) = P^+_{pump} \\ P^-(L) = 0 \\ S^+(0) = R_1 S^-(0) \\ S^-(L) = R_2 S^+(L) \end{cases}, \quad (2.6)$$

where R_1 and R_2 are the mirror reflectivities at $z = 0$ and $z = L$, respectively, and P^+_{pump}

is the pump power launched as shown in Figure 2.3b. The simulation considered amplification of the fundamental mode only, using the same material parameters for both cylindrical fiber and TDCF.

To take the tapered shape into account in the simulation, the concentration of active ions was varied axially with the relative volume $\Delta V_{TDCF}/\Delta V_{cylinder}$ of the active medium, i.e.

$$N_{TDCF}(z) = \frac{\Delta V_{TDCF}}{\Delta V_{cylinder}} N = \frac{r_{TDCF}^2(z)}{r_0^2} N, \tag{2.7}$$

where r_{TDCF} is the taper core radius, and $r_0 = \min(r_{TDCF})$ is the core radius of the cylindrical reference fiber. With this assumption, the TDCF ion concentration approaches the actual concentration at the narrow end of the taper; however, the axial change in overlap of the fundamental mode and the active medium is neglected. Furthermore, a TDCF has a higher absorption per unit length compared to regular fibers with the same dopant concentration in the core, because the doped volume in a TDCF is always higher than the doped volume of a regular fiber with core diameter similar to the narrow side of TDCF. Although the absorption is generally determined by the core-cladding area ratio, the TDCF exhibits higher absorption due to mode mixing introduced by the tapered cladding shape, and near core-pumping due to the large core size at launch end. The simulation conducted by varying the active ion concentration according to Equation 2.7 overestimates these effects; however, it serves to qualitatively illustrate the differences between the two fiber types, i.e. the consequences of the increased asymmetric absorption in the TDCF.

Pump vignetting was implemented as [52]

$$\frac{dP^+}{dz} = \frac{dP_P^+}{dz} - \frac{dP_v}{dz}, \tag{2.8}$$

where P_P^+ is the pump power without vignetting and [P2]

$$\frac{dP_v}{dz} = \frac{1}{L}\left(1 - \frac{r^2(L)}{r^2(0)}\right)\exp(-\alpha_p z). \tag{2.9}$$

With these assumptions, Equation 2.4 was solved for co- and counter-propagating configurations for a cylindrical fiber and for a TDCF with equal narrow end diameter, to yield the output power as a function of laser length and pump conversion efficiency as a function of absorbed pump power (Figures 2.4a and b, respectively). The power and power density distributions were calculated for all four schemes with results shown in

Figure 2.5. The results presented here were simulated with typical parameters, similar to those used in [P2].

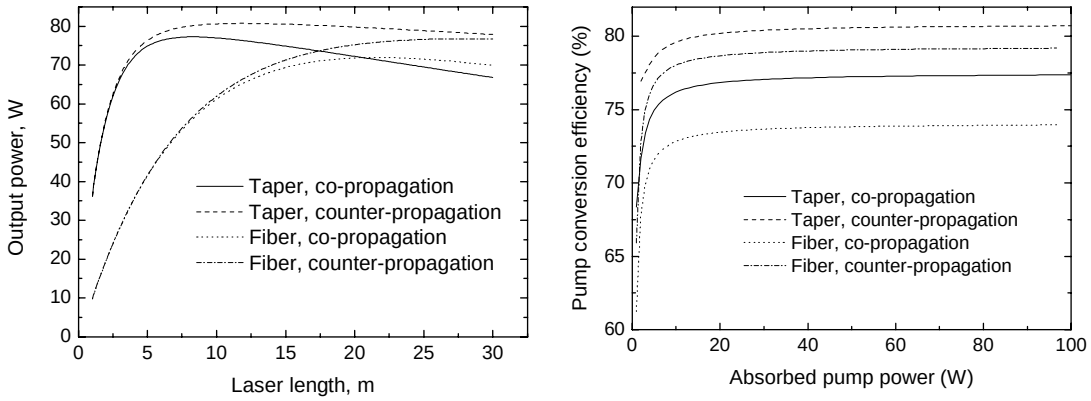

(a) (b)

Figure 2.4: (a) Simulated output power as a function of cavity length for different laser configurations. (b) Pump conversion efficiency versus absorbed pump power for the same configurations.

As noted above, pump absorption in the TDCF is higher, resulting in shorter optimal TDCF laser lengths in Figure 2.4a, which leads to higher PCEs for TDCF configurations in Figure 2.4b due to lower background loss. Although co- and counterpropagating schemes only differ in the location of the output coupler, their characteristics are quite distinct due to the much higher active volume in the pump launch side of the tapered fiber. Qualitatively, the uneven ion distribution and end pumping lead to optical power being generated mainly in the wide side, from where it either propagates through the narrowing fiber (co-propagation) before exiting the fiber, or exits the fiber directly (counter-propagation). Therefore, the background loss for counter-propagation scheme is lower, resulting in higher PCE in Figure 2.4b.

The effect is further illustrated by the power distributions in Figure 2.5a. As can be seen in the figure, similar behavior takes place in a regular end-pumped fiber laser; however, the TDCF enhances the asymmetry of the power distribution. In the counter-propagating configuration, this asymmetry is beneficial due to the synergic fiber geometry, as shown in Figure 2.5b. The power density over the entire fiber, and especially at the output endface is reduced due to this effect, which in turn reduces fiber nonlinearity. This was confirmed experimentally in terms of the threshold of self-pulsing, an effect commonly encountered in high-power density fiber lasers [53]. In [P2], a sevenfold in-

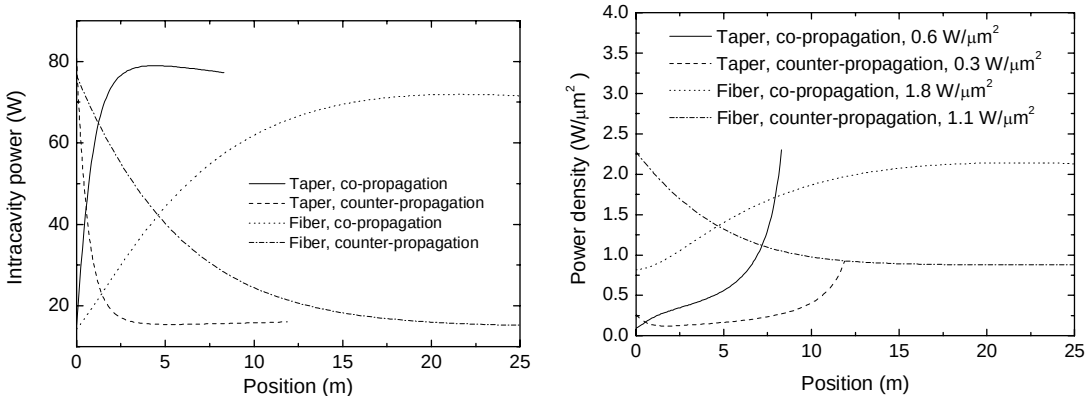

(a) (b)

Figure 2.5: Simulated intracavity power (a) and power density (b) for different laser schemes. The numerical values in the legend in (b) are the (average) power densities per unit length.

crease in self-pulsing threshold was measured for counter-propagation laser compared with otherwise identical co-propagation scheme.

Furthermore, the two laser schemes differ in terms of mode coupling, and the associated deterioration of PCE and beam quality. In the co-propagating scheme, the output beam quality is diffraction-limited because the narrow end core supports only a single mode (SM). However, the presence of mode coupling can lead to filtering of a large fraction of power into the cladding. The power leaked into the cladding contributes to cavity loss, reducing pump conversion efficiency. Conversely, in the counter-propagation scheme, the deterioration PCE is minimal. Consequently, in a narrow-to-wide traveling-wave (TW) TDCF amplifier the only adverse effect for the signal due to fiber geometry is the potential reduction in beam quality in the presence of mode coupling.

2.3 Mode Coupling

Mode coupling inevitably exists in non-regular waveguides [54, 55], and can have a significant effect on TDCF devices. In a TDCF laser, mode coupling can lead to signal leakage into the cladding, degrading pump conversion efficiency, whereas in both lasers and amplifiers the effect can result in beam quality deterioration. There are two basic mechanisms for mode coupling in tapered fibers; mode coupling induced by the core diameter variation [54–58], and by bending of the tapered fiber [59, 60].

The magnitude of mode coupling between modes m and n can be characterized in terms of the mode coupling coefficient Ω_{mn}. The mode field ε in the wave equation in scalar approximation

$$\frac{\partial^2\varepsilon}{\partial r^2}+\frac{1}{r}\frac{\partial\varepsilon}{\partial r}+\frac{\partial^2\varepsilon}{\partial z^2}+n^2(r,z)k^2\varepsilon=0, \tag{2.10}$$

where $k=2\pi/\lambda$ is the vacuum wavenumber, can be expressed as a superposition of local normal modes φ_m at any point of the tapered fiber [61]. The expansion coefficients c_m of the normal mode expansion are interdependent, and satisfy the coupled-wave equations [62]

$$\frac{dc_m}{dz}=\sum_n \Omega_{mn}c_n e^{i\int_0^z(\beta_m-\beta_n)dz'}, \tag{2.11}$$

where β_m is the propagation constant for mode m. Utilizing the normal mode expansion, the coupling coefficient resulting from core size variation for a step-index taper at core radius r can be shown to be [55]

$$\Omega_{mn}^{(r)}=\frac{2\pi k(n_{core}-n_{clad})}{\beta_m-\beta_n}r\frac{\partial r}{\partial z}[\varphi_m\varphi_n], \tag{2.12}$$

proportional to $\partial r/\partial z$, which corresponds to the taper angle for a linear taper. The power loss for the dominant mode was shown to decrease rapidly with decreasing taper angle in [55] for several taper shapes. A linear step-index taper with a tapering angle of 0.44 mrad exhibited $< 10^{-3}$ dB loss from the dominant mode due to tapering-induced mode coupling. For the tapered fibers discussed in this work with typical tapering angles of the order of 10^{-6} rad – 10^{-5} rad, the corresponding loss can be expected to be even lower, and allows concluding that the effect of mode coupling induced by changing core diameter in TDCFs is negligible.

Mode coupling due to local bending of adiabatically tapered single-mode fibers has been studied theoretically and experimentally in [59, 60, 63]. The tapered fiber bent at a given angle can be modeled as a sequence of cylindrical segments with a step-wise varying diameter, so that the longitudinal axis of each segment is rotated in an angle ψ (the total bend angle divided by the number of segments) towards the direction of the bend. The mode coupling coefficient resulting from such a local bend is given by [60]

$$\Omega_{mn,pq}^{\psi}=\int_0^{\infty}\int_0^{2\pi}\varepsilon_{mn}^{(k)}\varepsilon_{pq}^{(k+1)}(J_0(\beta_{mn}^{(k)}\psi r)+2iJ_1(\beta_{mn}^{(k)}\psi r)\cos\phi)rdrd\phi, \tag{2.13}$$

where subscripts m, p and n, q refer to the radial and azimuthal mode numbers, respectively, $\varepsilon_{mn}^{(k)}$ and $\varepsilon_{pq}^{(k)}$ are the transversal input and output mode field functions at segment k of the bent taper, respectively, J_0 and J_1 are Bessel functions, $\beta_{mn}^{(k)}$ is the propagation constant of mode mn at segment k, and r and ϕ are the radial and azimuthal coordinates, respectively. It has been shown that even small bends can lead to substantial mode coupling, e.g. ~ 10 % for a one-degree bend [59, 60]; the effect is significant enough to be utilized in sensing applications [63].

Furthermore, distributed bending due to coiling of a long adiabatic taper for practical purposes effectively constitutes another mode coupling mechanism that can be significant in a TDCF. In this case, although each local bending angle for a large coiling radius r_c is small, the aggregate mode coupling coefficient can be significant, defined as the integral over the fiber length

$$\Omega = \int_0^L \Omega_{mn,pq}^{1/r_c}(z)dz, \tag{2.14}$$

where $\Omega_{mn,pq}^{1/r_c}(z)$ is the coupling coefficient caused by the local bend at location z.

As noted in the previous section, the impact of mode coupling is different in co- and counter-propagating laser configurations and in TDCF amplifiers. The main distinction between the laser configurations is, qualitatively, that in the co-propagating scheme most of the generated power propagates through large part of the taper towards the narrow side, whereas in the counter-propagating scheme it does not. In wide-to-narrow propagation (prevalent in the co-propagating scheme), the number of available modes decreases along with the core diameter during propagation, and assuming the common nearest-neighbor coupling, eventually cladding modes will be excited [64]. This leads to signal leakage into the cladding, contributing to cavity loss. In addition, in the co-propagating configuration, the high-reflection (HR) mirror is located in the highly multimode section of the fiber and any defects in the reflector, non-ideal alignment of a free-space mirror, or any fiber Bragg grating (FBG) [65] can result in significant additional mode coupling. Conversely, in narrow-to-wide propagation, strong coupling to cladding modes requires excitation of nearly all core modes, because at each subsequent section of the fiber the modes near cut-off would need to be excited. Therefore, little cladding mode coupling takes place, and intracore coupling can only degrade beam quality, not PCE. Furthermore, in the counter-propagating laser configuration the HR mirror is located in the single-mode section and any non-idealities can only result in parasitic loss

without effect on mode coupling.

2.4 Geometric Limitations

In general, bearing in mind the manufacturing limits for the NA (Chapter 1), the core size of a step-index fiber has an upper limit to maintain near-diffraction-limited beam quality. A commonly used parameter to characterize the SM cut-off for operating wavelength λ is the normalized frequency [66]

$$V = \frac{2\pi r}{\lambda} NA, \tag{2.15}$$

where r is the core radius and $V \lesssim 2.4$ corresponds to single-mode operation for a circular waveguide. Although LMA fibers rarely are strictly single-mode waveguides, typically guiding a few modes, they can not significantly deviate from this condition when regular fibers are utilized. Furthermore, the double-clad absorption in a DCF is determined by the core-to-cladding area ratio and can be estimated by [67]

$$\gamma_{dc} = \gamma_{core} \frac{A_{core}}{A_{clad}}, \tag{2.16}$$

i.e. the core size restriction immediately imposes a limitation for the cladding size, as it is necessary to maintain a reasonable level of pump absorption in practical devices.

Enhancement of double-clad absorption for a given core-to-cladding area ratio can be achieved either by increasing the core doping level (to increase γ_{core}) or by implementing special features in the preform. To maintain high efficiency, feasible core doping levels typically limit the in-core absorption approximately to 600 dB/m – 800 dB/m at 980 nm pump wavelength due to photodarkening [68–70] and background loss [71]. Absorption enhancement methods independent of core doping include increasing the (effective) core size with respect to the cladding size while maintaining good beam quality e.g. by controlled bending of the fiber [14, 27] or by utilizing a PCF [30, 72], although it is debatable whether high-power rod-type PCFs should be regarded as fiber devices. To alleviate the effect of saturation of pump absorption due to the presence of weakly-absorbed pump modes arising from waveguide properties [73–75], several additional techniques can be employed. These include transversal shaping of the preform [76–78] (Figure 2.6a), introducing mechanical perturbations in the cladding [79, 80], and again, controlled bending of the fiber [81, 82]. However, the above approaches typically suffer

either from parasitic pump or signal loss, or from poor reproducibility. In addition, the problem of pump absorption saturation is not eliminated, but the saturation length merely increases.

As noted above, it is generally desirable to pump DCF devices by low-brightness pump sources, as the pump diode cost is directly proportional to the brightness. Due to the near-single-mode limitation for the core size (Equation 2.15) and the core-to-cladding area ratio restriction induced by the absorption requirement (Equation 2.16), the size of the cladding can not be increased arbitrarily even if additional absorption-enhancement methods are utilized. The restraint in cladding size, in turn, limits the pump power launched through the fiber end for a given pump brightness (unless side pumping is utilized, cf. Section 4.1.2).

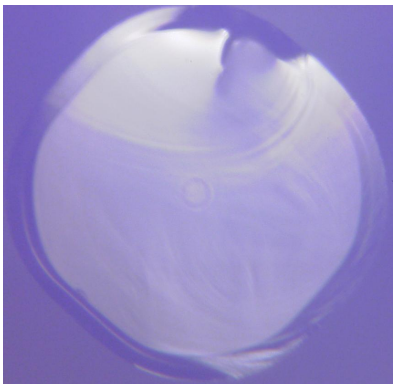

(a)

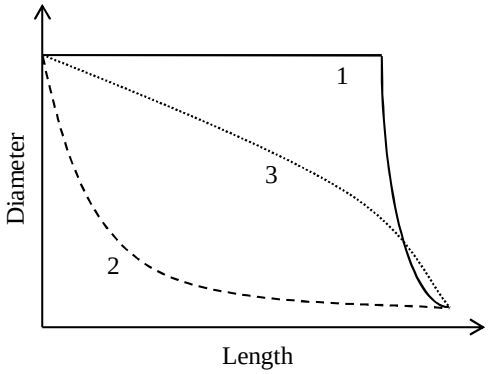

(b)

Figure 2.6: (a) A micrograph of the wide endface of one of the TDCFs used in this work. The preform has been transversally shaped (truncated four times) to improve double-clad absorption. Outer cladding diameter $\sim$ 1 mm, core diameter $\sim$ 60 μm. (b) Schematic of taper profiles utilized in [83–87] (1), [P1,P4,P5] (2), and [P6] (3).

In a TDCF, the above restraint is significantly relaxed, as the pump launch endface of the fiber can be very large without severely compromising either pump absorption or beam quality. Considering two fibers with similar output beam quality; a TDCF with wide end cladding diameter D, tapering ratio T, and cladding numerical aperture NA, and a uniform double-clad fiber with diameter D/T and the same NA, the theoretical pump launch efficiency into the DCF is [88, 89]

$$K_{DCF} = \left(\frac{D \cdot NA \cdot F_{DCF}}{2BPP \cdot T}\right)^2, \tag{2.17}$$

where F_{DCF} is the pump launch fill factor for the DCF, and BPP is the beam parameter product (BPP) of the pump source. For the same pump source, the launch efficiency into the TDCF is

$$K_{TDCF} = (\frac{D \cdot NA \cdot F_{TDCF}}{2BPP})^2, \tag{2.18}$$

where F_{TDCF} is the fill factor for the TDCF, and thus,

$$\frac{K_{TDCF}}{K_{DCF}} = (\frac{F_{TDCF}}{F_{DCF}}T)^2. \tag{2.19}$$

Usually $F_{DCF} = 1$ as there is no need for pump launch underfill in a cylindrical DCF, i.e. the pump launch efficiency into a TDCF is $(F_{TDCF}T)^2$ times higher than for a cylindrical fiber with similar output beam quality. Assuming similar slope efficiency and no beam quality degradation due to mode coupling, the brightness enhancement ratio between TDCF and DCF scales with $(F_{TDCF}T)^2$ as well. The exact limitations of F_{TDCF} and T depend on the paraxial absorption and the acceptable level of pump vignetting (Figure 2.2); however, typical experimental values used in this work with high slope efficiency yield brightness enhancement several times higher compared to a regular DCF, e.g. 3 – 8 in [P6].

Additional limitation for the tapering ratio can arise from HOM coupling in a TDCF laser. In the above, the output beam quality of the TDCF was assumed to be equal to that of a regular DCF with diameter similar to the narrow end taper diameter. In the presence of mode coupling in the taper; however, this is not exactly the case (cf. Section 3.2). In a TDCF laser with bidirectional signal propagation, mode coupling leads to filtering of coupled HOMs to the cladding in the narrow (single-mode) end of the fiber, i.e. part of the signal can propagate in the cladding, characterized by *contrast* of the output beam $C = S_{core}/S_{total}$, where S_{core} is the signal power propagating in the core and S_{total} is the total signal power. If $C < 1$, the brightness enhancement is correspondingly deteriorated; therefore, the tapering ratio is limited to relatively low values in a TDCF laser [P6]. Notably, in a traveling-wave TDCF amplifier with solely narrow-to-wide signal propagation, $C = 1$.

Another design consideration in a TDCF is the longitudinal shape of the taper, affecting not only pump vignetting (Section 2.1) but also mode coupling in the taper (Section 2.3). Figure 2.6b schematically illustrates three taper profiles . Assuming pumping from the wide side, profile type 1 exhibits very low vignetting loss, because nearly all pump power is absorbed in the wide side of the fiber, and is largely depleted at the steep slope

section where significant vignetting would start to occur. However, the lasers constructed using such tapers generally resulted in low slope efficiencies of 30% – 54% in [85–87]. This is likely due to strong mode coupling effects arising from the large tapering angle, which would be further aggravated by any (micro)bending of the tapered region (cf. Section 2.3). The power coupled into HOMs is subsequently filtered out of the core in the next wide-to-narrow pass through the short tapered section. The type 2 profile, in turn, suffers from significant pump vignetting due to the large slope near the pump launch end where unabsorbed pump power is substantial. Finally, the type 3 profile represents a compromise between the two former cases with low vignetting loss and minor mode coupling effects, and such a profile was used to achieve the highest CW powers within this work [P6].

Chapter 3

Experimental Study of Tapered Double-Clad Fiber

Nowadays, most high-purity (low-loss) optical fibers are fabricated by heating a glass preform, typically a few cm thick and tens of cm long cylinder, in a furnace located in a tower several meters high. The half-molten glass is drawn down while it cools to yield thin glass fiber with an inner structure corresponding to that of the preform. Subsequently, the fiber is coated with a protective jacket, typically made of acrylate polymer or polyimide. The fiber diameter can be continuously monitored below the furnace, and an automatic feedback loop is used to adjust the drawing speed and the furnace temperature to keep the diameter constant. For the tapered fibers used in this work, such a feedback loop was instead used to controllably vary the diameter during the drawing with an appropriate algorithm.

There are various methods currently available for fabrication of the preform, and although other approaches exist (e.g. [90]), the predominant techniques for step-index fiber fabrication are based on some form of chemical vapor deposition (CVD). The fibers studied in this work were fabricated by surface-plasma chemical vapor deposition (SPCVD) [91–93], a high-precision method utilizing microwaves to heat the deposition region. The higher index required for the fiber core is typically realized by adding Al-, Ge-, or P-oxides to the reactant flow, i.e. by doping of the same glass used for the cladding. Additional dopants can also be utilized e.g. to improve the solubility of the active rare-earth dopants added in the core. Furthermore, the index of the (outer) cladding can be lowered by doping with F- or B-oxides. Whereas pulling of the fiber

can be considered a somewhat standard procedure, the fabrication of special preforms requires careful process management, as the material parameters of the end product are determined solely at this stage. Particularly for a TDCF, the paraxial absorption (Section 2.1) is determined by the properties of the preform; not only by the rare-earth doping of the core, but also by geometric parameters such as transversal preform shape and the size of the core relative to the cladding. Whereas paraxial absorption and background loss are determined by the preform, several other factors affect the pump conversion efficiency, and will be discussed next.

3.1 Pump Conversion Efficiency

The pump conversion efficiency of a DCF laser is defined as the product of pump launch efficiency, slope efficiency, and beam contrast. A TDCF laser was compared to a regular (cylindrical) fiber laser in terms of PCE in [P2]. Both fibers were pulled from the same preform, i.e. they were only different in terms of fiber geometry. The wide end of the TDCF had 40 μm / 650 μm core/cladding diameter, tapered down to 6.5 μm / 110 μm over the length of 20 m, as shown in Figure 3.1a. The transverse dimensions of the regular DCF (L = 25 m) were equal to the narrow end of the TDCF, with strictly SM core at 1 μm wavelength; all other fiber parameters were identical. Each active fiber was used in both co- and counterpropagating laser configuration, and the slope efficiencies were measured using the end-pumped setup schematically shown in Figure 3.1b.

The same highly MM pump source was used for both fibers, with measured launch efficiencies of 5.5 % and 78 % for DCF and TDCF, respectively. The very large difference in launch efficiencies could be expected (cf. Section 2.4), as the cylindrical DCF would require much higher pump brightness for efficient launching compared to a TDCF with similar narrow end transverse dimension and relatively high tapering ratio.

The measured slope efficiencies in copropagating configuration were 50 % (DCF) and 51 % (TDCF), and in counterpropagating configuration 57 % (DCF) and 60 % (TDCF). The slope efficiency was slightly higher for the TDCF laser, whereas the higher values in counterpropagating configuration are typical for end-pumped fiber lasers with uneven population inversion distribution.

The beam contrast could be readily measured only in the copropagating scheme, with the results C = 98 % and C = 70 % for DCF and TDCF lasers, respectively. Both fibers had a core NA of 0.11, yielding high contrast due to strong confinement for the DCF

laser. The 70 % contrast for the TDCF in copropagating configuration can be taken as an estimate for the fundamental mode power, with approximately 30 % of the power distributed to HOMs. In the counterpropagating scheme, although the contrast could not be examined directly, the output divergence was measured to be 0.03 rad for the 0.11-NA core. This suggests that the output aperture is not fully filled, indicating a contrast of 1 for the counterpropagating scheme, i.e. all the output power propagated in the core. Despite the $\sim$ 30 % HOM content, the output beam quality was near-diffraction-limited with $M^2 = 1.06/1.2$ for two orthogonal axes.

The above comparison indicated that, using each fiber type in the more favorable counterpropagating configuration with the same low-brightness pump source, the TDCF allowed achieving a 15-fold increase in PCE with 35 times larger output mode field area compared to the DCF. The only disadvantage was the HOM content in the output signal due to mode coupling, resulting in slightly degraded beam quality of $M^2 < 1.2$. This effect will be discussed in more detail in the next section.

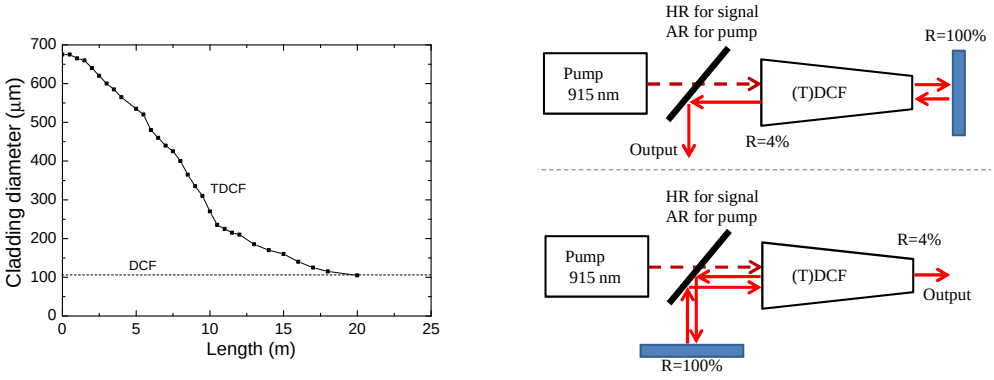

(a) (b)

Figure 3.1: (a) Cladding diameter versus length of the studied DCF and TDCF. (b) Schematic counter- (upper) and copropagating (lower) fiber laser setups used for slope efficiency measurements.

3.2 Mode Coupling

Several methods for experimental mode power decomposition have been proposed to date [94–97]. In this work, the recently demonstrated S^2-method (spatially and spectrally

resolved) [98, 99] was used in a simplified form to characterize mode coupling effects in a TDCF. The S^2-method is based on launching single-mode broadband emission into an LMA fiber and measuring the spectral modal beats at a number of locations over the output near field. Fourier transforms of the beat patterns can then be used to reconstruct the spatial distributions of the propagated modes. In this work, the broadband single-mode source was input at the SM end of the taper, and the output was measured by an optical spectrum analyzer through a SM fiber (acting as a spatial filter) directly coupled to the output endface at a given location. In the absence of mode coupling, the intensity after the spatial filter is determined by the spatial function of the single fundamental mode and the transmission function of the filter. However, in the presence of multiple modes (due to mode coupling) the intensity becomes frequency-dependent, containing the sum of modal functions with periods equal to the intermodal group delay [P2]

$$\tau_{mn} = \frac{\Delta n_{eff,mn} L_p}{c}, \tag{3.1}$$

where $\Delta n_{eff,mn}$ is the difference between effective indices of modes m and n, and L_p is the distance between the mode conversion location and the output end of the fiber. Thus, periodic spectral modulation after propagation through fiber under study and the spatial filter indicates mode coupling in the fiber. In general, the value of τ_{mn}, the amplitude of the harmonic with the period τ_{mn}, and the shape of the intermodal group delay spectrum (the Fourier transform of the optical spectrum) give information on the type of interfering modes, the coupling coefficient of the modes, and the type of mode coupling (distributed or discrete), respectively.

Mode coupling in a TDCF was studied experimentally in [P2] for a 20 m long fiber tapered down with an approximately linear axial profile from (core/cladding diameter in μm) 650/40 to 110/6.5, i.e. with a tapering ratio of 6.5, and with core and cladding NAs of 0.11 and 0.4, respectively. In such a fiber, the narrow end supports only the fundamental mode, whereas in the wide end with $V = 14$ up to 100 modes can be guided. The measurements were performed for coiling radii of 25 cm and 15 cm, and the effect of local bending was studied for bends of 5 cm radius separately at one meter from the wide end and three meters from the narrow end; both locations were in the multi-mode section of the TDCF. An example measurement is shown in Figure 3.2 for the coiling radius of 15 cm without local bending.

The results showed a few modes at the TDCF output, and an increasing number of coupled modes with decreasing coil radius. The beam contrast measured for the co-

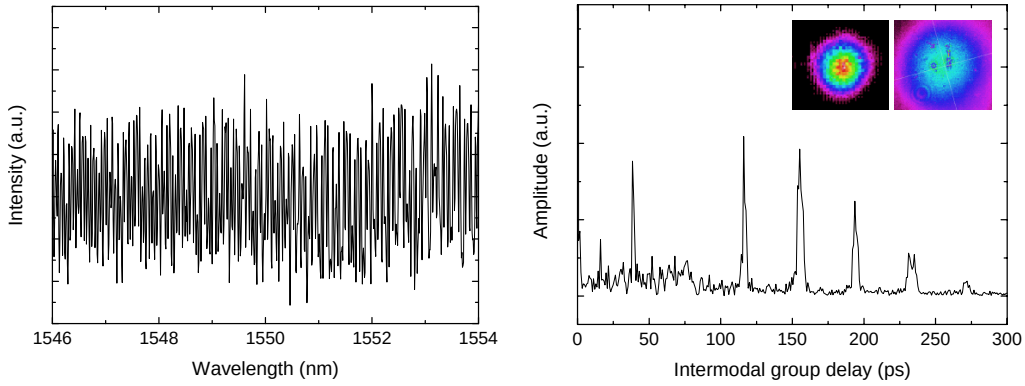

(a) (b)

Figure 3.2: (a) Optical spectrum measured after narrow-to-wide propagation through a TDCF with a coiling radius of 15 cm and a SMF spatial filter. (b) The intermodal delay spectrum, i.e. Fourier transform of the optical spectrum, and the near field (left inset) and far field (right inset) beam profiles.

propagating scheme was found to be ~ 70 % independent of the coiling radius, indicating that up to 30 % of the signal propagated in the higher order modes. The power coupled out of the fundamental mode was distributed over an increasing number of modes with decreasing radius of coiling. It was also found that local bending at the wide section had little effect on mode coupling, whereas bending at the narrow (still multi-mode) section caused strong coupling, essentially resulting in a multi-mode speckle pattern at the output. This was attributed to the strong dependence of mode coupling coefficients on the outer diameter of the fiber, i.e. $\Omega_{mn} \sim D^{-6}$ [100], and emphasizes the importance of avoiding local bends especially in the narrow part of the multi-mode section of a TDCF in practical operation.

The beam quality of the same TDCF was characterized by M^2 and divergence measurements for the 15 cm coil radius. Whereas the beam quality from the narrow single-mode end was naturally diffraction limited, the wide end output beam from the 40 μm core with NA=0.11 was measured to have an M^2 of 1.06/1.2 and a divergence of 0.03 rad, characterized in the counter-propagation laser scheme. Theoretically, in the absence of mode coupling the divergence would be even lower, approximately $NA/T = 0.018$ due to conservation of brightness. This discrepancy and the corresponding degradation in beam quality result from the HOM excitation. The presence of a few high-brightness

modes, however, has little effect on beam quality [98, 99, 101, 102], and therefore allows the realization of bright practical devices, although the HOM content could impede some applications requiring e.g. high pointing stability.

3.3 Fundamental Mode Evolution

As noted in Chapter 1, in addition to low-NA LMA fibers with controlled bending [14, 27] and various types of microstructured fibers [33, 103], selective excitation of a single mode (fundamental or another) in MM fiber has been found a feasible mode area scaling method [23, 104]. The results of preceding studies allow concluding that the contribution to mode coupling by macrobending in DCFs with sufficiently large cladding diameter is small, and it is possible for a single excited mode to propagate over long distances without significant mode coupling, even if the core would support a very large number of modes.

Typically, single mode excitation in a highly MM fiber requires either careful free-space launching to the fundamental mode, or special techniques such as utilization of a long-period fiber Bragg grating [24]. Adiabatic tapering in a TDCF is a simple method for fundamental mode excitation with the input signal launched through the narrow SM guiding end. Mode area scaling by tapering has been demonstrated e.g. in [105]; however, only few-cm-long tapers up to ~ 50 μm maximum core diameter have been studied before.

Within this work, fundamental mode evolution was studied in several meters long passive TDCFs by launching an input signal through the narrow end and recording the output beam parameters at different axial locations via cut-back measurement [P3]. The studied tapers were strictly SM in the narrow end and had an output core diameter up to 117 μm, V up to 38, and T up to 18. Minimal defects and a uniform refractive index profile of the fiber core were ensured by fabricating the tapers with the so-called rod-in-tube method, i.e. the core was formed by a solid silica rod inserted into a cladding tube, and the fibers were pulled directly from the aggregate.

Robust single fundamental mode propagation in the studied tapers was confirmed by several techniques, including measurements on divergence and degree of polarization at various cut-back lengths, as well as mode beating measurements. However, despite the single-mode character of the output signal, the mode field at the output was found to exhibit annular deformation in the near field (Figure 3.3). Since the mode content

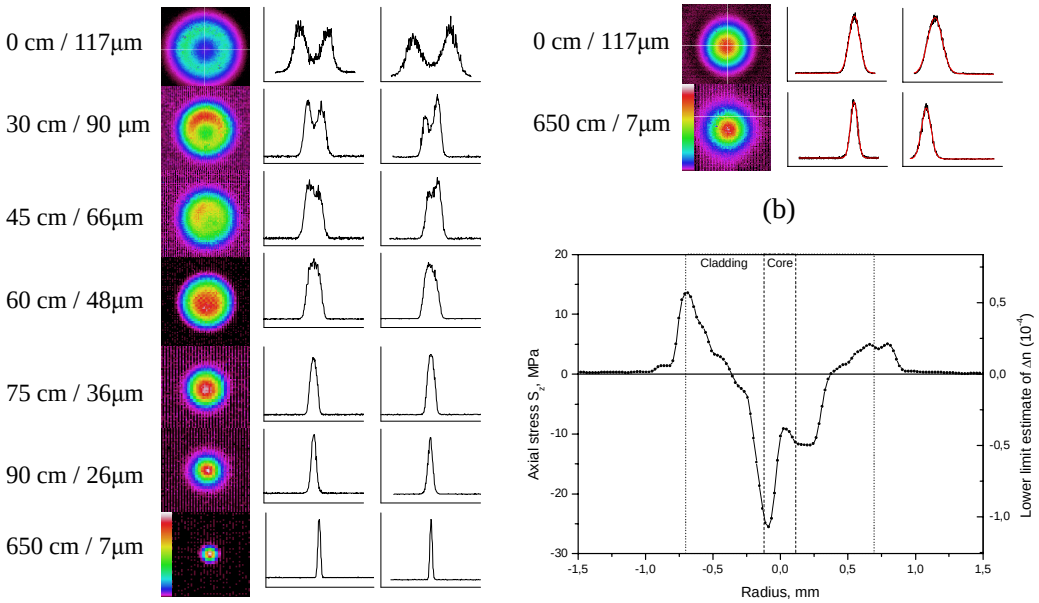

Figure 3.3: (a) The wide end output near field beam profiles of a 7-m passive TDCF at various cut lengths / output core diameters. (b) The far field beam profiles at the largest and smallest output core diameters with gaussian fits (red). (c) Measured axial stress and lower limit estimation of the corresponding index change.

was unchanged, this deformation was attributed to built-in stress in the fibers, which was measured to have an annular shape near the core-cladding boundary, resulting in a significant annular distortion of the core index profile [106]. Thermal annealing performed on a short fiber piece was found to significantly reduce the built-in stress. The stress likely arose due to inhomogeneous cooling of the fiber structure during drawing, or due to the mismatch of the thermal expansion coefficients of core and cladding materials [107]. The requirements of rare-earth doping and bending can present problems in terms of stress prevention [108, 109]; however, minimization of the built-in stress by annealing procedures and varying the chemical compositions of the materials can be expected to allow fundamental mode area scaling to very high core diameters.

Chapter 4

Continuous-Wave Fiber Lasers and Amplifiers

As outlined in Chapter 1, the last two decades have seen tremendous progress in power scaling of fiber devices. Recently, the theoretical upper limit for near-diffraction limited output power from a single fiber was estimated to be as high as 36 kW, mostly based on currently available technology [110]. However, various power scaling issues such as thermal management may need to be considered already at output powers of a few tens of watts, depending on application. Since the vast majority of fiber laser sales lies in the mid-power marking and micromachining sector, it is often more important to minimize the cost and complexity of a practical system than to aim for highest possible output powers, and as noted above, pump diode cost typically constitutes most of the fiber laser cost. In this chapter, state-of-the-art pump sources and pumping methods, as well as their applicability to TDCFs will be discussed, followed by an overview of the main limitations of power scaling of CW fiber devices and selected high-power results obtained within this work.

4.1 Diode Pumping

Optical pumping is utilized in lasers and amplifiers based on doped-dielectric gain media, such as fiber lasers, to provide the required energy into the system. Although edge-emitter diode pumping is nowadays by far the most common method, pumping by discharge lamps or by other laser types are utilized for certain applications due to either

low cost per watt or maximum achievable performance (e.g. pump brightness or spectral versatility), respectively.

Compared to lamp pumping, the most important advantages of diode pumping include high electrical-to-optical conversion efficiency, long lifetime, compactness, high beam quality, and narrow emission bandwidth. The two last-mentioned properties contribute to higher overall wall-plug efficiency of the system, because the overlap of the pump and signal emission can be higher, and the narrow line enables efficient direct pumping of certain transitions of the active medium.

Diode pumps can be fabricated as single-emitters, diode bars or diode stacks, depending on the required power. Diffraction-limited single emitters can be utilized in very compact, even battery-powered, systems, and yield output powers up to 1 W. Broad-area single-emitters with somewhat decreased beam quality can reach several watts, and diode bars with multiple emitters side by side are capable of >100 W. Diode stacks, i.e. multiple vertically stacked bars, can produce multiple kilowatts in a compact assembly. However, the output beam quality and brightness decrease with increasing power, and the asymmetric output beam often requires the use of beam shapers.

4.1.1 Pump Source Brightness

Although alternatives exists, direct diode pumping remains the most feasible approach for the majority of solid state laser (SSL) applications. The lowest cost per watt is achieved by lamp pumping; however, their low brightness and short lifetime considerably limit the applicability. On the other hand, it is possible to use other high-brightness pump lasers, such as in tandem pumping of fiber lasers; such schemes have been utilized in all highest-power HPFL systems demonstrated to date [111]. In fact, tandem pumping can remove the issue of pump brightness from HPFL power scaling consideration altogether [112]. However, such an approach significantly adds to footprint and complexity, and if the overall system cost is of concern, direct diode pumping is more reasonable for most applications. Therefore, the diode pump brightness remains an important design aspect in cost-effective industrial systems.

Brightness of a laser beam increases with increasing output power and beam quality. The beam quality is commonly characterized by the BPP, defined as

$$BPP = w_0\theta_d \quad [mm \cdot mrad], \tag{4.1}$$

where w_0 is the beam waist radius and θ_d is the (far-field) beam divergence half-angle. The beam quality factor M^2 relates to BPP as

$$M^2 = \frac{\pi}{\lambda} \cdot BPP. \tag{4.2}$$

For a diffraction-limited beam, $M^2 = 1$ and BPP ~ 0.3 mm $\cdot$ mrad at 1 μm. Essentially, both parameters describe the focusability of the beam for a given divergence angle, typically limited by the NA of the focusing lens.

HPFLs can be pumped by either a large number of broad-area single emitters or by a smaller number of multi-emitter bars (or stacks). Over the recent years, a fierce debate has been going on about the advantages of one method over the other, see e.g. [113]. Generally, single emitters offer much longer lifetimes, increased process yield, and somewhat higher efficiency, whereas highest brightness can arguably be achieved with diode bar pumps and the overall HPFL pump assembly can be significantly simplified [114–116]. Furthermore, single emitters typically do not require water cooling, whereas bars exhibit less thermally-induced wavelength shift, and bar-pumped systems are more robust due to facile elimination of back-reflections with a dichroic element in the bulk pump assembly. Lower cost per watt of raw pump power arguably favors single emitters; however, direct comparison is difficult due to varying required brightness, limited disclosure, and often biased views of the manufacturers. Complications arise from the need to consider several factors simultaneously for each application, including the cost per watt, required brightness, and the integration cost, i.e. the cost of the entire pumping scheme. State-of-the-art pump assemblies often pursue a compromise between the two approaches, either by integrated packaging of multiple single emitters or by utilizing short, few-emitter bars to gain some of the benefits typically associated to single emitters.

4.1.2 Pumping Methods

Optically pumped lasers act as brightness converters, producing more applicable high-brightness output from low-brightness pump light. The desirable feature of DCF devices is that they are capable to perform the conversion at a very high efficiency. Furthermore, as shown in [P6], the use of a TDCF can provide several times higher brightness enhancement compared to regular DCFs. The increased performance results from the

possibility to launch the pump through the wide taper end, enabling the use of low-brightness (low-cost) pump sources in a simple coupling scheme.

In general, the pump light is launched into an optically-pumped gain medium either by side pumping or by end pumping. Depending on the type of the laser, either approach can offer certain advantages. In the case of HPFL pumping, side pumping allows multi-point pump injection providing higher damage threshold and leaves the fiber ends available for handling the signal. However, the pump scheme is typically rather complicated and requires critical components, e.g. side pump combiners susceptible to thermal damage and high brightness sources.

Examples of side pumping methods include the V-groove technique [117], fused [118, 119] or non-fused [120] side pump couplers, and evanescent coupling [121]. The first method is based on small grooves etched on the side of the fiber that can be used to launch the pump light perpendicularly from outside the fiber and allows good distribution of the pump light as well as a scalable number of injection points, as do the side pump couplers. However, the launching schemes for these methods are often laborious to implement and not very robust. The evanescent coupling methods are based on bringing the signal fiber cladding and the multi-mode pump fiber(s) into optical contact during fiber fabrication or by fusing them manually at a later stage. This technique has been utilized successfully in commercial high-power systems.

The end-pumped HPFL scheme, widely used due to its simplicity, can be realized by directly launching the pump light from a beam-shaped bar or stack, or via delivery cable by either splicing it to the active fiber or by free-space coupling between the two fibers. Directly integrated launching of bar or stack emission decreases the system cost; however, the use of hermetically packaged fiber-coupled pump unit(s), as in this work, is often more robust and flexible especially for research purposes. Furthermore, splicing the single pump fiber directly to the active fiber protects the vulnerable end face; however, it requires cavity termination between the fibers by a fiber Bragg grating (FBG) and denies signal output from the pump side. For a TDCF device, inherently suitable for single-end pumping, the simplest method is to use free-space coupling between the fibers, allowing facile pump-side signal delivery with a dichroic element in addition to high flexibility.

Another approach, enabling both the fiber end protection by splicing and the pump-side signal output, is to utilize a pump combiner (fiber bundle) spliced to the active fiber. Figure 4.1 shows example combiners used in this work and pump units with pigtails

spliced to the combiner ports. The current "industry-standard" end-pump combiners are rather similar, with six multi-mode pump fibers (e.g. D = 200 μm, NA = 0.22) surrounding a double-clad signal fiber. State-of-the-art fiber-coupled pump units are capable of delivering near-kW power into one standard pump port with BPP = 44 mm · mrad (775 W in [116]). Such a brightness would allow all-fiber (6+1)-to-1 single-end delivery of up to 4.5 kW of pump power into an all-glass TDCF with a relatively modest wide end cladding diameter of 1 mm and a typical fill factor of 0.15/0.22. Allowing robust monolithic integration, pump combiners are often the go-to solution for commercial devices, although they typically need to be tailored for each active fiber type, and the fabrication of custom high-quality combiners is not trivial.

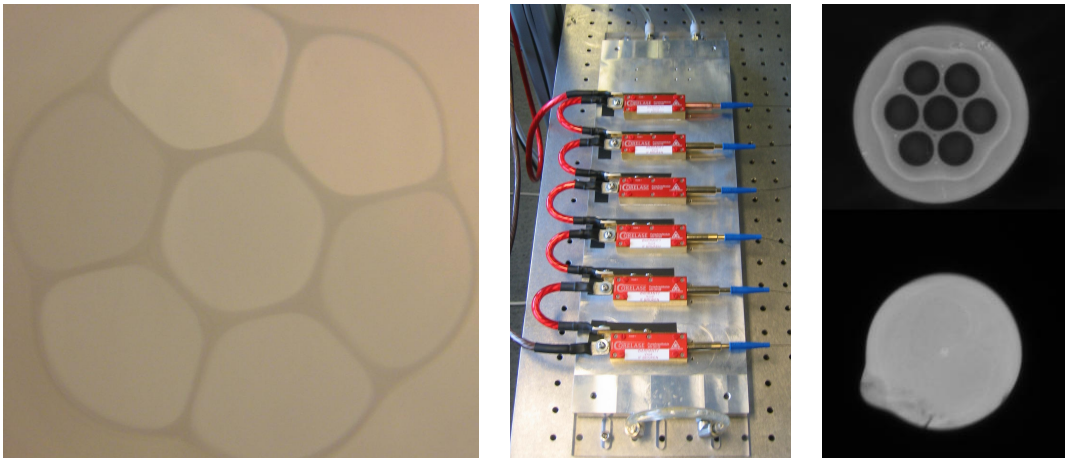

(a) (b) (c)

Figure 4.1: (a) An exemplar of a 7-port pump combiner. The central fiber is often double-clad to yield a (6+1)-to-1 combiner with signal delivery. (b) Fiber-coupled pump units used with the combiner in (a). (c) Micrographs of fused combiners fabricated within this work: the endface of a 7-to-1 tapered fiber bundle for end pumping (upper) and a 1-to-1 side pump combiner cleaved near the narrow end of the tapered pump fiber, partially fused into the active DCF (lower).

4.2 Power Scaling Considerations

As noted in Chapter 1, significant efforts to pursue ever higher output brightness from fiber devices are in active progress. It has become common to refer to any improvement

in device output power as *power scaling* regardless of the method, although it can be debated whether e.g. end-pumped fiber lasers should be considered power-scalable at all [122]. Nevertheless, single-fiber near-diffraction-limited devices with several tens of kW CW output seem to be manageable. Some of the methods and problems related to generation and handling of high power levels will be discussed in this section. Although the approach proposed in this thesis mainly targets practical kW CW level devices, most of the covered topics related to power scaling become relevant already at much lower power levels.

It should be noted that MM fiber devices with up to 100 kW output power and BPP $\sim$ 10 mm $\cdot$ mrad are nowadays commercially available [18] with several hundred kW to be expected in the near future. However, such systems are typically realized by incoherently combining the output of many SM devices into a single MM delivery fiber. In this section, only power scaling of near-diffraction-limited devices will be considered.

4.2.1 Thermal and Material Limitations

Due to the nonzero quantum defect and non-radiative decay mechanisms, significant amount of heat can be generated in the active core of a fiber laser or amplifier. Although optical (glass) fibers can safely withstand relatively high temperatures up to hundreds of $^{\circ}$C, in the absence of appropriate cooling the excess heat can lead to thermal fracture, melting of the core, or thermal lensing. These effects have been analyzed in [110, 123], indicating that fracture and melting generally do not fundamentally limit the achievable CW power, provided that sufficiently robust coating material is utilized along with forced cooling. Typically, air cooling is not sufficient for output power levels beyond a few hundred watts, and water cooling must be used instead (Figure 4.2a).

Thermal lensing, on the other hand, was established as a fundamental limit in [110] for step-index fibers with very large core sizes. A thermal lens forms in the fiber core when the transversal temperature gradient either modifies the refractive index via the thermo-optic effect, or gives rise to mechanical stresses that in turn result in a transversal index gradient. Until recently, fiber devices were regarded as largely immune to thermal lensing due to the inherent excellent heat dissipation. The pursuit for higher brightness has, however, led to higher thermal loads per meter and higher core areas, i.e. designs with thermal issues resembling those of solid-state rod lasers. Furthermore, recent studies indicate problems with thermally-induced degradation of the modal con-

tent [124–127]. This so-called mode instability seems to arise in several types of active fibers at relatively low output powers of a few hundred watts, often with a very sharp onset, and currently hinders the bleeding-edge work on CW HPFL power scaling. The origin of the effect has been traced to local variation of deposited quantum defect heat load caused by intermodal beating, and resulting in an index grating due to the emerged temperature gradient [128]. However, for coherent coupling of the fundamental mode to a HOM, a phase shift between the irradiance profile and the index perturbation is required. Such a phase shift can be produced by a moving irradiance pattern that could result from a frequency shift between the light in the two modes [124]. The effect was recently identified as a manifestation of stimulated thermal Rayleigh scattering, and it is somewhat analogous to SBS (Section 4.2.2) [129, 130]. The frequency offset corresponding to maximum gain for the HOM is inversely proportional to the effective mode area of the LMA fiber [131], indicating that the effect could be mitigated to some extent in a TDCF with continuously longitudinally varying effective mode area. However, this mitigation effect remains to be experimentally confirmed.

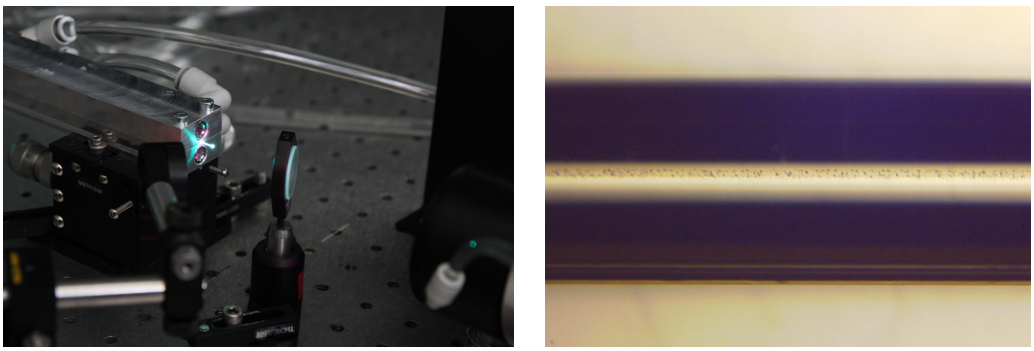

(a) (b)

Figure 4.2: (a) Cooling of a TDCF HPFL pump end under kW-level pumping. The part of the active fiber with the highest heat load is sandwiched in a groove between two water-cooled aluminum blocks with silicone heat-sink paste in between to provide better thermal contact. (b) COD in the core near signal output resulting from a fiber fuse effect. The effect arises when plasma ignited by e.g. a burning dust particle at the fiber end face propagates along the core by creating high-absorption spots at the extremely heated locations.

Despite the low signal absorption in silica-based HPFLs, high peak intensities particularly at the output end face of the fiber can lead to catastrophic optical damage (COD)

for the intensity range of $\sim$ 10-20 W/μm^2 [111, 132]. Due to the complexity of the topic (particularly for pulsed devices), clear-cut damage thresholds are difficult to establish. The damage threshold may depend on host glass composition and doping, and can be significantly different for bulk and surface of the fiber, depending on surface quality. The latter issue often necessitates the utilization of end caps to expand the mode prior to exiting the fiber, raising the damage threshold level to that of the bulk glass. In addition, damage mechanisms arising exclusively in fibers, such as the fiber fuse effect [133, 134] (Figure 4.2b) may need to be considered. However, in CW devices COD does not fundamentally limit the achievable output power for currently available pump diode brightness, although the situation may change in the near future with the ever-increasing brightness of diode pump sources [110].

4.2.2 Fiber Nonlinearities

While nonlinear effects in fibers present an extensively studied branch of optics with numerous useful applications, in the context of (peak) power scaling they impose certain limitations and are generally considered parasitic. In CW devices, typically only stimulated Raman scattering (SRS) and stimulated Brillouin scattering need to be considered, as the thresholds of other nonlinear effects by far exceed those of SRS and SBS. In addition, the susceptibility of a device to each effect directly depends on the emission linewidth; broadband emission is generally limited by SRS, whereas narrow-line devices are limited by SBS at much lower output power.

Raman scattering refers to the scattering of an incident photon by a molecule that results in a frequency-downshifted photon and excitation of the molecule to a higher-energy vibrational state. SRS arises from the Raman effect much like laser operation arises from spontaneous emission, and can transfer a large fraction of the optical energy to the Stokes wave at a longer wavelength. The output power at which the transferred power becomes significant is referred to as the SRS threshold [135]. The SRS threshold increases with mode area and decreases with increasing fiber length; therefore, despite the low Raman gain coefficient in silica ($\sim 10^{-13}$ m/W [136]), the large intensity and long interaction length in HPFLs can easily meet the threshold condition. In fused silica, the Raman-gain spectrum peaks at 13.2 THz [137], resulting in a Stokes line shifted from e.g. a 1080-nm pump wave to 1130 nm. The broadband nature of the Raman-gain spectrum in silica is utilized in widely-tunable Raman lasers, or in broadband Raman

amplifiers. Furthermore, the generated Stokes wave can generate a second-order wave and so on, yielding multiple cascaded Stokes orders separated by 13.2 THz frequency gaps. Finally, approaches for SRS suppression are based on wavelength-dependent loss mechanisms [138, 139]; however, their implementation is not straightforward. SRS fundamentally limits the output power of broadband CW HPFLs for long fiber lengths and small to moderate core sizes [110].

Stimulated Brillouin scattering can be described as the scattering of the pump wave from a moving refractive index grating in the fiber core. The index grating emerges due to a longitudinally propagating acoustic wave induced by the pump field via electrostriction [140]. The pump-induced Bragg grating scatters the pump light resulting in a Stokes wave with frequency downshifted according to the Doppler shift from the grating moving at the acoustic velocity. The acoustic frequency depends on the scattering angle with the maximum effect in the backward direction, and SBS in practice produces only a backscattered wave [137]. The Brillouin frequency shift and gain bandwidth are orders of magnitude smaller than the corresponding values for SRS, due to being related to the acoustic frequency and damping time of the acoustic wave (acoustic phonon lifetime), respectively. The SBS threshold is determined by the Brillouin gain coefficient, which in silica fiber depends on the pump linewidth with a peak value of $5 \cdot 10^{-11}$ m/W [135] for a very narrow line. Sufficiently narrow emission bandwidth with Brillouin gain coefficient near the peak value limits the operation to much lower power levels compared to broadband devices; up to 2 kW maximum achievable power in Yb:silica HPFLs compared to 36 kW for SRS-limited broadband emission [110]. Methods for increasing the SBS threshold include waveguide modification with longitudinally-varying core diameter [47, 141], refractive index profile [142], or strain distribution [143], and introduction of an acoustic-guiding layer around the core [144]. Special doping profiles can be used to efficiently reduce the overlap of optical and acoustic modes in the fiber core [145]. Furthermore, SBS can be mitigated by a longitudinal temperature gradient, either externally applied, or naturally present due to pump absorption in end-pumped devices [146]. A combination of the above methods has allowed generation of more than 500 W single-frequency output with high beam quality by utilizing a SBS-mitigating fiber with tailored dopant profile [147].

Another notable manifestation of nonlinear effects in CW fiber devices is sustained self-pulsing (SSP), first reported in 1997 [53] and consequently investigated in a number of studies. The effect arises either due to the interplay of cascaded Rayleigh scatter-

ing and SBS [53, 148], or relaxation oscillations and saturable signal reabsorption in a weakly-pumped section of the fiber [149,150]. SSP generally becomes more pronounced with decreasing cavity Q-factor, i.e. with increasing output coupler transmission and parasitic cavity loss [151, 152]. The high peak powers generated by the initial SSP mechanism may initiate a cascade of nonlinear processes, namely SRS, self-phase modulation (SPM), cross-phase modulation (XPM), and four-wave mixing (FWM), leading to supercontinuum (SC) generation. The SSP effect can be suppressed in some cases by improving the intracavity pump distribution [153] or by extending the active fiber with a passive section [154]. Figure 4.3 shows an exemple of a temporal instability and the optical spectrum associated to SSP [P2].

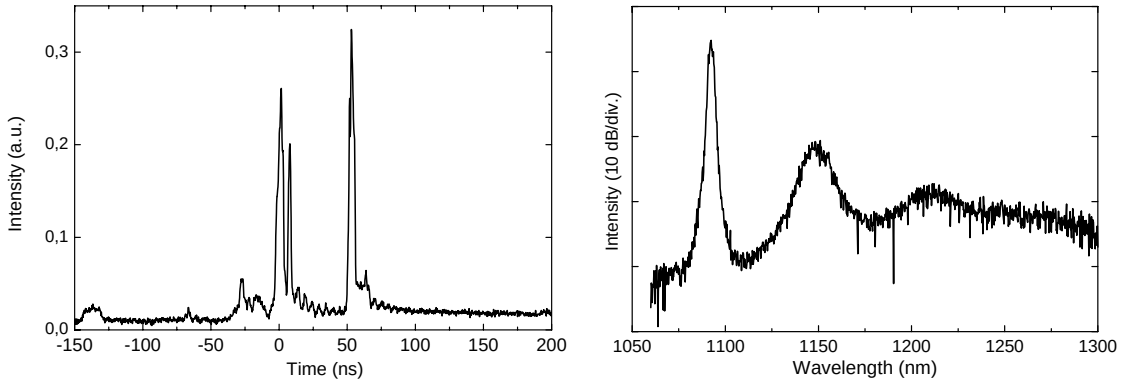

(a) (b)

Figure 4.3: (a) An example of a chaotic SSP pulse. (b) Typical optical spectrum of SSP with sufficient peak power to exceed SRS threshold. In addition to the signal at 1090 nm, two Stokes orders emerged at approximately 13 THz intervals are visible.

4.2.3 Other Limitations

For practical diode-pumped Yb-doped CW HPFLs, pump brightness (Section 4.1.1) may limit power scaling for devices with relatively small core area and short active fiber length. The small core area alleviates thermal lensing and the short fiber length allows to mitigate SRS and SBS; however, both adversely affect the absorption of pump light. For efficient laser operation, nearly all pump radiation needs to be absorbed in the active core, however, the core absorption (doping level) is limited by quenching effects [155]

and photodarkening [68]. For a given core absorption, the high-absorption requirement in turn limits the cladding diameter, and thus the launchable pump power with given brightness. However, the pump power limitation should not be taken as a hard limit, as the progress in diode technology constantly increases the available brightness. Novel materials may allow higher doping levels, relaxing the brightness limit. Furthermore, methods such as tandem pumping may be utilized to circumvent the problem, albeit at the expense of increased system complexity. These approaches will be discussed further in Section 4.2.4.

In any LMA technology, the mode size is scaled up to reduce the in-core intensity. The increase in mode field diameter (MFD) involves two detrimental effects, namely increased susceptibility to coupling to other modes, and sensitivity to mode shape and area changes due to bending (coiling) of the fiber. The former effect stems from the fact that increasing the effective area of the (fundamental) mode in most conventional fiber designs leads to a decrease in the effective index difference between neighboring modes, facilitating coupling between the modes [110]. Furthermore, bending of an LMA fiber contracts the effective mode area, and may severely limit the realization of practical devices for core diameters larger than a few tens of μm, as the use of long fibers is necessary due to the high-absorption requirement and bending can not be avoided altogether [110, 156].

Finally, for broadband ASE sources required for certain applications, output power is limited to much lower level by parasitic lasing due to the characteristic high fiber gain. Nevertheless, superfluorescent fiber devices have been demonstrated up to 100-W level by utilizing sophisticated feedback suppression techniques [157].

4.2.4 Auxiliary Scaling Methods

To reach extremely high powers, it has become common to utilize master oscillator – (fiber) power amplifier schemes in both CW and pulsed devices. In fact, many commercial ”fiber lasers” consist of a low-power seed laser (often not a fiber laser), and one or several amplifier stages; the (average) in-core intensity is always lower in an amplifier than in a laser with similar output power. In addition, the length of the power amplifier stage can be minimized to mitigate nonlinearities, and by counter-pumping the effective length can be shortened further. Another significant advantage of a MOPA system is increased flexibility; system architecture can be modular, different gain fibers

can be utilized for the stages, and bandwidth control and wavelength tuning are substantially easier to realize in a low-power seed source. As an example, a high-power single-frequency fiber source is difficult to establish, whereas amplification of an external low-power source is relatively simple. However, there are drawbacks to the fiber MOPA approach, namely higher sensitivity to back reflections and increased system complexity. The high gain typically requires feedback suppression by angle-cleaved fiber ends and optical isolators after each amplifier stage. The major advantages still make MOPAs worthwhile particularly in pulsed applications (cf. Section 5.2.4); the scheme is even more common due to the facile pulse parameter control at the low-power seed oscillator.

A somewhat less common technical development is the tandem-pumping approach, i.e. pumping of a fiber laser (amplifier) by fiber lasers. Recently, the maximum output power from a tandem-pumped single-fiber Yb device was estimated to be more than 70 kW [112], nearly twice the power limit estimated for directly diode-pumped devices. The scaling limit increase stems from the substantially increased brightness compared to diode pumps, essentially removing the pump brightness limitation from power scaling consideration altogether. Furthermore, the decreased overall thermal load resulting from the lower achievable quantum defect, reduced gain for unwanted modes, and potential mitigation of photodarkening significantly benefit the tandem-pumped architecture [158]. However, the increased system complexity and reduced wall-plug efficiency may limit the practicality of tandem-pumped devices. Near-diffraction-limited single-fiber output power of 10 kW at 1070 nm, demonstrated experimentally by IPG [159], was realized via tandem-pumped MOPA system, utilizing several sub-kW Yb-doped fiber lasers at 1018 nm as pump units. Although kW-class near-diffraction-limited powers have been achieved from directly diode-pumped fiber lasers [160], all reported output powers above $\sim$3 kW have to date been achieved via tandem pumping [111].

Because the hard limits of power handling in Yb^{3+}:silica fibers are already in sight, alternative dopant and host materials have started to attract attention in terms of highest achievable powers. Recently, it was estimated that the limits for Tm^{3+}-doped silica fibers are similar to, and for Er^{3+}-doped even higher than, their Yb^{3+}-doped counterparts, assuming the core area could be scaled accordingly without loss of brightness [161]. Phosphate host glasses could offer another interesting prospect due to the shorter possible fiber lengths achievable with higher absorption due to increased rare-earth solubility. However, currently available phosphate hosts suffer from extremely high background

loss [162], severely limiting the practical length of the active fiber. Finally, rod-like Yb-doped yttrium-aluminum-garnet (YAG) fibers with low Brillouin gain could potentially exhibit an order of magnitude higher narrowband (SBS-limited) output powers than silica fibers, though not with currently achievable background loss. Although promising in terms of hard physical limits, such new approaches still require substantial advances in materials development to become practical. [161]

Finally, the techniques of beam combining offer a scaling method independent of single-device limitations. Albeit not limited to scaling of fiber systems, recent results in spectral and coherent beam combining of fiber lasers and amplifiers have been promising. Beam combining potentially allows significant increase in output power, and more importantly, brightness, with the final combined output power emerging from a passive component, e.g. a delivery fiber. Beam-combined fiber systems have been realized with various different combining methods, with multi-kW output powers demonstrated with both spectral [163] and coherent [164] beam combining, and attractive prospects for further scaling. Arguably, an order-of-magnitude combined single-aperture power increase should be within reach [165]. However, due to challenging technical issues, the output powers currently achievable from single devices have not yet been reached with beam combining.

4.3 Practical High-Power Devices

As noted above, the fundamental limit for single-aperture, diode-pumped Yb-doped fiber lasers (amplifiers) was recently estimated to be approximately 36 kW for SRS-limited and 2 kW for SBS-limited devices. In addition to the limit due to nonlinear scattering for long fibers, both cases were found to be limited by pump brightness for short-length and small-core fibers, and by thermal lensing for large-core fibers. However, these levels can only be achieved assuming perfect scaling of the fundamental mode for very large core diameters. With state-of-the-art pump technology, the minimal core diameters required to achieve the above mentioned maxima were more than 60 μm in both cases, corresponding to approximate MFD of 50 μm and effective mode area of 2000 μm^2 for step-index fiber [110]. Although much larger effective mode areas have been reported in the laboratory, the practicality of many scaling approaches remains unclear. The mode area of a standard SMF is only $\sim$ 100 μm, and commercial LMA devices are typically limited to mode areas below 1000 μm^2. An additional practical limitation in conven-

tional step-index fibers arises from decrease in effective mode area due to bending of large-core fibers [166].

As mentioned in Chapter 1, several MFD scaling methods are currently actively studied. Most of these methods are based on either low-NA fibers with controlled bending, microstructured PCFs or LCFs, or selective excitation of the fundamental mode or certain HOM in a multi-mode fiber. In a TDCF, mode area scaling can be achieved with inherent selective fundamental mode excitation without cumbersome free-space launch schemes or problems with large-core fusion splices that may induce HOM coupling. The difficulties with low-NA engineering, bend control, and application-specific microstructure design can be alleviated, while the bendable long fiber still retains the advantages regarding thermal management and substantial absorption length. Nevertheless, care must be taken with bending to avoid significant mode coupling and bend-induced mode area deformation in the large-core section. Moreover, the preform should be fabricated so that the radial refractive index profile of the core is flat, as the large-area mode essentially follows the profile in the wide part of the TDCF, and e.g. a central dip in the profile common to CVD-preforms can be detrimental to the output beam quality [160]. Even with careful index control, difficulties may arise due to mechanical stress built in the fiber during drawing, as explained in section 3.3.

In addition to fundamental power limits and mode area scaling, multiple practical aspects need to be considered when assessing the expediency of a fiber device for a given application. These factors include the choice of pump source (diode bar or single emitter), cavity design and feasibility of MOPA approach, cooling arrangement and packaging issues, required brightness, and the overall system cost. The inherent benefits of TDCFs mentioned above can be exploited to realize highly practical trade-offs between these factors. In this work, various types of TDCF devices have been studied in different optical configurations, some of which are shown schematically in Figure 4.4.

The novel type of active medium and non-existent preceding HPFL research at ORC posed significant technical challenges in the early stages of the work. Near-diffraction-limited CW TDCF lasers were first demonstrated as proof of principle in [P1], followed by efforts to increase output power by improvements in pumping technology and fiber design [P4, P5], finally resulting in a high-power, highly efficient 750-W laser, still limited only by pump power [P6]. This progress is summarized in Figure 4.5, and leaves significant room for further scaling with respect to fundamental limits. However, investments in significantly more powerful pump units is not sensible for small-footprint de-

vices targeted for $\lesssim$1 kW. At later stages of the work, the studied devices were designed mountable into a standard 19" rack, and a fully packaged $\sim$ 100-W turn-key prototype was assembled for pre-commercialization testing in materials processing applications (Figure 4.6).

Whereas a TDCF laser suffers from contrast degradation due to mode coupling and other associated problems (Section 2.3), a in narrow-to-wide propagation TW TDCF amplifier such drawbacks can be avoided. Therefore, several TDCF MOPA systems were constructed throughout the work, and a high-gain CW amplifier was demonstrated in [P7] (Figures 4.4b and 4.7). High-power LMA amplifiers are often based on cascaded design (e.g. [167, 168]), with successively increasing mode areas of the active fibers. Typically, this approach requires careful free-space alignment into each (few-moded) fiber, or multiple fusion splices with mode conversion, potentially inducing mode coupling or compromising the practicality of the system. Conversely, a TDCF gain medium can be used to replace two or more stages to form a compact, monolithic scheme with a single pump launch point, enabling the use of simple diode-bar pump units. Furthermore, in applications requiring narrow linewidth, a TDCF device inherently benefits from both the varying core diameter and temperature gradient induced by end-pumping, both of which have been found to significantly mitigate SBS [47, 141, 146]. Narrowband and single-frequency fiber sources, preferred for applications such as beam combining, range finding and LIDAR, and nonlinear frequency conversion, typically comprise multiple amplifier stages with moderate gain of 18 dB – 22 dB [147, 167, 169–171] in the final power amplifier stage. The single-stage high-power TDCF amplifier demonstrated in [P7] featured a gain of more than 25 dB for narrow line signal amplification, and nearly 40 dB gain for broadband ASE seed amplification.

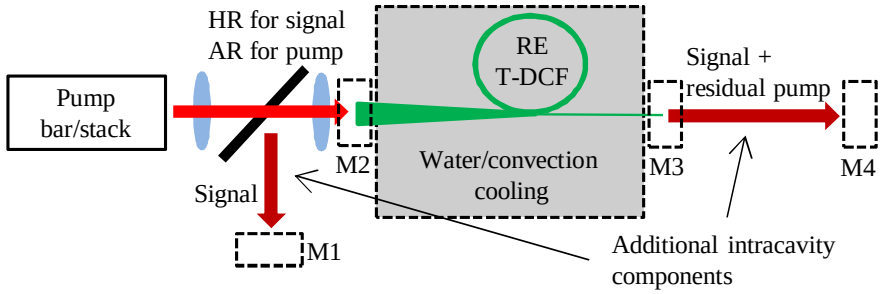

M1, M4: Free-space HR mirror / beam diagnostics
M2: 4 % Fresnel reflection / angle cleave / end cap / thin-film mirror
M3: 4 % Fresnel reflection / angle cleave / FBG

(a)

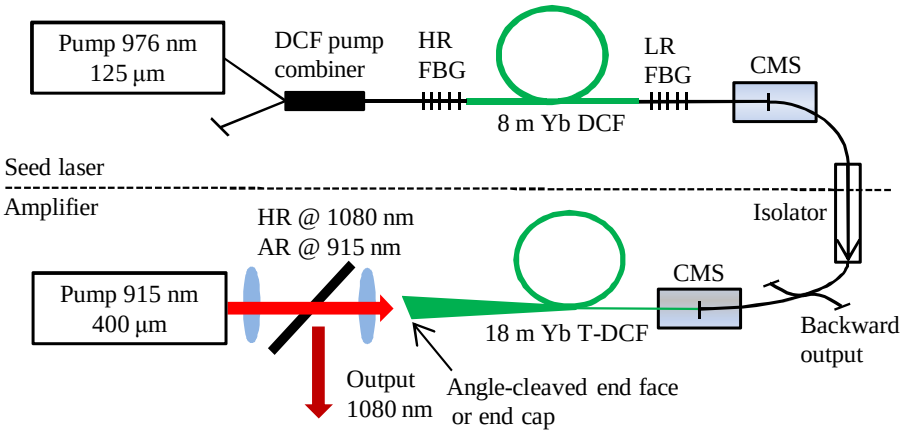

(b)

Figure 4.4: Schematics of optical setups used in this work. (a) A generic free-space-pumped setup, utilized in this work to construct different types of TDCF lasers or superfluorescent sources. A monolithic scheme can be realized with fiberized versions of the components, and by replacing the pump coupling with a pump/signal combiner at the wide end of the taper as described in Section 4.1.2. AR — anti-reflection. (b) A typical MOPA setup, as utilized e.g. in [P7]. The choice of seed source depends on desired characteristics, microchip lasers, (modulated) diodes, and distributed feedback (DFB) lasers are fairly common. In high-power, narrowband, and pulsed systems one or several preamplifier stages are often used between the seed source and the final power amplifier, and cascaded schemes typically require isolators and ASE filters between stages. A monolithic MOPA can be realized with in-line components much like its laser counterpart. CMS — cladding mode stripper, LR — low-reflection.

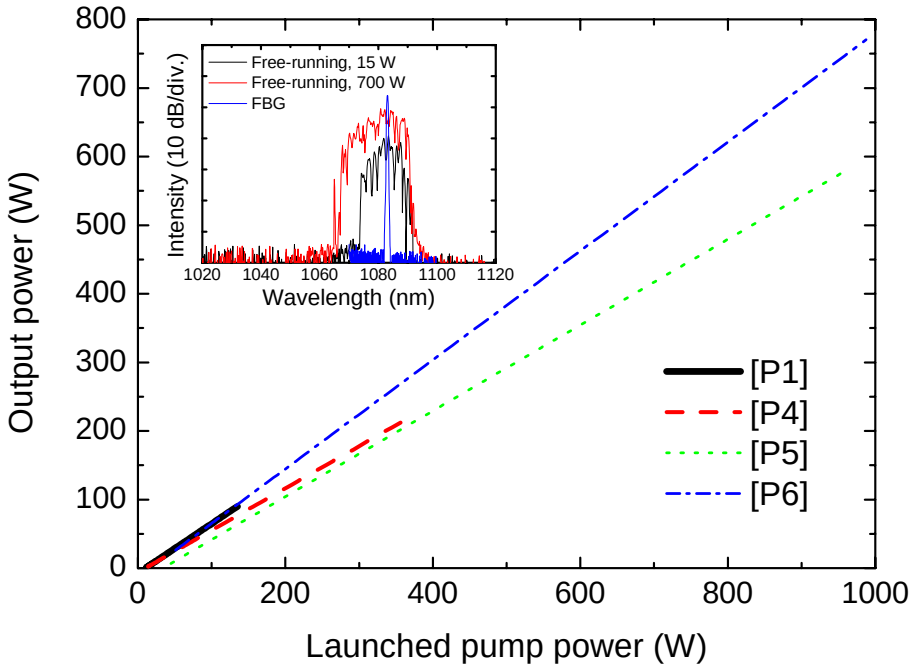

Figure 4.5: Output power versus launched pump power for several near-diffraction-limited CW fiber lasers demonstrated in this work. The inset shows typical output spectra in free-running and FBG cavities.

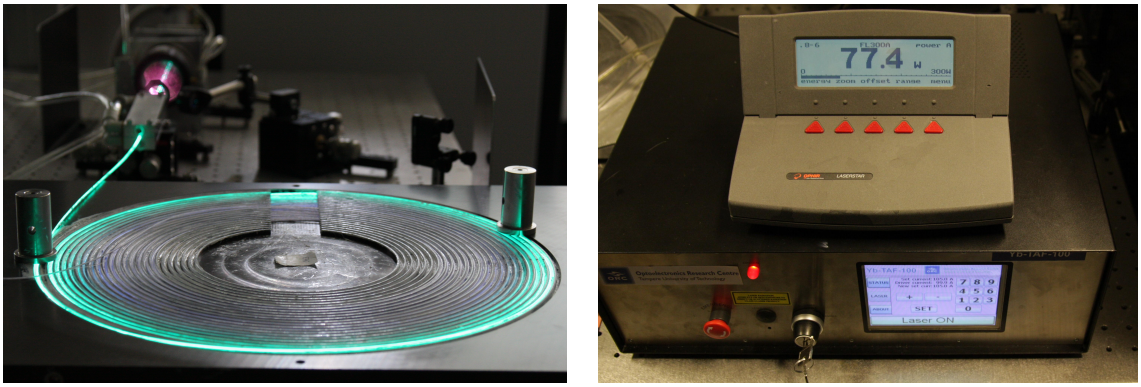

(a) (b)

Figure 4.6: (a) A 750-W TDCF laser operating in the laboratory. Most of the fiber rests on grooves etched on a water-cooled aluminum plate, and the free-space pump launch unit and cooling element for the pump launch end of the fiber can be seen in the background. (b) A packaged mid-power laser prototype featuring a touch-screen user interface.

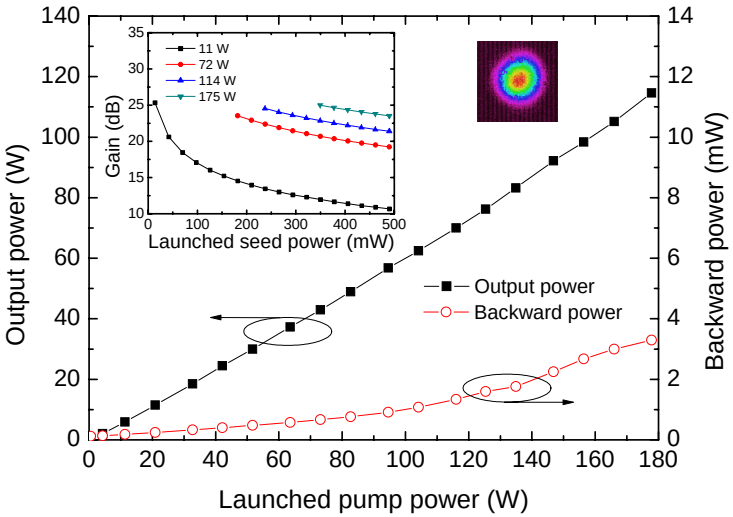

(a)

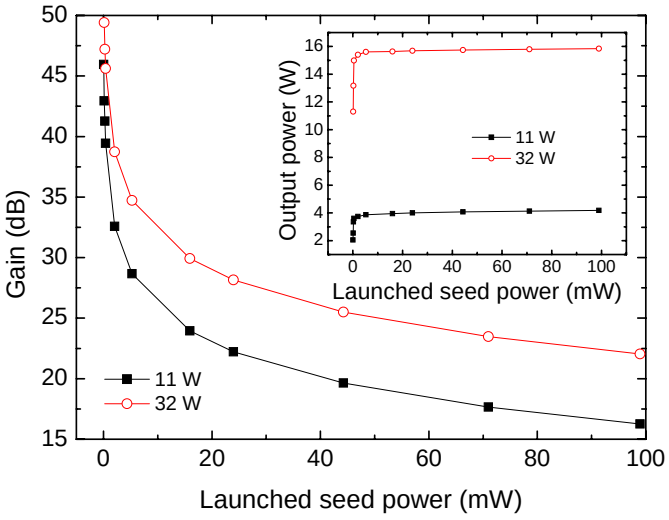

(b)

Figure 4.7: (a) Output power and backward-propagating power of the narrowband TDCF amplifier demonstrated in [P7], with the insets showing the gain as a function of launched seed power for several launched pump powers, and the near field output beam profile. The output power was limited by available pump power, whereas the maximum gain was limited to 24 dB – 26 dB by the onset of self-pulsing due to the interplay of ASE, distributed Rayleigh backscattering, and SBS. (b) The same amplifier seeded by broadband ASE was limited to lower output power by spurious lasing; however, nearly 40 dB gain could be achieved without output power degradation due to the absence of temporal instabilities triggered by SBS.

Chapter 5

Pulsed Fiber Lasers and Amplifiers

Several inherent features of fiber devices would make them a desirable choice for various purposes requiring short optical pulses, particularly in the important application ranges of remote sensing and micromachining. Traditionally, such applications have been dominated by bulk diode-pumped solid state lasers (DPSSL), although they suffer from thermally induced aberrations with increasing average powers. Conversely, in fiber devices the well-distributed thermal load and robust waveguiding substantially mitigate such problems. However, the high in-fiber intensities and long interaction lengths can result in various nonlinear effects, limiting the use of pulsed fiber devices to telecommunications and certain niche applications with modest pulse energies and peak powers. Using methods developed primarily for CW power scaling, state-of-the art pulsed fiber devices can nowadays produce ns-pulse energies in the 10-mJ range [172], and kW-class average powers of ultrafast pulse trains [173] with near-diffraction-limited beam quality. In this chapter, common methods of pulse generation are introduced. Power scaling of pulsed fiber devices, nonlinear effects in fibers, and their operational impact are discussed addressing primarily TDCF devices. Finally, several pulsed fiber device applications will be covered, particularly the generation of high-energy supercontinuum demonstrated within this work.

5.1 Pulse Generation Methods

Different types of laser sources can be utilized to produce very short pulse durations and high spatial coherence that enable very high focused intensities. Compared to CW

lasers, pulsed laser sources offer additional degrees of freedom for applications, namely pulse duration, pulse energy, peak power, and repetition rate (duty cycle). Several laser pulse generation methods exists; however, the most utilized methods are mode locking, gain switching, and Q-switching.

Mode locking is the dominant technique for ultrashort pulse generation with typical repetition rates of tens of MHz to 100 GHz, determined by the round-trip time of the resonator. Mode locking refers to the oscillation of axial resonator modes with a fixed phase relationship. It is convenient to consider the technique in the time domain with a single pulse circulating in the cavity and amplifying during each round trip in the gain medium. The pulse duration is typically between tens of fs to tens of ps, determined by various effects during propagation through the resonator. Due to relatively high repetition rate, the pulse energy from a mode-locked laser is low, typically from picojoules to hundreds of nanojoules [174]. Mode-locked operation requires fast intracavity loss modulation opening the low-loss time window resulting in pulse shaping, and leading to a steady state with the shortening effect balanced by pulse-broadening effects such as chromatic dispersion. The modulation needs to be synchronized with the resonator round-trip time, and can be realized actively e.g. by an electro-optic modulator (EOM) or passively by a saturable absorber. Mode-locked RE-doped fiber lasers are typically realized with passive modulators, resulting in compact and robust setups that enable sub-ps pulse durations due to the large gain bandwidth. However, the long interaction length and small mode area lead to high nonlinearity and dispersion that need to be taken into account. In this work, a mW-level ultrafast mode-locked fiber laser was utilized as a seed source for proof-of-concept demonstration of amplification in a TDCF to 10 W average output power with high efficiency and free from SBS [P1].

Gain switching refers to pulse generation by modulating the pump power of the laser. Although different types of lasers can be gain-switched, the method is most commonly applied to semiconductor lasers to produce nanosecond or even shorter pulses with facile electronic control of pulse duration, pulse shape, and repetition rate. Albeit the directly achievable pulse energy is low, the simplicity of pulse generation and good control of pulse parameters make gain switching an attractive technique e.g. for seeding a fiber amplifier with a modulated diode. Fiber gain media are too slow for practical gain-switching, thus Q-switching is typically used for direct high-energy pulse generation.

Q-switching is based on modulation of the cavity Q-factor by varying the resonator loss. Initially, the high-loss modulator state prevents lasing and allows high energy stor-

age in the cavity. Then the loss is abruptly reduced, resulting in substantial net gain and exponential increase in intracavity power until the gain is saturated and the power begins to decay. Most of the energy stored in the gain medium can be extracted by the short pulse; therefore, high active volume and long upper state lifetime are desirable to achieve energetic pulses. Q-switching is a relatively simple method for direct generation of intense ns-pulses, and although ultrashort pulses can not be generated, the high achievable energies make Q-switching the method of choice for many applications. Q-switching can be active or passive, using e.g. an acousto-optic modulator (AOM), or a passive saturable absorber, respectively. Due to the omission of the active modulator and control electronics, passive Q-switching is significantly simpler to implement, although it provides less pulse control and typically lower pulse energy. Pulse energies of several joules are possible with large-footprint systems, whereas pulses generated directly from fiber lasers are typically limited to the mJ-level. In-line modulators required for Q-switched all-fiber setups are usually limited to SM fiber devices, which lead to nonlinearity and damage issues for high pulse energies, and bulk modulators are required to achieve the highest energies. Figure 5.1 shows a typical setup for high-energy actively Q-switched LMA fiber laser utilized in [P8] with a TDCF gain fiber.

High-energy pulsed sources are preferably realized using MOPA configurations for better pulse parameter control. Particularly in the ultrafast regime with relatively high repetition rate, the directly-generated pulse energy is low, and further amplification is usually required. Ultrashort pulse amplification schemes include single- or multi-pass bulk solid-state amplifiers, regenerative amplifiers with an auxiliary resonator and an external switch, and optical parametric amplifiers. Fiber amplifiers, in particular, offer a large gain bandwidth and a high gain, and are suitable for scaling the signal to very high average powers. However, the achievable peak power is limited by nonlinearities, thus fiber amplifiers are typically used for relatively high repetition rates and mid-range pulse energies.

5.2 Pulse Energy and Peak Power Scaling

Generally, both nanosecond-range and ultrafast fiber systems are limited to somewhat lower average powers than corresponding CW devices due to high peak power and energy of the short pulses. Factors limiting the output power include COD in the bulk or at surfaces, nonlinear optical effects, and extraction of energy from the gain fiber. Al-

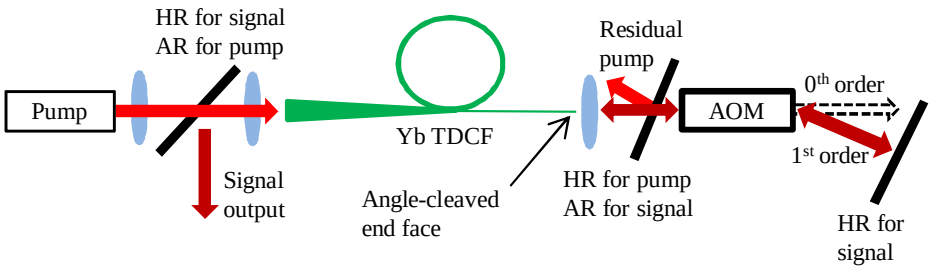

Figure 5.1: A high-energy Q-switched TDCF laser setup with the loss modulation provided by a free-space AOM [P8].

though thermal effects are often a lesser concern, for pulsed devices with high average power all the issues discussed in Section 4.2.1 need to be taken into account as well.

5.2.1 Fiber Damage

Material damage ultimately limits the achievable peak power in fiber devices, and the underlying physical processes responsible for the dielectric breakdown include various mechanisms. The critical peak intensity in Yb-doped silica fibers has been estimated to be approximately 450 GW/cm^2 (4.5 kW/μm^2) independent of pulse duration above 50 ps, i.e. the damage fluence increases linearly with the pulse duration τ_p [175, 176]. Several preceding experimental studies, however, reported a $\tau_p^{0.5}$ fluence dependence with significantly lower damage thresholds [177, 178]. For pulses shorter than a few tens of picoseconds the damage fluence in silica increases with the pulse duration as well, albeit with a weaker dependence ($\tau_p^{0.33}$ in [179]).

Enlargement of the mode area alleviates damage issues by reducing the in-fiber intensity. However, the critical intensity only scales with the mode area up to certain critical power set by self-focusing due to the intensity-dependent refractive index (Kerr effect, Section 5.2.2). The critical power for the fundamental mode LP_{01} in silica fibers can be estimated to be ~ 5 MW for 1 μm wavelength independent of mode area [180, 181], thus exhibiting a fundamental limit for peak power scaling in silica fibers. The damage threshold for the fiber facets can be significantly lower than the bulk threshold. Although the difference should theoretically be small, up to an order of magnitude lower thresh-

olds (40 GW/cm^2) are often observed in practice due to non-ideal cleaving or polishing processes [42]. However, the issue of surface damage can usually be avoided by end-capping, i.e. splicing a short segment of non-guiding silica at the output end face to substantially expand the beam prior to the glass-air interface, without degradation of the beam quality.

5.2.2 Fiber Nonlinearities

The combination of very high intensity and long interaction length in fiber devices makes them highly susceptible to various nonlinear effects. Whereas many of the effects can be exploited for applications, in terms of peak power scaling they are considered detrimental, and in practical devices encountered in the form of SBS, SRS, SPM, XPM, FWM, and self-focusing.

The effects of SBS and SRS were already considered in Section 4.2.2; however, in the pulsed regime some additional details should be noted. SBS is typically not an issue for pulses shorter than a few ns due to the large bandwidth of a short pulse, and reduced spatial overlap over the fiber length. For instance, the spectral width of a transform-limited 3-ns pulse already exceeds the typical Brillouin gain bandwidth, and the (spatial) length of such a pulse in fiber is less than 1 m, resulting in a relatively short overlap with the counterpropagating Stokes pulse. Several factors may affect the susceptibility to SBS, e.g. effective seeding of SBS by signal components at the Stokes frequency, cumulative SBS build-up by several pulses of a high-repetition-rate train with period less than the phonon lifetime, and the contribution of parasitic optical feedback on SBS. In contrast, the gain bandwidth of SRS is large enough to generate Stokes components even for very short pulses, and the generated Stokes pulse co-propagates with the input beam. However, due to the large group velocity dispersion, ultrashort pulses accumulate significant delay with respect to the generated Stokes pulse (temporal walk-off), resulting in substantial mitigation of the effect for $\tau_p \lesssim$ 10-ps pulses.

In contrast to CW devices, in addition to stimulated inelastic scattering, several other nonlinear effects can be significant in short-pulse operation. The intensity-dependent refractive index, i.e. the Kerr effect, causes an intrapulse phase shift referred to as SPM. The phase shift in turn leads to chirping of the pulse, detrimental for ultrashort pulse quality, and broadening of the output spectrum, which may hinder linewidth-sensitive applications. If the signal exhibits multiple frequencies, their nonlinear phase shifts can

become coupled (XPM), with potentially further increased spectral broadening. Whereas SPM can be regarded as a temporal manifestation of the Kerr effect, its spatial counterpart is self-focusing due to peaking of local intensity at the beam axis. As noted above, the critical power for self-focusing is independent of mode area, resulting in a fundamental peak power scaling limit. Finally, the effect of FWM leads to power transfer to spectral sidebands and can become important for applications demanding high spectral purity, especially if the sideband frequencies are effectively seeded by adjacent signal frequency components similarly to seeding of SBS mentioned above. [137]

5.2.3 Amplified Spontaneous Emission

The maximum extractable pulse energy is a key characteristic of a fiber device, and in Q-switched fiber lasers it scales linearly with effective mode area. Given the peak intensity below material damage threshold and a tolerable level of nonlinear distortions, the limit to energy extraction is ultimately amplified spontaneous emission. ASE is problematic especially in low-repetition-rate devices, as the long inter-pulse period allows for significant ASE accumulation. In addition, ASE co-propagating with the output signal reduces the signal-to-noise ratio. Furthermore, the presence of spurious reflections in an amplifier enhances all the adverse effects of ASE due to the emerging multi-pass behavior. Although high inversion (gain) between pulses is required for high energy extraction, it also favors ASE and can lead to spurious lasing e.g. by distributed Rayleigh scattering, even if isolators and other feedback suppression mechanisms are applied.

Energy scaling of Q-switched fiber lasers is of interest particularly because many industrial and LIDAR applications require energetic pulses with tens of ns duration at low duty cycles. Suitable high-energy fiber sources include rod-type PCFs and low-NA LMA DCFs; however, sources of this type are generally limited to relatively high duty cycles of 10^{-5} for few-ns pulses and 10^{-4} – 10^{-3} for > 100 ns pulses [25, 182, 183]. Typically, ASE is the main limitation in this type of fiber sources. Some techniques for alleviating the problem have been proposed, including doping the fiber with a saturable absorber, spectral filtering, and ring doping [43, 184, 185]. In a TDCF, a major fraction of wide-to-narrow propagating ASE is filtered out of the core due to vignetting. Furthermore, since the amount of spontaneous emission scales with the number of supported fiber modes, narrow-to-wide propagating ASE is weaker than in a cylindrical fiber with similar average core area, due to mode selection in the narrow part. In the Q-switched

TDCF laser reported in [P8], the M^2 of the wide end output ASE was measured to be 4.2, with an estimated number of modes $(M^2)^2 \sim 18$, whereas an estimation based on the V-parameter at the output would give $V^2/2 \sim 430$ modes, indicating substantial reduction in narrow-to-wide propagating ASE modes due to mode selection [20, 100]. With the Q-switched TDCF source, high-energy, sub-100-ns pulses were produced in a direct-generation setup [P8] that allowed achieving multi-mJ pulse energy [186] at very low duty cycles, up to single-shot regime (Figure 5.2).

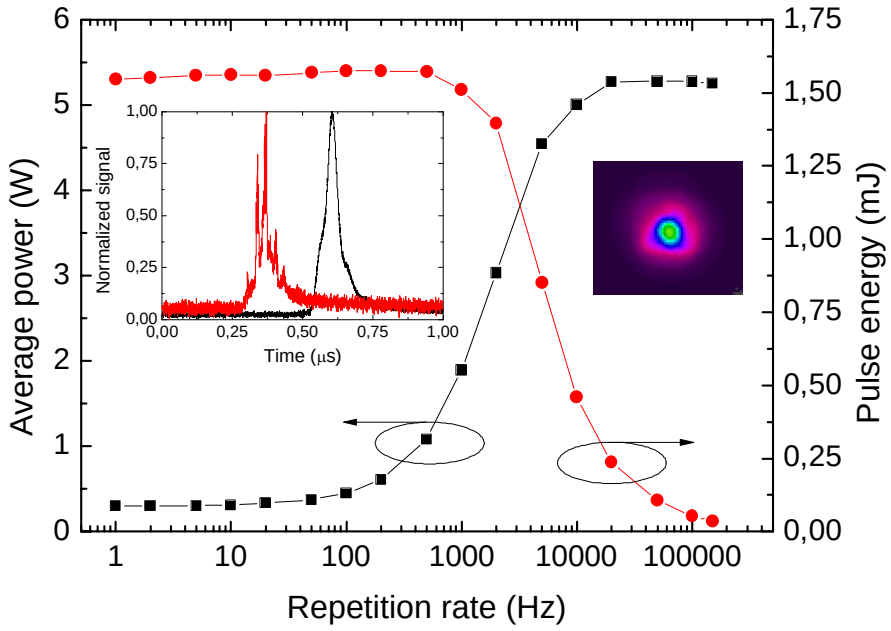

Figure 5.2: Average power and pulse energy versus repetition rate for a fixed pump power of the 1.6 mJ actively Q-switched TDCF laser in [P8]. The left inset shows the output pulse right before (black) and after (red) SBS-induced pulse breakdown, and the right inset shows the output beam profile at maximum pulse energy.

5.2.4 Master Oscillator — Power Amplifier

The characteristics of CW MOPAs noted in Section 4.2.4 are also applicable to pulsed amplification. In the pulsed regime, MOPA systems are widely utilized due to several important advantages. The potential advantages include improved spectral and temporal

pulse parameter control, utilization of multiple gain fiber types, and facile ASE mitigation via gain staging. For pulse durations of picoseconds and longer, a common alternative for direct pulse generation is a diode- or microchip-seeded MOPA with one or several fiber amplifier stages. Fiber-coupled SM diodes modulated by a pulsed current source provide excellent control over repetition rate, pulse duration, and pulse shape. On the other hand, they are susceptible to damage by parasitic back reflections, and the generated ns seed pulse energies are typically in the nJ-range, requiring a very high-gain amplifier (chain) to achieve practical level of pulse energy. Microchip sources are able to generate significantly higher energies of several μJ; however, they are less flexible in terms of pulse parameter control due to pulse generation by passive Q-switching. An amplifier scheme allows utilizing different types of gain fibers e.g. with successively increasing mode areas, which can be useful to minimize nonlinearities while maximizing the overall efficiency. A multi-stage amplifier also allows filtering of ASE between stages, either spectrally with bandpass filters, or temporally with pulse pickers.

Finally, due to very high peak intensities, ultrashort pulse amplification in fibers is usually realized by temporally stretching the pulses prior to coupling to the gain fiber, followed by subsequent compression at the output. The technique is referred to as chirped pulse amplification (CPA), and it is a dominant technique in moderate to high-energy systems. The ultrashort seed pulses are typically generated by a mode-locked oscillator and broadened temporally via dispersive stretcher up to $\sim$ 1 ns duration. The stretched pulse can then be amplified up to $\sim$ 5 MW peak power limited by self-focusing, and finally compressed back to the ultrafast regime resulting in an output peak power of the order of gigawatts [31]. While the resulting peak powers remain substantially lower than those achievable by bulk lasers, high-repetition-rate (hundreds of kHz) fiber CPA systems allow generating very high average powers of hundreds of watts [187, 188].

5.3 Applications

A wide variety of laser applications require fast or ultrafast pulsed sources, typically with high brightness and sometimes with high brilliance as well. Fiber devices excel in many such applications due to their inherent advantages outlined in previous chapters, combined with ruggedness that allows facile packaging for non-laboratory environments, and relatively low total cost of ownership due to long-term reliability and low maintenance.

Important applications for pulsed high-energy fiber devices include materials pro-

cessing (e.g. precision drilling and marking), remote sensing (e.g. ranging and terrain mapping), spectroscopy, and fundamental science. For instance, in high-precision micromachining, short or even ultrashort pulses are often essential to reduce collateral damage on the workpiece due to small heat affected zones. The wide range of remote sensing applications, in turn, requires pulsed sources for temporal resolution. Furthermore, for many applications short pulses with peak intensities (fluences) orders of magnitude higher than those possible with CW devices are needed. The extreme intensities are particularly useful for experimental nonlinear optics. In this work, a high-energy Q-switched TDCF laser was used as a pump source to initiate a cascade of nonlinear effects in a PCF to generate a supercontinuum, discussed in the next section.

5.3.1 Supercontinuum Generation

The process of SC generation refers to frequency conversion of laser emission by several nonlinear effects into light with very broad spectral bandwidth while retaining high spatial coherence. Broadband SC sources find applications e.g. in optical coherence tomography, fiber-optic communication systems, and fluorescence microscopy. Optical fibers are a favorable medium for the process due to long interaction length and high in-fiber intensity. High-nonlinearity PCFs, the workhorse of SC generation during the last decade [29, 32], have allowed broadband generation even with CW pumping [189, 190]; however, short pulses are more commonly used to enable efficient generation in a short length of fiber [191]. Widely used compact and ultrafast SC sources are typically high-repetition rate systems with relatively low pulse energy. However, many applications require spectral slicing of the continuum, reducing the output energy, and would benefit from more energetic sources.

In this work, a ns-range PCF SC source was constructed with a directly Q-switched TDCF laser as a pump source [P9]. In the ns pump regime, where the SC mechanics significantly differ from the more common ultrashort pulse pumping [192–194], previously achieved pulse energies are of the order of 10 μJ [195–198]. The utilized TDCF laser source allowed the generation of 250-μJ, 50-ns SC pulses spanning over 1000 nm spectral bandwidth from 600 nm to beyond 1600 nm within 5 dB intensity deviation (Figure 5.3). The maximum pulse energy was eventually limited by COD at the input end face of the PCF, and to the best of the authors knowledge, represents the highest energy generated from a broadband supercontinuum source at the time of writing.

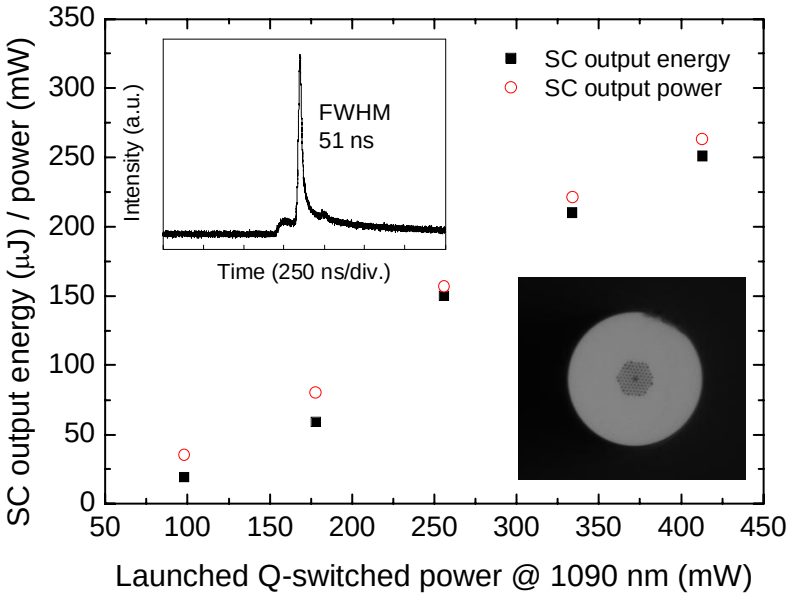

(a)

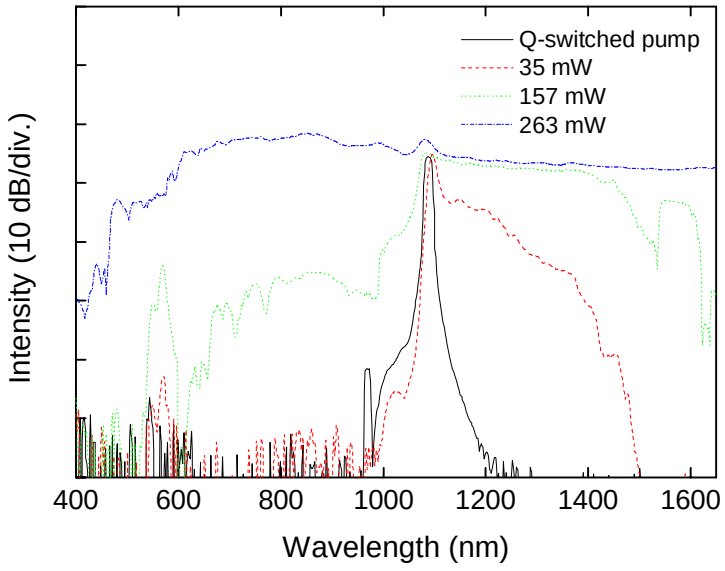

(b)

Figure 5.3: (a) The average output power and pulse energy of the supercontinuum demonstrated in [P9]. The insets show the 50-ns pump pulse shape (left) and the endface of the PCF used to generate the continuum (right). (b) The output spectra of the supercontinuum at different average output power levels.

Chapter 6

Conclusions

In this thesis, double-clad active fibers adiabatically tapered along the entire fiber length were proposed and studied as a gain medium for high-power fiber lasers and amplifiers. Various aspects related to the axially non-uniform fiber geometry were considered theoretically and experimentally in a number of laser and amplifier configurations, including potential applications and prototyping. During the course of this study, a HPFL infrastructure was established at ORC, and various related technical problems were tackled.

Different types of CW TDCF lasers were studied and compared with analogues based on cylindrical fibers. Properly engineered end-pumped TDCF lasers were found to be advantageous in terms of brightness enhancement, pump conversion efficiency, and tolerance of nonlinearities, due to the TDCF geometry enabling low-brightness pumping, higher absorption, and axially varying core diameter. The limitation imposed on pump launch aperture (fill factor) due to vignetting of the pump light was thoroughly studied. Practical TDCF devices exhibiting several times higher brightness enhancement factors compared to cylindrical fibers were demonstrated.

Fundamental mode evolution, mode coupling and associated beam contrast deterioration in a TDCF laser were studied in detail. Whereas intermodal coupling due to adiabatic tapering in long fibers was found negligible, mode coupling could be enhanced due to local or distributed bending of the taper, or by fabrication-related defects or features. Fundamental mode propagation through a passive taper with more than 100 μm output core diameter without mode coupling was demonstrated, although the fundamental mode shape revealed some annular distortion due to built-in stress. TDCF lasers were found to exhibit beam contrast deterioration due to mode coupling, particularly in co-propagating

configurations. Consequently, counter-propagating traveling-wave TDCF-based amplifiers were judged to be most appropriate for high-power applications.

The initial proof-of-concept CW TDCF laser demonstration was gradually improved, and the output power was scaled to near-kW regime by fiber design optimization, pump scheme engineering, and developments in thermal management. The optimized fiber parameters included active ion doping level, core-to-cladding area ratio, transversal cladding shape, tapering ratio, and axial profile shape, of which the two latter parameters are TDCF-specific. In addition, a high-gain, high-brightness CW TDCF amplifier with excellent power scaling prospects was demonstrated. Furthermore, a high-energy actively Q-switched TDCF laser with good-quality beam was shown to offer an interesting alternative for widely used complex multi-stage ns-MOPA systems. The potential of this type of devices was demonstrated by generation of the highest pulse energy supercontinuum reported to date.

To conclude, the TDCF platform was found to offer substantial advantages compared to regular cylindrical fibers. The shortcomings associated with tapered geometry were shown to be adequately manageable by careful fiber and device design. The tapered fiber technology was validated as a practical means for advanced mode control in high-power fiber systems. The output brightness of a TDCF device can be to a certain extent compromised by provoked mode coupling, or by refractive index profile irregularities, and eliminating such shortages should be the focus of future research efforts. Furthermore, experimental confirmation of supposed mitigation of thermal mode instability by tapered active fiber provides an intriguing direction of study. Overall, counter-propagating CW and pulsed TW TDCF amplifier devices appear most interesting for practical applications demanding bright, compact, and cost-efficient devices.

References

[1] T. H. Maiman, "Stimulated optical radiation in ruby," *Nature*, vol. 187, no. 4736, pp. 493–494, 1960.

[2] M. Peng, "Research on CO_2 shipborne laser anti-missile weapons," *Ship Electronic Engineering*, vol. 11, 2009.

[3] F. Dubin, C. Russo, H. Barros, A. Stute, C. Becher, P. Schmidt, and R. Blatt, "Quantum to classical transition in a single-ion laser," *Nature Physics*, vol. 6, no. 5, pp. 350–353, 2010.

[4] National Ignition Facility. [Online]. Available: https://lasers.llnl.gov/about/nif/about.php, accessed on 2013/01/06

[5] E. Snitzer, "Optical Maser Action of Nd^{+3} in a Barium Crown Glass," *Phys. Rev. Lett.*, vol. 7, pp. 444–446, 1961.

[6] E. Desurvire, J. Simpson, and P. Becker, "High-gain erbium-doped traveling-wave fiber amplifier," *Optics Letters*, vol. 12, no. 11, pp. 888–890, 1987.

[7] E. Snitzer, H. Po, F. Hakimi, R. Tumminelli, and B. McCollum, "Double clad, offset core Nd fiber laser," in *Optical Fiber Sensors*. Optical Society of America, 1988.

[8] J. D. Minelly, E. R. Taylor, K. P. Iedrzueswski, J. Wang, and D. N. Payne, "Laser-diode pumped neodymium-doped fibre laser with output power > 1 W," in *Conf. Lasers and Electro-optics,CWE-6*, 1992.

[9] H. Po, J. Cao, B. Laliberte, R. Minns, R. Robinson, B. Rockney, R. Tricca, and Y. Zhang, "High power neodymium-doped single transverse mode fibre laser," *Electronics Letters*, vol. 29, no. 17, pp. 1500–1501, 1993.

[10] H. Zellmer, A. Tünnermann, H. Welling, and V. Reichel, "Double-clad fiber laser with 30 W output power," in *Optical Amplifiers and Their Applications*. Optical Society of America, 1997.

[11] V. Dominic, S. MacCormack, R. Waarts, S. Sanders, S. Bicknese, R. Dohle, E. Wolak, P. Yeh, and E. Zucker, "110 W fibre laser," *Electronics Letters*, vol. 35, no. 14, pp. 1158–1160, 1999.

[12] N. Platonov, D. Gapontsev, V. Gapontsev, and V. Shumilin, "135W CW fiber laser with perfect single mode output," in *Lasers and Electro-Optics, 2002. CLEO'02. Technical Digest. Summaries of Papers Presented at the*. IEEE, 2002, pp. CPDC3–1.

[13] J. Limpert, A. Liem, H. Zellmer, and A. Tunnermann, "500 W continuous-wave fibre laser with excellent beam quality," *Electronics Letters*, vol. 39, no. 8, pp. 645–647, 2003.

[14] Y. Jeong, J. Sahu, D. Payne, and J. Nilsson, "Ytterbium-doped large-core fiber laser with 1.36 kW continuous-wave output power," *Optics Express*, vol. 12, no. 25, pp. 6088–6092, 2004.

[15] V. Gapontsev, D. Gapontsev, N. Platonov, O. Shkurikhin, V. Fomin, A. Mashkin, M. Abramov, and S. Ferin, "2 kW CW ytterbium fiber laser with record diffraction-limited brightness," in *Lasers and Electro-Optics Europe, 2005. CLEO/Europe. 2005 Conference on*. IEEE, 2005, p. 508.

[16] V. Fomin, A. Mashkin, M. Abramov, A. Ferin, and V. Gapontsev, "3 kW Yb fibre lasers with a single-mode output," in *International Symposium on High-Power Fiber Lasers and their Applications (St. Petersburg, 2006)*, 2006.

[17] E. Stiles, "New developments in IPG fiber laser technology," in *5th International Workshop on Fiber Lasers, Dresden, Germany*, 2009.

[18] IPG Photonics Co. [Online]. Available: www.ipgphotonics.com, accessed on 2013/01/06

[19] N. Broderick, H. Offerhaus, D. Richardson, R. Sammut, J. Caplen, and L. Dong, "Large mode area fibers for high power applications," *Optical Fiber Technology*, vol. 5, no. 2, pp. 185–196, 1999.

[20] C. Ranaud, H. Offerhaus, J. Alvarez-Chavez, C. Nilsson, W. Clarkson, P. Turner, D. Richardson, and A. Grudinin, "Characteristics of Q-switched cladding-pumped ytterbium-doped fiber lasers with different high-energy fiber designs," *Quantum Electronics, IEEE Journal of*, vol. 37, no. 2, pp. 199–206, 2001.

[21] Optics.org: Fibre lasers look to large mode areas. [Online]. Available: http://optics.org/article/38646, accessed on 2013/01/06

[22] P. Facq, F. de Fornel, and F. Jean, "Tunable single-mode excitation in multimode fibres," *Electronics Letters*, vol. 20, no. 15, pp. 613–614, 1984.

[23] C. Stacey, R. Jenkins, J. Banerji, and A. Davies, "Demonstration of fundamental mode only propagation in highly multimode fibre for high power EDFAs," *Optics Communications*, vol. 269, no. 2, pp. 310–314, 2007.

[24] S. Ramachandran, J. Nicholson, S. Ghalmi, M. Yan, P. Wisk, E. Monberg, and F. Dimarcello, "Light propagation with ultralarge modal areas in optical fibers," *Optics letters*, vol. 31, no. 12, pp. 1797–1799, 2006.

[25] J. Alvarez-Chavez, H. Offerhaus, J. Nilsson, P. Turner, W. Clarkson, and D. Richardson, "High-energy, high-power ytterbium-doped Q-switched fiber laser," *Optics Letters*, vol. 25, no. 1, pp. 37–39, 2000.

[26] J. Dawson, R. Beach, I. Jovanovic, B. Wattellier, Z. Liao, S. Payne, and C. Barty, "Large flattened-mode optical fiber for reduction of nonlinear effects in optical fiber lasers," in *Proceedings of SPIE*, vol. 5335, 2004, p. 132.

[27] J. Koplow, D. Kliner, and L. Goldberg, "Single-mode operation of a coiled multimode fiber amplifier," *Optics Letters*, vol. 25, no. 7, pp. 442–444, 2000.

[28] J. Knight, T. Birks, P. Russell, and D. Atkin, "All-silica single-mode optical fiber with photonic crystal cladding," *Optics letters*, vol. 21, no. 19, pp. 1547–1549, 1996.

[29] P. Russell, "Photonic crystal fibers," *Science*, vol. 299, no. 5605, p. 358, 2003.

[30] J. Limpert, O. Schmidt, J. Rothhardt, F. Röser, T. Schreiber, A. Tünnermann, S. Ermeneux, P. Yvernault, and F. Salin, "Extended single-mode photonic crystal fiber lasers," *Optics Express*, vol. 14, no. 7, pp. 2715–2720, 2006.

[31] T. Eidam, J. Rothhardt, F. Stutzki, F. Jansen, S. Hädrich, H. Carstens, C. Jauregui, J. Limpert, and A. Tünnermann, "Fiber chirped-pulse amplification system emitting 3.8 GW peak power," *Optics Express*, vol. 19, no. 1, pp. 255–260, 2011.

[32] J. Dudley and J. Taylor, "Ten years of nonlinear optics in photonic crystal fibre," *Nature Photonics*, vol. 3, no. 2, pp. 85–90, 2009.

[33] L. Dong, X. Peng, and J. Li, "Leakage channel optical fibers with large effective area," *JOSAB*, vol. 24, no. 8, pp. 1689–1697, 2007.

[34] L. Dong, T. Wu, H. McKay, L. Fu, J. Li, and H. Winful, "All-glass large-core leakage channel fibers," *Selected Topics in Quantum Electronics, IEEE Journal of*, vol. 15, no. 1, pp. 47–53, 2009.

[35] S. Huang, C. Zhu, C. Liu, X. Ma, C. Swan, and A. Galvanauskas, "Power scaling of CCC fiber based lasers," in *Conference on Lasers and Electro-Optics/International Quantum Electronics Conference*. Optical Society of America, 2009.

[36] M. Vogel, M. Abdou-Ahmed, A. Voss, and T. Graf, "Very-large-mode-area, single-mode multicore fiber," *Optics letters*, vol. 34, no. 18, pp. 2876–2878, 2009.

[37] J. Fini, "Large-mode-area multicore fibers in the single-moded regime," *Optics Express*, vol. 19, no. 5, pp. 4042–4046, 2011.

[38] A. Siegman, "Propagating modes in gain-guided optical fibers," *JOSAA*, vol. 20, no. 8, pp. 1617–1628, 2003.

[39] S. Suzuki, A. Schülzgen, and N. Peyghambarian, "Single-mode fiber laser based on core-cladding mode conversion," *Optics letters*, vol. 33, no. 4, pp. 351–353, 2008.

[40] "Fiber and industrial laser market review and forecast," Strategies Unlimited, Mountain View, CA , USA, 2009.

[41] Optics.org: Cautious Rofin details fiber laser strategy. [Online]. Available: http://optics.org/news/2/11/6, accessed on 2013/01/06

[42] T. S. McComb, M. C. Richardson, and M. Bass, *Handbook of optics, vol. V, ch. 25*, 3rd ed. New York, NY: McGraw-Hill, 2009.

[43] M. Digonnet, *Rare-earth-doped fiber lasers and amplifiers*, 2nd ed. Marcel Dekker, 2001.

[44] Y. Jeong, S. Yoo, C. Coderaard, J. Nilsson, J. Sahu, D. Payne, R. Horley, P. Turner, L. Hickey, A. Harker, *et al.*, "Erbium: ytterbium codoped large-core fiber laser with 297-W continuous-wave output power," *Selected Topics in Quantum Electronics, IEEE Journal of*, vol. 13, no. 3, pp. 573–579, 2007.

[45] T. Ehrenreich, R. Leveille, I. Majid, K. Tankala, G. Rines, and P. Moulton, "1-kW, all-glass Tm: fiber laser," in *Proc. SPIE*, vol. 7580, 2010, pp. 7580–112.

[46] A. Hemming, S. Bennetts, N. Simakov, A. Davidson, J. Haub, and A. Carter, "High power operation of cladding pumped holmium-doped silica fibre lasers," *Opt. Express*, vol. 21, no. 4, pp. 4560–4566, Feb 2013. [Online]. Available: http://www.opticsexpress.org/abstract.cfm?URI=oe-21-4-4560

[47] K. Shiraki, M. Ohashi, and M. Tateda, "Suppression of stimulated Brillouin scattering in a fibre by changing the core radius," *Electronics letters*, vol. 31, no. 8, pp. 668–669, 1995.

[48] Optics.org: Tapered fibre improves laser performance. [Online]. Available: http://optics.org/article/32979, accessed on 2013/01/06

[49] V. Filippov, Y. Chamorovskiy, O. Okhotnikov, and M. Pessa, "Active optical fiber and method for fabricating an active optical fiber," 2008, US patent app. 12/681,480.

[50] I. Kelson and A. Hardy, "Strongly pumped fiber lasers," *Quantum Electronics, IEEE Journal of*, vol. 34, no. 9, pp. 1570–1577, 1998.

[51] V. Ustimchik, S. Nikitov, and Y. Chamorovskii, "Simulation of radiation generation in an active double-clad optical tapered fiber," *Journal of Communications Technology and Electronics*, vol. 56, no. 10, pp. 1249–1255, 2011.

[52] V. Bagan, S. Nikitov, Y. Chamorovskii, and A. Shatrov, "Studying the properties of double-clad active cone optic fibers," *Journal of Communications Technology and Electronics*, vol. 55, no. 10, pp. 1154–1161, 2010.

[53] S. Chernikov, Y. Zhu, J. Taylor, and V. Gapontsev, "Supercontinuum self-Q-switched ytterbium fiber laser," *Optics Letters*, vol. 22, no. 5, pp. 298–300, 1997.

[54] A. Snyder, "Coupling of modes on a tapered dielectric cylinder," *Microwave Theory and Techniques, IEEE Transactions on*, vol. 18, no. 7, pp. 383–392, 1970.

[55] D. Marcuse, "Mode conversion in optical fibers with monotonically increasing core radius," *Lightwave Technology, Journal of*, vol. 5, no. 1, pp. 125–133, 1987.

[56] T. Ozeki and B. Kawasaki, "Mode behaviour in a tapered multimode fibre," *Electronics Letters*, vol. 12, no. 16, pp. 407–408, 1976.

[57] Y. Li and J. Lit, "Mode changes in step-index multimode fiber tapers," *JOSAA*, vol. 3, no. 1, pp. 161–164, 1986.

[58] A. Fielding, K. Edinger, and C. Davis, "Experimental observation of mode evolution in single-mode tapered optical fibers," *Journal of lightwave technology*, vol. 17, no. 9, p. 1649, 1999.

[59] P. Shankar, L. Bobb, and H. Krumboltz, "Coupling of modes in bent biconically tapered single-mode fibers," *Lightwave Technology, Journal of*, vol. 9, no. 7, pp. 832–837, 1991.

[60] L. Bobb, P. Shankar, and H. Krumboltz, "Bending effects in biconically tapered single-mode fibers," *Lightwave Technology, Journal of*, vol. 8, no. 7, pp. 1084–1090, 1990.

[61] A. W. Snyder and J. D. Love, *Optical Waveguide Theory*. London: Kluwer Academic Publishers, 2000.

[62] D. Marcuse, *Theory of Dielectric Optical Waveguides*. New York: Academic, 1974.

[63] L. Bobb, H. Krumboltz, and P. Shankar, "Pressure sensor that uses bent biconically tapered single-mode fibers," *Optics letters*, vol. 16, no. 2, pp. 112–114, 1991.

[64] R. Olshansky, "Mode coupling effects in graded-index optical fibers," *Applied Optics*, vol. 14, no. 4, pp. 935–945, 1975.

[65] A. Iho, A. Tervonen, K. Ylä-Jarkko, S. Tammela, and S. Honkanen, "Characterization of modal coupling of Bragg gratings in large-mode-area fibers," *Journal of Lightwave Technology*, vol. 29, no. 13, pp. 2031–2038, 2011.

[66] M. Young, *Optics and lasers: including fibers and optical waveguides*. Springer Verlag, 2000.

[67] D. Young and C. Roychoudhuri, "Results and comparison of a cladding pumped fiber simulation using a decagon-shaped fiber," *Optics Express*, vol. 11, no. 7, pp. 830–837, 2003.

[68] J. Koponen, M. Söderlund, H. Hoffman, and S. Tammela, "Measuring photodarkening from single-mode ytterbium doped silica fibers," *Opt. Express*, vol. 14, no. 24, pp. 11 539–11 544, 2006.

[69] B. Morasse, S. Chatigny, É. Gagnon, C. Hovington, J. Martin, and J. de Sandro, "Low photodarkening single cladding ytterbium fibre amplifier," in *Proceedings of SPIE*, vol. 6453, 2007, p. 64530H.

[70] S. Yoo, C. Basu, A. Boyland, C. Sones, J. Nilsson, J. Sahu, and D. Payne, "Photodarkening in Yb-doped aluminosilicate fibers induced by 488 nm irradiation," *Optics letters*, vol. 32, no. 12, pp. 1626–1628, 2007.

[71] J. Kirchhof, S. Unger, V. Reichel, and A. Schwuchow, "Background loss and devitrification in Nd-doped fiber laser glass," in *Optical Fiber Communications, 1996. OFC'96*. IEEE, 1996, pp. 60–61.

[72] J. Knight, "Photonic crystal fibers and fiber lasers," *JOSAB*, vol. 24, no. 8, pp. 1661–1668, 2007.

[73] D. Kouznetsov, J. Moloney, and E. Wright, "Efficiency of pump absorption in double-clad fiber amplifiers. I. Fiber with circular symmetry," *JOSAB*, vol. 18, no. 6, pp. 743–749, 2001.

[74] D. Kouznetsov and J. Moloney, "Efficiency of pump absorption in double-clad fiber amplifiers. II. Broken circular symmetry," *JOSAB*, vol. 19, no. 6, pp. 1259–1263, 2002.

[75] ——, "Efficiency of pump absorption in double-clad fiber amplifiers. III. Calculation of modes," *JOSAB*, vol. 19, no. 6, pp. 1304–1309, 2002.

[76] A. Liu and K. Ueda, "The absorption characteristics of circular, offset, and rectangular double-clad fibers," *Optics Communications*, vol. 132, no. 5-6, pp. 511–518, 1996.

[77] P. Leproux, S. Fevrier, V. Doya, P. Roy, and D. Pagnoux, "Modeling and optimization of double-clad fiber amplifiers using chaotic propagation of the pump," *Optical Fiber Technology*, vol. 7, no. 4, pp. 324–339, 2001.

[78] V. Doya, O. Legrand, and F. Mortessagne, "Optimized absorption in a chaotic double-clad fiber amplifier," *Optics letters*, vol. 26, no. 12, pp. 872–874, 2001.

[79] A. Carter, K. Tankala, and N. Jacobson, "Cladding-pumped optical fiber," Sept. 23 2003, US Patent 6,625,363.

[80] A. Carter, K. Tankala, and M. Seifert, "Double-clad optical fiber for lasers and amplifiers," Feb. 3 2004, US Patent 6,687,445.

[81] D. Marcuse, "Coupled power equations for lossy fibers," *Applied Optics*, vol. 17, no. 20, pp. 3232–3237, 1978.

[82] J. Nilsson, S. Alam, J. Alvarez-Chavez, P. Turner, W. Clarkson, and A. Grudinin, "High-power and tunable operation of erbium-ytterbium co-doped cladding-pumped fiber lasers," *Quantum Electronics, IEEE Journal of*, vol. 39, no. 8, pp. 987–994, 2003.

[83] J. Alvarez-Chavez, A. Grudinin, J. Nilsson, P. Turner, and W. Clarkson, "Mode selection in high power cladding pumped fibre lasers with tapered section," in *Lasers and Electro-Optics, 1999. CLEO'99. Summaries of Papers Presented at the Conference on*. IEEE, 1999, pp. 247–248.

[84] M. Dejneka, J. Minelly, and L. Zenteno, "Tapered fiber laser," Nov. 27 2001, US Patent 6,324,326.

[85] M. Dejneka, B. Hanson, S. Crigler, L. Zenteno, J. Minelly, D. Allan, W. Miller, and D. Kuksenkov, "La2O3-Al2O3-SiO2 glasses for high-power, Yb^{3+}-doped, 980-nm fiber lasers," *Journal of the American Ceramic Society*, vol. 85, no. 5, pp. 1100–1106, 2002.

[86] H. Jeong, S. Choi, and K. Oh, "Continuous wave single transverse mode laser oscillation in a Nd-doped large core double clad fiber cavity with concatenated adiabatic tapers," *Optics Communications*, vol. 213, no. 1-3, pp. 33–37, 2002.

[87] L. Li, Q. Lou, J. Zhou, J. Dong, Y. Wei, S. Du, and B. He, "High power single transverse mode operation of a tapered large-mode-area fiber laser," *Optics Communications*, vol. 281, no. 4, pp. 655–657, 2008.

[88] M. Hudson, "Calculation of the maximum optical coupling efficiency into multimode optical waveguides," *Applied Optics*, vol. 13, no. 5, pp. 1029–1033, 1974.

[89] A. Kosterin, V. Temyanko, M. Fallahi, and M. Mansuripur, "Tapered fiber bundles for combining high-power diode lasers," *Applied optics*, vol. 43, no. 19, pp. 3893–3900, 2004.

[90] J. Koponen, L. Petit, T. Kokki, V. Aallos, J. Paul, and H. Ihalainen, "Progress in direct nanoparticle deposition for the development of the next generation fiber lasers," *Optical Engineering*, vol. 50, p. 111605, 2011.

[91] K. Golant, "Surface plasma chemical vapor deposition: 20 years of application in glass synthesis for lightguides (a review)," in *XXI International Congress on Glass, Strasbourg, Proc. on CD ROM, paper L*, vol. 13, 2007.

[92] I. Bufetov, K. Golant, S. Firstov, A. Kholodkov, A. Shubin, and E. Dianov, "Bismuth activated alumosilicate optical fibers fabricated by surface-plasma chemical vapor deposition technology," *Applied optics*, vol. 47, no. 27, pp. 4940–4944, 2008.

[93] A. Kholodkov and K. Golant, "Surface plasma CVD as a new technological platform for Er-doped waveguide amplifiers and lasers fabrication," in *Optical Fiber Communication Conference*. Optical Society of America, 2004.

[94] S. Golowich, W. Reed, and A. Ritger, "A new modal power distribution measurement for high-speed short-reach optical systems," *Lightwave Technology, Journal of*, vol. 22, no. 2, pp. 457–468, 2004.

[95] D. Beom Soo Soh, J. Nilsson, S. Baek, C. Codemard, Y. Jeong, and V. Philippov, "Modal power decomposition of beam intensity profiles into linearly polarized modes of multimode optical fibers," *JOSAA*, vol. 21, no. 7, pp. 1241–1250, 2004.

[96] N. Andermahr, T. Theeg, and C. Fallnich, "Novel approach for polarization-sensitive measurements of transverse modes in few-mode optical fibers," *Applied Physics B: Lasers and Optics*, vol. 91, no. 2, pp. 353–357, 2008.

[97] C. Schulze, O. Schmidt, D. Flamm, M. Duparré, and S. Schröter, "Modal analysis of beams emerging from a multi-core fiber using computer-generated holograms," in *Proceedings of SPIE*, vol. 7914, 2011, p. 79142H.

[98] J. Nicholson, A. Yablon, S. Ramachandran, and S. Ghalmi, "Spatially and spectrally resolved imaging of modal content in large-mode-area fibers," *Optics Express*, vol. 16, no. 10, pp. 7233–7243, 2008.

[99] J. Nicholson, A. Yablon, J. Fini, and M. Mermelstein, "Measuring the modal content of large-mode-area fibers," *Selected Topics in Quantum Electronics, IEEE Journal of*, vol. 15, no. 1, pp. 61–70, 2009.

[100] M. Fermann, "Single-mode excitation of multimode fibers with ultrashort pulses," *Optics letters*, vol. 23, no. 1, pp. 52–54, 1998.

[101] H. Yoda, P. Polynkin, and M. Mansuripur, "Beam quality factor of higher order modes in a step-index fiber," *Journal of lightwave technology*, vol. 24, no. 3, p. 1350, 2006.

[102] S. Wielandy, "Implications of higher-order mode content in large mode area fibers with good beam quality," *Optics Express*, vol. 15, no. 23, pp. 15 402–15 409, 2007.

[103] J. Limpert, A. Liem, M. Reich, T. Schreiber, S. Nolte, H. Zellmer, A. Tünnermann, J. Broeng, A. Petersson, and C. Jakobsen, "Low-nonlinearity single-transverse-mode ytterbium-doped photonic crystal fiber amplifier," *Optics Express*, vol. 12, no. 7, pp. 1313–1319, 2004.

[104] S. Hurand, L. Chauny, H. El-Rabii, S. Joshi, and A. Yalin, "Mode coupling and output beam quality of 100–400 μm core silica fibers," *Applied Optics*, vol. 50, no. 4, pp. 492–499, 2011.

[105] N. Amitay, H. Presby, F. Dimarcello, and K. Nelson, "Optical fiber tapers–A novel approach to self-aligned beam expansion and single-mode hardware," *Lightwave Technology, Journal of*, vol. 5, no. 1, pp. 70–76, 1987.

[106] G. Scherer, "Stress-induced index profile distortion in optical waveguides," *Applied Optics*, vol. 19, no. 12, pp. 2000–2006, 1980.

[107] M. Hutsel, R. Ingle, and T. Gaylord, "Accurate cross-sectional stress profiling of optical fibers," *Applied optics*, vol. 48, no. 26, pp. 4985–4995, 2009.

[108] F. Just, H. Müller, S. Unger, J. Kirchhof, V. Reichel, and H. Bartelt, "Ytterbium-doping related stresses in preforms for high-power fiber lasers," *Journal of Lightwave Technology*, vol. 27, no. 12, pp. 2111–2116, 2009.

[109] D. Donlagic and B. Culshaw, "Propagation of the fundamental mode in curved graded index multimode fiber and its application in sensor systems," *Lightwave Technology, Journal of*, vol. 18, no. 3, pp. 334–342, 2000.

[110] J. Dawson, M. Messerly, R. Beach, M. Shverdin, E. Stappaerts, A. Sridharan, P. Pax, J. Heebner, C. Siders, and C. Barty, "Analysis of the scalability of diffraction-limited fiber lasers and amplifiers to high average power," *Optics express*, vol. 16, no. 17, pp. 13 240–13 266, 2008.

[111] D. J. Richardson, J. Nilsson, and W. A. Clarkson, "High power fiber lasers: current status and future perspectives [Invited]," *Journal of Optical Society America B*, vol. 27, no. 11, pp. B63–B92, 2010.

[112] J. Zhu, P. Zhou, Y. Ma, X. Xu, and Z. Liu, "Power scaling analysis of tandem-pumped Yb-doped fiber lasers and amplifiers," *Optics Express*, vol. 19, no. 19, pp. 18 645–18 654, 2011.

[113] B. Samson and G. Frith, "Diode pump requirements for high power fiber lasers," in *Proc. ICALEO*, 2007, p. #501.

[114] K. Price, S. Patterson, S. Karlsen, A. Brown, R. Mehl, R. Martinsen, K. Kennedy, D. Schulte, and J. Bell, "Progress in fiber-coupled, high-brightness, high-power diode laser pump sources," in *21st Annual Solid State and Diode Laser Technology Review*. Directed Energy Professional Society, 2008.

[115] V. Gapontsev, I. Berishev, G. Ellis, A. Komissarov, N. Moshegov, A. Ovtchinnikov, O. Raisky, P. Trubenko, V. Ackermann, and E. Shcherbakov, "9xx nm single emitter pumps for multi-kW systems," in *Proc. SPIE*, vol. 6104, 2006, p. 61040K.

[116] P. Wolf, B. Köhler, K. Rotter, S. Hertsch, H. Kissel, and J. Biesenbach, "High-power, high-brightness and low-weight fiber coupled diode laser device," in *Proceedings of SPIE*, vol. 7918, 2011, p. 79180O.

[117] D. Ripin and L. Goldberg, "High efficiency side-coupling of light into optical fibres using imbedded v-grooves," *Electronics Letters*, vol. 31, no. 25, pp. 2204–2205, 1995.

[118] Q. Xiao, P. Yan, S. Yin, J. Hao, and M. Gong, "100 W ytterbium-doped monolithic fiber laser with fused angle-polished side-pumping configuration," *Laser Physics Letters*, vol. 8, no. 2, pp. 125–129, 2011.

[119] G. Valentin and S. Igor, "Coupling arrangement between a multi-mode light source and an optical fiber through an intermediate optical fiber length," Dec. 7 1999, US Patent 5,999,673.

[120] J. Xu, J. Lu, G. Kumar, J. Lu, and K. Ueda, "A non-fused fiber coupler for side-pumping of double-clad fiber lasers," *Optics Communications*, vol. 220, no. 4-6, pp. 389–395, 2003.

[121] P. Polynkin, V. Temyanko, M. Mansuripur, and N. Peyghambarian, "Efficient and scalable side pumping scheme for short high-power optical fiber lasers and amplifiers," *Photonics Technology Letters, IEEE*, vol. 16, no. 9, pp. 2024–2026, 2004.

[122] R. Paschotta, "Power scalability as a precise concept for the evaluation of laser architectures," *Arxiv preprint arXiv:0711.3987*, 2007.

[123] D. Brown and H. Hoffman, "Thermal, stress, and thermo-optic effects in high average power double-clad silica fiber lasers," *Quantum Electronics, IEEE Journal of*, vol. 37, no. 2, pp. 207–217, 2001.

[124] A. Smith, J. Smith, *et al.*, "Mode instability in high power fiber amplifiers," *Opt. Express*, vol. 19, no. 11, pp. 10 180–10 192, 2011.

[125] K. Hansen, T. Alkeskjold, J. Broeng, and J. Lægsgaard, "Thermo-optical effects in high-power ytterbium-doped fiber amplifiers," *Optics Express*, vol. 19, no. 24, pp. 23 965–23 980, 2011.

[126] F. Jansen, F. Stutzki, H. Otto, T. Eidam, A. Liem, C. Jauregui, J. Limpert, and A. Tünnermann, "Thermally induced waveguide changes in active fibers," *Optics Express*, vol. 20, no. 4, pp. 3997–4008, 2012.

[127] B. Ward, C. Robin, and I. Dajani, "Origin of thermal modal instabilities in large mode area fiber amplifiers," *Optics Express*, vol. 20, no. 10, pp. 11 407–11 422, 2012.

[128] C. Jauregui, T. Eidam, H. Otto, F. Stutzki, F. Jansen, J. Limpert, and A. Tünnermann, "Physical origin of mode instabilities in high-power fiber laser systems," *Optics Express*, vol. 20, no. 12, pp. 12 912–12 925, 2012.

[129] A. V. Smith and J. J. Smith, "A steady-periodic method for modeling mode instability in fiber amplifiers," *arXiv preprint arXiv:1301.1296*, 2013.

[130] L. Dong, "Stimulated thermal rayleigh scattering in optical fibers," *Optics Express*, vol. 21, no. 3, pp. 2642–2656, 2013.

[131] A. V. Smith and J. J. Smith, "Frequency dependence of mode coupling gain in yb doped fiber amplifiers due to stimulated thermal rayleigh scattering," *arXiv preprint arXiv:1301.4277*, 2013.

[132] R. Menzel, *Photonics: linear and nonlinear interactions of laser light and matter*. Springer Verlag, 2001, vol. 24.

[133] R. Kashyap and K. Blow, "Observation of catastrophic self-propelled self-focusing in optical fibres," *Electronics Letters*, vol. 24, no. 1, pp. 47–49, 1988.

[134] E. Dianov, I. Bufetov, and A. Frolov, "Destruction of silica fiber cladding by the fuse effect," *Optics letters*, vol. 29, no. 16, pp. 1852–1854, 2004.

[135] R. Smith, "Optical power handling capacity of low loss optical fibers as determined by stimulated Raman and Brillouin scattering," *Applied Optics*, vol. 11, no. 11, pp. 2489–2494, 1972.

[136] R. Stolen, E. Ippen, and A. Tynes, "Raman oscillation in glass optical waveguide," *Applied Physics Letters*, vol. 20, no. 2, pp. 62–64, 1972.

[137] G. P. Agrawal, *Nonlinear fiber optics*, 3rd ed. San Diego, CA: Academic Press, 2001.

[138] E. Kuzin, G. Beltran-Perez, M. Basurto-Pensado, R. Rojas-Laguna, J. Andrade-Lucio, M. Torres-Cisneros, and E. Alvarado-Mendez, "Stimulated Raman scattering in a fiber with bending loss," *Optics Communications*, vol. 169, no. 1-6, pp. 87–91, 1999.

[139] J. Fini, M. Mermelstein, M. Yan, R. Bise, A. Yablon, P. Wisk, and M. Andrejco, "Distributed suppression of stimulated Raman scattering in an Yb-doped filter-fiber amplifier," *Optics letters*, vol. 31, no. 17, pp. 2550–2552, 2006.

[140] R. W. Boyd, *Nonlinear optics*, 2nd ed. San Diego, CA: Academic Press, 2003.

[141] B. Stiller, A. Kudlinski, M. Lee, G. Bouwmans, M. Delque, J. Beugnot, H. Maillotte, and T. Sylvestre, "SBS mitigation in a microstructured optical fiber by periodically varying the core diameter," *Photonics Technology Letters, IEEE*, no. 99, pp. 1–1, 2012.

[142] M. Ohashi and M. Tateda, "Design of strain-free-fiber with nonuniform dopant concentration for stimulated Brillouin scattering suppression," *Lightwave Technology, Journal of*, vol. 11, no. 12, pp. 1941–1945, 1993.

[143] N. Yoshizawa and T. Imai, "Stimulated Brillouin scattering suppression by means of applying strain distribution to fiber with cabling," *Lightwave Technology, Journal of*, vol. 11, no. 10, pp. 1518–1522, 1993.

[144] P. Dragic, C. Liu, G. Papen, and A. Galvanauskas, "Optical fiber with an acoustic guiding layer for stimulated Brillouin scattering suppression," in *Lasers and Electro-Optics, 2005.(CLEO). Conference on*, vol. 3. IEEE, 2005, pp. 1984–1986.

[145] S. Gray, D. Walton, X. Chen, J. Wang, M. Li, A. Liu, A. Ruffin, J. Demeritt, and L. Zenteno, "Optical fibers with tailored acoustic speed profiles for suppressing stimulated Brillouin scattering in high-power, single-frequency sources," *Selected Topics in Quantum Electronics, IEEE Journal of*, vol. 15, no. 1, pp. 37–46, 2009.

[146] V. Kovalev and R. Harrison, "Suppression of stimulated Brillouin scattering in high-power single-frequency fiber amplifiers," *Optics letters*, vol. 31, no. 2, pp. 161–163, 2006.

[147] S. Gray, A. Liu, D. Walton, J. Wang, M. Li, X. Chen, A. Ruffin, J. DeMeritt, and L. Zenteno, "502 Watt, single transverse mode, narrow linewidth, bidirectionally pumped Yb-doped fiber amplifier," *Optics Express*, vol. 15, no. 25, pp. 17 044–17 050, 2007.

[148] A. Fotiadi, M. Blondel, *et al.*, "Dynamics of a self-Q-switched fiber laser with a Rayleigh-stimulated Brillouin scattering ring mirror," *Optics letters*, vol. 29, no. 10, pp. 1078–1080, 2004.

[149] B. Upadhyaya, A. Kuruvilla, U. Chakravarty, M. Shenoy, K. Thyagarajan, and S. Oak, "Effect of laser linewidth and fiber length on self-pulsing dynamics and output stabilization of single-mode Yb-doped double-clad fiber laser," *Applied optics*, vol. 49, no. 12, pp. 2316–2325, 2010.

[150] S. Fu, X. Feng, L. Si, Z. Guo, X. Jia, Y. Zhao, S. Yuan, and X. Dong, "Self-pulsing dynamics of high-power Yb-doped fiber lasers," *Microwave and optical technology letters*, vol. 48, no. 11, pp. 2282–2285, 2006.

[151] B. Ortaç, A. Hideur, T. Chartier, M. Brunel, G. Martel, M. Salhi, and F. Sanchez, "Influence of cavity losses on stimulated Brillouin scattering in a self-pulsing side-pumped ytterbium-doped double-clad fiber laser," *Optics Communications*, vol. 215, no. 4-6, pp. 389–395, 2003.

[152] A. Martinez-Rios, I. Torres-Gomez, G. Anzueto-Sanchez, and R. Selvas-Aguilar, "Self-pulsing in a double-clad ytterbium fiber laser induced by high scattering loss," *Optics Communications*, vol. 281, no. 4, pp. 663–667, 2008.

[153] S. Jackson, "Direct evidence for laser reabsorption as initial cause for self-pulsing in three-level fibre lasers," *Electronics Letters*, vol. 38, no. 25, pp. 1640–1642, 2002.

[154] W. Guan and J. Marciante, "Complete elimination of self-pulsations in dual-clad ytterbium-doped fiber lasers at all pumping levels," *Optics letters*, vol. 34, no. 6, pp. 815–817, 2009.

[155] R. Paschotta, J. Nilsson, P. Barber, J. Caplen, A. Tropper, and D. Hanna, "Lifetime quenching in Yb-doped fibres," *Optics Communications*, vol. 136, no. 5-6, pp. 375–378, 1997.

[156] J. Fini, "Bend-resistant design of conventional and microstructure fibers with very large mode area," *Optics Express*, vol. 14, no. 1, pp. 69–81, 2006.

[157] P. Wang, J. Sahu, and W. Clarkson, "Power scaling of ytterbium-doped fiber superfluorescent sources," *Selected Topics in Quantum Electronics, IEEE Journal of*, vol. 13, no. 3, pp. 580–587, 2007.

[158] C. Codemard, J. Sahu, and J. Nilsson, "Tandem cladding-pumping for control of excess gain in ytterbium-doped fiber amplifiers," *Quantum Electronics, IEEE Journal of*, vol. 46, no. 12, pp. 1860–1869, 2010.

[159] V. Fomin, M. Abramov, A. Ferin, A. Abramov, D. Mochalov, N. Platonov, and V. Gapontsev, "10 kW single-mode fiber laser," in *International Symposium on High-Power Fiber Lasers and their Applications*, 2010.

[160] Y. Jeong, A. Boyland, J. Sahu, S. Chung, J. Nilsson, and D. Payne, "Multi-kilowatt single-mode ytterbium-doped large-core fiber laser," *Journal of the Optical Society of Korea*, vol. 13, no. 4, pp. 416–422, 2009.

[161] J. Dawson, M. Messerly, J. Heebner, P. Pax, A. Sridharan, A. Bullington, R. Beach, C. Siders, C. Barty, and M. Dubinskii, "Power scaling analysis of fiber lasers and amplifiers based on non-silica materials," in *Proc. SPIE*, vol. 7686, 2010, p. 768611.

[162] Y. Lee, M. Digonnet, S. Sinha, K. Urbanek, R. Byer, and S. Jiang, "High-power Yb^{3+}-doped phosphate fiber amplifier," *Selected Topics in Quantum Electronics, IEEE Journal of*, vol. 15, no. 1, pp. 93–102, 2009.

[163] C. Wirth, O. Schmidt, I. Tsybin, T. Schreiber, T. Peschel, F. Brückner, T. Clausnitzer, J. Limpert, R. Eberhardt, A. Tünnermann, *et al.*, "2 kW incoherent beam combining of four narrow-linewidth photonic crystal fiber amplifiers," *Optics Express*, vol. 17, no. 3, pp. 1178–1183, 2009.

[164] C. Yu, S. Augst, S. Redmond, K. Goldizen, D. Murphy, A. Sanchez, and T. Fan, "Coherent combining of a 4 kW, eight-element fiber amplifier array," *Optics letters*, vol. 36, no. 14, pp. 2686–2688, 2011.

[165] H. Injeyan and G. Goodno, *High power laser handbook*. McGraw-Hill Professional, 2011.

[166] J. Fini, "Design of large-mode-area amplifier fibers resistant to bend-induced distortion," *JOSAB*, vol. 24, no. 8, pp. 1669–1676, 2007.

[167] Y. Jeong, J. Nilsson, J. Sahu, D. Payne, R. Horley, L. Hickey, and P. Turner, "Power scaling of single-frequency ytterbium-doped fiber master-oscillator power-amplifier sources up to 500 W," *Selected Topics in Quantum Electronics, IEEE Journal of*, vol. 13, no. 3, pp. 546–551, 2007.

[168] O. Okhotnikov and J. Sousa, "Flared single-transverse-mode fibre amplifier," *Electronics Letters*, vol. 35, no. 12, pp. 1011–1013, 1999.

[169] O. Schmidt, M. Rekas, C. Wirth, J. Rothhardt, S. Rhein, A. Kliner, M. Strecker, T. Schreiber, J. Limpert, R. Eberhardt, *et al.*, "High power narrow-band fiber-based ASE source," *Optics Express*, vol. 19, no. 5, pp. 4421–4427, 2011.

[170] M. Hildebrandt, M. Frede, and D. Kracht, "Narrow-linewidth ytterbium-doped fiber amplifier system with 45 nm tuning range and 133 W of output power," *Optics letters*, vol. 32, no. 16, pp. 2345–2347, 2007.

[171] A. Liem, J. Limpert, H. Zellmer, and A. Tünnermann, "100-W single-frequency master-oscillator fiber power amplifier," *Optics letters*, vol. 28, no. 17, pp. 1537–1539, 2003.

[172] F. Stutzki, F. Jansen, A. Liem, C. Jauregui, J. Limpert, and A. Tünnermann, "26 mJ, 130 W Q-switched fiber-laser system with near-diffraction-limited beam quality," *Optics Letters*, vol. 37, no. 6, pp. 1073–1075, 2012.

[173] A. Tünnermann, T. Schreiber, and J. Limpert, "Fiber lasers and amplifiers: an ultrafast performance evolution," *Applied optics*, vol. 49, no. 25, pp. F71–F78, 2010.

[174] R. Paschotta, *Field guide to laser pulse generation*. Bellingham, WA: SPIE, 2008.

[175] A. Smith and B. Do, "Bulk and surface laser damage of silica by picosecond and nanosecond pulses at 1064 nm," *Applied optics*, vol. 47, no. 26, pp. 4812–4832, 2008.

[176] A. Smith, B. Do, G. Hadley, and R. Farrow, "Optical damage limits to pulse energy from fibers," *Selected Topics in Quantum Electronics, IEEE Journal of*, vol. 15, no. 1, pp. 153–158, 2009.

[177] B. Stuart, M. Feit, A. Rubenchik, B. Shore, and M. Perry, "Laser-induced damage in dielectrics with nanosecond to subpicosecond pulses," *Physical Review Letters*, vol. 74, no. 12, pp. 2248–2251, 1995.

[178] A. Tien, S. Backus, H. Kapteyn, M. Murnane, and G. Mourou, "Short-pulse laser damage in transparent materials as a function of pulse duration," *Physical review letters*, vol. 82, no. 19, p. 3883, 1999.

[179] M. Mero, J. Liu, W. Rudolph, D. Ristau, and K. Starke, "Scaling laws of femtosecond laser pulse induced breakdown in oxide films," *Physical Review B*, vol. 71, no. 11, p. 115109, 2005.

[180] R. Farrow, D. Kliner, G. Hadley, and A. Smith, "Peak-power limits on fiber amplifiers imposed by self-focusing," *Optics letters*, vol. 31, no. 23, pp. 3423–3425, 2006.

[181] G. Fibich and A. Gaeta, "Critical power for self-focusing in bulk media and in hollow waveguides," *Optics Letters*, vol. 25, no. 5, pp. 335–337, 2000.

[182] O. Schmidt, J. Rothhardt, F. Röser, S. Linke, T. Schreiber, K. Rademaker, J. Limpert, S. Ermeneux, P. Yvernault, F. Salin, *et al.*, "Millijoule pulse energy Q-switched short-length fiber laser," *Optics letters*, vol. 32, no. 11, pp. 1551–1553, 2007.

[183] A. Galvanauskas, M. Cheng, K. Hou, and K. Liao, "High peak power pulse amplification in large-core Yb-doped fiber amplifiers," *Selected Topics in Quantum Electronics, IEEE Journal of*, vol. 13, no. 3, pp. 559–566, 2007.

[184] J. Marciante and J. Zuegel, "High-gain, polarization-preserving, Yb-doped fiber amplifier for low-duty-cycle pulse amplification," *Applied optics*, vol. 45, no. 26, pp. 6798–6804, 2006.

[185] J. Nilsson, R. Paschotta, J. Caplen, and D. Hanna, "Yb^{3+}-ring-doped fiber for high-energy pulse amplification," *Optics letters*, vol. 22, no. 14, pp. 1092–1094, 1997.

[186] J. Kerttula, V. Filippov, Y. Chamorovskiy, K. Golant, and O. Okhotnikov, "2-mJ actively Q-switched ytterbium tapered fiber laser operating in the single-shot regime," in *4th EPS-QEOD Europhoton conference*, 2010.

[187] T. Eidam, S. Hanf, E. Seise, T. Andersen, T. Gabler, C. Wirth, T. Schreiber, J. Limpert, and A. Tünnermann, "Femtosecond fiber CPA system emitting 830 W average output power," *Optics letters*, vol. 35, no. 2, pp. 94–96, 2010.

[188] J. Limpert, F. Roser, D. Schimpf, E. Seise, T. Eidam, S. Hadrich, J. Rothhardt, C. Misas, and A. Tunnermann, "High repetition rate gigawatt peak power fiber laser systems: challenges, design, and experiment," *Selected Topics in Quantum Electronics, IEEE Journal of*, vol. 15, no. 1, pp. 159–169, 2009.

[189] A. Mussot, M. Beaugeois, M. Bouazaoui, and T. Sylvestre, "Tailoring CW supercontinuum generation in microstructured fibers with two-zero dispersion wavelengths," *Optics Express*, vol. 15, no. 18, pp. 11 553–11 563, 2007.

[190] J. Travers, A. Rulkov, B. Cumberland, S. Popov, and J. Taylor, "Visible supercontinuum generation in photonic crystal fibers with a 400W continuous wave fiber laser," *Optics Express*, vol. 16, no. 19, pp. 14 435–14 447, 2008.

[191] K. Chen, S. Alam, J. Price, J. Hayes, D. Lin, A. Malinowski, C. Codemard, D. Ghosh, M. Pal, S. Bhadra, *et al.*, "Picosecond fiber MOPA pumped supercontinuum source with 39 W output power," *Optics express*, vol. 18, no. 6, pp. 5426–5432, 2010.

[192] J. Dudley, G. Genty, and S. Coen, "Supercontinuum generation in photonic crystal fiber," *Reviews of Modern Physics*, vol. 78, no. 4, p. 1135, 2006.

[193] J. Dudley, G. Genty, F. Dias, B. Kibler, and N. Akhmediev, "Modulation instability, Akhmediev breathers and continuous wave supercontinuum generation," *Optics express*, vol. 17, no. 24, pp. 21 497–21 508, 2009.

[194] J. Travers, "Blue solitary waves from infrared continuous wave pumping of optical fibers," *Optics Express*, vol. 17, no. 3, pp. 1502–1507, 2009.

[195] J. Cascante-Vindas, A. Díez, S. Torres-Peiro, J. Cruz, and M. Andrés, "Enhanced supercontinuum generation in the nanosecond pump regime using specialty microstructured fibers," in *Transparent Optical Networks, 2009. ICTON'09. 11th International Conference on*. IEEE, 2009, pp. 1–4.

[196] J. Cascante-Vindas, A. Díez, J. Cruz, and M. Andrés, "Supercontinuum Q-switched Yb fiber laser using an intracavity microstructured fiber," *Optics letters*, vol. 34, no. 23, pp. 3628–3630, 2009.

[197] J. Stone and J. Knight, "Visibly "white" light generation in uniform photonic crystal fiber using a microchip laser," *Optics Express*, vol. 16, no. 4, pp. 2670–2675, 2008.

[198] S. Kobtsev, S. Kukarin, Y. Fedotov, and S. Smirnov, "All-fiber supercontinuum generator with high-energy pulses," in *Conference on Lasers and Electro-Optics/International Quantum Electronics Conference*. IEEE, 2009.

Appendices

Appendix 1

Publication 1

V. Filippov, Y. Chamorovskii, J. Kerttula, K. Golant, M. Pessa, and O. G. Okhotnikov, "Double clad tapered fiber for high power applications", *Optics Express*, vol. 16, no. 3, pp. 1929–1944, 2008.

Double clad tapered fiber for high power applications

V. Filippov[1*], Yu. Chamorovskii[2], J. Kerttula[1], K. Golant[3], M. Pessa[1], and O. G. Okhotnikov[1]

[1]*Optoelectronics Research Centre, Tampere University of Technology, 33101 Tampere, Finland*
[2]*Institute of Radio and Electronics of the Russian Academy of Sciences, Mokhovaya 11, bld.7, 125009 Moscow, Russia*
[3]*Fiber Optics Research Centre, Russian Academy of Sciences, 38 Vavilov Str., 119333 Moscow, Russia*
[*]*Corresponding author: valery.filippov@tut.fi*

Abstract: We report a novel type of active fiber – tapered double clad fiber suitable for pumping by low brightness sources with large beam parameter product of 50÷300 mm×mrad. Ytterbium double clad all-silica fiber (core/1st clad/2nd clad diameters 27/834/890 μm, NA_{core}=0.11, NA_{clad}=0.21), tapered down by a factor 4.8 for a length of 10.5 m was drawn from a preform fabricated by plasma chemical technologies. At a moderate Yb-ion concentration and 1:31 core/cladding ratio, the tapered double clad fiber demonstrates 0.9 dB/m pump absorption at 976 nm and excellent lasing slope efficiency. An ytterbium fiber laser with 84 W of output power and 92% slope efficiency, a 74 W superfluorescent source with 85% slope efficiency and amplifiers operating both in CW and pulsed regimes have been realized. All devices demonstrated robust single mode operation with a beam quality factor of M^2=1.07.

OCIS codes: (060.2280) Fiber design and fabrication; (060.2320) Fiber optics amplifiers and oscillators; (060.3510) Lasers, fiber

References and Links

1. www.ipgphotonics.com
2. Y. Jeong, J. K. Sahu, D. N. Payne, and J. Nilsson, "Ytterbium-doped large-core fiber laser with 1.36 kW continuous-wave output power," Opt. Express **12**, 6088-6092 (2004).
3. D. Young and C. Roychoudhuri, "Results and comparison of a cladding pumped fiber simulation using a decagon-shaped fiber," Opt. Express **11**, 830-837 (2003).
4. J. J. Koponen, M. J. Soderlund, H. J. Hoffman, and S. K. Tammela, "Measuring photodarkening from single-mode ytterbium doped silica fibers," Opt. Express **14**, 11539-11544 (2006).
5. B. Morasse, S. Chatigny, E. Gagnon, C. Hovington, J-P. Martin, and J-P. de Sandro, "Low photodarkening single cladding ytterbium fiber amplifier," Proc. SPIE **6453**, 64530H-1-64530H-9 (2007).
6. S. Yoo, C. Basu, A. J. Boyland, C. Sones, J. Nilsson, J. K. Sahu, and D. Payne, "Photodarkening in Yb-doped aluminosilicate fibers induced by 488nm irradiation," Opt. Lett. **32**, 1626-1628 (2007).
7. J. Kirchhof, S. Unger, V. Reichel, and A. Schwuchow, "Background loss and devitrification in Nd-doped fiber laser glass," *Optical Fiber Conference Technical Digest*, 60-61 (1996).
8. P. Koplow, D. Kliner, and L. Goldberg, "Single-mode operation of a coiled multimode fiber amplifier," Opt. Lett. **25**, 442-444 (2000).
9. J. Limpert, N. Deguil-Robin, I. Manek-Honninger, F. Salin, F. Roser, A. Liem, T. Schreiber, S. Nolte, H. Zellmer, A. Tunnermann, J. Broeng, A. Petersson, and C. Jacobsen, "High-power rod-type photonic crystal fiber laser," Opt. Express **13**, 1055-1058 (2005), http://www.opticsinfobase.org/abstract.cfm?URI=oe-13-4-1055
10. J. Limpert, O. Schmidt, J. Rothhardt, F. Roser, T. Schreiber, A. Tunnermann, S. Ermeneux, P. Yvernault, and F. Salin, "Extended single-mode photonic crystal fiber lasers," Opt. Express **14**, 2715-2720 (2006).
11. A. Liu and K. Ueda, "The absorption characteristics of circular, offset, and rectangular double-clad fibers," Optics Commun. **132**, 511-518 (1996).
12. P. Leproux, S. Fevrier, V. Doya, P. Roy, and D. Pagnoux, "Modeling and optimization of double-clad fiber amplifiers using chaotic propagation of pump," Opt. Fiber Technol. **6**, 324-339 (2001).
13. V. Doya, O. Legrand, and F. Mortessagne, "Optimized absorption in a chaotic double-clad fiber amplifier," Opt. Lett. **26,** 872-874 (2001).
14. D. Kouznetsov, J. Moloney, and E. Wright, "Efficiency of pump absorption in double-clad fiber amplifiers. I. Fiber with circular symmetry," J. Opt. Soc. Am. B **18**, 743-749 (2001).

#89552 - $15.00 USD Received 9 Nov 2007; revised 20 Dec 2007; accepted 14 Jan 2008; published 28 Jan 2008

15. D. Kouznetsov and J. Moloney, "Efficiency of pump absorption in double-clad fiber amplifiers. II. Broken circular symmetry," J. Opt. Soc. Am. B **19**, 1259-1263 (2002).
16. D. Kouznetsov and J. Moloney, "Efficiency of pump absorption in double-clad fiber amplifiers. III. Calculation of modes," J. Opt. Soc. Am. B **19**, 1304-1309 (2002).
17. H. Po, "Ring core fiber," PCT patent WO 02/079829 A1.
18. H. Po, "Optical fiber," PCT patent WO 03/010578 A1.
19. A. Carter, K. Tankala, and N. Jacobson, "Cladding-pumped optical fiber," US patent 6.625.363 B2
20. M. Fermann, "Single-mode excitation of multimode fibers with ultrashort pulses," Opt. Lett. **23,** 52-54 (1998).
21. A. Carter, K. Tankala, and M. Seifert, "Double-clad optical fiber for lasers and amplifiers," US patent 6.687.445 B2.
22. D. Marcuse, "Coupled power equations for lossy fibers," Appl. Opt. **17**, 3232-3237 (1978).
23. J. Nilsson, S.-U. Alam, J. A. Alvarez-Chavez, P. W. Turner, W. A. Clarkson, and A. B. Grudinin, "High-power and tunable operation of erbium-ytterbium co-doped cladding-pumped fiber lasers," IEEE J. Quantum Electron. **39**, 987-994 (2003).
24. D. Marcuse, *Light Transmission Optics*, (Van Nostrand Reinhold Company, New York, 1972), Chap. 9.
25. E. M. Dianov, K. M. Golant, V. I. Karpov, R. R. Khrapko, A. S. Kurkov, V. N. Protopopov, S. L. Semenov and A. G. Shebuniaev, "Application of reduced-pressure plasma CVD technology to the fabrication of Er-doped optical fibers," Opt. Mater. **3**, 181-185 (1994).
26. A. C. Boucouvalas and G. Georgiou, "External refractive-index response of tapered coaxial couplers," Opt. Lett. **11**, 257-259, (1986).
27. K. Kieu and M. Mansuripur, "Tuning of fiber lasers by use of a single-mode biconic fiber taper," Opt. Lett. **31**, 2435-2437 (2006).
28. S. A. Kingsley and D. E. N. Davies, "Multimode optical-fibre phase modulators and discriminators: I-Theory," Electron. Lett. **14**, 322-324 (1978).
29. V. B. Veinberg and D. K. Sattarov, *Waveguide Optics*, (Mashinostroenie, Leningrad, 1977), Chap.5 (in Russian).
30. N. S. Kapany and J. J. Burke, *Optical Waveguides*, (Academic Press, New York, 1972).
31. P. Wang and W. A. Clarkson, "High-power, single mode, linearly polarized, ytterbium-doped fiber superfluorescent source," Opt. Lett. **32**, 2605-2607 (2007).
32. O. G. Okhotnikov and J. M. Sousa, "Flared single-transverse-mode fiber amplifier," Electron. Lett. **35**, 1011-1013, (1999).
33. A. Liem, J. Limpert, H. Zellmer, and A. Tunnermann, "100-W single-frequency master-oscillator fiber power amplifier," Opt. Lett. **28**, 1537-1539, (2003).
34. Y. Jeong, J. Nilsson, J. Sahu, D. Payne, R. Horley, L. Hickey, and P. Turner, "Power scaling of single-frequency ytterbium-doped fiber master-oscillator power-amplifier sources up to 500W," IEEE J. Sel. Top. Quantum Electron. **13,** 546-551 (2007).
35. V. I. Kovalev and R. G. Harrison, "Suppression of stimulated Brillouin scattering in high-power single-frequency fiber amplifiers," Opt. Lett. **31**, 161-163 (2006).
36. J. Hansryd, F. Dross, M. Westlund, P. A. Andrekson and S. N. Knudsen, "Increase of the SBS threshold in a short highly nonlinear fiber by applying a temperature distribution," J. Lightwave Technol. **19,** 1691-1697 (2001).
37. K. Shiraki, M. Ohashi, and M. Tateda, "Suppression of stimulated Brillouin scattering in a fiber by changing the core radius," Electron. Lett. **31**, 668-669 (1995).
38. http://www.laserline.de/

1. Introduction

Fiber laser technology has attracted significant interest during the last decade. The breakthrough in ytterbium fiber laser power scaling looks especially remarkable. Kilowatt-level fiber lasers and amplified laser systems have been demonstrated recently [1, 2].

A double clad amplifying fiber is a key component of a fiber laser. This fiber usually contains a core doped with rare earth elements and the cladding, where pump radiation propagates. Small-signal cladding pump absorption can be estimated from the expression [3]:

$$\alpha_{DCfiber} = \alpha_{core} \cdot \frac{A_{core}}{A_{clad}} \qquad (1)$$

where α_{core} is core absorption, A_{core}, A_{clad} are core and cladding areas, correspondingly.

It can be seen from this equation that the pump absorption increases with the core absorption α_{core}, i.e. with doping level and/or with the core/clad ratio. These two options available for improvement of the efficiency of pump absorption are, however, restricted.

#89552 - $15.00 USD Received 9 Nov 2007; revised 20 Dec 2007; accepted 14 Jan 2008; published 28 Jan 2008

Particularly, the photodarkening effect [4-6] and background loss [7] set the upper level of rare ions concentration. The acceptable level of in-core absorption limited by the photodarkening effect is about 600-800 dB/m at 976 nm. But even when photodarkening effect is low, a high concentration of dopants may lead to a notable background loss of up to 50-200 dB/km caused by partial glass crystallization in the presence of rare earth ions [7]. The high level of background loss would obviously result in poor efficiency of the fiber lasers and amplifiers. This is one reason why the typical slope efficiency observed experimentally from ytterbium double clad fiber lasers and amplifiers is below 70-80 % [2, 8-10], though the theoretical limit is over 90 %.

Another method of pump absorption enhancement is scaling of the core/clad ratio. This can be achieved in two ways. First, an increase of the core diameter with simultaneous reduction in the numerical aperture (e.g., down to 0.05 in [2]) allows the V-parameter to be kept relatively small, e.g. V=5.7 in [2] and V=7.4 in [8]. With appropriate bending of the fiber, a nearly diffracted-limited beam quality could be maintained even with enlarged core diameter, e.g. M^2=1.4÷1.6, as shown in [2, 8]. Another way to increase the core/clad ratio is to use a photonic crystal fiber (PCF) with a large outer fiber size [9, 10]. However, such devices can not, however, be anymore regarded as truly fiber systems since PCF now represents an unbendable rod-like gain medium with a diameter of a few millimeters. The quality of the fundamental mode regime and the corresponding value of M^2 that can be achieved using this approach are still to be reported [10]. It should be noted that the analysis made using Eq. (1) is incomplete since it does not take into account saturation of pump absorption. Indeed, the pump radiation in a cladding propagates in a highly multimode regime. Effectively, it is possible to sort out all these modes into two groups – "well absorbed" and "weakly absorbed" modes. The modes of the first type have an axially symmetrical field distribution with a maximum of intensity at the doped core in the center of a fiber, and are well absorbed, thus contributing efficiently to gain. The other group includes the modes that have poor overlap with the doped core and, therefore, do not contribute notably to pump absorption. These modes could, however, carry a significant fraction of pump power.

In terms of ray optics, there are meridian rays which propagate along the fiber crossing an optical axis of the fiber and skew rays, which are also guided, but propagate in spiral trajectories without core crossing and, as result, without significant absorption. Schematically pump absorption occurs according to the following scenario. The "meridian" modes are absorbed very quickly during the propagation through the initial meters of fiber, while the residual unabsorbed pump corresponding to the "skew" modes propagates practically without significant absorption. Consequently, the first meters of a fiber have significantly higher absorption since the modal content of the pump in double clad fiber is varies strongly along the fiber.

The decrease in pump absorption with propagation distance could be prevented by using a fiber with broken axial symmetry. Among numerous shapes of proposed fiber cross-section, the most popular are truncated or D-shaped, double truncated or double D-shaped, core-offset, octagonal and helical fibers [3, 11-18]. Generally, this method, however, does not eliminate the saturation of pump absorption; instead, the saturation length just becomes slightly longer [12]. An essential problem with non-symmetrical fiber is practical handling. Indeed, the splice of non-symmetrical and conventional circular fibers usually exhibits optical losses for both pump and signal.

An alternative solution for enhancing the pump absorption is introducing the non-regularity in the mode propagation by external mechanical perturbations. Granular matter embedded chaotically in the cladding would cause a non-regular periodical bending of the fiber and lead to a chaotic mode coupling [19]. This mode coupling would direct power from "weakly absorbed" modes to "well absorbed" modes. This technique could be effectively applied only to thin fibers, typically up to 125 μm of outer diameter because the mode coupling coefficient is inversely proportional to the sixth power of the fiber outer diameter [20]. The embedding of "truncated regions" or "filaments" directly into the cladding enhances

#89552 - $15.00 USD Received 9 Nov 2007; revised 20 Dec 2007; accepted 14 Jan 2008; published 28 Jan 2008

the scattering of pump light propagated in the cladding [21]. Obviously, this causes efficient mode mixing; however, it would also inevitably lead to a certain loss of pump.

Marcuse has shown that the bending could induce an efficient mode coupling to the waveguide [22]. Based on this observation, non-regular properties could simply be achieved by coiling fibers with special shapes, e.g. kidney, figure-eight, etc. that apply different radii of bending to different fiber locations. As it was shown in [23], bending of one-meter-long piece of Er-Yb fiber could increase absorption by 10.7 dB: from 2.7 dB for straight fiber to 13.4 dB after figure-eight bending. Unfortunately, since the absorption depends strongly on the specific shape of a fiber, this technique has poor reproducibility. Apparently, this approach can be applied only to relatively thin fiber, typically with a diameter less than 400 μm.

Thus, considering that the pump absorption can be essentially increased by using various mode mixing methods, Eq. (1) should be modified by introducing a *mode scrambling factor* ***S***:

$$\alpha_{DCfiber} = \alpha_{core} \cdot \frac{A_{core}}{A_{clad}} \cdot S \qquad (2)$$

The value of the factor ***S*** depends on the exact mechanism of mode mixing applied for a given fiber and could describe the observed increase in pump absorption [23].The factor S is a ratio of pump absorption in an arbitrary, e.g. longitudinally or transversally non-uniform DCF relative to absorption in a circular, symmetrical and uniform double clad fiber with the same in-core absorption and core/clad area ratio. The value of S factor, therefore, shows an increase in the pump absorption induced by the enhancement of the mode mixing owing to the broken transversal symmetry or longitudinal scrambling in a fiber.

In this work we propose and demonstrate a tapered double clad fiber (T-DCF) that offers a significantly enhanced capability for pump absorption. The proposed fiber design allows for efficient launching of pump light, could have high immunity to photodarkening, and superior slope efficiency. Such fiber has a number of obvious advantages as compared to regular fibers:

- Efficient intrinsic mode scrambling mechanism for cladding modes. Significant pump absorption in a fiber is due to large value of mode scrambling factor ***S*** rather than to a high dopants concentration or a large core/clad ratio. Therefore, using an active tapered fiber allows remarkable properties to be achieved - a high pump absorption in combination with low dopants concentration featuring low background loss. A low doping level would also result in substantial suppression of the photodarkening effect and background losses would allow for efficiency approaching the ultimate value of 90 % attainable for ytterbium fiber;
- Large clad diameters, perhaps up to 2 mm, make T-DCF suitable for using pump sources with poor beam parameter product (BPP) (50- 300 mm×mrad) and would allow for essential increase in output power;
- Fundamental mode operation could be preserved for large core diameter (tens of microns).

2. Properties of tapered double clad fibers with active core

Tapered active double clad fiber can offer attractive features as compared to ordinary, axially uniform, fibers. The most important properties are a high rate of cladding pump absorption, non-reciprocity of spectral response and high slope efficiency (or pump conversion efficiency). In this section we will discuss the special features of light propagation caused by tapered geometry.

#89552 - $15.00 USD Received 9 Nov 2007; revised 20 Dec 2007; accepted 14 Jan 2008; published 28 Jan 2008

2.1. Pump absorption in T-DCF

As it was mentioned above, the saturation of the pump absorption caused by preferable absorption of certain modes is a main disadvantage of axially regular double clad fibers. The intrinsic reason of this property is the identical characteristics of the regular DCF waveguide over the entire length. T-DCF as an essentially non-regular waveguide has a distinguishing difference owing to the gradual change in the mode content along the fiber. Strictly speaking, the modes in T-DCF should be identified for every given cross-section independently and it is unconstructive to introduce the modes for entire T-DCF.

Following to Marcuse [24], the T-DCF can be approximately modeled with a sequence of uniform multimode fibers with different diameters, as it is shown in Fig. 1. Each of these "partial fibers" guides the specific set of modes. The excitation of *all guided* modes then occurs in the consecutive fiber by illumination from the preceding fiber with larger diameter thus recovering the quasi-equilibrium mode distribution broken by the mode-dependent absorption [24].

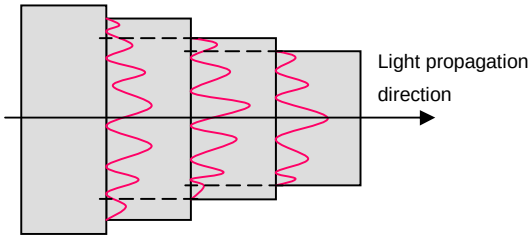

Fig. 1. T-DCF: the optical equivalent scheme

The different overlap of modes with fiber core allows to distinguish well and weakly absorbed modes in each partial uniform fiber in this step-like taper structure. The fraction of the pump power initially concentrated in the "well absorbed" modes will be rapidly depleted; therefore, the mode content gradually evolves in a partial fiber due to different mode absorption in favor of weakly absorbed modes. This schematic presentation of the tapered structure simulates the mechanism when the "quasi-equilibrium" mode content lost by the selective mode absorption in the uniform part of the guide is recovered at the step-like transition by excitation all guided modes thus ensuring the efficient mechanism for mode mixing. Similarly, the mode content modified by different mode absorption during the light propagation in T-DCF is continuously recovered and thus the population of "well absorbed" modes is maintained.

Ytterbium doped T-DCF was made by drawing on a tower with special pulling regime. The total length was 10.5 m and cladding diameter was dependent on the length as shown in Fig. 2. The preform fabricated by plasma chemical deposition technology [25] has been polished at one side with a 1:0.88 ratio. The preform was then coated by fluorosilicate glass with a low refractive index. Core/clad diameter ratio was 1:31 and numerical apertures of core and cladding were 0.114 and 0.21, respectively. The cross section of fiber is shown in the Fig. 2 as an inset. The core and cladding diameters of the wide part of the tapered fiber were 27 and 834 μm, respectively; the dimension of the truncated part was 732 μm. The core and cladding diameters of the narrow part were 5.8 and 177 μm. The length-dependent outer diameter and corresponding normalized frequency $\boldsymbol{V}$ with a maximum value of $\boldsymbol{V}$=9.1 is shown in Fig. 2. The taper ratio is 1:4.8. The shape of the fluorosilicate glass cladding was slightly non-uniform and varied within a 35-54 μm range, as seen from Fig. 2, inset.

#89552 - $15.00 USD Received 9 Nov 2007; revised 20 Dec 2007; accepted 14 Jan 2008; published 28 Jan 2008

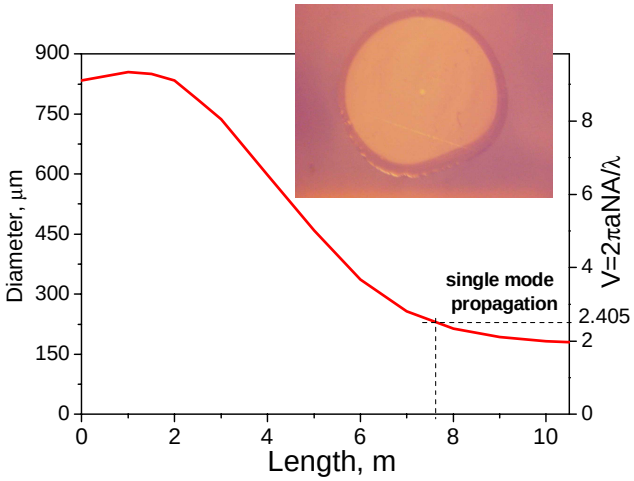

Fig. 2. T-DCF clad diameter and normalized frequency as function of fiber length.

The small-signal in-core pump absorption is 280 dB/m at 976 nm. The measured pump absorption in T-DCF was 9.6 dB or 0.9 dB/m. The background loss of T-DCF found from measurement was 10 dB/km at 1μm.

Double clad pump absorption of uniform (non-tapered) fiber with 1:31 core/clad ratio and core absorption of 280 dB/m was found from Eq. (1) to be 0.29 dB/m. The experimentally measured pump absorption of longitudinally uniform fiber pulled from the same preform as the taper has demonstrated an even lower value of 0.22 dB/m at 976 nm. By contrast, the pump absorption of the double clad T-DCF was 0.9 dB/m. In other words, the pump absorption increases compared with ordinary double clad fiber due to a higher value of the mode scrambling factor ***S*** [Eq. (2)] which rises from 1 for uniform fiber to 4.1 for T-DCF. The higher level of double clad pump absorption can be explained by efficient cladding mode mixing occurring in the T-DCF.

2.2. Non-reciprocity of T-DCF

The non-reciprocal spectral response is an interesting property of a T-DCF. Indeed, the taper has demonstrated essentially different spectral characteristics for different directions of light propagation. Generally speaking, the taper spectral selectivity is a known effect which has been observed earlier [26, 27], though it was not studied in detail.

The T-DCF spectral selectivity has been studied experimentally. The spectral response of the tapered fiber has been measured with an optical spectrum analyzer and light from the broadband source launched into the fiber core.

The results of experiment displayed in Fig. 3 show the spectral transmission for light propagation from wide-core end towards narrow-core end (black line) and for the opposite direction (red line).

The physical mechanism behind this phenomenon is the multimode character of light propagation in a wide section of the taper, whereas the narrow part of it is a single-mode waveguide. Due to modal interference in the wide multimode part of the taper and subsequent spatial filtering in the single-mode part, the intermodal phase delays are converted into a light intensity modulation. This effect has been studied earlier for multimode fiber as a technique for differential phase modulation [28]. Obviously, the intensity of this intermodal interference pattern has strong wavelength dependence.

#89552 - $15.00 USD Received 9 Nov 2007; revised 20 Dec 2007; accepted 14 Jan 2008; published 28 Jan 2008

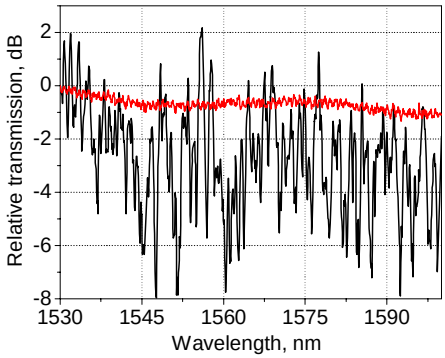

Fig. 3. Transmission characteristic of T-DCF: from wide end towards narrow end (black line) and in the opposite direction (red line).

Spectral selectivity can be observed only for light propagating towards a narrow single-mode section of the taper and when the multimode radiation has been excited in the wide section of taper. Conversely, when light propagates from the narrow to the wide section of the T-DCF, the spatial filtering owing to the interference pattern and, consequently, the spectral selectivity will not be developed. Spectral selectivity will obviously be suppressed when only the fundamental mode has been launched into the multimode end of taper.

As expected from the above consideration, T-DCF displays a strong spectral selectivity with a contrast up to 10 dB for the propagation direction from the wide end towards the narrow end, as seen from Fig. 3 (black line). The specific shape of the spectral dependence is determined by the spectrum of the guided modes excited in the fiber core at the wide end of a taper. In the opposite direction for light propagating from the narrow towards the wide end there is no signature of any spectral selectivity, as can be seen from Fig. 3 (red line).

Another distinctive feature of an active tapered fiber is a difference in the numerical apertures for light propagating in different directions. We assume that the light with large angle divergence, e.g. amplified spontaneous emission (ASE), propagates in a taper, as schematically illustrated in Fig. 4.

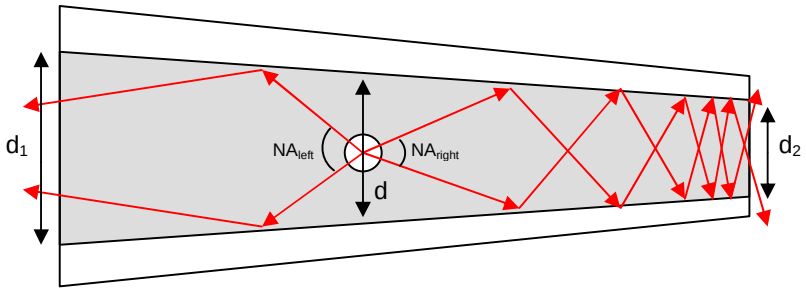

Fig. 4. Ray traces in a cladding of T-DCF.

The numerical apertures for ASE propagating from the fiber position with the local diameter ***d*** towards the narrow end and wide end, respectively, without vignetting are different and can be expressed in the form [29]:

$$NA_{right} = \frac{d_2}{d} \cdot NA_{core} - \theta \sqrt{n^2{}_{core} - NA_{core}{}^2 \cdot \left(\frac{d_2}{d}\right)^2} \quad \text{and} \tag{3}$$

#89552 - $15.00 USD Received 9 Nov 2007; revised 20 Dec 2007; accepted 14 Jan 2008; published 28 Jan 2008

$$NA_{left} = \frac{d_1}{d} \cdot NA_{core} + \theta \sqrt{n^2{}_{core} - NA_{core}{}^2 \cdot \left(\frac{d_1}{d}\right)^2} \quad , \tag{4}$$

where d_1, d_2 are core diameters at the wide and narrow ends of taper, respectively, $NA_{core} = \sqrt{n^2{}_{core} - n^2{}_{clad1}}$, θ is the angle of the core taper, equal approximately to $(d_1 - d_2)/2L$, L is the length of the taper.

The angle θ is small, about 1 μrad and, therefore, the ratio of numerical apertures can be found from Eqs. (3) and (4):

$$\frac{NA_{right}}{NA_{left}} = \frac{d_2}{d_1} \tag{5}$$

This expression shows that for any local cross-section of the taper, the ASE power emitted towards the wide end is higher than the power guided to the opposite direction by a factor d_1^2/d_2^2.

2.3. Pumping of T-DCF

The rays propagating in an axially uniform cylindrical optical fiber undergo multiple total internal reflections and maintain the certain angle of propagation with respect to the fiber axis. In contrast, the ray trajectory of light traveling in the T-DCF gradually changes its angle relative to the optical axis of the fiber after each reflection [29, 30]. Eventually, when the propagation angle of the pump radiation exceeds the critical angle of total internal reflection, the light could not be confined within the pump cladding, i.e. it radiated away from the fiber by the so-called vignetting process.

Thus, the two basic mechanisms of pump depletion in T-DCF are vignetting and absorption in the active core. The contribution of each mechanism can be estimated using the numerical aperture for pump radiation guided by the cladding. The numerical aperture of the cladding NA_{clad} for the light propagating from large to small end of the taper without vignetting can be found from the expression [29]:

$$NA_{clad} = \frac{D_2}{D_1} \cdot NA - \Omega \sqrt{n^2{}_{clad1} - NA^2 \cdot \left(\frac{D_2}{D_1}\right)^2} \quad , \tag{6}$$

where D_1, D_2 are cladding diameters for wide and small ends of the taper, respectively, $NA = \sqrt{n^2{}_{clad1} - n^2{}_{clad2}}$, Ω – angle of a taper cone, approximately equals to $(D_1 - D_2)/2L$, L – length of the taper.

The estimation for the numerical aperture of the cladding for the light propagating towards the small-diameter taper end obtained from this expression is then NA_{clad} =0.044.

The fraction of the pump power lost due to a vignetting in T-DCF has been experimentally estimated using the laser setup shown in Fig. 5(b). The lens with a high numerical aperture of NA=0.15 (>>NA_{clad}=0.044) was used for pump launching. The pump conversion efficiency of the laser of 82 % found from the measurement was close to the theoretical limit of 92 % determined by the quantum defect, i.e. by $\lambda_{pump}/\lambda_{signal}$ ratio. This feature gives evidence that the pump loss due to vignetting could be neglected and the actual loss of pump power is mainly due to ytterbium ions absorption.

Additionally, the launching scheme with fully filled numerical aperture (NA=0.21) had been studied to illustrate this effect. The slope efficiency of the laser was found to drop down to 30% providing direct evidence of high pump loss due to vignetting when the angle aperture

#89552 - $15.00 USD Received 9 Nov 2007; revised 20 Dec 2007; accepted 14 Jan 2008; published 28 Jan 2008

is entirely filled. Therefore, the pump light should be launched into a taper by filling only the fraction of the angle aperture to avoid early vignetting before significant depleting of the pump occurred.

3. Experimental demonstration of T-DCF applications

3.1. Ytterbium doped tapered fiber laser and superluminescent source

Several optical sources based on T-DCF have been constructed during the course of this study – the lasers and a high power superfluorescent source.

The fiber lasers with T-DCF are shown in Figs. 5(a) and 5(b). The emission of a multimode-fiber coupled pump diode laser was used as a pump source with a core/clad ratio and numerical aperture of the multimode fiber of 200/220 μm and NA=0.22, respectively. 135 W at 976 nm from the multimode fiber output of the pump diode laser were launched into a wide part of taper via lenses and dichroic filter resulting in a total coupling efficiency of 85%.

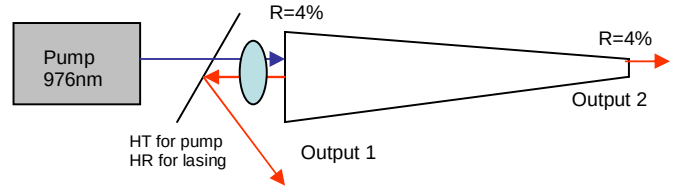

a. Laser with 4%-4% cavity

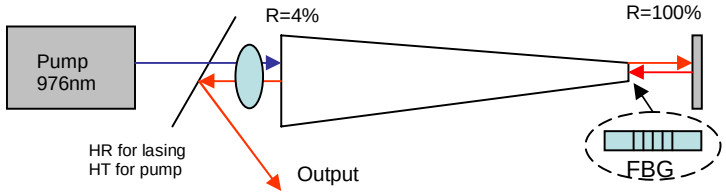

b. Laser with HR broad band mirror or FBG

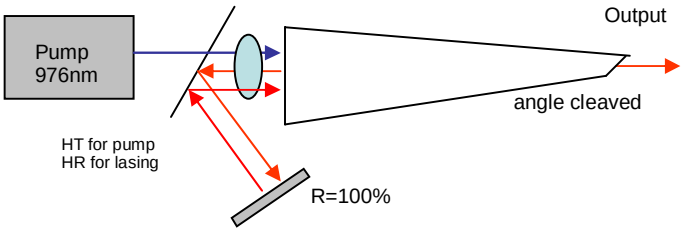

c. Superluminescent source

Fig. 5. Schematics of optical sources with T-DCF.

Three different laser configurations have been investigated experimentally. First, a cavity was formed by 4% Fresnel reflections from both taper ends, as shown in Fig. 5(a). The second cavity uses Fresnel reflections from the wide-core end of the taper and high reflecting (HR) broadband mirror as the other cavity reflector, see Fig. 5(b). The third laser cavity tested contains a fiber Bragg grating (FBG) spliced with the narrow-core side of the taper, see Fig. 5(b), inset.

The of output power as a function of absorbed pump power for the $R_{1,2}$=4%;4% cavity is shown in Fig. 6. The laser generates dominantly throughout a wide-core output 1 indicated in Fig. 5(a) with a ratio of powers radiated through output 1 and output 2 of approximately 1:25.

#89552 - $15.00 USD Received 9 Nov 2007; revised 20 Dec 2007; accepted 14 Jan 2008; published 28 Jan 2008

The slope efficiency for output 1 in this laser is 91.8%, and the slope efficiency for the total power (output 1 plus output 2) is 93.2%, both with respect to the absorbed pump power.

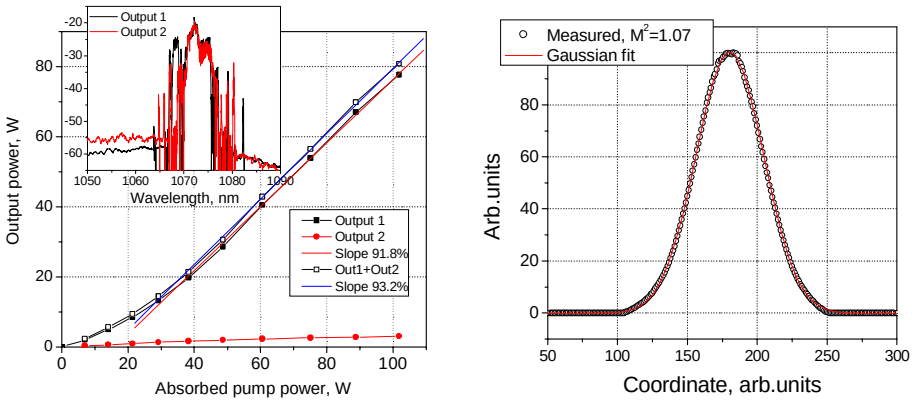

(a) (b)

Fig. 6. Output characteristics of T-DCF laser with $R_{1,2}$=4%;4%. (a) Output power versus absorbed pump power; Inset : emission spectra for output 1 (black line) and output 2 (red line). (b): beam profile (dots) and Gaussian fit (red line) for output 1. M^2=1.07.

Highest pump conversion efficiency achieved for both outputs is 79.3%. It can be seen from Fig. 6 (inset), that the spectra of emission coming from wide and narrow ends of a tapered laser are essentially different.

The output power versus absorbed pump power for the laser with a broadband high reflective mirror [Fig. 5 (b)] is shown in Fig. 7(a) with a spectrum plotted in Fig. 7(b).

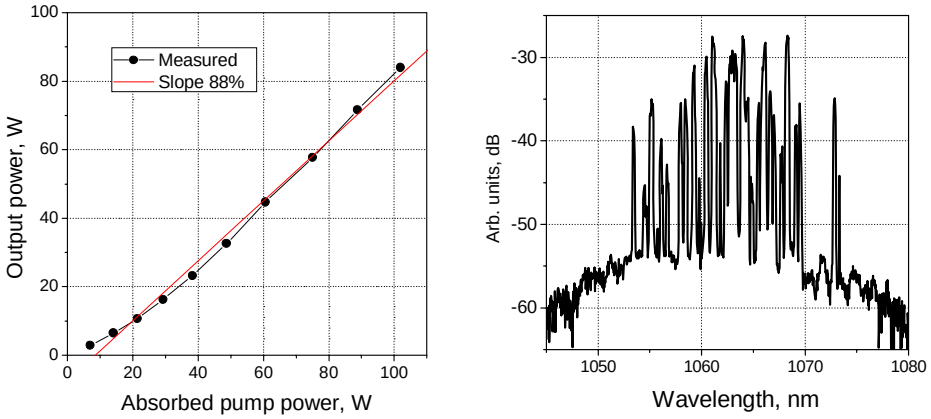

(a) (b)

Fig. 7. Output characteristics of T-DCF laser with broadband HR mirror: (a) output power versus absorbed pump power (b) spectrum of output radiation.

The slope efficiency of this laser with respect to the absorbed pump power is 88 %. Pump conversion efficiency is 82% for available pump power.

#89552 - $15.00 USD Received 9 Nov 2007; revised 20 Dec 2007; accepted 14 Jan 2008; published 28 Jan 2008

The dependence of output power as a function of absorbed pump power for the laser cavity with FBG as a reflector is shown in Fig. 8(a). Three FBGs operating with center wavelengths of 1063 nm, 1080 nm and 1083 nm have been investigated experimentally.

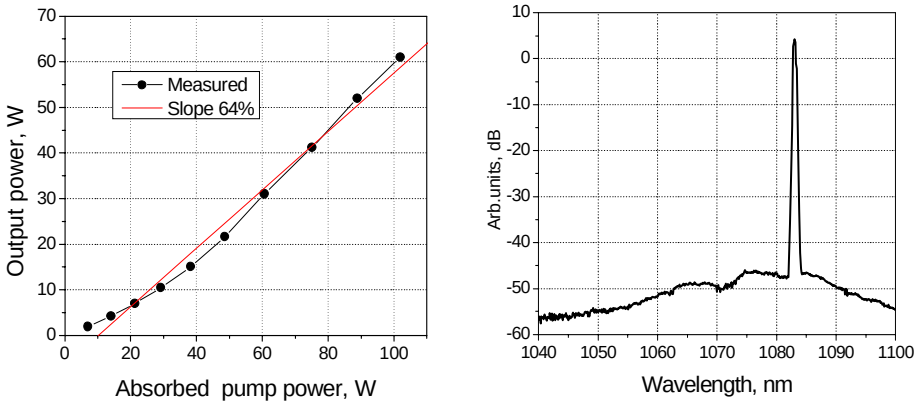

(a) (b)

Fig. 8. Output characteristics of T-DCF laser with FBG : (a) output power versus absorbed pump power (b) spectrum of output radiation.

The typical output radiation spectrum for the laser with FBG is presented in Fig. 8(b). The slope efficiency of the laser with λ=1083 nm was 64 %. All configurations of tapered fiber laser demonstrate robust single transverse mode operation with M^2=1.07, as seen from Fig. 6(b). The beam quality factor M^2 has been measured using calibrated BeamScope-P7, DataRay Inc. The measurements did not reveal measurable difference in beam factor M^2 for both outputs.

A high power superluminescent source based on T-DCF has also been studied experimentally. The setup of the source is shown in Fig. 5(c). The radiation coming from the wide-core side of the taper was coupled back into the core by a lens and broadband mirror, as seen from Fig. 5(c). The narrow end of tapered fiber was angle cleaved with 8 degrees.

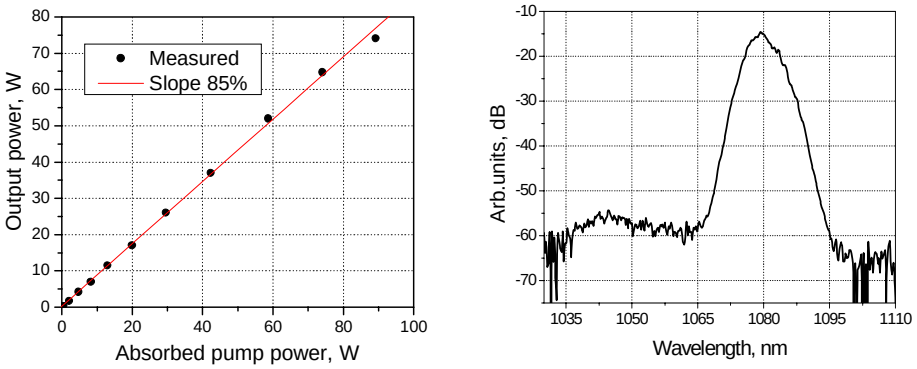

(a) (b)

Fig. 9. Output characteristics of T-DCF superluminescent source: (a) output power versus absorbed pump power (b) spectrum of output radiation.

#89552 - $15.00 USD Received 9 Nov 2007; revised 20 Dec 2007; accepted 14 Jan 2008; published 28 Jan 2008

The dependence of the output power of the superluminescent source on absorbed pump power is shown in Fig. 9(a).Superluminescent source generates broadband radiation with a FWHM of 5.5 nm and a central wavelength at 1079 nm [Fig. 9(b)]. The threshold-free dependence of the output power versus absorbed pump power reveals that the slope efficiency of 85% is equal to the pump conversion efficiency.

3.2. Ytterbium doped tapered fiber amplifier

Efficient operation of a T-DCF amplifier has been achieved experimentally, as described below. The scheme of the experimental setup is shown in the Fig. 10. The seed signal was launched into a single-mode narrow-core taper end via an optical isolator and 1:99 tap coupler. We have examined the performance of tapered amplifier for two types of seed signals - pulsed and continuous-wave narrowband.

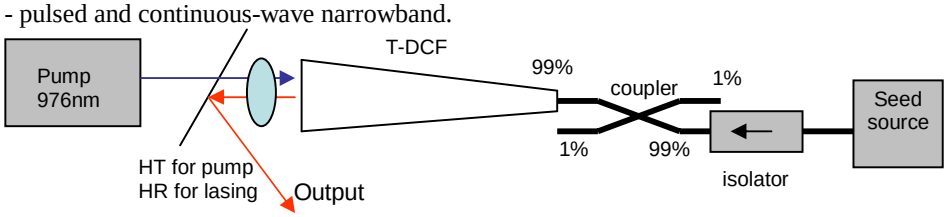

Fig. 10. Amplifier with T-DCF: experimental set up

A mode locked picosecond fiber laser with τ_{pulse}=4 ps, $f_{reprate}$=100 MHz, P_{ave}=50 mW and λ=1063 nm has been used as a seed source. The spectrum and autocorrelation function of the seed signal are shown in Fig. 11(a), inset and Fig. 11(b) with black lines, respectively.

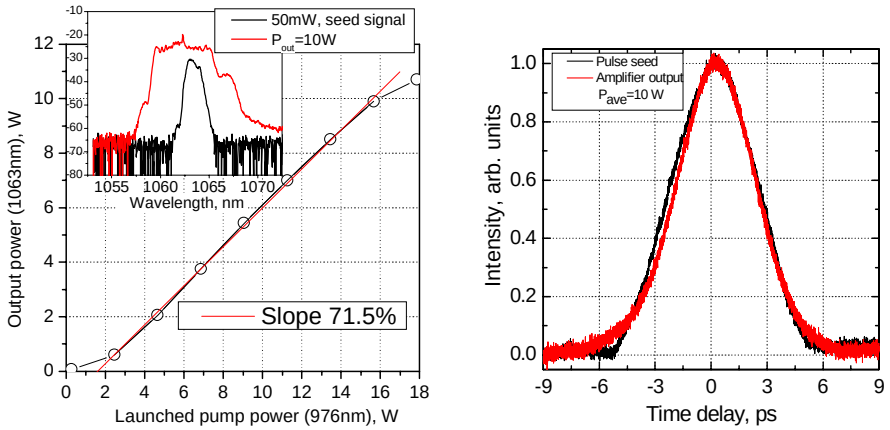

(a) (b)

Fig. 11. Output characteristics of T-DCF pulsed amplifier : (a) average output power versus launched pump power (circles); inset : seed source spectrum (black line) and amplified signal spectrum (red line). (b) autocorrelation function of seed signal (black line) and amplified signal (red line).

The dependence of the average output power versus launched pump power is shown in Fig. 11(a). We obtained 10.7 W of average output power for a 50-mW seed signal corresponding to a 23.3 dB gain. Slope efficiency was 71.5 % with respect to the launched pump power. The spectrum and autocorrelation function of the amplified signal are displayed in Fig. 11(a) inset and Fig. 11(b) with red color, respectively.

The performance of T-DCF for amplification of a CW signal with linewidth less then 100 kHz at FWHM has been studied. This amplification regime is usually affected severely by a

#89552 - $15.00 USD Received 9 Nov 2007; revised 20 Dec 2007; accepted 14 Jan 2008; published 28 Jan 2008

stimulated Brillouin scattering (SBS). In experiments we have used a DFB fiber laser with 30 mW of output power as a seed source. The back scattered emission was recorded through a 1% coupler port as shown in Fig. 10.

The dependence of the output power signal as a function of launched pump power is shown in Fig. 12(a). The amplifier has demonstrated 80% slope efficiency with respect to launched pump power and 25.4 dB gain. The spectra of input and amplified signals are shown in Fig. 12(a) inset.

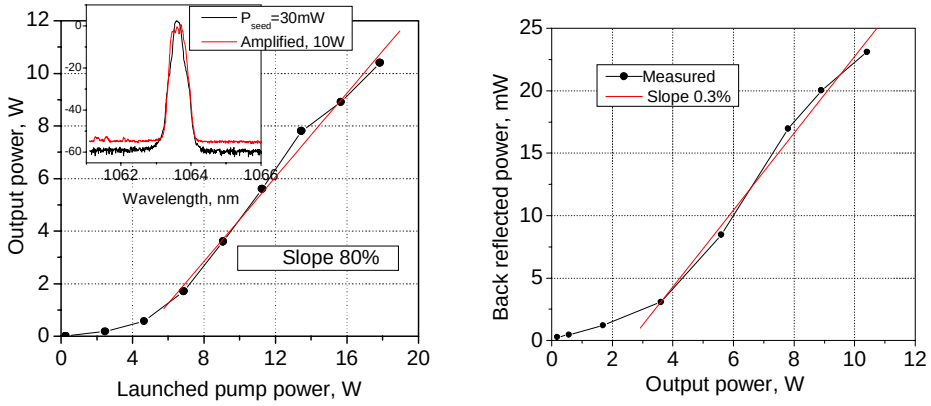

(a) (b)

Fig. 12. Output characteristics of T-DCF amplifier with CW seed signal: a. output power versus launched pump power (black circles); inset: seed source spectrum (black line) and amplified signal spectrum (red line). b. back reflected light power as a function of output power.

The level of backscattered power has been detected as a function of output power and plotted in Fig. 12(b). As we can see, less than 0.3% of output power is scattered back, providing clear evidence of strong SBS suppression. The output beam has a Gaussian shape with M^2=1.07.

4. Discussion

The tapered double-clad gain fiber proposed and demonstrated here represents a novel design of optical amplifier (laser) with unique feature offering a diffraction-limited large-area mode and efficient pump absorption. The wide end of tapered fiber cone allows to couple efficiently the pump radiation from the sources with large beam parameter product, BPP, and to expand the mode field of the radiation guided by the core. The narrow section of the taper acts as a spatial mode filter for higher-order modes resulting in a diffraction-limited quality of the output beam. A significant increase in the pump absorption due to efficient mode scrambling in a fiber taper allows the use a moderate concentration of the dopants in the core thus reducing the background loss to the level below 10 dB/km and preventing the photodarkening effect. The pump-to-signal conversion of 82% and the slope efficiency of 93.2% observed in the experiments have been obtained owing to low cavity losses achievable with tapered gain fiber.

Apparently, the T-DCF using is most prominent for pumping by high power pump sources with poor BPP. The requirement of just partially filling numerical aperture imposes certain limitations on the BPP of the pump source. Although theoretically, the pump source with BPP of 80 mm×mrad can be used for T-DCF with 830 μm cladding diameter and NA=0.21, the above mentioned aperture limitation dictates the use of pump sources with BPP below 60 mm×mrad. Technically, it is possible to fabricate the T-DCF with clad diameter increased up to 2-mm and raise the aperture to NA=0.37 using the fluorosilicate glass coating or to NA=0.5

#89552 - $15.00 USD Received 9 Nov 2007; revised 20 Dec 2007; accepted 14 Jan 2008; published 28 Jan 2008

with polymer coating. Taking into account the requirement for partial, possibly below 70 %, filling of the numerical aperture, for a taper with a 2-mm clad diameter and NA=0.37, pump sources with BPP 250 mm×mrad can be used. When the fiber aperture is increased to NA=0.5, the pump could have a beam parameter of 350 mm×mrad.

There is another practical advantage of the taper. For large outer diameters, the longitudinally uniform PCF cannot be bended because of the large effective diameter-to-length ratio. Instead, T-DCF with comparable length has significantly lower diameter-to-length ratio, i.e. the fraction of wide part in the taper could be short and, consequently, the tapered fiber can be easily bended even for diameters of 2 mm.

The non-reciprocal pump absorption and modal evolution in a tapered fiber provide a mechanism for preferable lasing in the direction towards the wide end of the taper. Indeed, the ratio of powers emitted through output 1 and output 2 in a laser with 4%-reflective cavity mirrors, shown in Fig. 5(a), is adequately described by the factor d_1^2/d_2^2 for the T-DCF mentioned in the previous section. The difference in the lasing spectra measured from output 1 and 2, seen in Fig. 6 at the inset, indicates the spectral non-reciprocity of the taper. Different dynamics of mode evolution in a taper for counter-propagating beams discussed above provide an effective "non-reciprocal" filtering effect that result in dissimilar spectra emerging from opposite ends of the taper.

The spectral spiking behavior in a laser with a HR broadband mirror, shown in Fig. 7(b), occurs in the laser because of the spectral selectivity of the taper. ASE is spectrally modulated during the propagation from the wide end towards the narrow end, as shown in Fig. 3 (black line), in agreement with the interferometric mode filtering mechanism discussed above. Simultaneously, the emission appears to be spatially single-mode at the narrow end of the laser cavity. After reflection from the HR mirror, as shown in Fig. 5(b), the single-mode light propagates back towards a wide section of taper and as a result, the output spectrum of the laser consists of discrete lines with a total spectral bandwidth of 20 nm.

Spectral selectivity of T-DCF, however, may limit the laser efficiency when using a fiber Bragg grating as a cavity reflector. The spectral response of the cavity affected strongly by the spectrum of excited modes in the wide part of the T-DCF core is irregular and rather complicated, as seen from Fig. 3. Therefore, insertion in the cavity of the FBG as a wavelength filter would be unavoidably accompanied with additional losses. Using FBGs with different reflectivities and center wavelengths, we have observed that the slope efficiency never exceeded 50-70%, as seen from Fig. 8.

The non-reciprocal spectral response of the taper affects the performance of high power superluminescent source, Figs. 5(c) and 9. During the first pass towards the wide taper end, ASE does not acquire any spectral modulation, as has been argued above. After reflection from the broadband mirror, the ASE propagates in a fundamental mode and is coupled back to the wide end of a taper. The spectral modulation due to differential modal phase modulation disappears since the laser operates at the fundamental mode during consecutive passes through the T-DCF. The design of a CW high power broadband single spatial mode optical source with output at the level of hundreds of watts is actively discussed in the literature [31]. Typically such optical sources are cumbersome devices based on the ASE seed source with good beam quality and power amplifier [31]. Using T-DCF pumped by a diode stack bar, a highly efficient and high power single-transverse-mode broadband source can be realized with rather straightforward technology. The preliminary results reported here demonstrate generation of 74-W fundamental mode broadband radiation (FWHM 5.5 nm) with excellent pump conversion efficiency of 85%. The output power is scalable and was limited only by available pump power.

Active tapered fiber is particularly attractive for use in high power amplifiers. The large core diameter of T-DCF offers an advanced capability for energy storage with reduced nonlinear distortion. An amplifier with gradually increased core diameter already has been investigated earlier, the so-called "flared amplifier" with three consecutive sections of fibers with different core diameters [32]. Using a T-DCF allows realization of a similar amplifier in a more practical way and avoids mode conversion and losses at the fiber splices.

#89552 - $15.00 USD Received 9 Nov 2007; revised 20 Dec 2007; accepted 14 Jan 2008; published 28 Jan 2008

A T-DCF based pulsed amplifier has been studied providing 23.3 dB gain for the input signal from the mode-locked seed source with a pulse duration of τ_{pulse}=4 ps and a repetition rate of f_{rep}=100 MHz. For an average output power of about 10 W, the amplified pulse shape remains practically undisturbed though the spectrum of the pulse acquires significant broadening due to self-phase modulation shown in Fig. 11(a), (inset). Apparently, the parameters of the T-DCF amplifier were not optimized for ultra short pulse seed signal. Namely, the length of T-DCF is too long, while the core diameter of the single-mode section is too small. Nevertheless, due to the good beam quality of the amplified signal, corresponding to M^2=1.07 for 27 μm core diameter with V=9.1, an essential improvement in the performance of the T-DCF amplifiers for high power ultra short pulse applications can be expected.

Amplification of highly coherent radiation is another important application where T-DCF could have a clear advantage. Efficient high power coherent beam combining requires laser beams with extremely long coherent lengths and with spectral bandwidths below 50 kHz (FWHM). The saturation power of such amplifiers should be on the order of hundreds of watts or even kilowatts. The main obstacle for power scaling with this technique is stimulated Brillouin scattering (SBS) which imposes a limitation on the output power of the single-frequency radiation [33]. Power scaling in such systems assumes an essential increase in the threshold of SBS [34, 35]. One proposed solution exploits the acoustic properties of fiber core when the temperature gradient is gradually varied along the fiber owing to the longitudinal change in the pump absorption [34]. Obviously, this approach requires an extraordinarily high pump power that ensures sufficient longitudinal temperature gradient in the fiber. Alternatively, the fiber could be heated with an external furnace, which is, however, unlikely to be the practical solution to the problem [36]. In contrast to the abovementioned techniques using an artificially induced longitudinal variation in the guide properties, the T-DCF amplifier has a natural immunity to SBS due to in-built axial non-uniformity. The increase in the SBS threshold in passive fiber with variable core diameter has been demonstrated earlier [37] and the tapered amplifier would clearly benefit from similar effect when using with narrow band seed signal. Use of an optically pumped T-DCF amplifier may, however, be accompanied by certain broadening of the Brillouin gain spectrum due to heating [34]. A 25.4 dB high gain amplifier reported here, producing over 10 W of output power for 30-mW seed signal, reveals no signature of SBS, as shown in Figs. 12(a), 12(b). The slope efficiency of the amplifier was 80% for a Gaussian beam shape with M^2=1.07 and only 0.3 % of output power was scattered back.

It is important to note that although the single-mode section of the amplifier has a core diameter of only 5.8 μm, the SBS signal has not been measurable. A further optimization of the T-DCF design should also allow for an essential increase in the saturation power of these amplifiers.

5. Conclusion

A double clad tapered fiber as a gain medium for high power lasers, superluminescent sources and amplifiers has been proposed and demonstrated in this study for the first time. A large clad diameter of tapered fiber allows optical pumping with low brightness sources available commercially with powers up to 6 kW [38]. The specific features of the tapered fiber, e.g. non-reciprocal spectral response and non-reciprocity of the numerical aperture, have been systematically studied. It was demonstrated that an efficient intrinsic mode scrambling mechanism ensures enhanced pump absorption in a tapered fiber with a relatively low doping level. The tapered fiber with modest doping level applicable due to enhanced pump absorption is expected to have a strongly suppressed photodarkening effect and reduced background losses. All these features result in the high efficiency of lasers and amplifiers demonstrated in this study.

A T-DCF based laser producing 84 W with a slope efficiency of 93% and pump conversion efficiency of 82%, a 74 W superluminescent source with pump conversion efficiency of 85% and an amplifier for both pulsed and CW high coherent radiation with slope

#89552 - $15.00 USD Received 9 Nov 2007; revised 20 Dec 2007; accepted 14 Jan 2008; published 28 Jan 2008

efficiency of 80% have been demonstrated. The output power of the devices is scalable and was limited here by the pump power available for these experiments. The output beam has a diffraction-limited property with a typical quality parameter of M^2=1.07.

We believe that double clad tapered fiber technology using low brightness pump sources represents an exciting opportunity for essential power scaling with excellent pump conversion efficiency and superior output beam quality.

#89552 - $15.00 USD Received 9 Nov 2007; revised 20 Dec 2007; accepted 14 Jan 2008; published 28 Jan 2008

Appendix 2

Publication 2

J. Kerttula, V. Filippov, Y. Chamorovskii, V. Ustimchik, K. Golant, and O. G. Okhotnikov, "Principles and Performance of Tapered Fiber Lasers: from Uniform to Flared Geometry", *Applied Optics*, vol. 51, no. 29, pp. 7025–7038, 2012.

Principles and performance of tapered fiber lasers: from uniform to flared geometry

Juho Kerttula,[1,*] Valery Filippov,[1] Yuri Chamorovskii,[2] Vasily Ustimchik,[2] Konstantin Golant,[2] and Oleg G. Okhotnikov[1]

[1]Optoelectronics Research Centre, Tampere University of Technology, P.O. Box 692, FIN-33101, Tampere, Finland

[2]Institute of Radio and Electronics, Russian Academy of Sciences, 125009 Moscow, Russia

*Corresponding author: juho.kerttula@tut.fi

Received 5 July 2012; accepted 21 August 2012;
posted 5 September 2012 (Doc. ID 172045); published 8 October 2012

We have studied the recently demonstrated concept of fiber lasers based on active tapered double-clad fiber (T-DCF) in copropagating and counterpropagating configurations, both theoretically and experimentally, and compared the performance to fiber lasers based on conventional cylindrical fibers in end-pumped configurations. Specific properties of T-DCFs were considered theoretically using a rate-equation model developed for tapered fibers, and a detailed comparative study was carried out experimentally. Furthermore, we have studied mode coupling effects in long adiabatic tapers due to coiling and local bending. The results allow us to conclude that, with proper fiber design, the T-DCF technology offers a high-potential alternative for bright, cost-effective fiber devices. © 2012 Optical Society of America

OCIS codes: 060.2280, 060.2320, 060.3510.

1. Introduction

Recently, we have demonstrated the concept of high-power fiber lasers and amplifiers based on a tapered double-clad fiber as an active medium [1–3]. The active tapered double-clad fiber (T-DCF) is an axially nonuniform double-clad active optical fiber with the diameter varied along its length. It is practical to use the wide end of the T-DCF for launching the pump radiation from low-brightness sources.

In this paper we analyze the operation of ytterbium-doped fiber lasers based on T-DCF and compare their characteristics with lasers based on a conventional cylindrical fiber with similar brightness. With a volume-equivalent fiber we refer to a uniform fiber with equal active volume, whereas a brightness-equivalent fiber is assumed to be a cylindrical fiber with the core diameter equal to the T-DCF narrow end core diameter. The paper considers two basic schemes of T-DCF lasers using either the narrow or wide end of the taper as an output coupler (copropagation and counterpropagation scheme, respectively). The pump conversion efficiency (PCE), self-pulsing threshold [4], and the output beam quality have been used as criteria for comparison.

This paper is organized as follows. In Section 2 a rate-equation model of a laser comprising an active T-DCF is presented. The pump absorption, pump conversion efficiency, longitudinal power distribution, and power density distribution for different configurations of lasers containing either a T-DCF or a regular fiber have been obtained numerically from a rate-equation model. The mode coupling mechanisms in a T-DCF and their effect on the operation of tapered lasers are also discussed in Section 2. In Section 3 we present an experimental comparative study of the parameters of fiber lasers with a T-DCF and a regular fiber. The pump conversion efficiency, mode coupling effects, and conditions of the parasitic self-Q-switch modulation are experimentally studied in Section 3 as well. In Section 4 the results of the preceding sections are discussed further.

1559-128X/12/297025-14$15.00/0

2. Theory and Simulation

Any optically pumped, double-clad fiber (DCF) laser acts as a brightness converter; therefore, the pump conversion efficiency is an essential parameter of the device. To determine this parameter for an end-pumped double-clad fiber laser we need to know the pump radiation launching efficiency, the slope efficiency, and the fraction of generated emission propagating in the core. The pump conversion efficiency is defined as

$$\mathrm{PCE} = S \cdot L \cdot C, \tag{1}$$

where S is the slope efficiency, L is the launch efficiency of pump radiation into the cladding, and C is the contrast of output radiation, i.e., the ratio of generated power propagating in the core to the total output power. In this section these parameters will be considered separately.

A. Slope Efficiency, Pump Absorption, and Power Distribution

Scheme of a fiber laser containing a T-DCF (or a regular fiber) of length L is shown in Fig. 1(a), and a typical energy-level diagram of the ytterbium ion is shown in Fig. 1(b) [5]. The pump radiation is launched into the pump cladding at the wide end of the tapered fiber and propagates to the narrow end $(0 \to L)$. Reflectivity of the cavity mirrors at signal wavelength are $R_1 = 100\%$, $R_2 = 4\%$, and $R_1 = 4\%, R_2 = 100\%$ for the copropagating and counterpropagating direction of the output beam relative to pump direction respectively. To simulate the pump absorption and signal generation in the laser, we have used the coupled-wave equations in adiabatic approximation [5]:

$$\begin{cases} \pm\frac{dS^{\pm}}{dz} = \Gamma_S \cdot [(\sigma_{\mathrm{es}} + \sigma_{\mathrm{as}}) \cdot N_2 - \sigma_{\mathrm{as}} \cdot N] \cdot S^{\pm} - \alpha_s \cdot S^{\pm} \\ \pm\frac{dP^{\pm}}{dz} = -\Gamma_P \cdot [\sigma_{\mathrm{ap}} \cdot N - (\sigma_{\mathrm{ap}} + \sigma_{\mathrm{ep}}) \cdot N_2] \cdot P^{\pm} - \alpha_p \cdot P^{\pm} \end{cases}, \tag{2}$$

where $S^{\pm}, P^{\pm}$ are the signal (S) and pump (P) powers propagating right $(+)$ and left $(-)$ in Fig. 1(a), $N = 5.57 \cdot 10^{19}$ cm^{-3} is the ytterbium concentration in the core of the fiber, N_2 is the active ion concentration in the excited state. $\sigma_{\mathrm{ap}} = 6.2 \cdot 10^{-21}$ cm^2, $\sigma_{\mathrm{ep}} = 3.4 \cdot 10^{-22}$ cm^2 are the cross sections of absorption and emission for pump, $\sigma_{\mathrm{as}} = 9.5 \cdot 10^{-24}$ cm^2, $\sigma_{\mathrm{es}} = 1.9 \cdot 10^{-21}$ cm^2 are the cross sections of absorption and emission for signal, $\alpha_s = 8.1 \cdot 10^{-5}$ cm^{-1}, $\alpha_p = 8.1 \cdot 10^{-5}$ cm^{-1} are the coefficients of the scattering loss for signal and pump, and Γ_p, Γ_s are the pump and signal fill factors respectively.

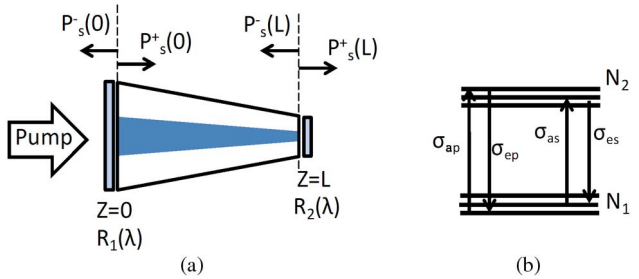

Fig. 1. (Color online) (a) Schematic illustration of the simulated laser geometry. For copropagating and counterpropagating configurations, pump direction $(0 \to L)$ coincides, or is opposite, to output beam direction respectively. (b) Energy level system of Yb^{3+} ions. Parameters are defined in the text.

The pump fill factor is determined by the core/cladding area ratio $\Gamma_p = S_{\mathrm{core}}/S_{\mathrm{clad}}$. The fill factor of signal $\Gamma_s = 0.82$ is assumed to be determined by overlapping of the core and lowest mode LP_{01} [5]. Taking into account the fact that the total concentration of Yb^{3+} is equal to the sum of the concentrations of Yb^{3+} ions in the ground and excited states, we can write the rate equations for the two-level system and solve for excited state population in the steady state [5]:

$$\begin{cases} N = N_1 + N_2 \\ \frac{\partial}{\partial t} N_1 = -\frac{1}{\tau_1} \cdot N_1 + \frac{1}{\tau_2} \cdot N_2 + \omega_{21} \cdot N_2 - \omega_{12} \cdot N_1 \\ \frac{\partial}{\partial t} N_2 = \frac{1}{\tau_1} \cdot N_1 - \frac{1}{\tau_2} \cdot N_2 - \omega_{21} \cdot N_2 + \omega_{12} \cdot N_1 \end{cases}, \tag{3}$$

$$\begin{aligned} N_2(z) = N(z) \cdot (\Gamma_p \cdot \sigma_{\mathrm{ap}} \cdot \lambda_p \cdot (P^+ + P^-) + \Gamma_s \cdot \sigma_{\mathrm{as}} \cdot \lambda_s \cdot \\ \times (S^+ + S^-)) / \left(\frac{Ahc}{\tau} + \Gamma_p \cdot \lambda_p \cdot (\sigma_{\mathrm{ap}} + \sigma_{\mathrm{ep}}) \cdot \right. \\ \times (P^+ + P^-) + \Gamma_s \cdot \lambda_s \cdot (\sigma_{\mathrm{as}} + \sigma_{\mathrm{es}}) \cdot \\ \left. \times (S^+ + S^-) \right), \end{aligned} \tag{4}$$

where N_1 is the ground state active ion population, τ_i is the lifetime of level i, ω_{ij} is the transition rate from level i to level j, A is the core area, h is the Planck constant, c is the speed of light in vacuum, $\tau = 10^{-3}$ s is the lifetime of ions in excited state, and $\lambda_p = 920$ nm, $\lambda_s = 1090$ nm are the wavelengths of pump and signal, respectively.

From Eqs. (4) and (2), we obtain the set of equations for modeling. The solution determined by fiber parameters gives the distribution of pump power and signal power along the length of the fiber given by the boundary conditions:

$$\begin{cases} P^+(0) = P^+ \\ P^-(L) = 0 \\ S^+(0) = R_1 \cdot S^-(0) \\ S^-(L) = R_2 \cdot S^+(L) \end{cases}, \tag{5}$$

where R_1 and R_2 are the mirror reflectivities at $z = 0$ and $z = L$, respectively, and P^+ and P^- are the pump powers launched in the positive $(0 \to L)$ and negative directions respectively. The analysis considers amplification of the fundamental mode only during its propagation in the T-DCF.

In the simulation, the T-DCF is modeled with the same equations as a regular cylindrical fiber with

constant core diameter, by appropriately varying the effective concentration of ytterbium ions along the length as well as taking the effect of vignetting into account. The longitudinal distribution of concentration is determined by the axial variation of the relative volume of the active medium:

$$N_{\text{taper}}(z) = \frac{\Delta V_{\text{taper}}}{\Delta V_{\text{cylinder}}} \cdot N_0 = \frac{r_{\text{taper}}^2(z)}{r_0^2} \cdot N_0, \quad (6)$$

where r_0 is the core radius of single-mode cylindrical fiber equal to the core radius at the narrow end of the T-DCF, and N_0 is the concentration of ytterbium ions in the preform. The effective concentration for two taper shapes shown in Fig. 2 approaches the actual concentration in the narrow (single-mode) part of the T-DCF. This assumption neglects the weakly-absorbed pump modes and the axial variation of the overlap of the propagating mode and active medium, and the simulation only considers the fundamental mode.

It has been shown earlier that the part of pump power which is vignetted (leaks out from the pump cladding due to a violation of the total internal reflection condition) is determined by the longitudinal profile $r(z)$ of the T-DCF and is given by [6]:

$$\frac{dP_{\text{vgnt}}}{dz} = -\frac{1}{r^2(0)} \cdot \exp(-\alpha \cdot z) \cdot \frac{dr^2(z)}{dz}. \quad (7)$$

Previous studies show that the optimal T-DCF shape is moderately parabolic [3,6]. Here we have used an axial profile of the form

$$\frac{r^2(z) - r^2(0)}{r^2(L) - r^2(0)} = \frac{z}{L}. \quad (8)$$

Substituting Eq. (8) into Eq. (7), we obtain an expression for vignetted pump power at the elementary length dz for parabolic shape of T-DCF:

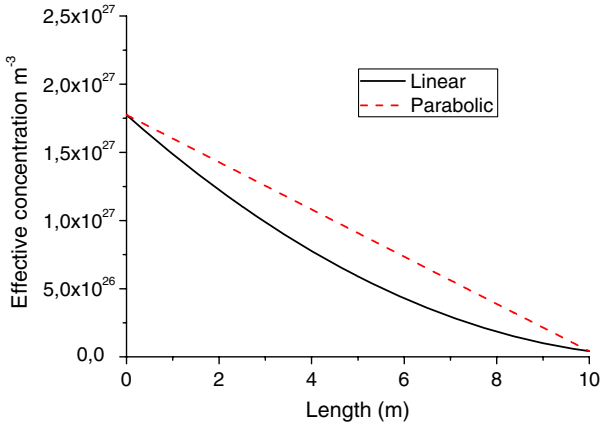

Fig. 2. (Color online) Effective concentration of ytterbium ions in a simulated cylindrical fiber representing the T-DCF.

$$\frac{dP_{\text{vgnt}}}{dz} = \frac{1}{L}\left(1 - \frac{r^2(L)}{r^2(0)}\right) \exp(-\alpha_p \cdot z). \quad (9)$$

Substituting the expression for the effective concentration Eq. (6) into Eq. (4), we obtain an equation describing the concentration of active ions in the excited state. The vignetting of pump power is taken into account as [6]:

$$\frac{dP_{\text{pump}}^{+}}{dz} = \frac{dP^{+}}{dz} - \frac{dP_{\text{vgnt}}}{dz}. \quad (10)$$

Taking Eq. (10) into account, substituting Eqs. (4) and (6), and solving the final equation set, Eq. (2), we obtain the distribution of the pump [Fig. 3(a)] and signal power [Fig. 3(b)] along the cavity. Furthermore, the calculated longitudinal distribution of the population inversion for copropagation and counterpropagation schemes of lasers with regular fiber and T-DCF is shown in Fig. 4. The parameters of the laser cavity are kept the same.

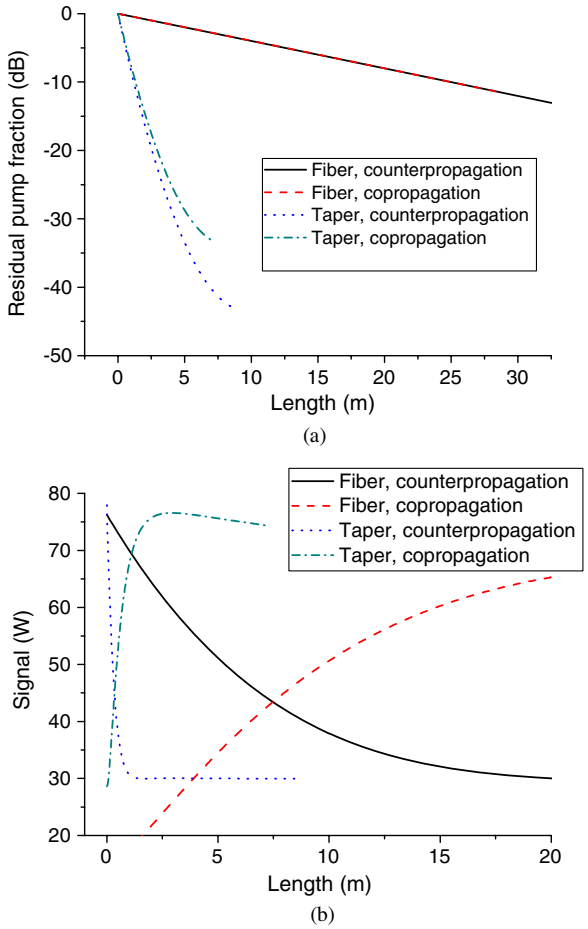

Fig. 3. (Color online) Longitudinal distributions of (a) pump and (b) signal power for simulated copropagating and counterpropagating laser schemes for 100 W of absorbed pump power. Fiber length for each configuration was selected to yield maximum output power.

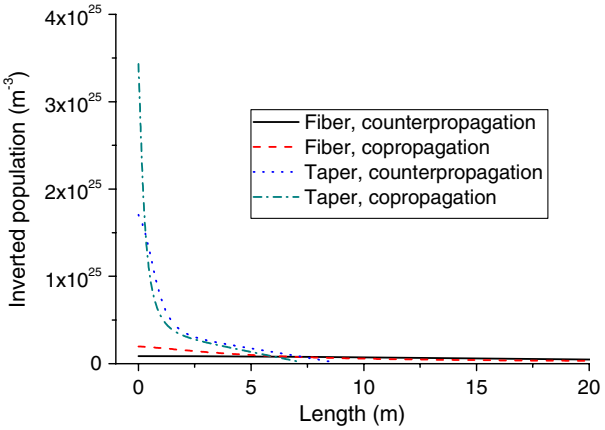

Fig. 4. (Color online) Small-signal inverted population distribution for the different laser configurations calculated for a 25 m fiber length.

The simulation results indicate that the population inversion is distributed in an extremely nonuniform manner in the T-DCF cavity. The highest inversion occurs in the wide part of the T-DCF. This dependence of inversion is a result of the end-pumping configuration and the larger number of active ions in the wide part of the T-DCF. Although the maximal value of power in the cavity of the copropagated scheme is higher, the output power is lower. This is due to high average power in the cavity of copropagated fiber laser resulting in higher scattering loss and thus lower pump conversion efficiency. Figure 5 shows the pump conversion efficiency as a function of absorbed pump power calculated for the copropagation and counterpropagation laser schemes with regular and tapered active fiber. The distribution of the intracavity power density for the copropagated and counterpropagated schemes for tapered and cylindrical fiber is shown in Fig. 6. As can be seen in Fig. 6, the (average) power density in a core of counterpropagated tapered laser is significantly lower than the power density in the core of copropagated laser.

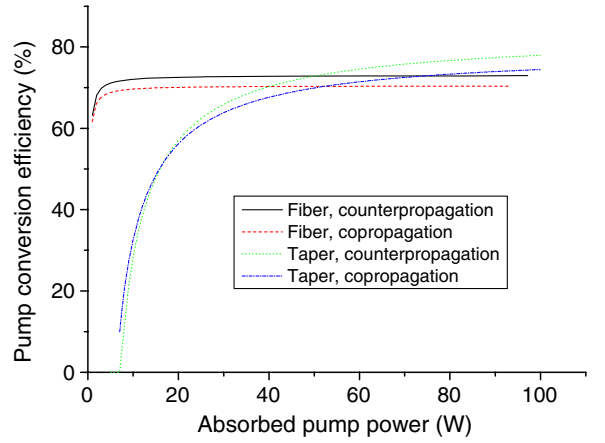

Fig. 5. (Color online) Pump conversion efficiency versus absorbed pump power.

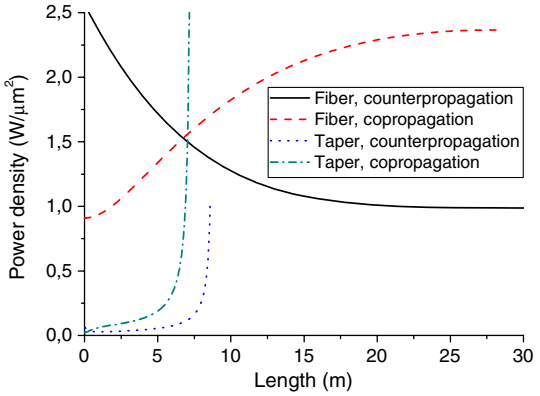

Fig. 6. (Color online) Intracavity power density distribution for different laser schemes. The numerical values in the legend refer to the average intracavity power density per unit length.

A T-DCF has a higher absorption per unit length compared to regular fibers with the same dopant concentration in the core because the doped volume in a T-DCF is always higher than the doped volume of brightness-equivalent regular fiber with a core diameter similar to the narrow side of T-DCF. Although the absorption is mostly determined by the core-cladding area ratio, the T-DCF exhibits higher absorption due to mode mixing introduced by the tapered cladding shape and partial core-pumping due to the large core size at launch end. As confirmed by the experimental results in Section 3, the simulation conducted by varying the active ion concentration substantially overestimates these effects as the measured absorption in the T-DCF was only twice higher than in the cylindrical fiber; however, it serves to qualitatively illustrate the consequences of the increased absorption in the T-DCF. It can be shown that the ratio of lengths of cylindrical and linear tapered fibers equivalent in terms of total volume and core diameter (in the narrow end of the taper) is determined as

$$\frac{L_{\text{cylinder}}}{L_{\text{taper}}} = \frac{1}{3}(T^2 + T + 1), \tag{11}$$

where L_{cylinder} is the length of equivalent cylindrical fiber, L_{taper} is the length of tapered fiber, and T is the tapering ratio. Figure 7 shows the ratio of the lengths for cylindrical and tapered fibers with the same active volume as a function of the tapering ratio. As can be seen from Fig. 7, the length of a tapered fiber with $T = 5$ could be 1/10 of the length of an equivalent cylindrical fiber. Of course, this estimation ignores vignetting, and the actual T-DCF is longer.

As indicated by Fig. 3(a) and confirmed by the experimental section, the absorption in the tapered fiber pulled from the same preform is higher than the absorption of the brightness-equivalent regular fiber. As a result, the optimal length of T-DCF in the laser cavity is shorter than the optimal length of the regular fiber. Since background loss per unit length is the same for regular and tapered fibers made of the

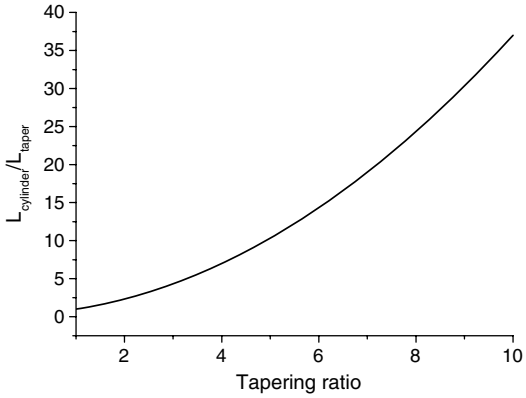

Fig. 7. The ratio of length for cylindrical and tapered fiber with equal volume of active material versus tapering ratio.

same preform, the intracavity losses for a fiber laser with T-DCF will be smaller than the intracavity losses for an equivalent laser with a regular fiber. As a result, the pump conversion efficiency of a T-DCF laser is always higher than that of a laser containing a brightness-equivalent regular fiber.

B. Contrast and Beam Quality

The contrast of the output radiation from the tapered fibers is defined as the ratio of the power propagating in the core and cladding, and is determined mostly by the mode coupling which inevitably exists in nonregular waveguides [7,8]. For emission propagating toward the wide end of the taper, mode coupling leads to the transfer of a fraction of the fundamental mode power to high-order modes. Though the power flow to higher-order modes does not increase cavity loss, it can degrade the beam quality (M^2) [9].

For emission propagating toward the narrow end, high-order modes excited due to mode coupling in the multimode part of the taper eventually violate the guiding condition and leak out of the core. This leads to an increase in the cavity loss and the deterioration of the contrast of the output radiation. Thus, the presence of mode coupling in the T-DCF significantly affects the operation of the laser or amplifier containing a T-DCF and will be discussed in next.

1. *Mode Coupling Mechanisms in a T-DCF*

Mode coupling in passive tapered fibers has been studied in [7–14]. Two basic mechanisms causing mode coupling in tapered fibers are longitudinal variation of the core diameter [7,8,10–12] and bending of the tapered fiber [13,14]. The mode coupling coefficient C_{nm} caused by longitudinal variation of the core diameter is given by [8,12]:

$$C_{nm} = 0.5\frac{n_1^2 - n_2^2}{n_{\text{eff},n} - n_{\text{eff},m}}\frac{1}{a}\frac{\partial a}{\partial z}, \tag{12}$$

where n_1, n_2 are the refractive indices of core and cladding, $n_{\text{eff},m}$, $n_{\text{eff},n}$ are the effective indices for modes with mode number m and n, respectively, and a is the core radius.

As it was shown in [7,8,10–12], the mode coupling caused by the core diameter variation is significant only for nonadiabatic short tapers (millimeters or even less) with relatively high tapering angles (0.01–0.1 rad). For long (meters to tens of meters) adiabatic tapers with a typical tapering angle of the order of 10^{-7} rad (as in this study), the mode coupling coefficient calculated from Eq. (12) has a negligible value in the range of 10^{-5}–10^{-6} m^{-1}. Thus, the mode coupling in long adiabatic tapers due to core diameter variations is small and does not lead to significant changes of the mode content [10,11].

The mechanism of the mode coupling caused by local bending of the adiabatically tapered fiber is described and studied theoretically and experimentally in [13–15]. The tapered fiber bent under the angle θ has been simulated as a sequence of M cylindrical fiber segments with successively decreasing diameter. The longitudinal axis of each fractional cylindrical fiber is rotated at an angle $\psi = \theta/M$ relative to the longitudinal axis of the neighboring fiber. A local mode coupling coefficient in an adiabatically tapered fiber locally bent under the angle ψ is defined by [14]:

$$C^{\psi}_{nm;pq} = \int_0^{\infty}\int_0^{2\pi} \varepsilon^{(i)}_{nm}\varepsilon^{(i+1)}_{pq}[J_0(\beta^{(i)}_{nm}\psi r) + 2jJ_1(\beta^{(i)}_{nm}\psi r)\cdot\cos\varphi]r\mathrm{d}r\mathrm{d}\varphi, \tag{13}$$

where n, p, and m, q are the radial and azimuthal mode numbers, respectively, ε^{i}_{nm} and ε^{i}_{pq} are the transversal input and output mode field functions at the elementary part i of the bent taper respectively, β^{i}_{nm} is the propagation constant of the (nm)-mode at the elementary part i of the bent taper, r, φ are the radial and azimuthal coordinates, and J_0, J_1 are Bessel functions. It was shown both theoretically and experimentally that even a small local bend of the order of one degree of adiabatically tapered fibers can lead to significant mode coupling, ~8–10% [13,14]. Furthermore, it has been shown that the effect can be significant enough to be used for sensing applications [15].

Distributed bending of adiabatically tapered long fibers due to coiling exhibit essentially different behavior. Since the long fibers are always coiled for practical use, they are inevitably bent. The mode conversion in coiled tapered fiber has not been considered so far. Although each local bending angle determined by the radius of fiber coiling $(1/R)$ is small, the long length of the coiled taper can result in a significant aggregate mode coupling coefficient. The mode coupling coefficient for a long tapered fiber coiled at radius R is defined as the integral over the taper length:

$$C_{nm,pq} = \int_0^L C^{\frac{1}{R}}_{nm,pq}(z)\mathrm{d}z, \tag{14}$$

where $C^{1/R}_{nm,pq}(z)$ is the mode coupling coefficient caused by coiling at location z. This parameter

describes the mode conversion mechanism in long adiabatic tapers, namely the distributed mode coupling caused by continuous bending due to coiling of the fiber. Since the entire taper is typically not coiled, to evaluate the coefficient Eq. (14) for each pair of coupled modes would represent a contour integral taking the real shape into account, which is out of the scope of this paper. Futhermore, fabrication defects are not taken into account although they may significantly contribute to the total mode coupling.

2. *Mode Coupling Characterization*

To date, several methods have been proposed to determine the mode power content. These methods are based on the analysis of either temporal [16] or spectral characteristics [17] of the radiation propagating through a multimode fiber. A method based on the measurement of various intermodal time delays requires, however, fiber lengths of a few hundred meters [16]. The mode power decomposition method based on the spectral measurements with a ring scanning cavity assumes that the transversal modes of the fiber coincide with the transversal modes of the ring resonator; a condition that is difficult to meet appropriately [17]. Some approaches are based on the analysis of the spatial pattern of radiation from a multimode fiber using a precomputed holographic filter [18] or a tomographic procedure [19]. These methods require *a priori* knowledge of spatial distribution of the mode that is difficult to derive practically.

Recently a new experimental technique for the analysis of large mode area (LMA) fiber mode content—the so-called S^2 method (spatially and spectrally resolved)—has been proposed [20,21]. The spectral modal beats measured for different points of the output of LMA fibers are used for Fourier transform and reconstruction of the spatial distribution of propagating modes. In this study we analyze the mode coupling in long adiabatic tapers using a similar method.

The S^2 method is applied here particularly to the long coiled adiabatic taper with narrow-to-wide propagation direction and only for a single spatial output point. The schematic measurement setup is shown in Fig. 8. The single-mode radiation is launched into the core of the T-DCF. The aperture of the single mode fiber, butt-coupled at taper output, acts as a spatial filter and delivers the signal to the optical spectrum analyzer. In the absence of mode coupling, the light intensity, after passing through a spatial filter with a transmission function S, can be written as

$$I = \int S \cdot E_1^2 \mathrm{d}s, \tag{15}$$

where E_1 is the spatial function of the fundamental mode. When high-order modes are excited at certain points located at the distance L_p from taper output, the intensity of the radiation passed through the spatial filter can be written as

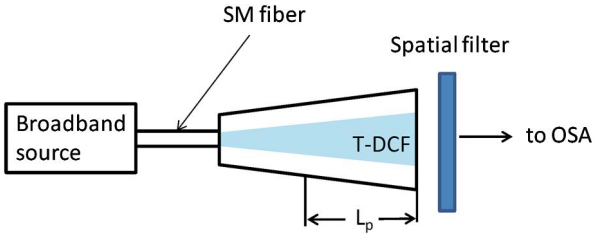

Fig. 8. (Color online) S^2-measurement setup for tapered fiber. OSA, optical spectrum analyzer.

$$I = \sum_{i=1}^{N} c_i^2 \int SE_i^2 \mathrm{d}s + 2 \sum_{i,j=1}^{N} c_i c_j \times \int E_i \cdot S \cdot E_j \mathrm{d}s \cdot \cos\left(\frac{2\pi \Delta n_{ij}^{\mathrm{eff}} L_p f}{c}\right), \tag{16}$$

where E_i is the spatial distribution of electrical field of mode i, N is the number of modes in the core, c_i is the excitation coefficient of mode i, $\Delta n_{ij}^{\mathrm{eff}} = \Delta n_i^{\mathrm{eff}} - \Delta n_j^{\mathrm{eff}}$ is the difference between effective indices of modes i and j respectively, c is the speed of light in vacuum, f is the optical frequency, and L_p is the distance between the point where the mode conversion occurs and the output end of the tapered fiber.

The mode coupling is described in Eq. (16) by the term containing the sum of modal functions with the period equal to the intermodal group delay:

$$\tau_{ij} = \frac{\Delta n_{ij}^{\mathrm{eff}} L_p}{c}. \tag{17}$$

Therefore, periodic modulation of the optical spectrum after passing through the tapered fiber and the spatial filter indicates the presence of mode coupling. The value of the intermodal delay τ_{ij} gives information on the type of interfering modes, whereas the amplitude of the harmonic with the period of τ_{ij} indicates the coupling coefficient of modes i and j.

In addition, the shape of the intermodal group delay spectrum (the Fourier transform of optical spectrum) allows determining the origin of the mode coupling. Two types of mode coupling—distributed and discrete—have been considered in [20]. The distributed mode coupling is defined as a coupling that occurs throughout the whole length of the fiber, e.g., due to distributed microbending, core diameter variations, or irregularities in the refractive index of the core. The discrete mode coupling occurs as a result of a local perturbation, e.g., a sharp bend or local fiber compression. The shape of the intermodal group delay spectrum for distributed and discrete disturbances have different properties. Since the delay Eq. (17) depends on the distance L_p, the spectrum of the intermodal group delay is smooth if distributed mode coupling dominates, whereas for discrete perturbations the spectrum becomes multilined. Thus, the shape of the intermodal group delay

spectrum suggests the principal mechanism of the mode coupling.

3. *Impact of Mode Coupling on the Operation of Tapered Fiber Lasers*

Mode coupling has a different effect on copropagating and counterpropagating T-DCF laser geometries. For a copropagating scheme, consider light propagating toward the wide end that is then reflected back by the mirror to the narrow end. The high-order modes excited in the wide part of the taper are reflected by the mirror and propagate as a multimode radiation towards the narrow single-mode taper section. The backreflected, higher-order modes leak to the cladding thus reducing the output contrast and pump conversion efficiency. Additionally, in the copropagating scheme, the end-mirror misalignment could further increase mode coupling/mixing in the multimode part of the system. As it was shown recently in [22], the use of fiber Bragg gratings may also lead to mode coupling. In the counterpropagation scheme, the situation is fundamentally different because the reflector cannot change the mode content in a single mode section but can only increase the loss.

The beam contrast deterioration is a result of coupling of the core and cladding modes. The strongest coupling to the cladding modes is expected for higher-order modes of the core having closest propagation constants, i.e., the core modes operating close to cutoff of the guiding [23]. Therefore, strong coupling to the cladding mode occurs when nearly all core modes are excited. The number of guided modes in the tapered fiber is proportional to the square of the core diameter. This means that even if at a certain location of the taper the next-to-cutoff modes are excited at the subsequent part of taper with larger core diameter, those modes are quite far from the cutoff and thus the coupling to the cladding modes are not efficient. Therefore, in the counterpropagation T-DCF, the degradation of contrast due to mode coupling is very low. Furthermore, as shown in [24], the increase in the number of propagated modes often does not lead to a significant degradation of the M^2.

To summarize, the presence of mode coupling in the cavity of a tapered laser has a significant influence on the parameters of a copropagated laser, namely the deterioration of the output beam contrast and pump conversion efficiency. On the other hand, the counterpropagation scheme is less prone to these effects of mode coupling. Though the excitation of high-order modes can slightly degrade the beam quality, it does not reduce the pump conversion efficiency.

C. Launching Efficiency

The launching efficiency into a uniform double-clad fiber with cladding diameter D/T and brightness-equivalent to a T-DCF with wide end cladding diameter of D, the tapering ratio of T, and the numerical aperture of the cladding of NA can be written as [25,26]:

$$L_{\mathrm{DCF}} = \left(\frac{D \cdot \mathrm{NA} \cdot F_{\mathrm{DCF}}}{2 \cdot \mathrm{BPP} \cdot T}\right)^2, \tag{18}$$

where BPP is the beam parameter product of the pump source, and F_{DCF} is the fill factor of the cladding aperture. The launching efficiency into a corresponding taper is given by

$$L_{T\text{-DCF}} = \left(\frac{D \cdot \mathrm{NA} \cdot F_{T\text{-DCF}}}{2 \cdot \mathrm{BPP}}\right)^2, \tag{19}$$

where $F_{T\text{-DCF}}$ is the fill factor of the T-DCF cladding aperture. Thus, the ratio of the launching efficiency coefficients of the tapered fiber and equivalent regular fiber is

$$\frac{L_{T\text{-DCF}}}{L_{\mathrm{DCF}}} = \left(\frac{F_{T\text{-DCF}}}{F_{\mathrm{DCF}}} T\right)^2. \tag{20}$$

This expression shows that for the pump source with given brightness, the launching efficiency into a T-DCF is always $(T \cdot F_{T\text{-DCF}})^2$ times higher than the launching efficiency into equivalent cylindrical fiber assuming a fully filled DCF cladding aperture. Although the T-DCF launch aperture should be underfilled to avoid excessive vignetting, brightness enhancement remains significantly higher than in a regular fiber, as shown in [3]. The maximum acceptable fill factor that ensures negligible vignetting loss is determined by the longitudinal taper shape and the incore pump absorption, i.e., the doping level.

3. Experimental Results

The ytterbium-doped preform fabricated by the surface-plasma chemical vapor deposition method [27], had an absorption of 150 dB/m at $\lambda = 920$ nm. The preform was shaped (four times truncated) for better absorption. The tapered fiber and the reference regular fiber with equivalent brightness were drawn from the same preform. The longitudinal profile of the tapered fiber is shown in Fig. 9.

The tapering ratio of the T-DCF was $T = 6.5$, and the distance between the flat side surfaces of the T-DCF in the wide end is 630 μm. The core diameter in the wide end was approximately 40 μm. The diameter of the regular (cylindrical) fiber was equal to the diameter of the T-DCF in the narrow end (110 μm). Both the T-DCF and the regular fiber were coated with a low-index polymer (NA = 0.4). The fiber-coupled (core 400 μm, NA = 0.22) laser diode bar with a maximum output of 140 W at $\lambda = 915$ nm was used as the pump source.

The pump absorption, pump conversion efficiency, and susceptibility to self-pulsing for copropagated and counterpropagated schemes were examined for both regular and tapered fibers. The mode coupling and its effect on contrast and beam quality was studied using the S^2-method and M^2-measurements.

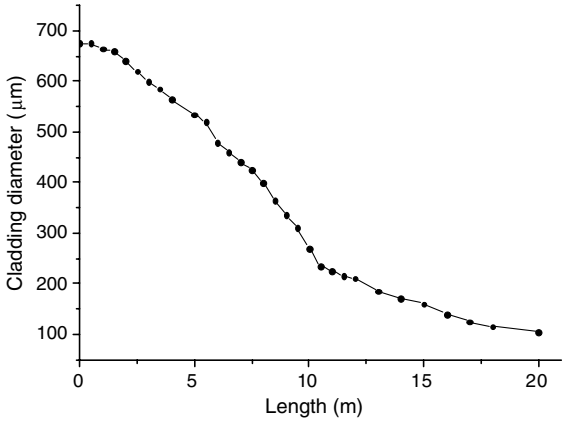

Fig. 9. Cladding diameter versus length of the tapered fiber.

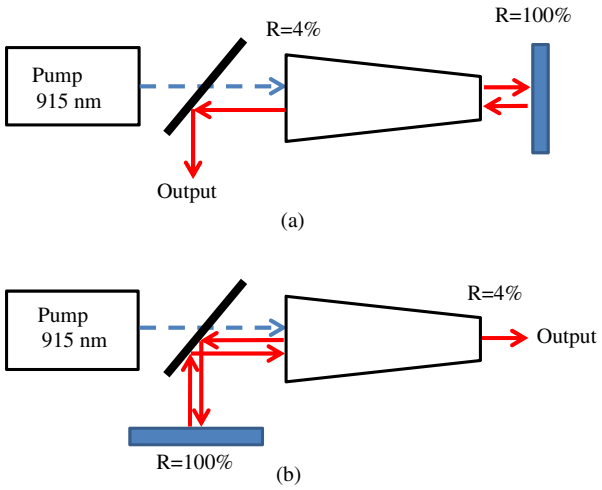

Fig. 10. (Color online) (a) Counterpropagation and (b) copropagation laser schemes.

A. Pump Absorption

The pump absorption in the tapered fiber was measured by launching pump source emission (915 nm) into the wide part of the T-DCF. The cladding aperture (NA = 0.4) of the T-DCF was only partially filled (NA = 0.15) to completely avoid the effect of vignetting [3]. A pump launch NA of 0.3 was used in the case of the regular fiber. The summary of results is shown in Table 1.

B. Pump Conversion Efficiency

As noted above in Eq. (1), the pump conversion efficiency of a double-clad fiber laser is determined by the product of pump launching efficiency, slope efficiency, and the fraction of power propagating in the core, i.e., beam contrast. The launching efficiency into the fiber (taper) was determined by coupling the pump radiation into a short piece of fiber (taper) and measuring the transmitted power (Table 1). The contrast of the radiation was measured only for copropagated schemes by removing part of the polymer coating at the output of fiber (taper) and applying a high-index gel to filter out the light propagated in the cladding to estimate its relative contribution to the total output power.

The slope efficiency was measured using the setup schematically shown in Fig. 10. The fiber-coupled diode bar at 915 nm was used as a pump source. The pump light was launched through a dichroic filter (highly transparent for pump and highly reflecting for signal) into the wide end of the T-DCF. The cavity is terminated by a highly reflective mirror on one side and 4% Fresnel reflection on the other fiber end. We measured the slope and pump conversion efficiencies for the two schemes for both the T-DCF and the regular fiber. The results are shown in Table 1.

C. Self-Pulsing Threshold

Passive Q-switching regime, frequently observed in fiber lasers, can be triggered by the cascaded effect of Rayleigh backscattering and stimulated Brillouin scattering (SBS) [4]. This regime was observed in lasers with tapered and regular fiber studied here and characterized by measuring pulse shape, spectrum, and launched pump power corresponding to the onset of pulsing. The pulsing pump threshold was 4 W for tapered copropagation laser setup, as seen from Table 1. This laser configuration demonstrated a strong tendency toward generation of an unstable train of pulses with the duration of several nanoseconds and with a repetition rate of several hundred kilohertz. A typical pulse shape and emission spectrum are shown in Fig. 11(a) and 11(b) respectively. Due to the relatively high peak power of several kW, considerable stimulated Raman scattering was

Table 1. Characterization Results for the Studied Laser Schemes

Measured Quantity	Regular Fiber, Co-pumping	Regular Fiber, Counter-pumping	Tapered Fiber, Co-pumping	Tapered Fiber, Counter-pumping
Length (m)	25.5	25.5	20	20
DC absorption (dB/m)	0.4	0.4	0.75	0.75
Slope efficiency (%)	49.7	57.1	51	60
Pump launching efficiency (%)	5.5 (NA 0.3)	5.5 (NA 0.3)	78 (NA 0.15)	78 (NA 0.15)
Contrast (%)	98	—	70	—
Pump conversion efficiency (%)	2.6	3.14	28	46.8
Self-pulsing threshold (W)	4	5	4.4	30
M^2	SMF	SMF	SMF	1.06/1.20
Output mode field diameter (μm)	5	5	5	30
Divergence (rad)	0.11	0.11	0.11	0.03

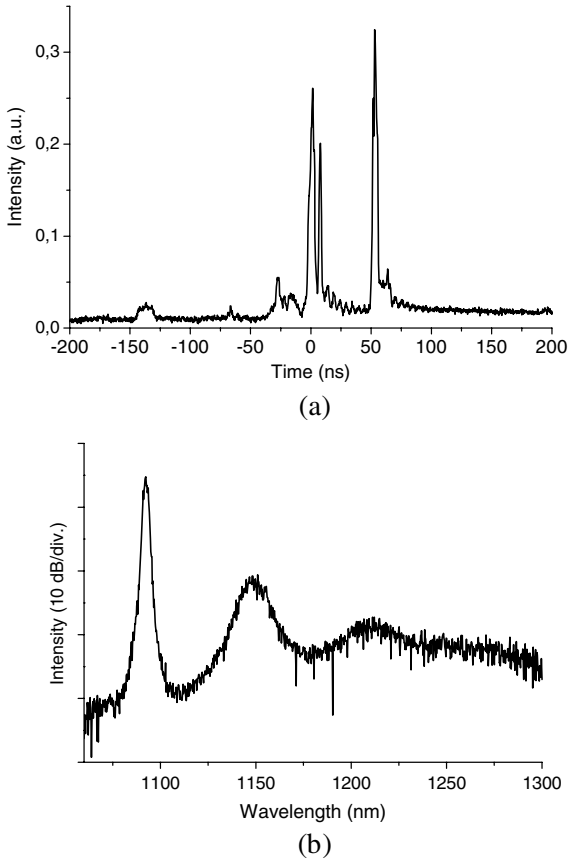

Fig. 11. (a) Typical output pulse shape and (b) spectrum for self-pulsing operation.

observed resulting in a typical spectrum shown in Fig. 11(b).

The threshold of a pulsed operation for a counterpropagation scheme of the laser with T-DCF was 30 W, more than seven times higher than the threshold for copropagation scheme. For the pump power below the threshold, steady CW lasing was observed with the optical spectrum shown in Fig. 12(a). Onset of the pulse regime is accompanied with an additional down-shifted spectral band seen in Figs. 12(b) and 12(c). The pulsed regime was observed for both directions of signal propagation with a regular fiber,

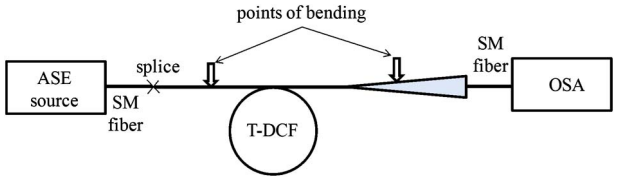

Fig. 13. (Color online) Mode coupling measurement setup.

see Table 1. The emission spectra were similar to those shown in Fig. 12. It should be noted that the pulses are always superimposed on a CW pedestal containing a large fraction of the output power.

D. Mode Coupling Measurements

Mode coupling in a long adiabatically tapered coiled fiber induced by distributed or local bending was studied using the S^2 method [20,21]. Experimental setup is shown in Fig. 13. A 1550 nm broadband source was spliced to the single-mode end of the T-DCF. It was necessary to utilize a source wavelength far away from the 1 μm line due to high absorption; however, for qualitative interpretation of the results the wavelength is not critical. A single-mode fiber, butt-coupled to the core at the wide end of the T-DCF, was used as a spatial filter. The spectral beats of the broadband light transmitted through the resulting optical system were measured for different bending geometries of the T-DCF.

The emission spectrum of broadband radiation passed through the T-DCF coiled with a 25 cm radius is shown in Fig. 14(a). The spectrum is modulated periodically with 0.73 dB average deviation. The Fourier transform of this spectrum representing an intermodal group delay spectrum is shown in Fig. 14(b). The results of a similar measurement performed for a coil radius of 15 cm are shown in Fig. 15. The measurements plotted in Figs. 14–17 have been done for the same optical power at the taper output. The power after spatial filtering by the single-mode fiber, however, depends on the bending condition.

Next, in the T-DCF, coiled with radius of 15 cm, an additional local bend with a 5 cm radius was introduced at one of two different locations: either one meter from the wide end or three meters from the

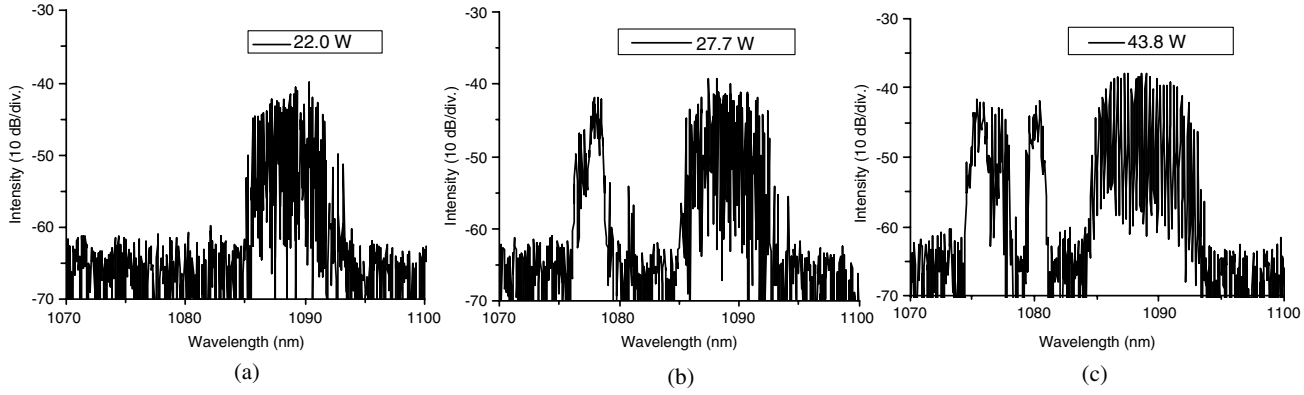

Fig. 12. Output signal spectra of counterpropagation tapered fiber laser for three different values of launched pump power.

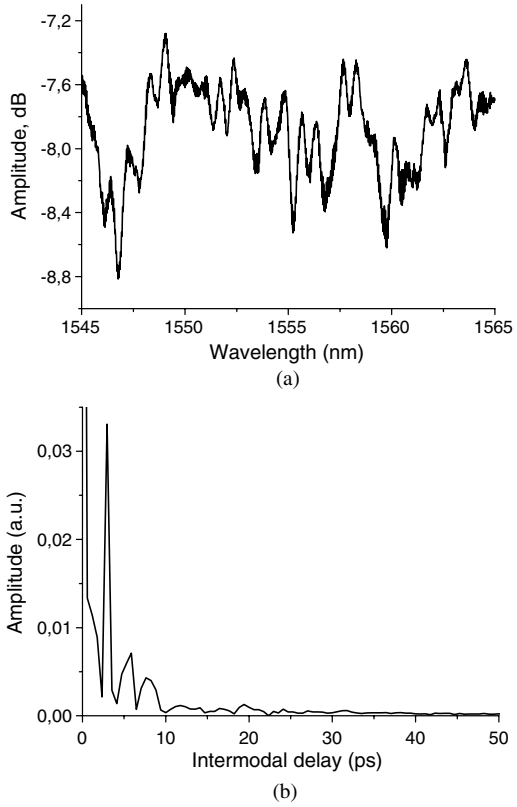

Fig. 14. (a) Spectrum of light transmitted through the optical system consisting of the taper and the spatial single-mode filter. Taper coil radius is 25 cm, mean deviation is 0.73 dB. (b) Fourier transform of the spectrum presented in (a).

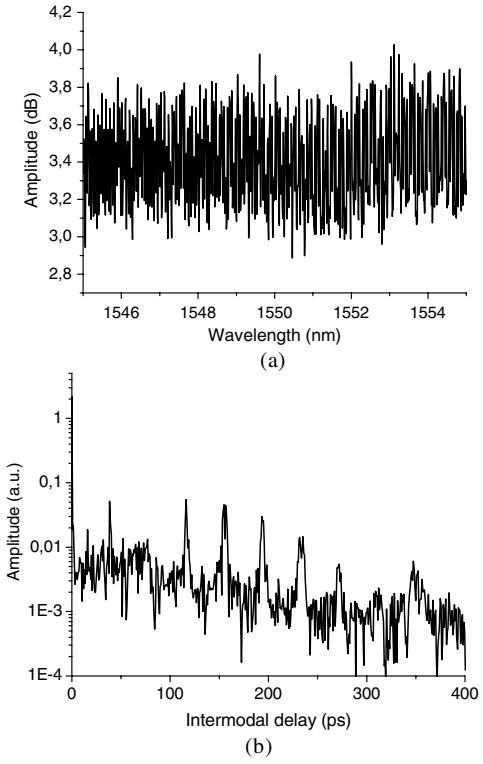

Fig. 15. (a) Spectrum of light propagated through the taper and the spatial filter. Taper coil radius is 15 cm, average signal is 3.38 dB, and deviation is 0.66 dB. (b) Fourier transform of the spectrum shown in (a).

narrow end, as schematically shown in Fig. 13. Spectra corresponding to these bends are shown in Figs. 16(a) and 17(a) respectively. Fourier transforms of these spectra are shown in Figs. 16(b) and 17(b) respectively. As can be seen from Fig. 16, the local bend imposed at the wide side of the taper results in a relatively small effect. The local bend with a 5 cm radius imposed in the wide part of T-DCF caused only a slight increase in the losses by 0.2 dB, while the deviation remains 0.66 dB, the same as for unperturbed case. The local bending of the narrow section of tapered fiber demonstrates different behavior, as shown in Fig. 17. The average signal level decreases by 9.4 dB down to −6.02 dB relative to the original level. The spectrum exhibits strong periodic modulation with a mean deviation of 1.61 dB.

E. Beam Quality Measurements

The core output beams from the single-mode reference fiber and the T-DCF narrow output are both diffraction-limited, as generally expected. The beam quality of the signal emitted from the wide end of the T-DCF with 40 μm core diameter measured using a clip level method corresponds to $M_x^2 = 1.06$/ $M_y^2 = 1.20$. The beam distribution in the near and far field is shown in Fig. 18. In addition, the output beam divergence was measured to be 0.03 rad. The beam quality measurements were performed for 15 cm coiling radius without local bending.

4. Discussion

A. Slope Efficiency

Comparison of the laser performance based on tapered and regular fibers shows that the slope efficiency of a tapered fiber laser is higher both for copropagation and counterpropagation geometries. Additionally, the slope efficiency for the counterpropagation scheme is superior with both fiber types as shown both numerically and experimentally (Table 1). It was also found from modeling and measurements that pump absorption in a T-DCF is higher than that in a regular fiber with an equivalent volume of active material. This feature originates from the mode mixing introduced by the taper shape, the larger active volume of a brightness-equivalent T-DCF, and the nonuniform distribution of active volume along the T-DCF, i.e., most of the gain material is located in its wide section at pump input end. Accordingly, pump absorption per unit length in a T-DCF is higher than in the equivalent regular fiber. This allows for shorter length of active fiber with the same density of the dopants, which in turn decreases the intracavity losses and improves the slope efficiency. Additionally, higher absorption per unit length in T-DCF allows fibers with modest concentrations of active ions to be used, which is beneficial e.g., in terms of photodarkening [28].

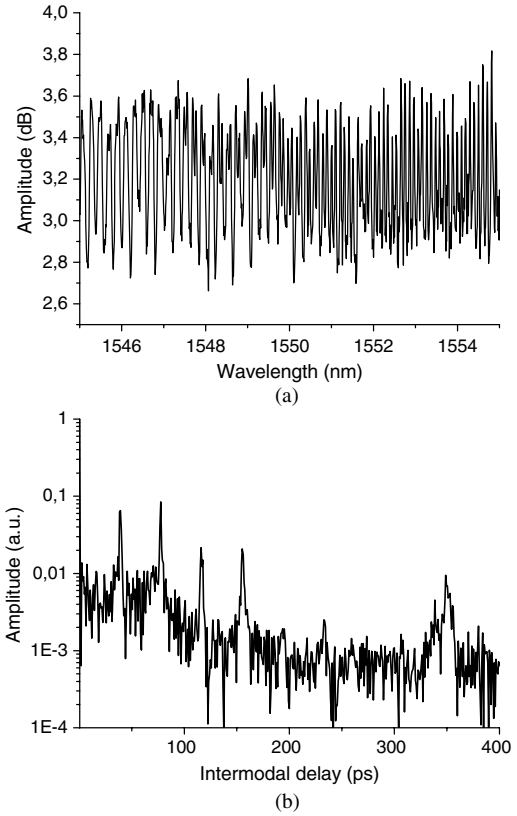

Fig. 16. Local bending of the wide side of the T-DCF with 5 cm radius: (a) Output spectrum with average level of 3.17 dB, deviation is 0.66 dB. (b) Fourier transform of the spectrum in Fig. 16(a).

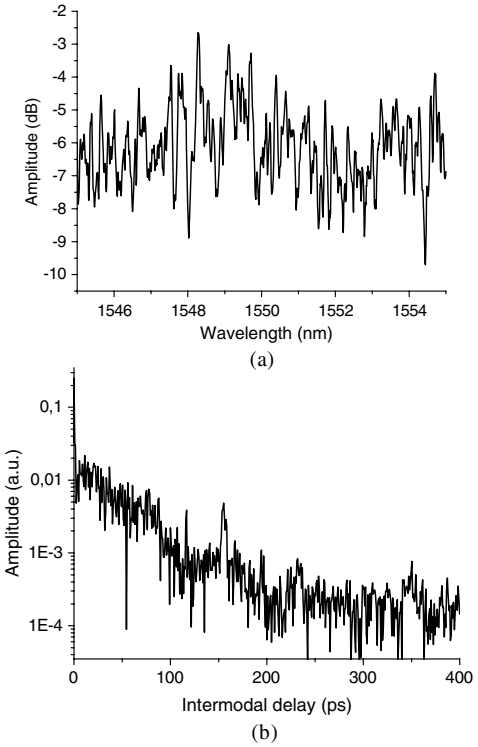

Fig. 17. Local bending of the narrow section of the T-DCF with 5 cm radius: (a) Output spectrum; the average level is −6.02 dB, deviation is 1.61 dB. (b) Fourier transform of the spectrum in Fig. 17(a).

B. Contrast

The beam contrast of a regular fiber laser derived from measurements is approximately 98% determined largely by the relatively high $NA_{core} = 0.11$ and a large radius of fiber coiling of 15 cm and indicates that coupling between the fundamental and cladding modes is prohibited.

The output divergence of 0.03 rad measured for counterpropagating T-DCF suggests that the aperture of the core is not fully filled and indicates a nearly perfect beam contrast for counterpropagated T-DCF. Ideally, without mode coupling, the aperture of the output emission should be even lower, i.e., $NA_{core}/T = 0.018$. The slightly higher divergence can be attributed to higher-order modes that are present due to mode coupling caused by the coiling of the taper.

The experimentally measured contrast of the output radiation of a copropagating tapered laser was 70% as shown in Table 1. Since the T-DCF is an efficient filter of high-order modes, reduced contrast provides estimation for the fraction of power contained in high-order modes of ~30%. The mode content was evaluated from the modulation features in the spectra measured by the S^2-method. Changing the coiling radius of the T-DCF from 25 to 15 cm, shown in Figs. 14 and 15 respectively, reveals that the beat spectrum depends directly on the bending condition. The number of intermodal delay harmonics in the Fourier spectra in Figs. 14(b) and 15(b) indicate the presence of up to three and six excited modes for a bend radius of 25 cm and 15 cm respectively. The beam contrast was approximately 70% for both coiling radii. The increase in coiling radius causes a reduction of the number of excited modes, i.e. the group of modes receiving power depends on the radius of periodic bending, as can be seen from Figs. 14 and 15, whereas the total amount of power converted from the fundamental mode to higher-order modes remains approximately constant and is likely to be determined by the length of the taper. It should be

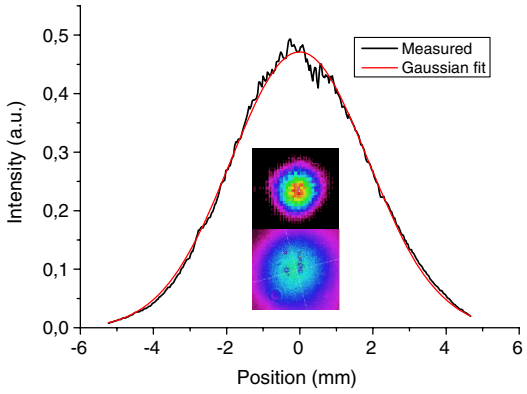

Fig. 18. (Color online) Far field distribution of the beam from the wide output of the T-DCF, and the near field (upper inset) and far-field (lower inset) two-dimensional images.

noted that in the large-core section of tapered fiber with $V = 14$, up to 100 modes can be guided. The fairly discrete character of the spectra indicates that the excitation of higher-order modes is resonant and dependent on the radius of coiling. Furthermore, the discrete nature of the intermodal delay spectra in Figs. 14–16 could result from relatively high local slopes in the taper profile that give rise to localized mode coupling when bent due to coiling. The intensity variations of the optical spectrum (0.66–0.73 dB) correspond closely to the observed beam contrast of 70%. Thus, the mode coupling caused by the coiling leads to the coupling of a significant fraction of the fundamental mode power (~30%) to higher-order modes.

It has been shown earlier that bending can induce strong mode coupling in a tapered fiber, while the sensitivity to the bending depends on the local taper diameter [13,14]. Figure 16 shows that local bending of the large-core section of the taper with a radius of 5 cm leads to a minor reduction of output power (0.2 dB), while the spectral intensity variation remains at the same level of 0.66 dB. However, local bending of the narrow section of the taper exhibits different behavior. As seen from Fig. 17, the average power decreases by 9.4 dB and the amplitude of intensity variations increases up to 1.61 dB. Corresponding intermodal delay spectrum given by Fourier transform is no longer discrete and has a rather smooth shape due to a large number of intermodal delay harmonics flattening the spectral envelope. The spectral behavior together with reduction in the average power indicates a multimode speckle pattern at the taper output.

Therefore, the mode coupling in the wide and narrow sections of the T-DCF exhibit significantly different sensitivity to bending. Apparently, this is due to the strong dependence of the mode coupling coefficient c_{ij} on the fiber outer diameter D, $c_{ij} \sim D^{-6}$ [29]. Furthermore, bending of the narrow part results in a larger number of modes early in the taper, which enhances further mode coupling to a larger number of neighboring modes, compared to a single mode propagating in the narrow part when bending is absent. For local bending at the wide part, the effect is smaller due to shorter remaining propagation distance. This behavior indicates that in order to minimize mode coupling, any small-radius bends, especially in the small-diameter section of the T-DCF, should be avoided.

Analysis of the beam contrast in a T-DCF laser shows that the bends during the coiling affect the performance of copropagating and counterpropagating tapered lasers differently. Though the mode content changes in both cases, in the copropagating scheme it leads to contrast deterioration and eventually to deterioration of PCE (Table 1). In the counterpropagation laser scheme, the changes of the mode content practically do not affect the contrast of the output radiation and only result in minor beam quality deterioration.

C. Launching Efficiency

Theoretical assumptions made in Subsection 2.C are supported by experimental results presented in Table 1. The theoretical launch efficiencies for the characterized T-DCF and regular fiber are 100% and 13% (taking into account the fill factors 0.375 and 0.75 used in measurements) respectively, for the pump source with a nominal BPP of 44 mm · mrad. The corresponding measured launching efficiencies were 78% and 5.5%. The discrepancy is partially attributed to free-space launch components, spherical lens aberrations for multimode pump radiation and Fresnel reflection from the fiber end face. In addition, we used a pump delivery cable without a cladding mode stripper, which can cause a significant part of the pump power to propagate in the cladding with lower brightness. These effects have not been considered in Eqs. (18)–(20). However, the requirement of very high pump brightness for a cylindrical fiber compared to a brightness-equivalent T-DCF remains apparent.

D. Self-Pulsing

We observed the phenomenon of self-pulsing in all studied laser configurations. The threshold of the effect was found to be significantly higher for a counterpropagating T-DCF scheme than for the other schemes, as can be seen in Table 1. The T-DCF laser can be expected to perform better in this respect due to the higher SBS threshold arising from the core diameter modulation, whereas the difference between T-DCF configurations can be partially attributed to the higher intracavity power density in the copropagating geometry (see Fig. 6).

Another mechanism for enhancement of the effect in copropagating geometry is illustrated schematically in Fig. 19. Once the threshold is exceeded, an effective SBS mirror develops in the relatively small-diameter section of T-DCF where the power density is sufficiently higher, as shown in Fig. 6. The laser cavity then effectively becomes a three-mirror resonator that functions differently for copropagation and counterpropagation geometry, as the bulk of the gain material, and thus the amplification is located in the large-core section of the T-DCF.

For the counterpropagation scheme, the arising cavity is formed by the SBS mirror and the 4% Fresnel reflection, Fig. 19(a). With the low-reflectivity output mirror, the cavity operates effectively in a two-pass regime with low-energy storage resulting in a high self-pulsing threshold (Table 1).

For the copropagation scheme, the cavity is formed by the highly reflective end mirror and the SBS mirror developed close to the narrow output end of the T-DCF. Since the reflectivity of the effective SBS mirror is relatively high, the emerged cavity can operate in a multiple-pass regime. Consequently, the copropagating T-DCF laser exhibits a low self-pulsing threshold, ~4 W of launched pump power (Table 1). High peak power produced with this configuration generated notable Stokes spectral components seen

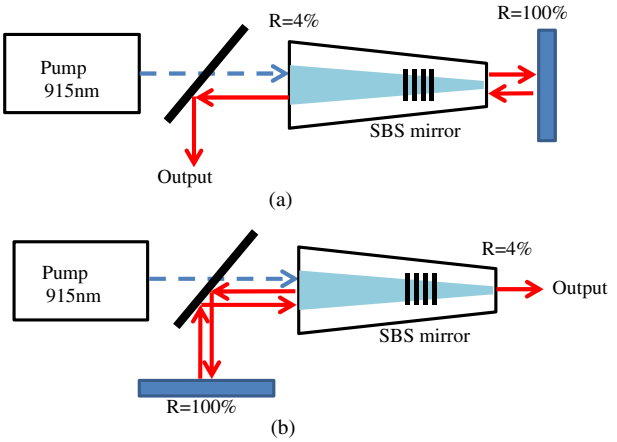

Fig. 19. (Color online) Schematic illustration of the development of self-pulsing in (a) counterpropagating and (b) copropagating configurations.

in Fig. 11(b). Therefore, a major disadvantage of the copropagation scheme is the susceptibility to self-pulsing, as well as to other nonlinearities. Although the pulsing threshold can be increased by e.g., increasing the diameter of the active core [3], the counterpropagating scheme will always have higher resistance to the effect.

E. Beam Quality

Given the strictly single-mode output core, the beam quality of a copropagated T-DCF laser is equal to the fiber laser with the regular fiber. However, the counterpropagated tapered laser typically emits a few modes as a result of mode coupling. The mode content of the output radiation is largely determined by the bending of the taper. Furthermore, the small-diameter section of the T-DCF is significantly more sensitive to bending than the large diameter section. Nevertheless, the output beam with counterpropagating geometry had a Gaussian shape and an $M^2 = 1.06/1.20$. The small number (~5–6) of higher-order modes with combined power contribution below 30% and relatively high brightness [9], provides a trade-off between output power and beam quality. These results agree well with results obtained for LMA and moderately multimode fibers [9,20,21,24].

5. Conclusion

In this study, we have analyzed the performance of fiber lasers based on tapered double-clad active fibers and compared them to the performance of regular active DCFs. The studied characteristics include pump conversion efficiency, susceptibility to self-pulsing, and output beam properties. The results of simulations and measurements allow us to conclude that tapered fiber lasers offer significant advantages especially in terms of low-brightness pump launching, self-pulsing threshold, and pump conversion efficiency compared to lasers built from regular fibers. The distinctive feature of tapered laser design is that enhanced power characteristics can be combined with good beam quality despite the mode coupling occurring in coiled tapers.

The performance of tapered fiber lasers has been examined for cavity configurations with output signal copropagating and counterpropagating relative to pump launch direction. The results show that a counterpropagation scheme exhibits superior pump conversion efficiency due to better beam contrast of the output radiation and higher slope efficiency. Furthermore, the counterpropagating design offers a substantially higher self-pulsing threshold compared with copropagating tapered lasers and lasers based on regular fibers. Although mode coupling exists in a coiled T-DCF, and the counterpropagating scheme uses a multimode output port, the output emission retains good beam quality. Therefore, we can conclude that the T-DCF concept offers a practical alternative for bright, high-power fiber oscillators pumped by cost-effective low-brightness sources.

References

1. V. Filippov, Y. Chamorovskii, J. Kerttula, K. Golant, M. Pessa, and O. G. Okhotnikov, "Double clad tapered fiber for high power applications," Opt. Express **16**, 1929–1944 (2008).
2. V. Filippov, Y. Chamorovskii, J. Kerttula, A. Kholodkov, and O. G. Okhotnikov, "600 W power scalable single transverse mode tapered double-clad fiber laser," Opt. Express **17**, 1203–1214 (2009).
3. V. Filippov, J. Kerttula, Y. Chamorovskii, K. Golant, and O. G. Okhotnikov, "Highly efficient 750 W tapered double-clad ytterbium fiber laser," Opt. Express **18**, 12499–12512 (2010).
4. S. V. Chernikov, Y. Zhu, J. R. Taylor, and V. P. Gapontsev, "Supercontinuum self-Q-switched ytterbium fiber laser," Opt. Lett. **22**, 298–300 (1997).
5. I. Kelson and A. Hardy, "Strongly pumped fiber lasers," IEEE J. Quantum Electron. **34**, 1570–1577 (1998).
6. V. A. Bagan, S. A. Nikitov, Yu. K. Chamorovskii, and A. D. Shatrov, "Studying the properties of double-clad active cone optic fibers," J. Commun. Technol. Electron. **55**, 1154–1160 (2010).
7. A. W. Snyder, "Coupling of modes on a tapered dielectric cylinder," IEEE Trans. Microwave Theory Tech. **18**, 383–392 (1970).
8. D. Marcuse, "Mode conversion in optical fibers with monotonically increasing core radius," J. Lightwave Technol. **5**, 125–133 (1987).
9. H. Yoda, O. Polynkin, and M. Mansuripur, "Beam quality factor of higher order modes in a step-index fiber," J. Lightwave Technol. **24**, 1350–1355 (2006).
10. T. Ozeki and B. S. Kawasaki, "Mode behaviour in a tapered multimode fibre," Electron. Lett. **12**, 407–408 (1976).
11. Y.-F. Li and J. W. Y. Lit, "Mode changes in step-index multimode fiber tapers," J. Opt. Soc. Am. A **3**, 161–164 (1986).
12. A. Fielding, K. Edinger, and C. Davis, "Experimental observation of modal evolution in single-mode tapered optical fibers," J. Lightwave Technol. **17**, 1649–1656 (1999).
13. P. M. Shankar, L. C. Bobb, and H. D. Krumboltz, "Coupling of modes in bent biconically tapered single-mode fibers," J. Lightwave Technol. **9**, 832–837 (1991).
14. L. C. Bobb, P. M. Shankar, and H. D. Krumboltz, "Bending effects in biconically tapered single-mode fibers," J. Lightwave Technol. **8**, 1084–1090 (1990).
15. L. C. Bobb, H. D. Krumboltz, and P. M. Shankar, "Pressure sensor that uses bent biconically tapered single-mode fibers," Opt. Lett. **16**, 112–114 (1991).
16. S. E. Golowich, W. A. Reed, and A. J. Ritger, "A new modal power distribution measurement for high-speed short-reach optical systems," J. Lightwave Technol. **22**, 457–468 (2004).

17. N. Andermahr, T. Theeg, and C. Fallnich, "Novel approach for polarization-sensitive measurements of transverse modes in few-mode optical fibers," Appl. Phys. B **91**, 353–357 (2008).
18. C. Schulze, O. Schmidt, D. Flamm, M. Duparre, and S. Schroter, "Modal analysis of beams emerging from a multicore fiber using computer-generated holograms," Proc. SPIE **7914**, 79142H1 (2011).
19. D. B. S. Soh, J. Nilsson, S. Baek, C. Codemard, Y. Jeong, and V. Philippov, "Modal power decomposition of beam intensity profiles into linearly polarized modes of multimode optical fibers," J. Opt. Soc. Am. A **21**, 1241–1250 (2004).
20. J. W. Nicholson, A. D. Yablon, S. Ramachandran, and S. Ghalmi, "Spatially and spectrally resolved imaging of modal content in large-mode-area fibers," Opt. Express **16**, 7233–7243 (2008).
21. J. W. Nicholson, A. D. Yablon, J. M Fini, and M. D. Mermelstein, "Measuring the modal content of large-mode-area fibers," IEEE J. Sel. Top. Quantum Electron. **15**, 61–70 (2009).
22. A. Iho, A. Tervonen, K. Ylä-Jarkko, S. Tammela, and S. Honkanen, "Characterization of modal coupling of Bragg gratings in large-mode-area fibers," J. Lightwave Technol. **29**, 2031–2038 (2011).
23. R. Olshansky, "Mode coupling effects in graded-index optical fibers" Appl. Opt. **14**, 935–945 (1975).
24. S. Wielandy, "Implications of higher-order mode content in large mode area fibers with good beam quality," Opt. Express **15**, 15402–15409 (2007).
25. M. C. Hudson, "Calculation of the maximum optical coupling efficiency into multimode optical waveguides," Appl. Opt. **13**, 1029–1033 (1974).
26. A. Kosterin, V. Temyanko, M. Fallahi, and M. Mansuripur, "Tapered fiber bundles for combining high-power diode lasers," Appl. Optics **43**, 3893–3900 (2004).
27. K. M. Golant, "Surface plasma chemical vapor deposition: 20 years of application in glass synthesis for lightguides (a review)," in *Proceedings of XXI International Congress on Glass* (CD) (2007), paper L13.
28. J. J. Koponen, M. J. Söderlund, H. J. Hoffman, and S. K. T. Tammela, "Measuring photodarkening from single-mode ytterbium doped silica fibers," Opt. Express **14**, 11539–11544 (2006).
29. M. E. Fermann, "Single-mode excitation of multimode fibers with ultrashort pulses," Opt. Lett. **23**, 52–54 (1998).

Appendix 3

Publication 3

J. Kerttula, V. Filippov, Y. Chamorovskii, V. Ustimchik, and O. G. Okhotnikov, "Mode Evolution in Long Tapered Fibers with High Tapering Ratio", *Optics Express*, vol. 20, no. 23, pp. 25461-25470, 2012.

Mode evolution in long tapered fibers with high tapering ratio

Juho Kerttula,[1,*] Valery Filippov,[1] Vasily Ustimchik,[2] Yuri Chamorovskiy,[2] and Oleg G. Okhotnikov[1]

[1]*Optoelectronics Research Centre, Tampere University of Technology, P.O. Box 692, 33101 Tampere, Finland*
[2]*Institute of Radio Engineering and Electronics of the Russian Academy of Sciences, Mokhovaya 11, bld.7, 125009 Moscow, Russia*
[*]*juho.kerttula@tut.fi*

Abstract: We have experimentally studied fundamental mode propagation in few meters long, adiabatically tapered step-index fibers with high numerical aperture, core diameter up to 117 μm (V = 38) and tapering ratio up to 18. The single fundamental mode propagation was confirmed by several techniques that reveal no signature of higher-order mode excitation. It can be, therefore, concluded that adiabatic tapering is a powerful method for selective excitation of the fundamental mode in highly multimode large-mode-area fibers. Annular near field distortion observed for large output core diameters was attributed to built-in stress due to thermal expansion mismatch between core and cladding materials. The mechanical stress could be avoided by an appropriate technique of fiber preform fabrication and drawing, which would prevent the mode field deformation and lead to reliable diffraction-limited fundamental mode guiding for very large core diameters.

OCIS codes: (060.2270) Fiber characterization; (060.2280) Fiber design and fabrication; (060.2400) Fiber properties.

References and links

1. J. P. Koplow, D. A. V. Kliner, and L. Goldberg, "Single-mode operation of a coiled multimode fiber amplifier," Opt. Lett. **25**(7), 442–444 (2000).
2. Y. Jeong, J. Sahu, D. Payne, and J. Nilsson, "Ytterbium-doped large-core fiber laser with 1.36 kW continuous-wave output power," Opt. Express **12**(25), 6088–6092 (2004).
3. V. Fomin, M. Abramov, A. Ferin, A. Abramov, D. Mochalov, N. Platonov, and V. Gapontsev, "10 kW single-mode fiber laser," presented at the Fifth International Symposium on High-Power Fiber Lasers and Their Applications, St. Petersburg, Russia, 28 Jun. - 1 Jul. 2010.
4. J. Limpert, A. Liem, M. Reich, T. Schreiber, S. Nolte, H. Zellmer, A. Tünnermann, J. Broeng, A. Petersson, and C. Jakobsen, "Low-nonlinearity single-transverse-mode ytterbium-doped photonic crystal fiber amplifier," Opt. Express **12**(7), 1313–1319 (2004).
5. O. Schmidt, J. Rothhardt, F. Röser, S. Linke, T. Schreiber, K. Rademaker, J. Limpert, S. Ermeneux, P. Yvernault, F. Salin, and A. Tünnermann, "Millijoule pulse energy Q-switched short-length fiber laser," Opt. Lett. **32**(11), 1551–1553 (2007).
6. F. Stutzki, F. Jansen, A. Liem, C. Jauregui, J. Limpert, and A. Tünnermann, "26 mJ, 130 W Q-switched fiber-laser system with near-diffraction-limited beam quality," Opt. Lett. **37**(6), 1073–1075 (2012).
7. L. Dong, X. Peng, and J. Li, "Leakage channel optical fibers with large effective area," J. Opt. Soc. Am. B **24**(8), 1689–1697 (2007).
8. M. E. Fermann, "Single-mode excitation of multimode fibers with ultrashort pulses," Opt. Lett. **23**(1), 52–54 (1998).
9. S. Ramachandran, J. W. Nicholson, S. Ghalmi, M. F. Yan, P. Wisk, E. Monberg, and F. V. Dimarcello, "Light propagation with ultralarge modal areas in optical fibers," Opt. Lett. **31**(12), 1797–1799 (2006).
10. C. D. Stacey, R. M. Jenkins, J. Banerji, and A. R. Davies, "Demonstration of fundamental mode only propagation in highly multimode fibre for high power EDFAs," Opt. Commun. **269**(2), 310–314 (2007).
11. S. Hurand, L.-A. Chauny, H. El-Rabii, S. Joshi, and A. P. Yalin, "Mode coupling and output beam quality of 100-400 μm core silica fibers," Appl. Opt. **50**(4), 492–499 (2011).
12. N. Amitay, H. Presby, F. DiMarcello, and K. Nelson, "Optical fiber tapers–A novel approach to self-aligned beam expansion and single-mode hardware," J. Lightwave Technol. **5**(1), 70–76 (1987).
13. Y. Jung, Y. Jeong, G. Brambilla, and D. J. Richardson, "Adiabatically tapered splice for selective excitation of the fundamental mode in a multimode fiber," Opt. Lett. **34**(15), 2369–2371 (2009).

#173704 - $15.00 USD Received 2 Aug 2012; revised 9 Oct 2012; accepted 18 Oct 2012; published 25 Oct 2012

14. Y. Jung, G. Brambilla, and D. Richardson, "Efficient higher-order mode filtering in multimode optical fiber based on an optical microwire," in Asia Optical Fiber Communication and Optoelectronic Exposition and Conference, OSA Technical Digest (CD) (Optical Society of America, 2008), paper SuB4.
15. J. Kerttula, V. Filippov, Y. Chamorovskii, V. Ustimchik, K. Golant, and O. G. Okhotnikov, "Theoretical and experimental comparison of different configurations of tapered fiber lasers," in *Conference on Lasers and Electro-Optics/European Quantum Electronics Conference,* Technical Digest (CD) (Optical Society of America, 2011), paper CJ1_6.
16. V. Filippov, Y. Chamorovskii, J. Kerttula, K. Golant, M. Pessa, and O. G. Okhotnikov, "Double clad tapered fiber for high power applications," Opt. Express **16**(3), 1929–1944 (2008).
17. V. Filippov, Y. Chamorovskii, J. Kerttula, A. Kholodkov, and O. G. Okhotnikov, "600 W power scalable single transverse mode tapered double-clad fiber laser," Opt. Express **17**(3), 1203–1214 (2009).
18. J. Kerttula, V. Filippov, Y. Chamorovskii, K. Golant, and O. G. Okhotnikov, "Actively Q-switched 1.6-mJ tapered double-clad ytterbium-doped fiber laser," Opt. Express **18**(18), 18543–18549 (2010).
19. J. W. Nicholson, A. D. Yablon, S. Ramachandran, and S. Ghalmi, "Spatially and spectrally resolved imaging of modal content in large-mode-area fibers," Opt. Express **16**(10), 7233–7243 (2008).
20. G. W. Scherer, "Stress-induced index profile distortion in optical waveguides," Appl. Opt. **19**(12), 2000–2006 (1980).
21. O. E. Shushpanov, A. N. Tuzov, I. V. Alexsandrov, S. P. Vikulov, M. E. Zhabotinskii, V. V. Romanovtzev, and S. J. Feld, "An automated system for measurement of mechanical stresses in optical fiber preforms with polarization-optical method," Radiotechnika **43**, 67–72 (1988) (in Russian).
22. M. R. Hutsel, R. Ingle, and T. K. Gaylord, "Accurate cross-sectional stress profiling of optical fibers," Appl. Opt. **48**(26), 4985–4995 (2009).
23. A. W. Snyder, "Coupling of modes on a tapered dielectric cylinder," IEEE Trans. Microw. Theory Tech. **18**(7), 383–392 (1970).
24. D. Marcuse, "Mode conversion in optical fibers with monotonically increasing core radius," J. Lightwave Technol. **5**(1), 125–133 (1987).
25. P. M. Shankar, L. C. Bobb, and H. D. Krumboltz, "Coupling of modes in bent biconically tapered single-mode fibers," J. Lightwave Technol. **9**(7), 832–837 (1991).
26. L. C. Bobb, P. M. Shankar, and H. D. Krumboltz, "Bending effects in biconically tapered single-mode fibers," J. Lightwave Technol. **8**(7), 1084–1090 (1990).
27. D. Donlagic and B. Culshaw, "Propagation of the fundamental mode in curved graded index multimode fiber and its application in sensor systems," J. Lightwave Technol. **18**(3), 334–342 (2000).
28. F. Just, H.-R. Müller, S. Unger, J. Kirchhof, V. Reichel, and H. Bartelt, "Ytterbium-Doping Related Stresses in Preforms for High-Power Fiber Lasers," J. Lightwave Technol. **27**(12), 2111–2116 (2009).
29. J. W. Dawson, M. J. Messerly, R. J. Beach, M. Y. Shverdin, E. A. Stappaerts, A. K. Sridharan, P. H. Pax, J. E. Heebner, C. W. Siders, and C. P. Barty, "Analysis of the scalability of diffraction-limited fiber lasers and amplifiers to high average power," Opt. Express **16**(17), 13240–13266 (2008).

1. Introduction

Fiber mode area enlargement is one of the key means for power scaling and nonlinearity mitigation. Currently, there are three main approaches for development of near single mode (SM) large mode area (LMA) fibers, namely, low numerical aperture (NA) fibers, microstructured fibers such as large-pitch photonic crystal fibers (PCF) and leakage-channel fibers (LCF), and selective mode excitation in multi-mode (MM) fibers.

In low-NA fibers, controlled bending is often utilized to induce large losses for the high-order modes (HOM) [1], and the method was used to realize the first kW laser [2] and recently a 10-kW amplifier [3]. However, the core diameter usually remains limited to below 50 μm due to the minimum core/cladding refractive index difference (typically NA = 0.05-0.06) achievable by modified chemical vapor deposition (MCVD) technology. In addition, the guiding properties of these fibers are weak due to the low NA, making them highly sensitive to environmental perturbations, especially uncontrolled bends.

An alternative technology for mode area scaling is based on different types of microstructured fibers. Active PCF with small hole-diameter-to-pitch ratio d/Λ (< 0.1) was demonstrated in [4], and core diameter as large as 70 μm has been achieved [5]. Recently, the core diameter of a large-pitch PCF was further increased to 135 μm [6]. Similarly to low-NA fibers, PCFs of this type possess weak guiding properties, and they are realized as unbendable rod-type fibers; furthermore, their mode content is strongly dependent on pump power [6]. The basic principle of these fibers, the delocalization of higher order modes out of the guiding core, is also utilized in the LCF design [7]. In LCFs, the single mode LMA core is formed by channels introduced in the cladding to make the core waveguide leaky for all modes. Such

#173704 - $15.00 USD Received 2 Aug 2012; revised 9 Oct 2012; accepted 18 Oct 2012; published 25 Oct 2012

fibers can potentially be several meters long and bendable to a small diameter, although high-power experimental results are yet to be demonstrated.

Finally, mode area scaling can be achieved by selective excitation of a certain mode in a multimode fiber. Using a lens system for selective excitation of the fundamental mode in a multimode fiber with a core diameter of 45 μm and NA of 0.13, single-mode propagation over 23.5 m was demonstrated in [8]. The excitation of the single LP_{07} mode by using a long period fiber Bragg grating (LPG) in a multimode fiber with an 86-μm core was demonstrated in [9]. Furthermore, fundamental mode propagation through a 20-cm straight fiber with 300 μm core diameter and NA = 0.39 was demonstrated in [10], and propagation through 2 m in 100-μm core fiber was demonstrated in [11] with output M^2 of 1.6. The results of [8–11] allow concluding that mode coupling induced by macro-bends in fibers with a sufficiently large cladding diameter is small, and after excitation of a single mode (fundamental or another), the lone mode can propagate in a highly multimode core over long distances without significant mode conversion.

In addition to the free-space [8, 10, 11] and LPG [9] approaches, adiabatic tapering can be used for fundamental mode excitation in multimode fibers by using the SM end as a launching port. In this paper, we investigate the fundamental mode evolution in long, adiabatic, high-NA tapers with high tapering ratio. Although mode area scaling by tapering a multimode optical fiber has been reported [12–14], only short (few-cm) tapers with up to ~50 μm core diameters have been studied experimentally. Previously, we have proposed the use of long active tapered fiber as a gain medium for fiber lasers and amplifiers [15]. Experimentally, we have shown that the wide side core diameter can be scaled up to 40-60 μm (NA 0.11) with a diffraction-limited beam, whereas further increasing the core diameter often leads to deterioration of the output beam quality [16–18]. The main aim of this paper is a detailed experimental study of the evolution of the beam characteristics (modal composition, state of polarization, transversal mode field distribution, and beam quality) after mode area expansion in a long (several meters) tapered passive fiber with high NA, high tapering ratio, and core diameter up to 117 μm.

2. Experimental results

The longitudinal profiles of the tapered fibers are shown in Fig. 1. The 7-m and 20-m fibers have tapered lengths of approximately 5 m and 13 m, tapering ratios of 18 and 12, and maximum core diameters of 117 μm and 86 μm, respectively. Both tapers had a W-profile with core NA of 0.11, core to cladding diameter ratio of 1:6, and core diameter to outer diameter ratio of 1:14. The narrow end core diameter was approximately 6.5 μm, strictly single-mode for the 1 μm wavelength used in most measurements. Special attention was paid to the uniformity of the core refractive index, as the maximum core diameter in the 100 wavelengths range renders the mode field sensitive to any perturbation of the transversal index profile. Therefore, the rod-in-tube technology was used for preform fabrication to ensure a uniform index profile of the core. The preform core was a pure silica glass rod (type F-300), and the cladding was formed by fluoro-silicate glass layers deposited inside an F-300 tube by MCVD technique. After deposition of the cladding layers, the core rod was inserted into the tube, and the tapered fibers were pulled directly from the aggregate. The tapers were coated by a high-index polymer to remove cladding modes, and the diameters of the pulled fibers were controlled and measured at several locations during the drawing.

2.1 Mode field distribution and beam quality

Single-mode excitation

A cut-back measurement was used to determine the modal evolution during propagation in the 7-m tapered fiber. A 1060-nm SM diode source was launched by splicing the diode pigtail in the narrow end of the taper. For several cutting locations, the fiber diameter, 1-D and 2-D beam profiles, divergence, and M^2-parameter were measured for both straight and coiled (R =

#173704 - $15.00 USD Received 2 Aug 2012; revised 9 Oct 2012; accepted 18 Oct 2012; published 25 Oct 2012

15 cm) fiber. The first 50 cm in the wide side were kept approximately straight also in the coiled case. Figures 2(a) and 2(b) show the beam profiles in the near field and far field at the wide side output after propagation through several cut lengths of the shorter taper, respectively, and Fig. 2(c) shows the near and far field profiles after propagation through the entire 20-m taper.

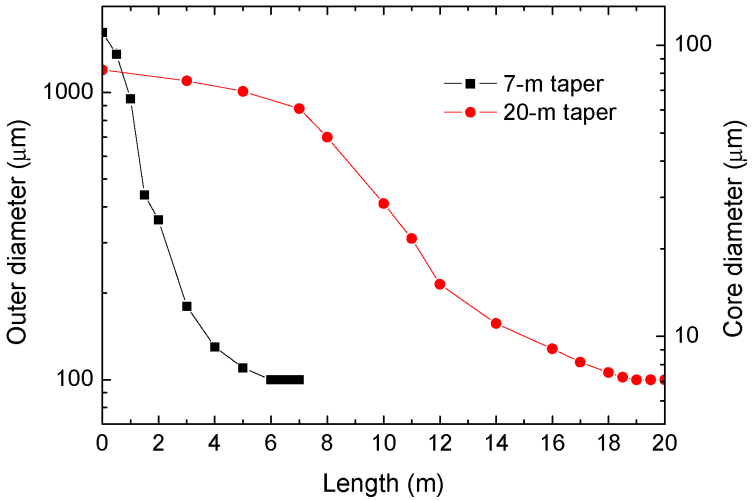

Fig. 1. Outer diameters (left axis) and core diameters (right axis) versus length of 7-m and 20-m tapers.

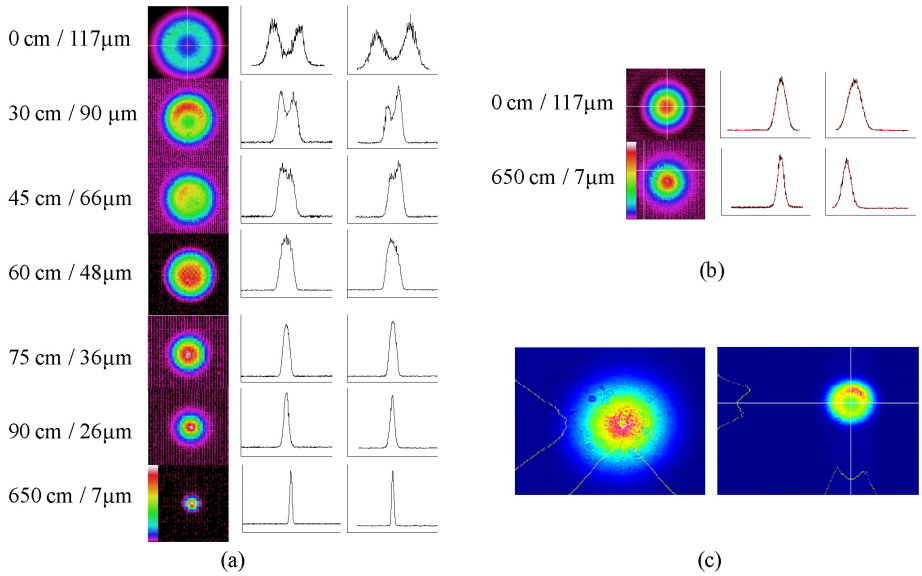

Fig. 2. (a) The core diameters and near field output beam profiles (2-D picture and 1-D graphs for two orthogonal axes) at different cut lengths measured from the large diameter output for straight 7-m taper. Bending or tension applied on the relatively rigid wide part of the taper resulted in a shift of the field distribution as shown in the second and third rows. (b) The far field beam profiles for the largest and smallest core diameters with Gaussian fits (red) in the 1-D profiles. Significant changes in the far field distribution were not observed at any output core diameter with any bending. (c) Far field (left) and near field (right) beam profiles for the uncut coiled 20-m taper.

#173704 - $15.00 USD Received 2 Aug 2012; revised 9 Oct 2012; accepted 18 Oct 2012; published 25 Oct 2012

The dependence of output beam quality on the cut-back was characterized by measuring the output beam divergence and M^2 (4σ-method, average of two measured orthogonal axes) at various cut lengths for both coiled and straight 7-m taper, with the results shown as a function of core diameter shown in Fig. 3. For the 20-m taper, the beam quality was measured for the uncut fiber with output core diameter 86 μm, with the results $M^2 = 1.31$ for R = 100 cm and $M^2 = 1.42$ for R = 15 cm. The output beam profiles are shown in Fig. 2(c).

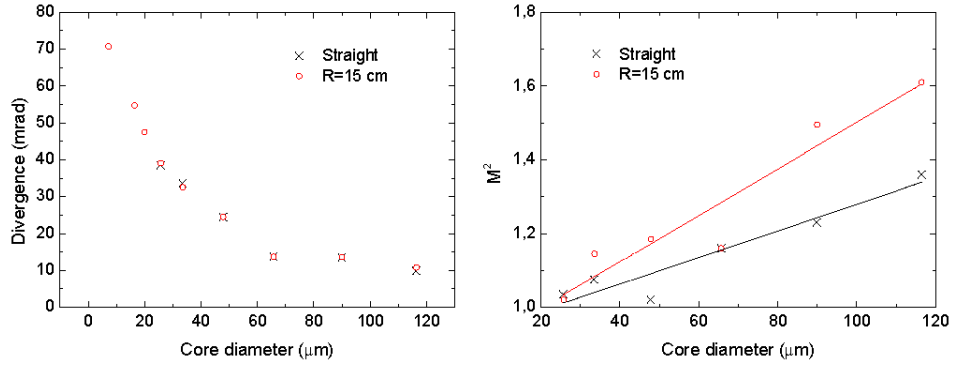

(a) (b)

Fig. 3. The output beam divergence (a) and M^2 (b) versus core diameter for straight and coiled 7-m taper.

Multi-mode excitation

Prior to the cut-back measurement, 532-nm and 1064-nm emission were launched into the narrow end of the 7-m taper from a frequency-doubled diode laser. At the wide end output, a dichroic filter was used to separate the two wavelengths. Figure 4(a) shows the wide output far field distribution for both wavelengths. As evident from Fig. 4(a), green excitation of the narrow input core (few-mode for green) led to apparent multi-mode output, whereas for the 1-μm excitation the far field had a Gaussian shape. The output divergence for both wavelengths was measured to be 10 mrad.

Furthermore, 1060-nm SM diode emission was launched into a highly multi-mode 30-cm taper section cut from the wide end with core diameter increasing from 90 μm to 117 μm. The SM diode pigtail was butt-coupled to the 90-μm core and the beam profiles, divergence, and polarization state were measured at the output. The output beam distributions are shown in Fig. 4(b) for centered and arbitrary excitation of the large core. The $1/e^2$ divergence measured after the 30 cm propagation was found to be 50 mrad and 86 mrad for centered and off-centered excitation, respectively.

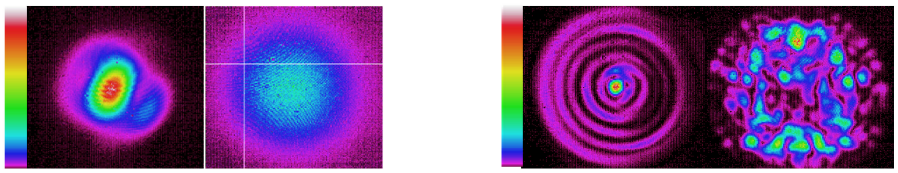

(a) (b)

Fig. 4. (a) The far field beam profiles from 117-μm output core for narrow-to-wide propagated green (left) and infrared (right) emission through the 7-m taper. (b) The near field beam profiles after propagation through the 30-cm fiber section cut from the 7-m taper with core diameter increasing from 90 μm to 117 μm. The butt-coupled SM input launching was centered for lowest order mode excitation achievable (left) or off-center core excitation (right).

#173704 - $15.00 USD Received 2 Aug 2012; revised 9 Oct 2012; accepted 18 Oct 2012; published 25 Oct 2012

2.2. State of polarization

The evolution of the state of polarization (SOP) during narrow-to-wide propagation through the long tapered fibers was studied with the 1060-nm SM diode emission. The Stokes parameters were determined after propagation through different taper sections shown in Table 1, and the degree of polarization (DOP), ellipticity ε, and azimuth θ of the SOP were calculated from the measured parameters. It should be noted that although ellipticity and azimuth are sensitive to perturbations such as bending of the pigtail, the DOP is not. The transmission through a polarizer for the 1060-nm SM diode pigtail output (99% DOP) and for the 7-m taper output is shown in Fig. 5. The degradation of DOP during propagation through the entire length of either taper was found negligible, whereas propagation through the 30-cm MM taper piece with core diameter 90 μm to 117 μm excited by butt-coupled SM fiber caused significant depolarization (Table 1).

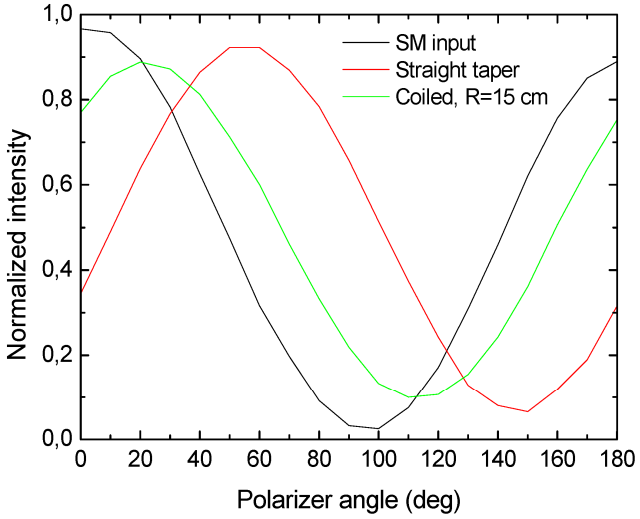

Fig. 5. (a) Transmission through a polarizer for the SM diode emission, and after narrow-to-wide propagation through coiled and uncoiled 7-m taper.

Table 1. Polarization measurements.

	DOP	ε	θ
SM diode pigtail	0.99	0.15	0.52
7-m taper, straight	0.98	0.20	0.51
7-m taper, R = 15 cm	0.97	0.14	0.34
20-m taper, straight	0.97	0.37	0.31
20-m taper, R = 15 cm	1.00	0.38	0.29
30-cm MM section of 7-m taper, centered excitation	0.80	0.15	0.067
30-cm MM section of 7-m taper, off-center excitation	0.84	0.18	0.081

DOP, ellipticity ε, and azimuth θ calculated from the measured Stokes parameters for various elements.

#173704 - $15.00 USD Received 2 Aug 2012; revised 9 Oct 2012; accepted 18 Oct 2012; published 25 Oct 2012

2.3. Mode content

Changes in mode content were experimentally studied for propagation through the entire 20-m taper based on the S^2-method [19]. Emission from a 1-μm broadband source was launched into the narrow end of the fiber, and a SM fiber acting as a spatial filter was butt-coupled to the wide output core. The SM fiber was not scanned over the entire output field, but only a few aperture locations were studied. The optical spectra at the source and at the output of the spatial filter were Fourier transformed to derive an intermodal group delay spectrum. The measurement was performed for various taper coiling radii and for different locations of the spatial aperture at the output core; however, coiling and aperture location had little effect on the beat spectrum. A typical group delay spectrum (R = 15 cm) is shown in Fig. 6. The spectrum of the broadband source exhibited some initial modulation resulting in harmonics in the Fourier domain; however, significant new harmonics could not be observed in the spectrum after propagation through the taper for any bending or aperture location.

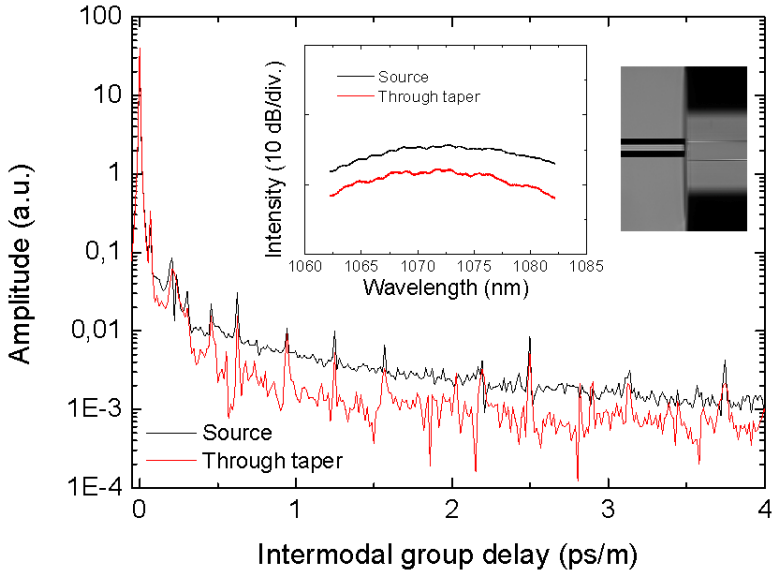

Fig. 6. Intermodal group delay spectrum normalized to fiber length for narrow-to-wide propagated broadband input. The insets show the optical spectra of the source before and after the 20-m taper, and an example location of the SM fiber (spatial filter) butt-coupled to the wide end taper core.

2.4. Impact of built-in mechanical stress

Built-in mechanical stresses in optical fibers may lead to significant changes in the refractive index profile of the core [20, 21]. We investigated the existence of such stresses in the studied tapers and their possible influence on the transverse field distribution of the output beam. A 37 mm long section with 1.6 mm outer diameter cut from the wide end of the 7-m taper was excited with a white light source to study the presence of mechanical stress. White light was launched into the fiber piece through a linear polarizer, and the output beam profile was measured as is, and through another (crossed) polarizer. The same measurement was performed after annealing the taper section for 4 h at 1000 °C. The observed output beam profiles are shown in Fig. 7.

#173704 - $15.00 USD Received 2 Aug 2012; revised 9 Oct 2012; accepted 18 Oct 2012; published 25 Oct 2012

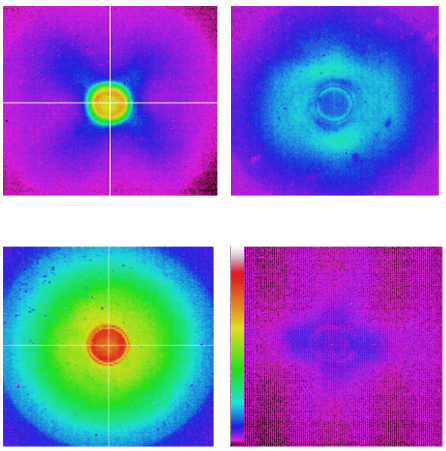

Fig. 7. The spatial distribution of linearly polarized white light propagated through a 37-mm taper section (117 μm core diameter) cut from the wide end of the 7-m taper (top left), and the same output after a crossed polarizer (top right). Bottom row: the same measurements after annealing of the fiber piece for 4 h at 1000 °C.

The cross-like structure resulting from mechanical stress is clearly visible in the spatial distribution at the taper output (Fig. 7, top left). The top right image in Fig. 7 shows the same output after transmission through a cross-state polarizer, illustrating the spatial distribution of mechanical stress in the transversal plane of the fiber. Two ring-shaped stress zones can be identified: a broad zone in the cladding, and a narrow zone at the core-cladding boundary. Thermal annealing led to almost complete elimination of the stress (Fig. 7, bottom row).

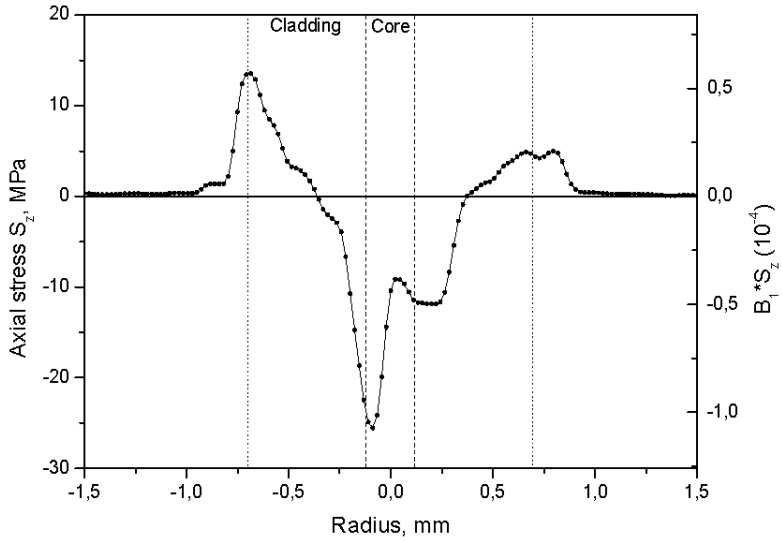

Fig. 8. The axial stress component (left axis) and the corresponding lower limit estimation of the stress-induced refractive index change (right axis).

Furthermore, a quantitative measurement of the intrinsic stress in the taper was carried out. A 1.6-mm diameter fiber segment was cut from the wide part of the 7-m taper and longitudinal mechanical stress was measured directly using a polarimetric setup [21, 22] with a spatial resolution of 20 μm. The result of this measurement shown in Fig. 8 reveals two

#173704 - $15.00 USD Received 2 Aug 2012; revised 9 Oct 2012; accepted 18 Oct 2012; published 25 Oct 2012

ring-like stress areas: a broad one in the cladding and a narrower one with an opposite sign at the core-cladding boundary, in agreement with the pictorial result presented in Fig. 7.

It should be noted that the stress measurement in Fig. 8 could only determine the axial (longitudinal) stress. The relevant radial refractive index change in an optical fiber in cylindrical coordinates is defined as $\Delta n_r = -B_2*S_r-B_1*(S_\theta + S_z)$, where B_1 and B_2 are the stress-optical coefficients for fused silica, and S_r, S_θ, S_z are the radial, tangential, and axial stress components, respectively [20]. Because B_1, $B_2 > 0$, $B_2 << B_1$, and the three stress components are of the same order of magnitude, B_1*S_z can be taken as a reasonable lower limit estimate for Δn_r (Fig. 8, right axis).

3. Discussion

The mode composition of multimode fiber output is determined mainly by three factors: initial mode excitation, local (e.g. due to a splice) or distributed (e.g. due to microbending) mode coupling, and differential modal attenuation or amplification. Thus, high-quality initial excitation and absence of significant mode coupling sources are essential for robust single-mode propagation. Adiabatic, splice-free fiber tapering is an excellent method for fundamental mode excitation in a large-core, highly-MM fiber. In an ideal taper, significant mode coupling can be caused either by changes of the core diameter [23, 24] or by local bending [25, 26]. Mode coupling in the tapered fiber due to varying core radius has been considered theoretically in [23, 24], and found negligible in long adiabatic tapers with small tapering angle. Furthermore, mode coupling in tapered fibers caused by local bends was studied in [25, 26], and the effect was shown to be strong only for local bends with radii of a few millimeters. This allows assuming that mode coupling in a long adiabatically tapered fiber is insignificant for practical coiling radii of tens of centimeters, given that the taper is free from imperfections such as abrupt diameter changes. In the present work, robust propagation of the solitary fundamental mode in long, step-index, highly-MM fiber tapers has been demonstrated for the first time with V up to 38 and fiber lengths of several meters. This became possible by the record tapering ratio (up to 18), and the absence of any significant structural flaws and splicing points, although some variation of core diameter due to small oscillation of the pull speed regulation system remains possible.

The solitary fundamental mode propagation has been confirmed by several experiments. First, the measured large-diameter output beam divergence of 10 mrad (Fig. 3(a)) closely corresponds to the theoretical limit $1.22\lambda/D$, where λ is the wavelength and D is the output core diameter. Second, the propagation of SM diode emission through the studied tapers did not cause noticeable degradation of DOP (Table 1). For comparison, propagation through a 30-cm highly-MM taper section caused up to 20% depolarization and increased divergence to 86 mrad for arbitrary excitation. Third, the 7-m taper was simultaneously excited in the narrow end by 1064-nm (V = 1.5) and 532-nm (V = 4.6) emission, revealing apparent MM output for green and a Gaussian far field for infrared. The output divergence for both wavelengths was the same (10 mrad), although the theoretical limit for green is 50% less. Finally, the near constancy of the mode composition of the 1060-nm SM input propagating through the 20-m taper was confirmed by a simplified S^2 method.

With increasing core size, the originally Gaussian field distribution gradually assumed a top-hat shape (~50 μm core), followed by an annular profile at larger diameters (Fig. 2(a)). The evolution of the near field distribution is accompanied by moderate increase in M^2 (Fig. 3(b)). Interestingly, the progressive mode field distribution change is characteristic only to the near field, whereas far field distribution remains nearly Gaussian for any core diameter (Fig. 2(b), 2(c)). Usually, such an annular near field shape is associated with a higher order mode (LP_{02}) excitation or a central dip in the core index profile. Since the mode content did not change, and the core index profile was uniform, this behavior was ascribed to built-in mechanical stress, which has a ring structure (Figs. 7, 8), modulates the magnitude of the refractive index by several percent, and distorts the fundamental mode field.

#173704 - $15.00 USD Received 2 Aug 2012; revised 9 Oct 2012; accepted 18 Oct 2012; published 25 Oct 2012

The internal mechanical stress associated with inhomogeneous cooling of the fiber structure during drawing (quenching stress), the mismatch of the thermal expansion coefficients of core and cladding materials [22] or external stress due to bends [27] can lead to a distortion of the mode field and finally limit the output beam quality. Furthermore, it was recently shown that the presence of rare-earth dopants may lead to additional stress [28]. As can be seen from Fig. 2(a), the distortion of the mode shape becomes significant around 700 μm outer diameter (~50 μm core diameter), likely determined by the magnitude of built-in stress induced by the specific dynamics of fiber cooling during the drawing process. Although the preform of the studied fibers was ensured to have a uniform core index profile, stress compensation or mitigation methods were not applied. By utilizing annealing procedures, modifying the chemical composition of the core and cladding to match their thermal expansion coefficients, and varying the geometry of the pulled fibers, it should be possible to avoid the observed deformation of the fundamental mode field.

In addition to the built-in stress, mechanical stresses due to bending exist in a long fiber which inevitably needs to be coiled for practical purposes [27]. As shown by our experiments, bending of the studied tapers leads to an asymmetric deformation of the beam. Whereas the cross-section of the beam after propagation through a straight taper has a symmetric ring structure (Fig. 2(a)), propagation through a coiled taper leads to a crescent-shaped near field profile (Fig. 2(c)) and results in moderate degradation of the beam quality (Fig. 3(b)). However, coiling did not induce changes in the output divergence (Fig. 3(a)), the DOP (Table 1), or mode composition (Fig. 6), which allows concluding that although the bend-induced stress in a coiled taper distorts the fundamental mode field, its effect on mode coupling is small. As in any LMA fiber, small-radius bending of the taper will eventually limit the achievable mode area [29] even if the built-in stress can be avoided, unless bend-compensation methods are utilized. However, with the single fundamental mode guiding, additional complications associated with HOM content can be avoided.

4. Conclusion

In this paper, robust single-mode propagation without depolarization in few-meter long, step-index, high-NA adiabatic tapers with core diameter up to 117 μm (V = 38) and tapering ratio up to 18 was experimentally demonstrated. Nevertheless, the field distribution of the fundamental mode was found to exhibit annular distortion in the near field for large core size. The distortion was attributed mainly to built-in stress in the cladding and at the core-cladding boundary, likely due to inhomogeneous cooling during drawing and mismatched thermal expansion coefficients of the core and cladding materials.

The robust fundamental mode propagation practically without mode coupling illustrates the potential of long adiabatic tapers particularly for traveling-wave LMA amplifiers and high power delivery. Avoiding the built-in stress by careful design of core and cladding materials, doping, and fiber geometry is expected to allow scaling to very high core diameters with diffraction-limited output.

Acknowledgments

The authors would like to thank O. E. Shushpanov for measurements of mechanical stresses in the fiber and G. A. Ivanov and I. L. Vorob'ev for help with the preform preparation. This research was supported in part by the Finnish Funding Agency for Technology and Innovation (Tekes) project MARTEC, the Graduate School in Electronics, Telecommunications and Automation (GETA), and the Walter Ahlstrom Foundation.

#173704 - $15.00 USD Received 2 Aug 2012; revised 9 Oct 2012; accepted 18 Oct 2012; published 25 Oct 2012

Appendix 4

Publication 4

V. Filippov, Y. Chamorovskii, J. Kerttula, A. Kholodkov, and O. G. Okhotnikov, "Single-mode 212 W tapered fiber laser pumped by a low-brightness source", *Optics Letters*, vol. 33, no. 13, pp. 1416–1418, 2008.

Single-mode 212 W tapered fiber laser pumped by a low-brightness source

Valery Filippov,[1,*] Yuri Chamorovskii,[2] Juho Kerttula,[1] Artem Kholodkov,[2] and Oleg G. Okhotnikov[1]

[1]*Optoelectronics Research Centre, Tampere University of Technology, 33101 Tampere, Finland*
[2]*Institute of Radio and Electronics of the Russian Academy of Sciences, Mokhovaya 11, Building 7, 125009 Moscow, Russia*
**Corresponding author: valery.filippov@tut.fi*

Received February 14, 2008; accepted April 24, 2008;
posted May 23, 2008 (Doc. ID 92794); published June 19, 2008

With a tapered double-clad all-glass ytterbium fiber as a gain medium, a maximum output power of over 200 W at 1079 nm and a slope efficiency of over 70% were demonstrated. The tapered double-clad fiber concept allows for using low-brightness diode bars and results in cost-effective and efficient high-power fiber lasers. The adiabatic conical fiber gain waveguide combines improved pump absorption owing to enhanced mode mixing in the pump cladding, low-noise single fundamental mode operation with $M^2 \leqslant 1.02$, and strong potential for significant power scaling. © 2008 Optical Society of America

OCIS codes: 060.2320, 060.2340, 060.3510, 140.3615.

Different types of lasers based on so-called tapered or flared waveguides have been demonstrated and studied during the past decade. The essential advantage of these lasers is that they can be pumped efficiently by low-brightness optical sources through the large-dimension end of the tapered structure. Another attractive characteristic of tapered design is the spatial filtering that occurs in a small cross-sectional part of the waveguide providing transverse mode selection. It has been demonstrated that tapered structure with proper mode control could exhibit robust fundamental mode operation.

Tapered waveguide systems reported to date include lasers using a planar waveguide based on an ion-exchanged Nd:glass [1] polymer fiber doped with Rhodamine-6G dye [2] and double-clad fiber [3–5]. Among those, the tapered planar waveguide and polymer fiber lasers exhibit poor slope efficiency, typically below 10%–20%, and low output power of up to tens of milliwatts. In contrast, the tapered double-clad glass fiber lasers demonstrate an essentially better performance [3–5]. For instance, a tapered fiber laser composed of a multimode ytterbium double-clad fiber with a core diameter of 15 μm, NA=0.15, and V=6.7 has revealed a 67% slope efficiency and 9 W of output power [3]. To introduce a significant insertion loss for high-order modes, a 3 cm long piece of active fiber has been tapered down. The tapered section inside the laser cavity enhanced the brightness by a factor of 3.5, though with a power penalty of ~20% [3]. Better beam quality with M^2=1.14 and output power scaling to 56.4 W have been reported recently [4]. However, the power penalty induced by the tapered structure was 30.6%, and the slope efficiency was only 54.1%. It should be noted that this type of tapered geometry has a significant disadvantage owing to poor mode control. Some modes, especially LP_{11}, could propagate through the taper with low loss as a leaking mode, and, consequently, higher-order modes propagation throughout the tapered section could not be prevented completely. As a result, truly single-mode operation could not be demonstrated and the best beam quality was limited to M^2=1.14–1.4 [3,4]. To resolve this problem, ytterbium double-clad fiber with a multimode core coupled to a piece of single-mode fiber through a few millimeter long adiabatic taper has been proposed [5]. Using a single-mode fiber in the cavity guarantees the fundamental mode operation; however, the slope efficiency was only 30% at 0.45 W of output power. The poor efficiency is expected with this design owing to significant intracavity losses caused by nonadiabatic mode conversion in the tapered part.

The tapered lasers discussed above contain double-clad fiber, and, therefore, they exhibit the disadvantages inherent for these fibers. The most serious issue is a low pump absorption in the active double-clad fiber originated from absorption saturation [6]. The poor pump absorption dictates the use of relatively long fibers that, in turn, leads to a mode coupling–conversion and higher-order mode excitation in the tapered core that could result in additional losses and degradation in the beam quality. The value of the outer clad diameter determines the highest pump power that could be launched into it, whereas the pump absorption in the double-clad fiber depends on core absorption, i.e., active ions concentration and core–cladding area ratio [7]. To keep reasonably small the value of the normalized frequency V, the core diameter should typically not exceed 15–20 μm. As a consequence, the outer cladding di-

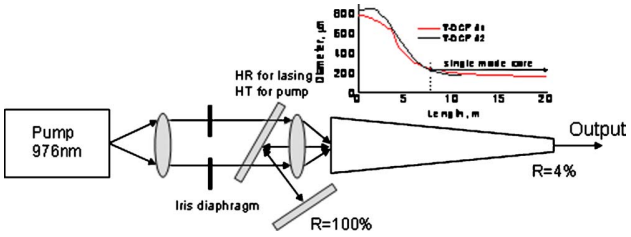

Fig. 1. (Color online) Schematic of fiber laser with a T-DCF. Inset, tapered double-clad fiber diameter as function of fiber length. T-DCF 1 has 780 μm OD [gray curve (red online)] and T-DCF 2 has 834 μm OD.

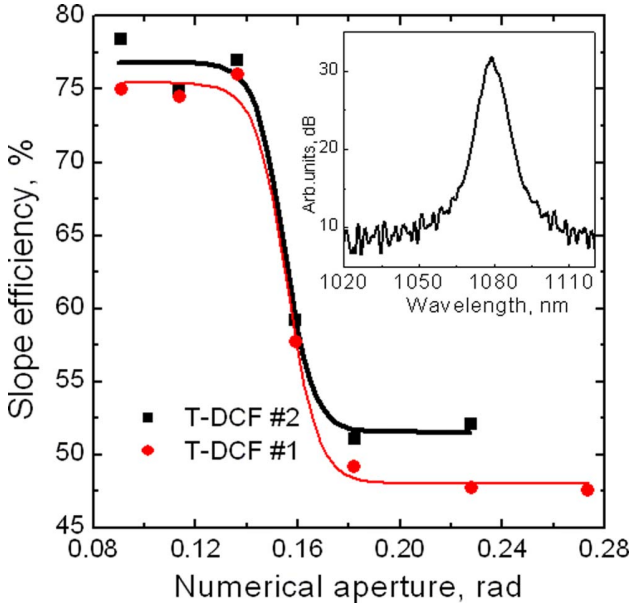

Fig. 2. (Color online) Slope efficiency versus NA of the launched pump radiation for T-DCF 1 (circles) and 2 (squares). Inset, spectrum of output emission taken at the highest output power (212 W).

ameter is limited to 300–400 μm, which imposes certain limitations to the pump source brightness. As becomes apparent from the above overview, the tapered guides studied previously represent composite "steplike" tapered structures obtained by joining fibers with different mode-field distributions. Consequently, they suffer from poor mode matching that eventually results in high loss and low efficiency.

In this Letter the power scaling, efficiency, and beam-quality enhancement have been achieved using a novel tapered double-clad fiber (T-DCF). The T-DCF is an active double-clad fiber with the diameter adiabatically varying over the *entire* length thus limiting the mode content exclusively to the fundamental mode by preventing the mode conversion. The properties of the T-DCF as an active medium were studied recently [8]. The large-dimension section of taper with a clad diameter of 700–900 μm could serve as a launching end for high-power pump radiation with low brightness. The downtapered single-mode section of the taper plays the role of an efficient spatial filter suppressing higher-order mode excitation in the fiber core. At the same time, the gradual change of the T-DCF diameter was shown to offer a strong mechanism of *mode mixing in a multimode pump cladding* and, as result, high pump absorption occurs even for a low doping level and a small core–clad ratio [8].

We prepared ytterbium-doped T-DCFs with different lengths and diameters downtapered adiabatically to ensure single-mode propagation [8]. The variation of the cladding diameter with the length for two samples of the T-DCF with a core–cladding ratio of 1:31 is shown in Fig. 1, inset. To avoid fiber overheating owing to pump absorption by polymer cladding [9], the all-glass cladding with NA=0.21 was implemented. The NA of the active core is NA=0.114. The measured in-core pump absorption was 280 dB/m, and the clad pump absorption was 0.9 dB/m, both at 976 nm.

The experimental setup used in our experiments is shown in Fig. 1. A 500 W fiber-coupled laser diode emitting at 976 nm with fiber diameter of 600 μm and NA=0.22 has been used as a pump source [Laserline, beam parameter product (BPP) is 66 mm mrad]. Pump radiation was launched into a wide end of the T-DCF via lenses and dichroic filter. The laser cavity was formed by a high-reflective mirror and Fresnel reflection from the small-diameter facet of the taper (Fig. 1).

We demonstrated earlier that to avoid optical losses owing to a vignetting and to get high slope efficiency, the aperture of the T-DCF should be filled only partially [8]. The pump absorption and the axial shape of the T-DCF determine the upper value of the NA of pump radiation required to achieve a given conversion efficiency (slope efficiency). To identify an optimal NA, the slope efficiency has been measured as a function of the NA of the pump radiation launched into two tapers. The adjustable iris diaphragm, shown in Fig. 1, was used to change the NA of the pump light. The results presented in Fig. 2 reveal the optimal value for a NA of 0.14–0.15 for both T-DCFs. The tapered fiber 2 with a diameter of 834 μm at the large end has been used in a laser, as shown in Fig. 1, inset. Analysis shows that only 89% of optical power can be coupled from a 600 μm NA =0.22 fiber to a 834 μm fiber with NA=0.15 [10]. Up to 350 W of pump power could be actually launched to a T-DCF. The measured coupling efficiency of 70% can be explained by taking into account the reflections from lenses, the uncoated side of dichroic filter, and the end face of the T-DCF.

Figure 3 shows that the laser output increases lin-

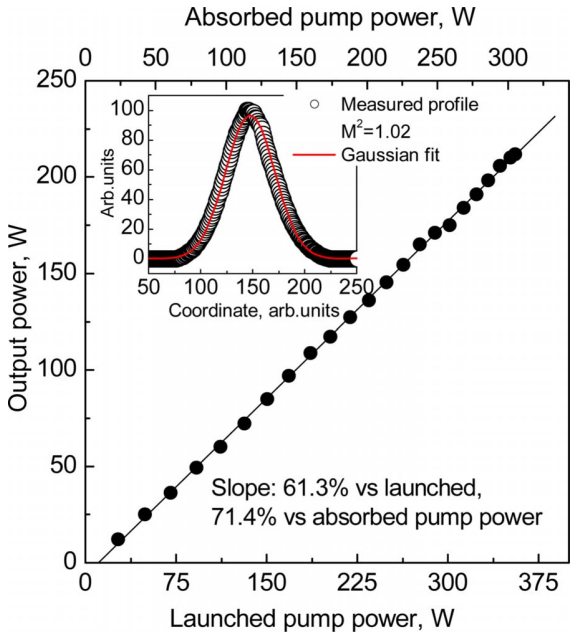

Fig. 3. (Color online) Output power of a fiber laser with a T-DCF as a function of the launched (absorbed) pump power. Inset, beam profile (circles) of output emission and Gaussian fit [gray curve (red online)].

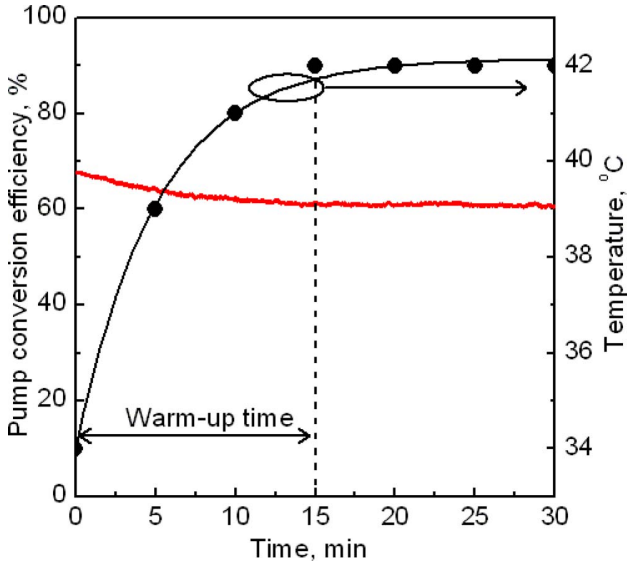

Fig. 4. (Color online) Temporal variation of the T-DCF laser pump conversion efficiency [gray curve (red online)] and corresponding temperature of the pump diode.

early with launched–absorbed pump power without evidence of rollover at the highest output power limited only by the available pump. The maximum output obtained with the laser was measured to be 212 W, resulting in a slope efficiency of 61.3% and 71.4% relative to a launched and absorbed pump power, respectively. The laser spectrum was centered at 1079 nm with a FWHM bandwidth of 7 nm, as shown in Fig. 2, inset. The laser beam has a nearly ideal Gaussian profile with $M^2=1.02$ (Fig. 3, inset).

The wide-core section of the T-DCF obviously represents a multimode waveguide, whereas the small-core part of the T-DCF guides only the fundamental mode. The adiabatic axial shape of the taper is essential because it causes spatial transformation of the fundamental mode without coupling to higher-order modes and preserves the single-mode character of oscillation. Otherwise, mode competition–conversion in a multimode section of the taper and subsequent spatial filtering in a single-mode part could be expected to result in a strong intensity noise. Thus, the existence strength of mode competition in the ytterbium-doped axially nonuniform core gain fiber could be indirectly estimated by monitoring the time behavior of the laser output. The temporal variation of pump conversion efficiency, i.e., output power–absorbed pump power, has been recorded during a time interval of 30 min. As can be seen from the results displayed in Fig. 4, without implementing any stabilization measures after a warm-up period of 10 min, the laser emits stably with an intensity variation below 1%. The "quiet" output characteristic confirms the single-mode property of the oscillation otherwise supported by the good beam quality confirmed above.

In summary, we have demonstrated a 212 W single-mode ytterbium fiber laser using a T-DCF suitable for pumping with low-brightness sources. The diameter of the wide end of the T-DCF can in principle be further increased up to 2 mm. Taking into account that the NA of pump radiation should not exceed 0.15 (Fig. 2), pumping sources with BPP ~150 mm mrad can be used. To date, pump sources with a few kilowatts of output power are commercially available featuring this value of BPP [11]. For lasers with low or medium power it is possible to exploit a polymer with low refraction index as a clad coating, which would further reduce the requirements to BPP of the pumping source. Hence, using the polymer with a refraction index of 1.37 would increase the acceptable NA for a pump radiation to NA=0.46 and allow the use of pump sources with BPP~300 mm mrad. The fiber lasers based on the T-DCF concept open up the opportunity for using cost-effective diode bars and will result in inexpensive and efficient high-power fiber lasers. The smooth conical fiber waveguide as a gain medium combines improved pump absorption owing to enhanced mode mixing in the pump cladding with low-noise single fundamental mode operation in an adiabatically tapered amplifying core and has a strong potential for significant power scaling.

The authors thank G. Rehmann for help in the preparation of an experiment.

References

1. S. J. Hettrick, J. Wang, C. Li, J. S. Wilkinson, and D. P. Shepherd, J. Lightwave Technol. **22**, 845 (2004).
2. Q. Peng, G. Wang, Y. Bo, X. Guo, A. Geng, Z. Xu, L. Ren, Y. Zhang, Y. Wang, W. Zhao, and L. Wang, Appl. Phys. Lett. **87**, 251101 (2005).
3. J. A. Alvarez-Chavez, A. B. Grudinin, J. Nilsson, P. W. Turner, and W. A. Clarkson, in *Conference on Laser and Electro-Optics*, OSA Technical Digest (Optical Society of America, 1999), p. 247.
4. L. Li, Q. Lou, J. Zhou, J. Dong, Y. Wei, S. Du, and B. He, Opt. Commun. **281**, 655 (2008).
5. M. J. Dejneka, B. Z. Hanson, S. G. Crigler, L. Zenteno, J. D. Minelly, D. C. Allan, W. J. Miller, and D. Kuksenkov, J. Am. Ceram. Soc. **85**, 1100 (2002).
6. P. Leproux, S. Fevrier, V. Doya, P. Roy, and D. Pagnoux, Opt. Fiber Technol. **6**, 324 (2001).
7. D. Young and C. Roychoudhuri, Opt. Express **11**, 830 (2003).
8. V. Filippov, Yu. Chamorovskii, J. Kerttula, K. Golant, M. Pessa, and O. G. Okhotnikov, Opt. Express **16**, 1929 (2008).
9. V. Reichel, S. Unger, K. Mörl, H.-R. Müller, T. Sandrock, and A. Harschak, in *Proceedings of the Conference on Lasers and Electro-optics (CLEO) Europe 2003* (IEEE, 2003), paper CL-3-FRI.
10. M. Hudson, Appl. Opt. **13**, 1029 (1974).
11. http://www.laserline.de/.

Appendix 5

Publication 5

V. Filippov, Y. Chamorovskii, J. Kerttula, A. Kholodkov, and O. G. Okhotnikov, "600 W power scalable single transverse mode tapered double-clad fiber laser", *Optics Express*, vol. 17, no. 3, pp. 1203–1214, 2009.

600 W power scalable single transverse mode tapered double-clad fiber laser

V. Filippov,[1*] Y. Chamorovskii,[2] J. Kerttula[1], A. Kholodkov[2] and O. G. Okhotnikov[1]

[1]*Optoelectronics Research Centre, Tampere University of Technology, 33101 Tampere, Finland*
[2]*Institute of Radio and Electronics of the Russian Academy of Sciences, Mokhovaya 11, bld.7, 125009 Moscow, Russia*
[*]*Corresponding author: valery.filippov@tut.fi*

Abstract: Pump propagation and absorption in active tapered double-clad fiber has been analyzed based on a ray optics approach. Optimization of the longitudinal shape, absorption and angular distribution of the pump beam allowed for power scaling of a ytterbium fiber laser up to 600 W with high beam quality ($M^2 \leq 1.08$) and a slope efficiency of 63%. It is shown that the influence of vignetting in a tapered fiber can be avoided, resulting in high overall efficiency, in good agreement with the presented model.

OCIS codes: (060.2280) Fiber design and fabrication; (060.2320) Fiber optics amplifiers and oscillators; (060.3510) Lasers, fiber

References and links

1. www.ipgphotonics.com
2. S. Gray, A. Liu, D. T. Walton, J. Wang, M. Li, X. Chen, A. B. Ruffin, J. A. DeMeritt, and L. A. Zenteno, "502 Watt, single transverse mode, narrow linewidth, bidirectionally pumped Yb-doped fiber amplifier," Opt. Express **15**, 17044-17050 (2007), http://www.opticsinfobase.org/oe/abstract.cfm?URI=oe-15-25-17044.
3. Y. Jeong, J. Sahu, D. Payne, and J. Nilsson, "Ytterbium-doped large-core fiber laser with 1.36 kW continuous-wave output power," Opt. Express **12**, 6088-6092 (2004), http://www.opticsinfobase.org/oe/abstract.cfm?URI=oe-12-25-6088.
4. G. Bonati, H. Voelckel, T. Gabler, U. Krause, A. Tunnermann, J. Limpert, A. Liem, T. Schreiber, S. Nolte and H. Zellmer, "1.53 kW from a single mode Yb-doped crystal fiber laser," Photonics West, Late Breaking Developments, Session 5709-2a (The International Society for Optical Engineering, 2005).
5. V. Filippov, Y. Chamorovskii, J. Kerttula, K. Golant, M. Pessa, and O. G. Okhotnikov, "Double clad tapered fiber for high power applications," Opt. Express **16**, 1929-1944 (2008), http://www.opticsinfobase.org/abstract.cfm?URI=oe-16-3-1929.
6. V. Filippov, Y. Chamorovskii, J. Kerttula, A. Kholodkov, and O. G. Okhotnikov, "Single-mode 212 W tapered fiber laser pumped by a low-brightness source," Opt. Lett. **33**, 1416-1418 (2008), http://www.opticsinfobase.org/ol/abstract.cfm?URI=ol-33-13-1416.
7. V. Filippov, Y. Chamorovskii, J. Kerttula, A. Kholodkov, and O. G. Okhotnikov, "High power tapered ytterbium fiber laser pumped by a low-brightness source," 3rd EPS-QEOD Europhoton Conference on Solid-State, Fiber and Waveguided Light Sources, 31 August – 05 September 2008, Paris (France), Europhysics Conference Abstract vol.32G, ISBN: 2-914771-55-X, paper TUoC.3, p. 33.
8. N. S. Kapany and J. J. Burke, *Optical waveguides* (Academic Press, New York, 1972).
9. V. B. Veinberg and D. K. Sattarov, *Waveguide Optics* (Mashinostroenie, Leningrad, 1977), Chap.5 (in Russian).
10. http://www.laserline.de/
11. J. Limpert, N. Deguil-Robin, I. Manek-Hönninger, F. Salin, F. Röser, A. Liem, T. Schreiber, S. Nolte, H. Zellmer, A. Tünnermann, J. Broeng, A. Petersson, and C. Jakobsen, "High-power rod-type photonic crystal fiber laser," Opt. Express **13**, 1055-1058 (2005), http://www.opticsinfobase.org/oe/abstract.cfm?URI=oe-13-4-1055.
12. L. Michaille, C. R. Bennett, D. M. Taylor, T. J. Shepherd, J. Broeng, H. R. Simonsen, and A. Petersson, "Phase locking and supermode selection in multicore photonic crystal fiber lasers with a large doped area," Opt. Lett. **30**, 1668-1670 (2005), http://www.opticsinfobase.org/ol/abstract.cfm?URI=ol-30-13-1668.

1. Introduction

The technology of high power fiber lasers and amplifiers has undergone a significant progress during last decade. These devices are either side-pumped by large number of relatively low

#103845 - $15.00 USD Received 11 Nov 2008; revised 24 Dec 2008; accepted 5 Jan 2009; published 16 Jan 2009

power (~10 W) fiber coupled diodes through pump combiners or end-pumped by diode bars through the end face of an active double clad fiber [1-2]. The highest output power demonstrated to date (1.36 kW in [3] and 1.53 kW in [4]) has been achieved with diode bars producing kilowatt level pump power and low brightness beam. The end pumped configuration usually implements the large mode area (LMA) active double clad fiber with clad diameter of 400÷600 μm. The pump absorption in the double clad fibers proportional to the core/clad area ratio which is typically in a range of $2.5\times(10^{-3}\div10^{-2})$. It should be noted that this approach has an intrinsic limitation determined by the trade-off between core and clad size. Indeed, since the core diameter is determined by the fundamental mode operation, the clad diameter cannot be increased considerably without reducing the pump absorption. Therefore, the clad diameter imposes eventually the limitation on the launched pump power and, consequently, on the output power of the end-pumped fiber laser.

Recently, we have proposed an active tapered double-clad fiber (T-DCF) as a gain medium for high power fiber lasers and amplifiers [4-7]. T-DCF was shown to have several distinct advantages as compared with regular fibers, particularly, it can be pumped with low brightness sources and offers an efficient intrinsic mode mixing mechanism resulting in enhanced pump absorption and robust single mode generation.

It should be mentioned that longitudinally irregular T-DCF generally exhibits additional loss of pump radiation owing to leakage to the cladding. Indeed, pump propagation in the cladding of tapered double-clad fiber is accompanied by a gradual increase of propagation angle relative to the fiber axis. As a result, when the condition of total internal reflection is violated, some rays leak to the pump cladding, leading to the so-called vignetting effect [8, 9]. The total pump power balance, therefore, includes pump absorbed by the active core, pump which passes through the fiber unabsorbed and appears at the small-core end of the taper as residual pump, and pump radiation which leaks out of the fiber. The pump power absorption can therefore not be estimated from the launched and unabsorbed pump power ratio, which is the usual method applied in the case of regular fibers. A model of pump propagation/absorption in tapered active fiber allowing accurate optimization of T-DCF operation has not been available until now.

In this paper, we present a theoretical model of tapered active fiber which provides an adequate tool for T-DCF optimization. Over 600 W output power in the fundamental spatial mode regime has been demonstrated. Good agreement with theoretical predictions suggests that a further increase of output power would be possible.

2. Theoretical model

The conceptual structure of T-DCF is shown in Fig. 1 (a). It contains a core doped with rare earth ions, a cladding with index of refraction $\boldsymbol{n}_{clad}$, where the pump emission propagates, and an outer cladding with low index of refraction. The diameter of T-DCF gradually decreases toward the narrow end, which ensuring single mode propagation regime.

The pump propagation throughout an active T-DCF has been analyzed using ray optics, taking into account meridional rays. The essential difference of T-DCF, as compared with regular fiber, is a gradual increase of the propagation angle relative to the fiber axis, shown in Fig. 1 (a). Eventually, the propagation angle exceeds the critical angle for total internal reflection, resulting in pump leakage (refraction) into the secondary cladding, which is known as the vignetting phenomenon [7, 8]. We consider the propagation of meridional rays through a taper whose diameter has a linear dependence on the axial length $\boldsymbol{L}$, with the diameters of the wide and narrow ends being $\boldsymbol{D_1}$ and $\boldsymbol{D_2}$, respectively (Fig. 1 (a)).

#103845 - $15.00 USD Received 11 Nov 2008; revised 24 Dec 2008; accepted 5 Jan 2009; published 16 Jan 2009

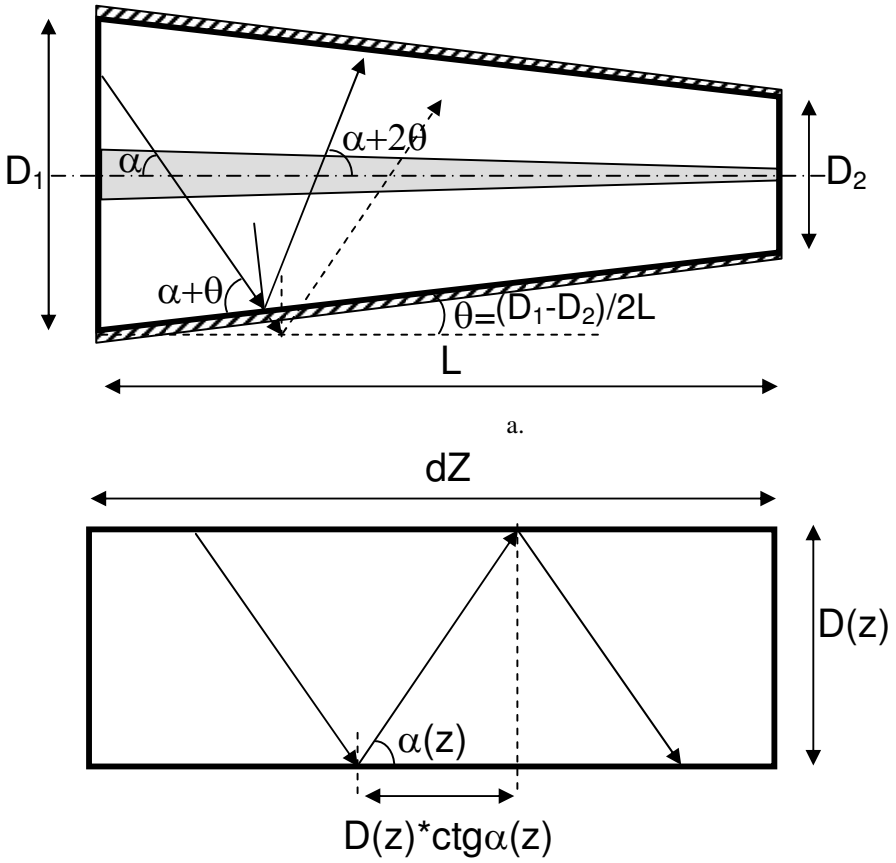

Fig. 1. Ray trajectory in: (a) tapered fiber and (b) cylindrical fiber.

The angle of linear taper is given by

$$\theta = \frac{D_1 - D_2}{2L} \tag{1}$$

and the diameter of the taper as a function of length can be written as

$$D(z) = D_1 - 2\theta \cdot z\,, \tag{2}$$

where z – is the axial coordinate of the tapered fiber.

Meridional rays propagating in a regular cylindrical fiber without undergoing refraction are reflected repeatedly at the boundary between two media of different refractive indices; the angles of reflection are always equal to the angles of incidence when they exceed the critical angle (Fig. 1 (b)). To the contrary, the angle of reflection in a linear taper increases after each reflection, by a value of 2θ. The ray changes its angle with the propagation length according to

#103845 - $15.00 USD Received 11 Nov 2008; revised 24 Dec 2008; accepted 5 Jan 2009; published 16 Jan 2009

$$\alpha(z) = {\alpha_{in}}/{n_{clad}} + 2\theta \cdot \eta(z), \tag{3}$$

where α_{in} – is the angle of incidence onto the taper, n_{clad} is the cladding refractive index and $\eta(z)$ is the number of multiple reflections in the taper occurring before the propagation distance z.

The angle θ is small, typically a few microradians, therefore, a tapered fiber with infinitesimal length dZ can be approximated by a cylindrical shape [8, 9]. The total number of reflections $\eta(z)$ of a ray propagating with the angle $\alpha(z)$ within a taper of length dZ and diameter $D(z)$ (see Fig.1 (b)) can then be approximated by

$$d\eta = \frac{dz}{D(z)} tg\alpha(z). \tag{4}$$

Combining equations (2), (3) and (4) we can obtain an equation for the number of meridional ray reflections in a circular linear taper

$$\frac{d\eta}{tg\left({\alpha_{in}}/{n_{clad}} + 2\theta \cdot \eta\right)} = \frac{dz}{D_1 - 2\theta \cdot z}. \tag{5}$$

To calculate the total number of reflections in a linear taper, one should integrate Eq.(5)

$$\eta(z) = \frac{a\sin\left(\dfrac{D_1 \cdot \sin\left({\alpha_{in}}/{n_{clad}}\right)}{D_1 - 2\theta \cdot z}\right) - {\alpha_{in}}/{n_{clad}}}{2\theta}. \tag{6}$$

Substituting Eq. (6) into (3) yields an expression for the meridional ray angle after a propagation distance z in a linear taper

$$\alpha(z) = a\sin\left(\frac{D_1 \cdot \sin\left({\alpha_{in}}/{n_{clad}}\right)}{D_1 - 2\theta \cdot z}\right). \tag{7}$$

Equation (7) can be simplified for a total taper length L to yield

$$\alpha = a\sin\left(\frac{D_1}{D_2}\sin\left({\alpha_{in}}/{n_{clad}}\right)\right) = a\sin\left(T\sin\left({\alpha_{in}}/{n_{clad}}\right)\right), \tag{8}$$

where $T=D_1/D_2$ is the tapering ratio.

The ray propagates throughout the taper without vignetting when the condition $n_{clad} \times \sin\alpha < NA_{clad}$ is satisfied over the whole length of the taper. The product $n_{clad} \times \sin\alpha$ gradually increases with light propagation towards the small diameter single mode end of the taper and approaches the value of the cladding numerical aperture NA_{clad} only at the very end of the taper. The critical incident angle, which ensures ray propagation without vignetting, can then be found from

#103845 - $15.00 USD Received 11 Nov 2008; revised 24 Dec 2008; accepted 5 Jan 2009; published 16 Jan 2009

$$\sin\left(\alpha_{in}/n_{clad}\right) = \frac{1}{T}\cdot\frac{NA}{n_{clad}}\ , \tag{9a}$$

or, for paraxial rays (small values of α_{in}), from

$$\alpha_{in} \approx \frac{NA}{T} \tag{9b}$$

Equations (9a), (b) are valid for a tapered fiber with an arbitrary longitudinal dependence of taper diameter. Indeed, a T-DCF with nonlinear complex shape can be represented by a sequence of small-length linear tapers. Using Eq. (8), the ray angle after propagation through the chain of linear tapers with arbitrary shape can be approximated by

$$\alpha = \frac{\alpha_{in}}{n_{clad}}\cdot\frac{d_1}{d_2}\cdot\frac{d_2}{d_3}\cdot\ldots\ldots\cdot\frac{d_{n-2}}{d_{n-1}}\cdot\frac{d_{n-1}}{d_n} = T\cdot\frac{\alpha_{in}}{n_{clad}}, \tag{10}$$

where $\boldsymbol{d_i}$ is the diameter of an elementary short linear taper.

When the condition $\boldsymbol{n_{clad}\times\sin\alpha<NA_{clad}}$ is violated over a certain length of the taper, the normalized length $\left(\frac{z}{L}\right)_{vgnt}$ of linear taper where this inequality is not satisfied and where, therefore, the vignetting occurs, can be expressed as a function of ray incidence angle $\boldsymbol{\alpha_{in}}$ using Eq.(7)

$$\left(\frac{z}{L}\right)_{vgnt} = \frac{T}{T-1}\left(1-\frac{n_{core}\sin\left(\alpha_{in}/n_{core}\right)}{NA}\right). \tag{11}$$

The similar dependence for an arbitrarily shaped taper can be found for an actual T-DCF axial profile by approximating it by a sequence of linear tapers and using Eq. (7) for each fractional taper. The dependence of diameter on length and an end face image for the T-DCF used in the experiments are shown in Figs. 2 (a) and 2 (b), respectively.

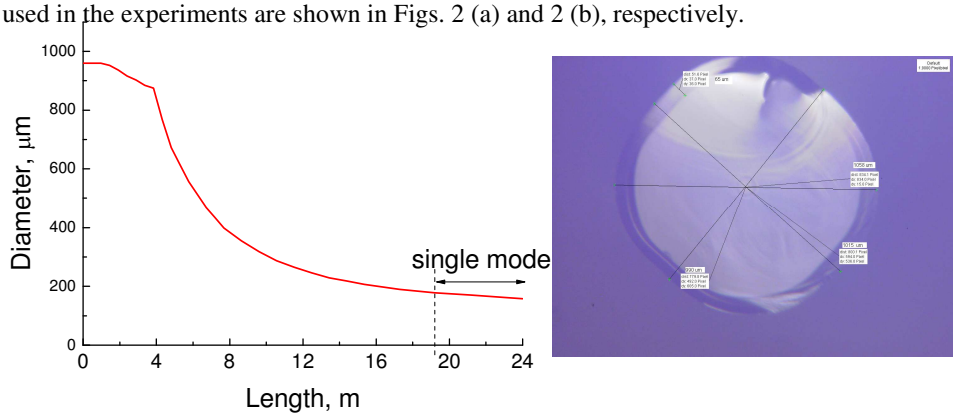

a. b.

Fig. 2. T-DCF characteristics: (a) clad diameter versus length and (b) image of taper end face.

#103845 - $15.00 USD Received 11 Nov 2008; revised 24 Dec 2008; accepted 5 Jan 2009; published 16 Jan 2009

The numerical aperture of the pump cladding is 0.22 and the tapering ratio T=6, as defined in (8). According to (9), rays launched into the taper with incident angles below 0.037 rad (NA/T~0.22/6) are expected to propagate without vignetting over the entire length of the taper. Rays launched at angles above 0.037 rad will be partially absorbed by the active core, and in part leak from the T-DCF cladding, due to vignetting. To quantify the amount of pump absorption and loss due to leakage from a taper, the characterization of the T-DCF has been performed for pump launch conditions which prevent vignetting. The practical beam delivery system used in this measurement employs launch optics to deliberately underfill the fiber aperture, by limiting the numerical aperture of the input pump beam to NA≤0.037. The pump absorption measured for rays with an aperture less then NA/T can be regarded as *paraxial ray pump absorption*.

The measured paraxial ray absorption for the T-DCF presented in Fig. 2(a), (b) which was used in this study was 1.2 dB/m at 915 nm, with an actual numerical aperture of pump light launched into the pump cladding of 0.0377.

The normalized length of vignetting for a T-DCF with arbitrary shape as function of launching angle can be calculated using the model of short-length linear tapers sequence, and applying it to each taper Eq. (8). The result of these calculations for the fabricated T-DCF is shown in Fig. 3.

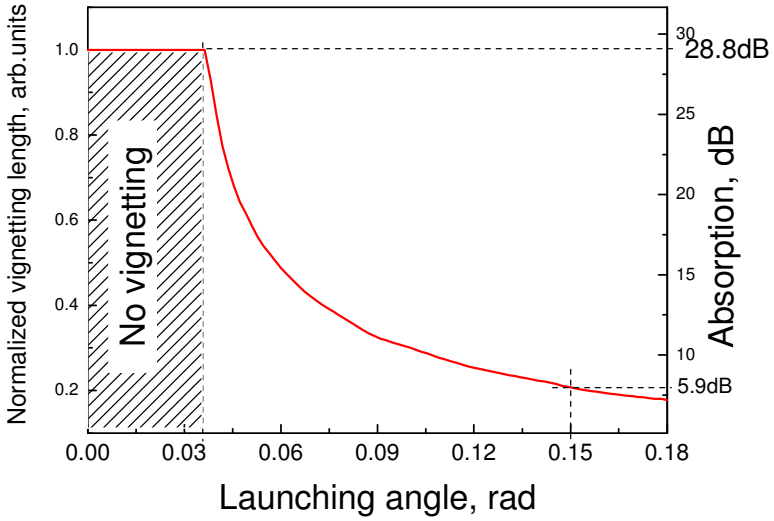

Fig. 3. Normalized vignetting length (left) and absorption (right) in T-DCF as a function of the launching angle.

Figure 3 illustrates that vignetting depends strongly on the incident angle of the cone of rays launched into the T-DCF. Since vignetting decreases pump absorption in the taper core, which is proportional to the propagation length, the pump efficiency reduces with increasing numerical aperture of the pump beam. Strong angular selectivity of the double clad taper absorption results in ~23 dB increase in absorption for beams with NA<0.037 rad, compared with absorption for beams with NA=0.15, corresponding to the overfill launching condition. The above analysis has been developed for taper excitation by a ray with a specific launching angle. In practice, however, the pump source produces a cone of rays with a Lorentzian angular power distribution. The measured angular power distributions for the launching optics, providing pump beam numerical apertures of 0.15 and 0.18, are shown in Figs. 4 (a) and 4 (b), respectively (black curves). The corresponding normalized angular distributions of absorbed pump power shown in Fig. 4 (a), (b) (red curves) have been calculated by taking into

#103845 - $15.00 USD Received 11 Nov 2008; revised 24 Dec 2008; accepted 5 Jan 2009; published 16 Jan 2009

account the dependence of pump absorption on the launching angle, presented in Fig. 3, and the angular pump power distribution shown, in Fig. 4.

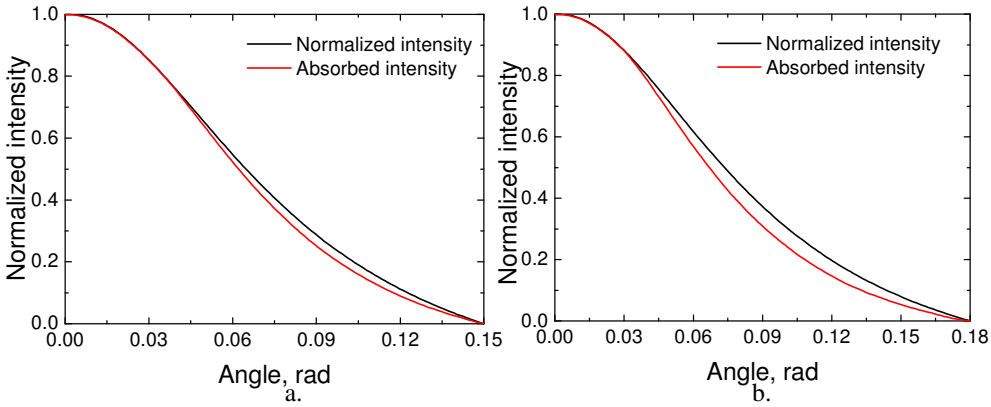

Fig. 4. Measured angular power distribution of pump sources with NA=0.15 (a) and NA=0.18 (b) and pump absorption (red curves).

Absorbed pump power, and pump power which is lost due to vignetting as a function of pump NA, can be calculated from the equations

$$P_{abs} = \frac{\int \left(P(\alpha) - P(\alpha)\exp(-\gamma L(\alpha))\right) d\alpha}{\int P(\alpha) d\alpha}, \tag{12a}$$

$$P_{vgnt} = 1 - P_{abs} - P_{unabs} \tag{12b}$$

where P(α) – angular power distribution of pump source, L(α) – vignetting length for ray, launched at the angle α, γ – absorption of double-clad taper per unit length for α≤NA/T, P_{unabs} – residual unabsorbed pump power transmitted throughout the T-DCF to the narrow end.

The pump absorption as a function of pump beam NA has been calculated using Eq.12(a) for the T-DCF with a diameter variation with length presented in Fig. 2. Fig. 5 demonstrates 15 dB (97%) absorption for a pump source with NA=0.15 and 1.2 dB/m paraxial ray absorption, which illustrates the tapered double-clad fiber's ability to pump absorption.

#103845 - $15.00 USD Received 11 Nov 2008; revised 24 Dec 2008; accepted 5 Jan 2009; published 16 Jan 2009

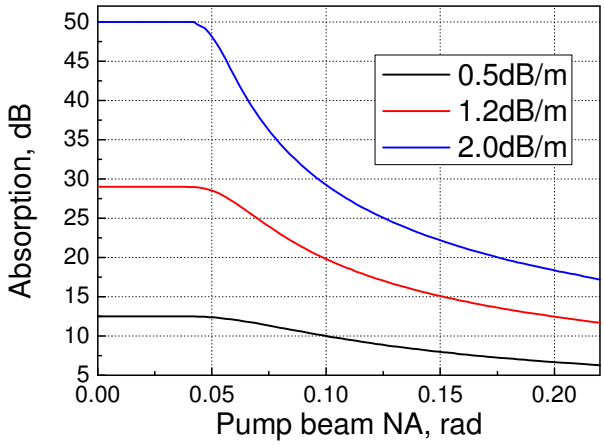

Fig. 5. Pump absorption in T-DCF versus numerical aperture of launched pump beam for actual shape of T-DCF and paraxial ray absorption of 0.2 dB/m (black), 1.2 dB/m (red) and 2 dB/m (blue).

A brief summary of the model presented above allows parameters determining the performance of tapered double-clad fiber lasers/amplifiers to be identified:

- Paraxial ray absorption;
- Shape of the taper;
- Angular power distribution of the pump source.

Importantly, the detrimental effect of vignetting can be largely suppressed by optimizing the shape of the taper, increasing paraxial ray absorption and using a pump beam with proper numerical aperture.

3. Experiment

The laser setup of the single mode ytterbium fiber laser with T-DCF as a gain medium is shown in Fig. 6. The diode source LDM 600-1500 (Laserline) operated at 915 nm provides pump radiation through an optical fiber with 600 μm core diameter and NA=0.22.

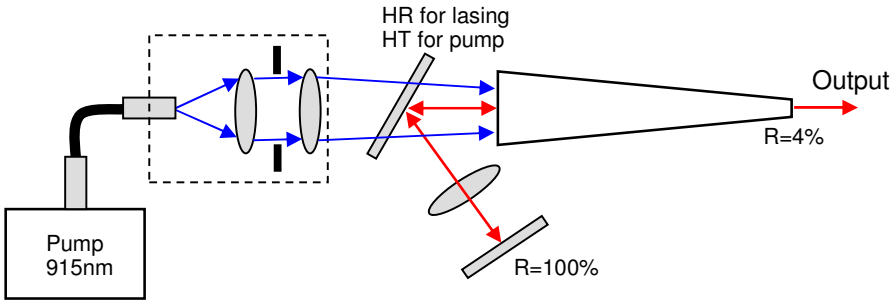

Fig. 6. The experimental setup

The maximum achievable power from this source was 1.3 kW. The output pump radiation was launched via optical cable into a beam shaping unit comprising a collimating lens,

#103845 - $15.00 USD Received 11 Nov 2008; revised 24 Dec 2008; accepted 5 Jan 2009; published 16 Jan 2009

diaphragm and focusing lens. The launched beam with Lorentzian intensity profile, as shown in Fig. 4 (a), (b), could be produced using simple coupling optics. By changing the lenses and the diaphragm we could adjust the numerical aperture and diameter of the pump beam launched into the T-DCF. The pump radiation was launched into the T-DCF through a dichroic beam splitter highly transparent for pump radiation and highly reflective for the lasing wavelength. The pump emission launch efficiency was 86%. The cavity was formed by a highly reflective dielectric mirror at the wide end of the T-DCF and by Fresnel reflections (~4%) from the facet of the narrow end. The total T-DCF length was 24 m, as shown in Fig. 2 (a). The fiber had a near-circular cladding cross-section, with the diameter at the wide side of the T-DCF varying in the range 835 - 890 μm, as shown in Fig. 2 (b). The fluorine glass coating with a NA of 0.22 was deposited on the pump guiding cladding. A low refractive index polymer was used for outer protection. The active core with a numerical aperture of 0.07 had a diameter of 65 μm at the wide end of the T-DCF. The core diameter at the narrow end of the taper was 11 μm, ensuring that at least five meters of the T-DCF was a single mode waveguide. The preform for the tapered fiber was fabricated by a plasma chemical vapor deposition (PCVD) method with in-core absorption of ~600 dB/m at 976 nm. As mentioned earlier, the paraxial ray absorption of double-clad pumped taper was measured to be 1.2 dB/m using a pump beam with NA=0.0377 to prevent losses due to vignetting.

The output characteristics of the laser are shown in Fig. 7 for two values of pump beam aperture adjusted using the diaphragm in the optical beam shaping unit. Though a decrease of the diaphragm diameter reduces the available pump, as expected, the output power at a specific pumping rate increases, demonstrating improvement in pumping efficiency due to reduced vignetting and increased pump absorption in the active core.

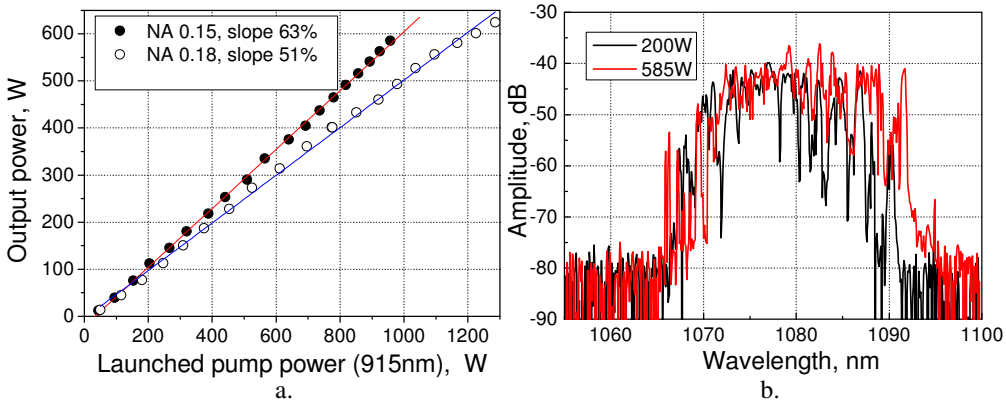

Fig. 7. Output characteristics of laser: (a) Output power versus launched pump power. The solid circles correspond to a pump beam with NA=0.15 and the open circles to pump with NA=0.18. (b) Spectrum of output radiation, pump beam with NA=0.15.

Consequently, the slope efficiency is 63% for a pump beam of NA=0.15, and reduces down to 51% for NA=0.18 (Fig. 7 (a)). The maximum achieved power was 624 W. The laser emits a broad spectrum with a FWHM bandwidth of 20 nm, as shown in Fig. 7 (b).

#103845 - $15.00 USD Received 11 Nov 2008; revised 24 Dec 2008; accepted 5 Jan 2009; published 16 Jan 2009

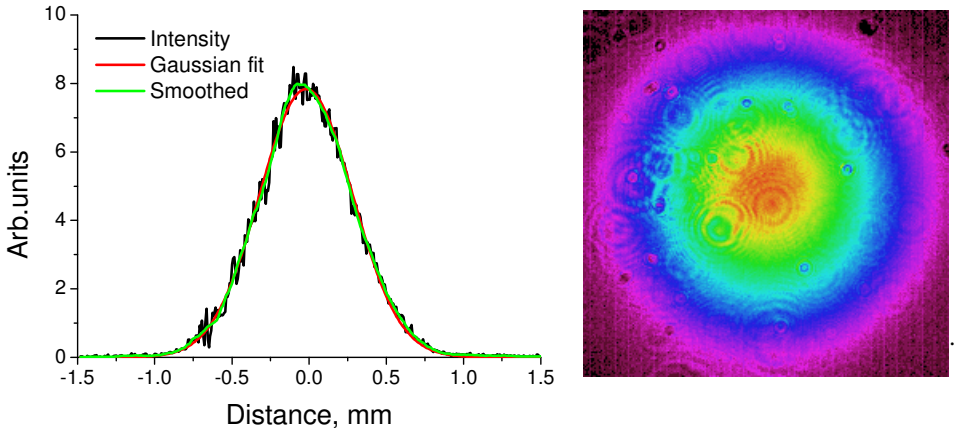

Fig. 8. Output beam profile with M^2=1.08.

Beam profile and two-dimensional intensity distribution of output beam are shown in Fig. 8. The laser operates on the fundamental mode with M^2=1.08.

4. Discussion

The important experimental observation, supported by the analysis, is that efficient optical pumping can be achieved even with pump beam apertures significantly exceeding the critical value needed for vignetting-free propagation. The significant practical result of this conclusion is the possibility for optical pumping with low-brightness sources, e.g. diode bars. The experimental dependence of slope efficiency on the numerical aperture of the launched pump beam (Fig. 7 (a)) is in good agreement with results of modeling presented in Fig. 5. The modeling of the tapered double clad amplifier presented here identifies the features and optimal design of the fiber for efficient operation. The fraction of pump power which leaks from the T-DCF due to vignetting increases with pump beam NA, resulting in slope efficiency deterioration. Therefore, to prevent the degradation of pumping efficiency with high-NA pump sources, a substantial fraction of the pump power should be absorbed in the active core well before vignetting sets in.

It is demonstrated that absorption for a Lorentzian pump beam with NA=0.15 reaches 15 dB and is sufficient for practical laser operation. However, a further increase in the beam NA up to 0.18 causes an increase in launched pump power (up to 1.3 kW, Fig. 7 (a)), is accompanied by a reduction in pump absorption (from 15 to 13.37 dB) and leads to slope efficiency reduction (Fig. 7). However, a practically acceptable value of absorption could be achieved even with higher NA pump sources, for highly-doped core fiber with a large value of paraxial absorption. Fig. 5 demonstrates 17.2 dB absorption for a beam with NA=0.22). This observation demonstrates the potential of high-NA pump sources for highly-doped T-DCF.

The analysis identifies key parameters responsible for pump absorption in tapered fiber, namely in-core absorption, cross-sectional geometry and longitudinal shape of the taper. The influence of paraxial ray absorption presented in Fig. 5 shows that the effect of vignetting becomes more significant for low paraxial ray absorption. Thus, the T-DCF absorption increases from 8 dB to 22.3 dB when the axial ray absorption increases from 0.5 dB/m to 2 dB/m, as shown in Fig. 5 for pumping with the beam having NA of 0.15. Another major parameter is the axial shape of the T-DCF, which affects its pump absorption dramatically since it determines the normalized vignetting length (Eqs.(11)). The profile of the T-DCF used in experiments, and the corresponding axial dependence of local taper angle proportional to the first derivative of diameter, are shown in Fig. 9 (red curves). It can be seen that the local cone angle is small at the large-core end of the taper and experiences a strong increase over the first 4 m, up to 200 μrad, followed by near exponential reduction. This rapid increase of

#103845 - $15.00 USD Received 11 Nov 2008; revised 24 Dec 2008; accepted 5 Jan 2009; published 16 Jan 2009

the local taper angle may be accompanied by significant losses due to vignetting, because this feature occurs at the very outset of the taper, where the unabsorbed pump power is high. The shape of T-DCF used in this study could, therefore, be improved, e.g. by using a design in which local taper angle gradually increases with length, achieving the maximum when a substantial part of the pump power is absorbed, i.e. a parabolic taper or a linear taper with constant cone angle.

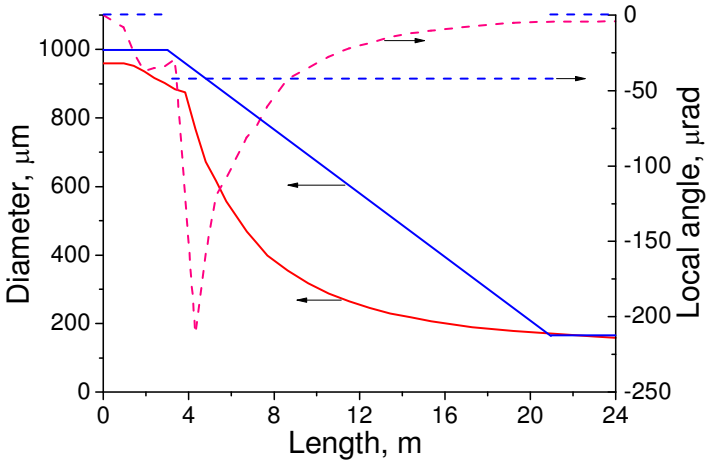

Fig. 9. Shape of the taper: diameter (solid line) and local angle (dashed line) as function of the length; red color – actual T-DCF used in the experiment, blue color – a hypothetical linear T-DCF.

An example of a linear taper with a constant cone angle of 46 μrad is shown in Fig. 9 (blue curves). The pump absorption as a function of numerical aperture of launched pump beam for these T-DCFs, calculated using Eq. (12a), is presented in Fig. 10. The results plotted in Fig. 10 demonstrate the crucial role of taper shape in pump absorption. Thus, the T-DCF with linear fiber diameter length dependence exhibits an absorption increase of ~6 dB compared with the taper of the same length used in this study, with the same pump beam aperture of 0.22.

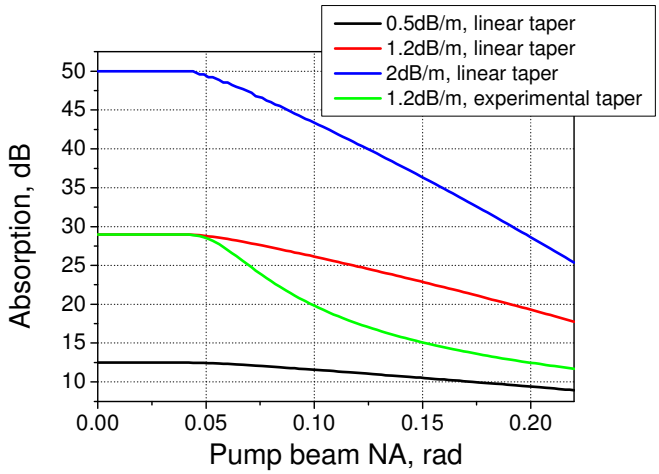

Fig. 10. Pump absorption versus numerical aperture of launched pump beam for linear T-DCF (corresponding to Fig. 9, blue curves) for different paraxial ray absorption, 0.2 dB/m (black curve), 1.2 dB/m (red) and 2 dB/m (blue). The green curve corresponds to the experimental T-DCF.

#103845 - $15.00 USD Received 11 Nov 2008; revised 24 Dec 2008; accepted 5 Jan 2009; published 16 Jan 2009

This result allows us to conclude that T-DCF with sufficient paraxial ray absorption and optimized longitudinal shape can operate efficiently under overfill launch conditions using low-brightness, high-NA, pump sources. It is expected that power scaling using tapered double-clad fiber technology can be achieved in the future, by implementation of the following:

- Enlargement of the T-DCF diameter. Current fiber technology is capable of producing T-DCF with a 2 mm large-end diameter, which would allow the launch of a few kilowatts of pump power [10];
- Increase of the mode field diameter would improve the energy storage capability of the fiber. Tapered active large-core microstructured fiber [11] or multicore fiber [12] hold significant potential for power scaling.

5. Conclusion

We have investigated the performance and major parameters governing the operation of tapered double-clad fiber amplifiers both theoretically and experimentally. A ray optics analysis applied to this fiber reveals good agreement with experimental observations. Paraxial ray absorption in the fiber core and the longitudinal shape of the tapered fiber have been found to be the major factors affecting the amplifier characteristics. The analysis and measurements show that low brightness sources with high numerical apertures can be used for efficient pumping of the tapered fiber, offering both high launching efficiency and low pump power losses. This is an important practical conclusion which opens up the opportunity of using high-power, cost-effective diode bars. Using this innovative design concept, we developed a single mode (M^2=1.08) ytterbium fiber laser with power exceeding 600 W. The potential of this approach for scaling to higher powers has been discussed.

#103845 - $15.00 USD Received 11 Nov 2008; revised 24 Dec 2008; accepted 5 Jan 2009; published 16 Jan 2009

Appendix 6

Publication 6

V. Filippov, Y. Chamorovskii, J. Kerttula, A. Kholodkov, and O. G. Okhotnikov, "Highly efficient 750 W tapered double-clad ytterbium fiber laser", *Optics Express*, vol. 18, no. 12, pp. 12499–12512, 2010.

Highly efficient 750 W tapered double-clad ytterbium fiber laser

Valery Filippov,[1*] Juho Kerttula[1],Yuri Chamorovskii,[2] Konstantin Golant[2] and Oleg G. Okhotnikov[1]

[1]*Optoelectronics Research Centre, Tampere University of Technology, 33101 Tampere, Finland*
[2]*Institute of Radio and Electronics of the Russian Academy of Sciences, Mokhovaya 11, bld.7, 125009 Moscow, Russia*
**valery.filippov@tut.fi*

Abstract: The results of theoretical and experimental studies of active tapered double-clad fibers, intending the optimization of its imperative parameters - tapering ratio, longitudinal profile, core/cladding diameters ratio, are presented. Using a refined taper geometry we have demonstrated power scaling of a ytterbium fiber laser pumped by low-brightness, cost-effective laser diodes up to 750 W, with 80% efficiency.

OCIS codes: (060.2280) Fiber design and fabrication; (060.2320) Fiber optics amplifiers and oscillators; (060.3510) Lasers, fiber

References and Links

1. V. Filippov, Y. Chamorovskii, J. Kerttula, K. Golant, M. Pessa, and O. G. Okhotnikov, "Double clad tapered fiber for high power applications," Opt. Express **16**(3), 1929–1944 (2008), http://www.opticsinfobase.org/abstract.cfm?URI=oe-16-3-1929.
2. V. Filippov, Y. Chamorovskii, J. Kerttula, A. Kholodkov, and O. G. Okhotnikov, "Single-mode 212 W tapered fiber laser pumped by a low-brightness source," Opt. Lett. **33**(13), 1416–1418 (2008).
3. V. Filippov, Y. Chamorovskii, J. Kerttula, A. Kholodkov, and O. G. Okhotnikov, "High power tapered ytterbium fiber laser pumped by a low-brightness source," Europhoton 2008, Paris.
4. V. Filippov, Y. Chamorovskii, J. Kerttula, A. Kholodkov, and O. G. Okhotnikov, "600 W power scalable single transverse mode tapered double-clad fiber laser," Opt. Express **17**(3), 1203–1214 (2009), http://www.opticsinfobase.org/oe/abstract.cfm?URI=oe-17-3-1203.
5. J. A. Alvarez-Chavez, A. B. Grudinin, J. Nilsson, P. W. Turner, and W. A. Clarkson, "Mode selection in high power cladding pumped fibre lasers with tapered section," in *Conference on Laser and Electro-Optics,* OSA Technical Digest (Optical Society of America, 1999), pp. 247–248.
6. J. D. Minelly, L. Zenteno, M. J. Dejneka, W. J. Miller, D. V. Kuksenkov, M. K. Davis, S. G. Crigler, and M. E. Bardo, "High power diode pumped single-transverse-mode Yb fiber laser operating at 976 nm," in *Dig. Optical Fiber Communication Conf.,* 2000, postdeadline paper PD2, **vol.4**, pp. 172–174.
7. M. J. Dejneka, J. D. Minelly, and L. Zenteno, "Tapered fiber laser," US patent # 6.324.326 B1 (2001).
8. M. J. Dejneka, B. Z. Hanson, S. G. Crigler, L. Zenteno, J. D. Minelly, D. C. Allan, W. J. Miller, and D. Kuksenkov, "La_2O_3-Al_2O_3-SiO_2 glasses for high-power, Yb^{3+}-doped 980-nm fiber lasers," J. Am. Ceram. Soc. **85**, 1100–1106 (2002).
9. H. Jeong, S. Choi, and K. Oh, "Continuous wave single transverse mode laser oscillation in a Nd-doped large core double clad fiber cavity with concatenated adiabatic tapers," Opt. Commun. **213**(1-3), 33–37 (2002).
10. L. Li, Q. Lou, J. Zhou, J. Dong, Y. Wei, S. Du, and B. He, "High power single transverse mode operation of tapered large-mode-area fiber laser," Opt. Commun. **281**(4), 655–657 (2008).
11. T. A. Birks, and Y. W. Li, "The shape of fiber tapers," J. Lightwave Technol. **10**(4), 432–438 (1992).
12. D. Marcuse, "Light transmission optics," Van Nostrand Reinhold Company, New York, chapter 8, (1972).
13. K. M. Golant, "Surface plasma chemical vapor deposition: 20 years of application in glass synthesis for lightguides (a review)", XXI International Congress on Glass, Strasbourg, July 1–6, 2007, Proc. on CD ROM, paper L13.

1. Introduction

Recently we proposed an active tapered double-clad fiber (T-DCF) as a gain medium for high power fiber lasers and amplifiers with nearly diffraction-limited beam quality [1–4]. Having large cladding diameters, these fibers can be pumped by high-power, low-brightness laser diode bars which establishes the basis for a cost-effective source. We have demonstrated a fundamental mode ytterbium fiber laser with 600 W of output power and 63% slope

#125834 - $15.00 USD Received 22 Mar 2010; revised 23 May 2010; accepted 24 May 2010; published 27 May 2010

efficiency [4]. However, due to the non-optimized longitudinal profile of the T-DCF used, the efficiency observed was somewhat lower than the theoretically expected figure of 85%.

The design strategy and operation of tapered active fibers with cladding pumping have been discussed earlier in our paper [4], which presents a precise description of absorption mechanism, guiding characteristics and amplification of T-DCFs.

The goal of this paper is the detailed analysis and optimization of an active tapered fiber, with the aim of improving the performance of lasers and amplifiers using this concept.

2. Parameters of a T-DCF and their optimization

The parameters of tapered fibers involved in the optimization procedure include

- Tapering ratio;
- Shape of the longitudinal profile;
- Core/cladding ratio;
- Dopants concentration;
- Cladding shape.

Their effect on laser performance is discussed in this section.

2.1. Tapering ratio

A double-clad pumping scheme is widely used to efficiently couple the radiation from high power sources into the fiber amplifier. As a result, the low brightness of pumping sources can be effectively converted to the high brightness exhibited by single-mode fiber emitters. For a conventional double-clad fiber the brightness enhancement factor $\boldsymbol{K_{DCF}}$ can be written as:

$$K_{DCF} = S \cdot \frac{A_{clad}}{A_{core}} \cdot \left(\frac{NA_{clad}}{NA_{core}} \right)^2 = S \cdot \left(\frac{D_{clad} \cdot NA_{clad}}{D_{core} \cdot NA_{core}} \right)^2, \quad (1)$$

where $\boldsymbol{S}$ is the slope efficiency of the laser, $\boldsymbol{A_{clad}}$, $\boldsymbol{A_{core}}$, $\boldsymbol{NA_{clad}}$, $\boldsymbol{NA_{core}}$ are the areas and numerical apertures, respectively, of the double-clad fiber cladding and core; and $\boldsymbol{D_{clad}}$ and $\boldsymbol{D_{core}}$ are the cladding and core diameters.

Typical parameters for a ytterbium double-clad fiber are S = 0.8, NA_{clad}/NA_{core}~3, A_{clad}/A_{core}~400 and K_{DCF}~3000. Modified for the tapered double-clad fiber, Eq. (1) takes the form:

$$K_{T-DCF} = S \cdot \frac{A_{clad\_input}}{A_{core\_output}} \cdot \left(\frac{NA_{launch}}{NA_{core}} \right)^2 = S \cdot \left(\frac{T \cdot D_{clad\_output} \cdot NA_{launch}}{D_{core\_output} \cdot NA_{core}} \right)^2 = \quad (2)$$
$$= T^2 \cdot F^2 \cdot K_{DCF},$$

where $\boldsymbol{NA_{launch}}$ is the numerical aperture of the launched pump beam, which preferably satisfies the condition $\boldsymbol{NA_{launch} < NA_{clad}}$[2,4], $\boldsymbol{T = D_{input}/D_{output}}$ is the tapering ratio, and $\boldsymbol{F = NA_{launch}/NA_{clad}}$ is the cladding filling factor. Obviously, it is assumed that the light is coupled to the T-DCF through the large diameter facet. Thus, for the tapered double-clad fiber operating in a laser regime, the brightness is increased by a factor of $\boldsymbol{(F*T)^2}$ as compared to the cylindrical (untapered) double-clad fiber. The tapering ratio beneficial for brightness improvement cannot, however, be increased above a certain value. It should be noted that in terms of ray optics the propagation of pump light through a T-DCF is accompanied by a gradual increase in the angle of the propagating ray relative to the fiber axis, which strongly affects the rate of pump absorption [1–4]. Consequently, the pump absorption for rays propagating in the T-DCF cladding at angles of $\alpha < NA_{clad}/T$ and $\alpha > NA_{clad}/T$ could be very different, due to their different interaction lengths with the active material.

#125834 - $15.00 USD Received 22 Mar 2010; revised 23 May 2010; accepted 24 May 2010; published 27 May 2010

Specifically, the absorption of pump radiation propagating at angles $\alpha<NA_{clad}/T$ is similar to pump absorption in untapered DCF with T = 1. Typically, $\alpha \le 5°$, which allows us to consider these pump rays as "near-paraxial". In this case the unabsorbed pump power $\mathscr{P}_{unabs}^{pump}$ exiting through the small diameter facet of the T-DCF is determined by the tapering ratio T and the so-called "paraxial" absorption coefficient $\boldsymbol{\gamma}$ which takes into account in-core absorption and pump ray tracing [4]:

$$\mathscr{P}_{unabs}^{pump} = \int_0^{NA_{clad}/T} I(\alpha)\cdot\exp(-\gamma L)d\alpha, \tag{3}$$

where $\boldsymbol{\alpha}$ – ray launching angle, $\boldsymbol{I(\alpha)}$ – normalized angular distribution of pump intensity, and $\boldsymbol{L}$ – length of the T-DCF.

Pump rays propagating at angles $\alpha>NA_{clad}/T$ have different absorption lengths, $L(\alpha)$, in T-DCF which depend strongly on launching angle α. These pump rays are depleted during the propagation through a T-DCF partly through absorption in the core, and partly through leakage from the fiber due to violation of the total internal reflection condition, the so-called vignetting effect [4]. The unabsorbed vignetting fraction of pump, which leaks from T-DCF through the side surface, can be expressed as [4]:

$$\mathscr{P}_{vgnt}^{pump} = \int_{NA_{clad}/T}^{NA_{clad}} I(\alpha)\exp(-\gamma \mathscr{L}(\alpha))d\alpha \tag{4}$$

Therefore, the total pump power launched into a T-DCF is divided as according to:

$$\mathscr{P}_{launch}^{pump} = \begin{cases} \mathscr{P}_{abs}^{'} + \mathscr{P}_{unabs}, \alpha < NA_{clad}/T \\ \mathscr{P}_{abs}^{''} + \mathscr{P}_{vgnt}, \alpha > NA_{clad}/T \end{cases}, \tag{5}$$

where the relative share of absorbed pump power for $\alpha<NA_{clad}/T$ and $\alpha>NA_{clad}/T$ could be very different. To avoid pump losses due to the vignetting effect, the aperture of T-DCF cladding should be underfilled, i.e. $NA_{launch}<NA_{clad}$ [1–4]. The fraction of pump power $\mathscr{P}_{parax}^{pump}$ which satisfies the condition $\alpha<NA_{clad}/T$ can be written as:

$$\mathscr{P}_{parax}^{pump} = -20\cdot\log(F\cdot T)[dB] \tag{6}$$

Figure 1 shows that the paraxial pump power $\mathscr{P}_{parax}^{pump}$ decreases strongly with an increase in tapering ratio and fill factor.

Since the rays propagating at angles $\alpha>NAclad/T$ exhibit lower absorption, preferential excitation of these rays could deteriorate the slope efficiency of the laser (amplifier).

Unlike the pump radiation in a tapered cladding, which enters the large diameter end and propagates in one direction, the laser light in a tapered core circulates in both directions. The single mode output is then preserved in tapered fiber by filtering out the higher-order modes to the cladding. The remarkable attribute of tapered geometry is nonreciprocal amplification. Specifically, the propagation from the large size multimode end of the tapered core to the small diameter single-mode section of the T-DCF suffers both amplification and loss due to the mode filtering effect, while the propagation in the opposite direction undergoes gain only.

#125834 - $15.00 USD Received 22 Mar 2010; revised 23 May 2010; accepted 24 May 2010; published 27 May 2010

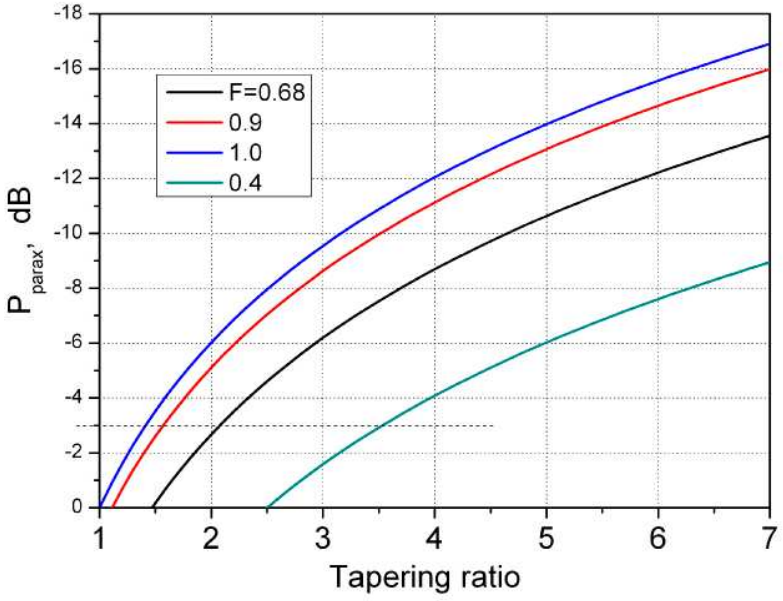

Fig. 1. Near-paraxial fraction of pump power $\mathcal{P}_{parax}^{pump}$ as function of tapering ratio.

Assuming that in the multimode section of the T-DCF the average number of guided modes is *N*, their power could be estimated as $P_{core} \approx \delta P \cdot N$, where $\boldsymbol{\delta P}$ is the partial average power of one mode, $\boldsymbol{N = 2\pi^2 a^2 NA^2_{core}/\lambda}$ is the number of guided modes in the fiber with core radius $\boldsymbol{a}$ and numerical aperture $\boldsymbol{NA_{core}}$ [12], and λ is the lasing wavelength. With the "worst" case assuming equal sharing of pump power over the guided modes, the estimation for the upper value of vignetting loss due to mode filtering during signal propagation towards the section with the small diameter core gives:

$$L_{vgnt} = \frac{P_{vgnt}^{core}}{P_{in}^{core}} = \frac{\delta P \cdot (N_{in} - N_{out})}{\delta P \cdot N_{in}} = \left(\frac{N_{in} - N_{out}}{N_{in}}\right) = \left(\frac{a_{in}^2 - a_{out}^2}{a_{in}^2}\right) = \\ = \frac{T^2 - 1}{T^2} \qquad (7)$$

Apparently the mode filtering (vignetting) loss vanishes for non-tapered fiber, $L_{vgnt} = 0$ for $T = 1$ and approaches $L_{vgnt} = 1$ for large tapering ratios. This feature imposes a limitation on the upper value of the tapering ratio.

The leakage of high-order modes from the fiber core to the cladding owing to the vignetting effect can result in a high density of light propagating as cladding modes, which negatively affects the quality of the output beam. The figure of merit describing this process is the core guiding ratio or beam contrast ***C,*** defined as the ratio of lasing power in the core to the total power propagating in the fiber. Therefore, although increasing the tapering ratio *T* improves the brightness enhancement factor $\boldsymbol{K_{DCF}} \sim T^2$, it could lead to a decrease in laser slope efficiency, an increase of the lasing threshold, and deterioration of the core guiding ratio due to reduced pump absorption and higher intracavity loss. $\boldsymbol{K_{DCF}}$ for T-DCF can be normalized to the similar factor for the non-tapered cylindrical double-clad fiber with an analogous geometry which gives

#125834 - $15.00 USD Received 22 Mar 2010; revised 23 May 2010; accepted 24 May 2010; published 27 May 2010

$$K_{DCF}^{norm} = \frac{S_{T-DCF} \cdot T^2 \cdot F^2 \cdot C}{S_{DCF}}, \quad (8)$$

where $\boldsymbol{S_{T\text{-}DCF}}$ – slope efficiency for the laser with T-DCF, $\boldsymbol{S_{DCF}}$ – slope efficiency for a laser with similar conventional DCF and $\boldsymbol{C}$ – contrast of the emitted light. Here, only the radiation coming out of the core is accounted for.

In T-DCF-based amplifiers the mode filtering from the core is entirely suppressed since the signal propagates unidirectionally towards the large core fiber end, therefore the tapering ratio in the amplifiers can be varied in a wider range.

2.2. Longitudinal shape of T-DCF profile

The axial taper shape should provide high output power supplied by preferential pump conversion in the large-core section, and preserve fundamental mode operation by spatial filtering in the single-mode section. The relative lengths of these sections, determined by the outer diameter variation along the fiber, affect the output beam characteristics. The multimode waveguide in the double-clad fiber should allow for efficient pump launching into the fiber, and intense absorption in the single-mode core. Moreover, in a T-DCF the longitudinal profile can be engineered to accept the radiation of low-brightness pump sources and guarantee robust fundamental mode operation of the tapered core. Figure 2 shows some feasible axial profiles of T-DCF.

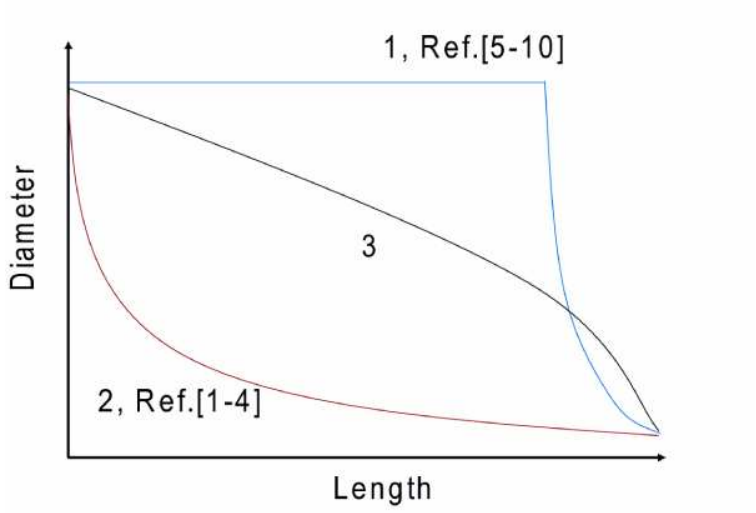

Fig. 2. Various axial taper profiles: (1) - “step-like” shape; (2) – bowl-shaped; (3) – “convex”.

As discussed above, the absorption of near-paraxial pump rays (α<NA/T) in T-DCF cladding is fairly insensitive to the longitudinal taper shape, while for rays with α>NA/T it is critically dependent on taper profile. The fraction of the latter rays with large values of α can be significant, as can be seen from Fig. 1. For example, 75% of the pump power propagates under this condition for a tapering ratio T = 3 and fill factor F = 0.68 ($\boldsymbol{NA_{launch}/NA_{clad}}$ = 0.15/0.22), and for tapering ratios above T~5-6 the fraction of these rays rises to 90%. The strategy for T-DCF profile optimization is to prevent the vignetting effect primarily in the large diameter section of the cladding, where the pump power density is high [4].

A “step-like” T-DCF longitudinal profile, as shown in Fig. 2 (blue curve 1), consisting of a regular cylindrical fiber and short tapered section has some attractive features. Particularly, a taper with this shape exhibits no vignetting in the regular non-tapered section of a double-clad fiber whose length and cross section are optimized primarily to ensure efficient pump absorption. Then, the residual pump light reaching the small-diameter tapered fiber section is

#125834 - $15.00 USD Received 22 Mar 2010; revised 23 May 2010; accepted 24 May 2010; published 27 May 2010

strongly depleted, which allows for a short (few cm-long) length of this section, thus making the vignetting effect negligible [5–10]. The "step-like" tapered fiber, however, exhibits low slope efficiency as compared to a uniform fiber, 30% in [6–8], 45% in [9] and 54.1% in [10]. This is due to the strong spatial mode filtering which is required because the length of the single-mode section is much shorter than the length of the multimode section. A significant fraction of pump power consumed by higher-order non-oscillating modes in the multimode section of a "step-like" taper is filtered out in the single-mode section, resulting in losses and reduced laser efficiency. Therefore, although application of the "step-like" shape of T-DCF prevents pump loss due to vignetting, it can cause losses for signal radiation propagating in the core because of spatial mode filtering.

Fundamental mode operation is one of the most important characteristics related to the T-DCF format. Another problem associated with a "step-like" design with a short length of the tapered single-mode section is low filtering extinction, especially for the LP_{11} mode, which can reduce output beam quality to M^2 ~1.3-1.7 [5,9,10].

Contrary to the "step-like" tapered fiber, the diameter of bowl-shaped "concave" T-DCF is gradually varied along the entire length, as shown in Fig. 2 (red curve 2), thus representing a certain compromise between output parameters and providing some advantages. An essential feature of axially non-uniform T-DCF is an efficient cladding mode mixing mechanism leading to enhanced pump absorption, which in turn leads to an improvement in the slope efficiency, as shown in [1]. Since the multimode section of bowl-shaped taper is short, the gain in the core is depleted mostly by fundamental and low-order modes, which allows for efficient and low-loss spatial mode filtering, occurring here over the long length of the taper.

Recently, we have demonstrated a 600 W single-mode fiber laser using long distributed T-DCF with a concave profile [4]. The slope efficiency and beam quality of this laser were 63% and M^2 = 1.07, respectively, demonstrating a significant improvement over the short-length step-like tapered laser producing a power of 56 W with a slope efficiency of 54% reported earlier [10]. It should be noted, however, that the upper limit for slope efficiency of a ytterbium laser pumped at 915 nm is 84%, which suggests that the laser efficiency could be further improved by advancing the taper parameters.

Another option is a fiber with an exponential axial shape, exhibiting a strong increase of the local tapering angle at the large-diameter (pump launching) input of the fiber where pump power is high. Nearly exponential axial variation of diameter can be fabricated by direct pulling from a drawing tower [1–4, 11]. Considerable vignetting of unabsorbed pump power is expected in T-DCFs with this geometry, which would impose losses, reduce the slope efficiency, and could lead to optical damage at the fiber segment with a large tapering angle.

Basically, the "step-like" and exponential bowl-shaped tapers are two extreme designs each suffering, respectively, from low fundamental mode selectivity and pump power losses. A compromising solution is a convex shape with a gradual increase of the tapering angle and a negative slope of diameter change with length, as shown in Fig. 2 (black curve 3). Specifically, linear or parabolic diameter distributions provide a reasonable trade-off between the "step-like" and the exponential profiles.

Ray optics analysis of the tapered fiber developed in [4] can be applied to determine the optimal structure of the taper. Efficient laser operation requires high absorbed pump power, $\mathscr{P}'_{abs} + \mathscr{P}''_{abs}$ (Eq. (5)), meaning that $\mathscr{P}_{unabs}$ and $\mathscr{P}_{vgnt}$ are low. $\mathscr{P}_{unabs}$ depends on the length of the T-DCF and its paraxial absorption coefficient γ, while $\mathscr{P}_{vgnt}$ is influenced by the taper shape. A T-DCF with arbitrary shape can be represented as a sequence of N elementary short-length linear tapers, as shown in Fig. 3. The propagation angle of a meridional ray at the output of the k^{th} elementary linear taper can be determined from the recurrent formula ([4], Eq. (7)):

$$\alpha_k = \frac{D(k\cdot\Delta z)\cdot\alpha_{k-1}}{D(k\cdot\Delta z) - D'(k\cdot\Delta z)\cdot k\cdot\Delta z}, \tag{9}$$

#125834 - $15.00 USD Received 22 Mar 2010; revised 23 May 2010; accepted 24 May 2010; published 27 May 2010

where ***D(z)*** is the outer diameter of the T-DCF as a function of length, ***D(z)´*** is the first derivative of ***D(z)***, and ***k*** and ***Δz*** are the number and length of the kth elementary linear taper, respectively.

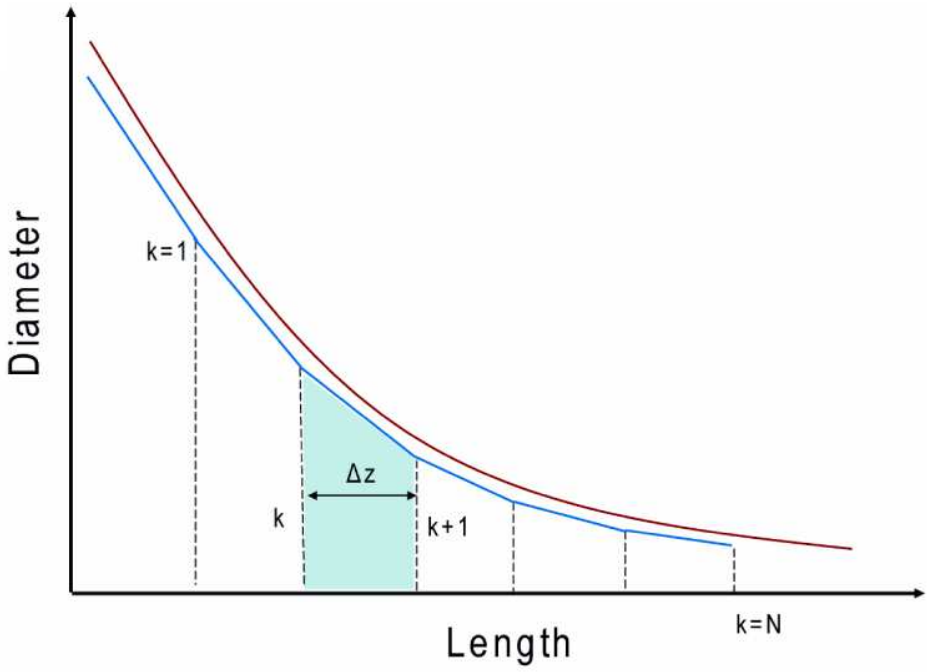

Fig. 3. Arbitrary shaped taper approximated by a sequence of N short-length linear tapers.

The meridional ray angle, after passing a T-DCF with length *L,* can be written as:

$$\theta(\alpha_0) = \sum_{k=1}^{N} \alpha_k = \sum_{k=1}^{N} \frac{D(k\cdot\Delta z)\cdot\alpha_{k-1}}{D(k\cdot\Delta z) - D'(k\cdot\Delta z)\cdot k\cdot\Delta z}. \tag{10}$$

Vignetting of a ray begins when the angle of propagation reaches the numerical aperture value, θ (α_0) = NA. L*(α)* depends on the numerical aperture of the fiber NA, and on the shape of the taper, ***D(z)***. The effective length of fiber L*(α)* when the vignetting starts, for given pump launch angle α, can be determined from the parametric equation

$$\sum_{k=1}^{N} \frac{D(k\cdot\Delta z)\cdot\alpha_{k-1}}{D(k\cdot\Delta z) - D'(k\cdot\Delta z)\cdot k\cdot\Delta z} = NA \tag{11}$$

The practical method for T-DCF engineering is based on numerical simulation using Eqs. (4) and (11) to define the effect of the angular pump intensity distribution and the longitudinal profile of the T-DCF on the fraction of pump power $\mathcal{P}_{vgnt}^{pump}$ vignetted from the cladding, for given values of $\boldsymbol{NA_{clad}}$ and the paraxial absorption coefficient ***γ***. For a certain acceptable level of vignetted power $\mathcal{P}_{vgnt}^{pump}$ and a given angular intensity distribution ***I(α)*** of the pump source, the optimal longitudinal shape ***D(z)*** of the T-DCF can be defined by solving Eqs. (4) and (11). Alternatively, by setting the parameters of the pump beam and T-DCF, these equations provide an estimate of vignetted $\mathcal{P}_{vgnt}^{pump}$ pump power. Obviously, the angular distribution of the pump source determines the optimal taper shape to achieve a low level of $\mathcal{P}_{vgnt}^{pump}$.

Assuming a parabolic shape of the taper, the diameter variation along the length ***L*** can be written as

#125834 - $15.00 USD Received 22 Mar 2010; revised 23 May 2010; accepted 24 May 2010; published 27 May 2010

$$D(z) = \frac{b_0 - b}{L} \cdot z^2 + b \cdot z + D_1, \qquad (12)$$

where b is the parabolic shape factor, $b_0 = (D_2-D_1)/L$ is the average angle of the taper, and D_1, D_2 are the diameters at the wide and narrow fiber ends, respectively.

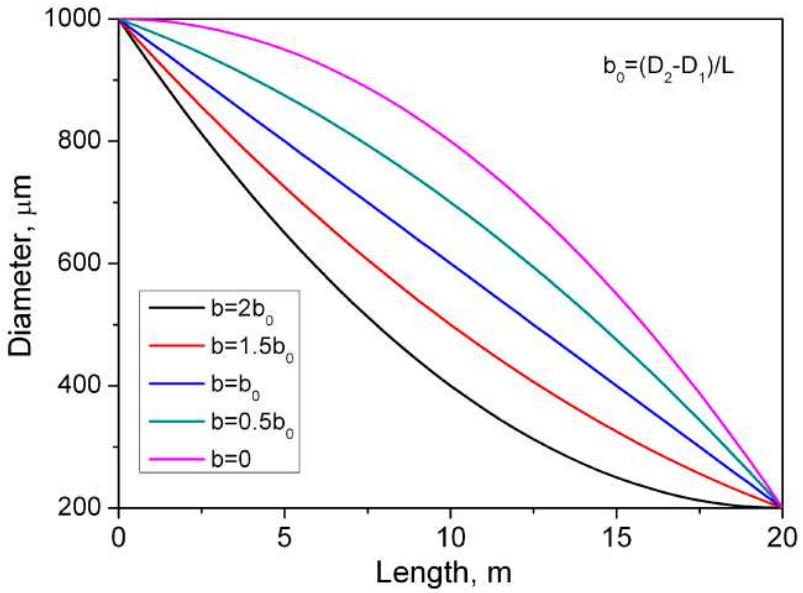

Fig. 4. Parabolic shapes of tapered fiber for different values of the shape factor b.

Figure 4 shows various T-DCF shapes for different parabolic factors. $b<b_0$, $b>b_0$, and $b = b_0$ correspond to concave, convex and linear shapes, respectively (Eq. (12). Assuming a Lorentzian angular distribution of the pump intensity, the dependence of vignetted power versus b can then be derived from Eqs. (4) and (11). This dependence, calculated for different values of the paraxial absorption coefficient γ, is shown in Fig. 5.

The concave taper shape exhibits larger vignetting losses for the pump, however, it provides better filtering of the fundamental mode and, therefore, improved output beam quality, as discussed above. In effect, an acceptable level of vignetting losses determines the optimal axial profile of the taper. For instance, Fig. 5 (inset) shows the T-DCF shape corresponding to a 0.5%-level of pump power losses caused by vignetting.

#125834 - $15.00 USD Received 22 Mar 2010; revised 23 May 2010; accepted 24 May 2010; published 27 May 2010

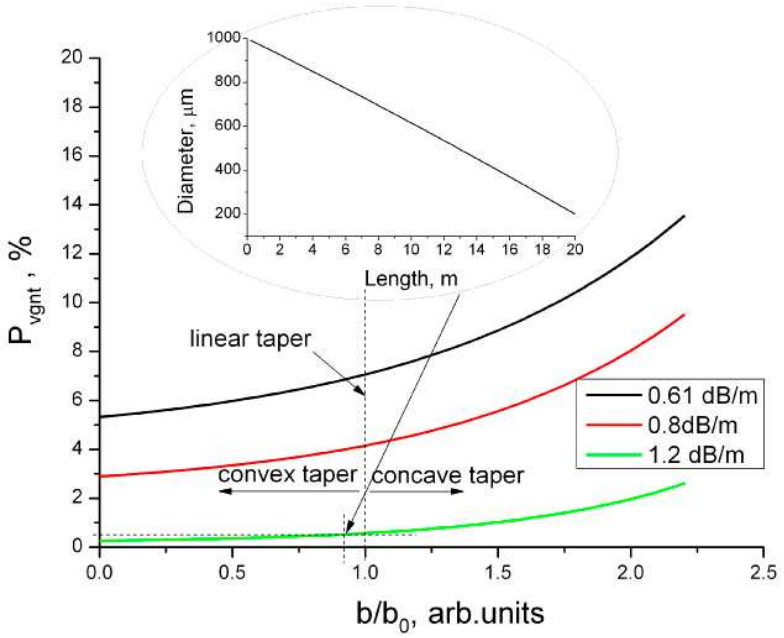

Fig. 5. Vignetted pump power as a function of the taper shape factor ***b***.

To sum up, the optimal longitudinal shape of T-DCF exhibiting the required level of pump power loss $\mathscr{P}_{vgnt}^{pump}$ is defined by the angular distribution of the pump source intensity, the paraxial absorption coefficient ***γ,*** and the tapering ratio ***T***.

2.3. Shape of the cladding, core-cladding ratio and dopant concentration profile

The shape of the cladding cross sections, the core-cladding diameter ratio, and the concentration of the dopants determine the paraxial absorption coefficient ***γ***, which is an essential characteristic of T-DCF. The dependence of the vignetted pump power on the absorption coefficient ***γ,*** derived from Eqs. (4) and (11), is shown in Fig. 6 for linear (b/b_0 = 1), concave (b/b_0 = 2) and convex (b/b_0 = 0) T-DCFs. As expected, the vignetted pump power $\mathscr{P}_{vgnt}^{pump}$ decreases rapidly with the increase of absorption coefficient ***γ***. For large values of absorption, γ>2 dB/m, the shape of the taper has little effect on the vignetted power, as seen from Fig. 6.

#125834 - $15.00 USD Received 22 Mar 2010; revised 23 May 2010; accepted 24 May 2010; published 27 May 2010

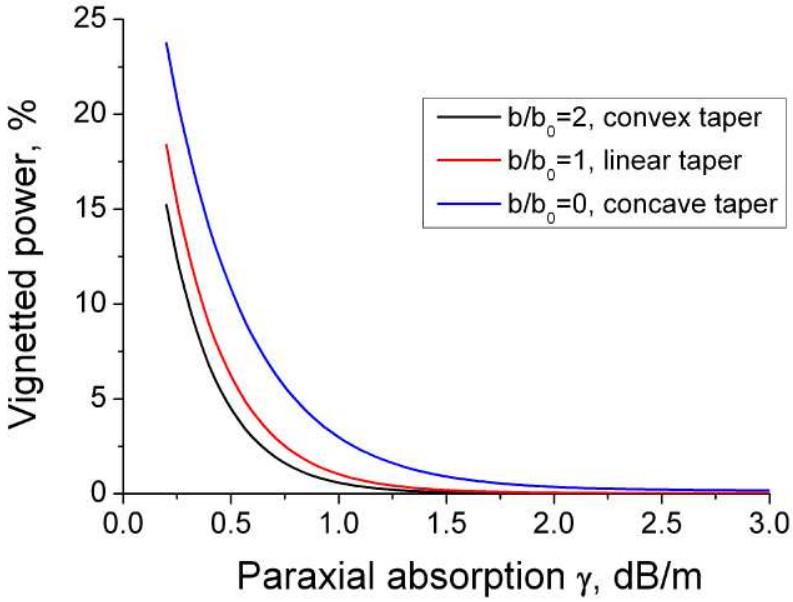

Fig. 6. Vignetted pump power versus paraxial pump absorption.

3. Experimental results

Three tapers with convex, concave and near-linear shapes with different tapering ratios have been pulled from the same preform. The all-silica fiber preform was fabricated with using plasma chemical deposition. First Yb-doped alumosilicate core layer was deposited on the inner surface of a silica substrate tube. After collapsing, redrawing and jacketing the cylindrical preform was mechanically shaped into an octagon; the perform surface has been polished then by flame. The secondary outer cladding of the octagon was formed by jacketing it with another silica tube comprising a fluorine-doped silica layer deposited on its inner surface. The entire structure was collapsed again resulted in a monolithic perform.

Both Yb-doped and F-doped silica layers were formed by the SPCVD process as described in [13] and references therein. The refractive index profile of the octagon preform is shown in the inset of Fig. 7. The essential advantage SPCVD technology as compared with conventional MCVD solution-doping technique is strong suppression of photodarkening confirmed with high-power fiber lasers. Fiber made by SPCVD technique did not reveal any measurable changes during long-term tests contrary to the lasers fabricated by conventional method which exhibit frequently decay of performance.

Tapered fiber has been formed at drawing tower during the pooling process. The axial shape of the tapered fiber depends on several factors: geometry of preform; the volume of melted part of preform in furnace determined by high temperature furnace design; drawing speed and speed of preform feed into a hot zone. Proper control of all above mentioned parameters allows to achieve a good reproducibility of longitudinal shapes of T-DCF for diameter range of 150-1000 μm and typical length 3-20 m. The accuracy of tapers shape is estimated to be better than 10% which is sufficient for control of laser parameters. The parameters of manufactured tapers are listed in Table 1. The shapes of tapers, expressed in the form of dependences of the outer diameter on the fiber length, are shown in Fig. 7.

#125834 - $15.00 USD Received 22 Mar 2010; revised 23 May 2010; accepted 24 May 2010; published 27 May 2010

Table 1. Parameters of T-DCF

# T-DCF	#1	#2	#3
Length, m	25	21.2	23.5
Core diameter at large end, µm	65	110	58
Core diameter at narrow end, µm	11	20	20
Clad diameter at wide side, µm	835/890	880/925	930/980
Clad diameter at narrow side, µm	140/150	158/165	320/340
Core/clad ratio	1:13	1:9.5	1:18
Tapering ratio	6	5.6	2.9
b, µrad	104.63	22.35	29.64
b_0 µrad	51	40	39.35
b/b_0	2.05	0.56	0.753
Shape of the cladding cross-section	octagonal	octagonal	Octagonal
Core NA	0.11	0.11	0.11
Clad NA	0.22	0.22	0.22
In-core pump absorption @ 915 nm, dB/m	600 dB/m	600 dB/m	600 dB/m
Paraxial ray absorption @ 915 nm, dB/m	0.8 dB/m	1.2 dB/m	0.61 dB/m

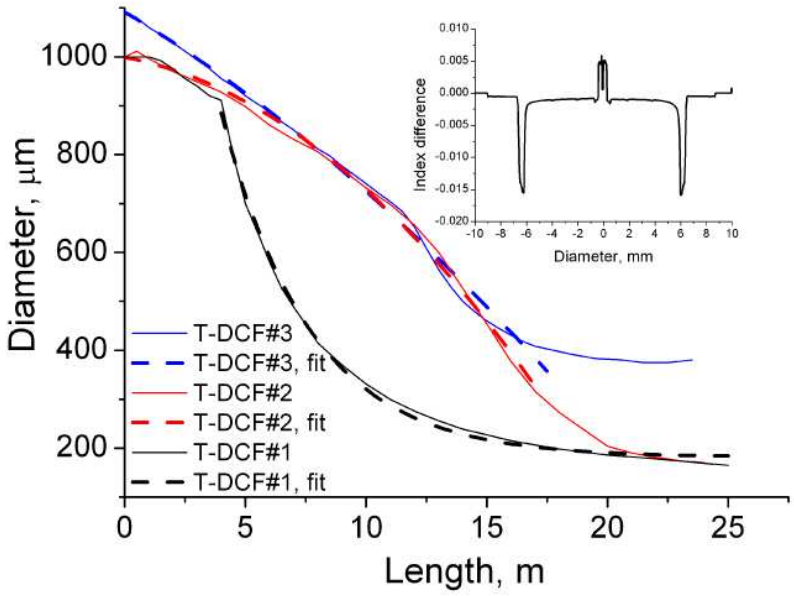

Fig. 7. Longitudinal profiles of experimental T-DCFs: solid lines – experimentally measured, dashed lines – parabolic fit. Inset: refractive index profile of the all-silica Yb-doped alumosilicate-core/F-doped-silica-cladding fiber preform synthesized with the help of SPCVD

.The fibers described in Table 1 were then incorporated into fiber laser configurations, as shown schematically in Fig. 8. This experimental set up is similar to that report in [2, 4]. The pump radiation from a 915 nm high-power source was launched via fiber cable with a core diameter of 600 µm and a NA = 0.22 into T-DCF using a beam shaping optical unit and dichroic filter. Beam shaping optics comprising lenses and a diaphragm forms the beam to a diameter of 880 µm and divergence corresponding to NA = 0.15. The laser cavity is terminated by a dielectric mirror located behind the wide end of the T-DCF, and 4% Fresnel reflection at the output small-diameter facet of the taper. The wide end of T-DCF was angle cleaved.

#125834 - $15.00 USD Received 22 Mar 2010; revised 23 May 2010; accepted 24 May 2010; published 27 May 2010

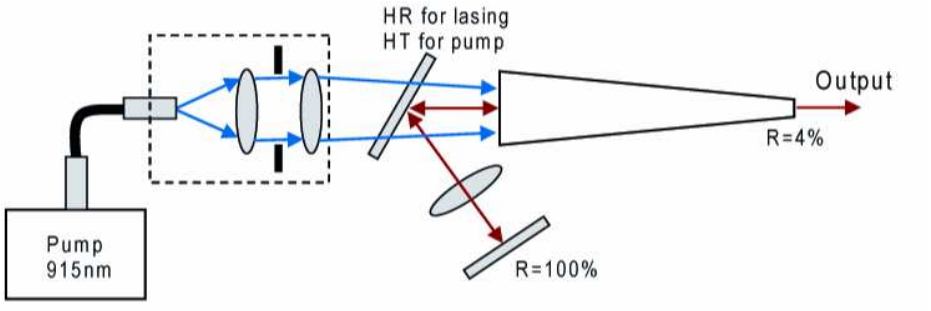

Fig. 8. Experimental setup.

The dependence of the output power on the launched pump power measured for each T-DCF reveals the slope efficiency and maximum output power shown in Fig. 9.

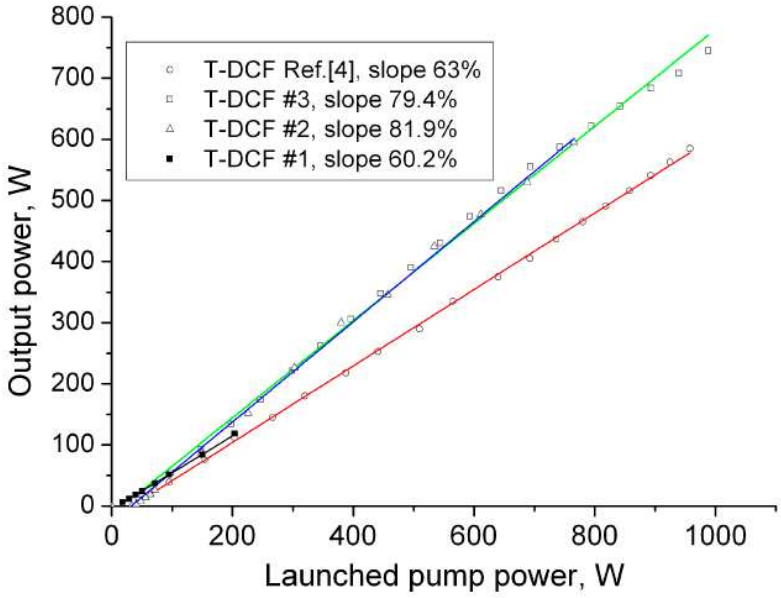

Fig. 9. Output power as function of launched pump power.

The contrast, defined as the relative fraction of output power emitted from the core, was determined by examining the angular distribution of output radiation in the far field. Pump power losses caused by vignetting $\mathcal{P}_{vgnt}^{pump}$ have been calculated for each T-DCF, as described above, using experimental parameters - absorption coefficient, taper shape and angular intensity distribution of the pump source. The results are summarized in Table 2.

Table 2. Parameters of lasers with T-DCF

	#1	**#2**	**#3**
Pump beam NA	0.15	0.15	0.15
P_{vgnt}, %	10.19	0.45	2.22
P_{unabs}, %	0.9	0.08	3.13
P_{vgnt} + P_{unabs}, %	11.09	0.53	5.35
Slope efficiency, %	60.2	81.9	77.9
Contrast, %	64.3	35	87
Normalized brightness enhancement factor	7.6	4.92	3.11

#125834 - $15.00 USD Received 22 Mar 2010; revised 23 May 2010; accepted 24 May 2010; published 27 May 2010

4. Discussion

Next, the characteristics of lasers using different T-DCFs have been examined.

T-DCF#1

T-DCF#1 has a concave parabolic shape with a pump absorption coefficient of 0.8 dB/m at 915 nm. The initial 4 m section of T-DCF has a nearly flat shape, which is followed by a concave section with rapid diameter decrease along the length. The tapering ratio and the parabolic factor of the concave section are 6 and 2.05, respectively. The measured slope efficiency of the laser using this taper was only 60.2%. The poor slope efficiency is caused by high pump vignetting losses of 10.19% due to both non-optimal T-DCF shape and a relatively small value of pump absorption coefficient. A similar concave T-DCF used previously in [2] has demonstrated a better slope efficiency of 71.4% due to a 3-4 times higher pump absorption coefficient, which made the laser performance tolerant to taper shape, in agreement with results presented in Fig. 6. The measured beam contrast for this T-DCF of 64.3% is determined by the high tapering ratio of $T = 6$ and the 4 m long large core diameter section. The relatively low value of contrast indicates a significant fraction of higher-order modes leaking from the core into the cladding.

T-DCF #2

T-DCF#2 is a convex shape taper with parabolic factor $b/b_0 = 0.56$, absorption coefficient γ = 1.2 dB/m and tapering ratio of 5.6, as shown in Fig. 7 (red curve). In accordance with the above analysis, it demonstrated a high slope efficiency of 81.9%, which is close to the theoretical limit of 85%. Record slope efficiency is the result of a low level of vignetting of 0.45%, and only 0.08% unabsorbed pump power. The parabolic shape with $b/b_0 = 0.56$ is actually close to the "step-like" shape shown in Fig. 2 (blue curve 1). The high-order modes efficiently deplete the population inversion and are amplified over significant lengths of the taper. The laser exhibited, however, a poor output beam contrast of only 35%. The taper section with a large core diameter of $2a = 110$ μm guides a large number of modes, $N \sim a^2$, (Eq. (7) thus reducing the relative fraction of fundamental and lower-order modes. In the narrow part of the T-DCF higher-order modes are filtered out from the core and afterwards propagate in the cladding, degrading the output beam contrast.

T-DCF #3

T-DCF#3 is a convex taper with parabolic factor of $\boldsymbol{b/b_0} = 0.753$, i.e. taper profile is close to the linear shape, paraxial absorption coefficient of 0.61 dB/m and tapering ratio of 2.9. Vignetted pump power and unabsorbed pump power losses are 2.22% and 3.13%, respectively, resulting in a total loss of pump power of 5.35% (see Table 2). The laser with this tapered fiber demonstrates a combination of good slope efficiency, 77.9%, and high output beam contrast, 87%.

An analysis of the simulations and experimental results allows the following conclusions to be drawn:

- The slope efficiency of a laser with T-DCF is determined by the axial profile of the taper diameter, for a given angular distribution of the pump beam. The slope efficiency of the tapered laser has been studied experimentally using a pumping source with NA = 0.15 for various longitudinal shapes of taper. We show that an optimized taper configuration could approach the theoretical limit of the efficiency.
- The slope efficiency is strongly dependent on the pump absorption coefficient. For absorption above 2 dB/m this effect, however, is less pronounced.
- The slope efficiency suffers from a pump-vignetting effect dependent on the tapering ratio. When the tapering ratio is low, the fraction of pump power leakage decreases and, consequently, slope efficiency increases.

#125834 - $15.00 USD Received 22 Mar 2010; revised 23 May 2010; accepted 24 May 2010; published 27 May 2010

- The contrast of the output beam, defined as the relative fraction of power propagating in the core, depends critically on the tapering ratio and shape of the taper. In the T-DCF with a large tapering ratio and parabolic shape factor, the population inversion is strongly depleted by high-order modes, thus reducing the beam contrast. It was shown that the beam contrast decreases with the tapering ratio *T*. Some discrepancy between calculations using Eq. (7) and experimental data summarized in Table 2 is due to the simplified assumption of uniform excitation of all guided modes.
- T-DCF with properly chosen parameters demonstrates superior brightness enhancement characteristics compared with regular double-clad fiber. The measured normalized brightness enhancement factors presented in Table 2 show an improvement up to a factor of 7.6. It should be noted that in T-DCF-based amplifiers there are no signal losses in the core due to mode filtering, and consequently no limitations on the tapering ratio. The brightness gain factor in tapered amplifiers can be significantly higher.

In summary, we demonstrate that T-DCF with appropriate parameters values allows considerable brightness improvements to be achieved, compared to regular non-tapered double-clad fiber. High brightness, efficiency and beam contrast from an active T-DCF are accomplished by means of high paraxial absorption, a modest tapering rate and a nearly linear (or slightly parabolic) shape.

5. Conclusion

In this paper, an optimization strategy for active tapered double-clad fibers has been developed based on ray optics formalism. In particular, the effect of the tapering ratio, the axial shape of the profile, and the absorption on the brightness enhancement and slope efficiency has been examined in detail. We have shown that T-DCF with an optimized design exhibits a slope efficiency close to the theoretical limit. The brightness characteristics of an active T-DCF, superior to regular non-tapered active DCF, have been demonstrated experimentally. Active T-DCF can be pumped with powerful laser diode bars, whose application is usually limited due to their low brightness. Experimentally, we have demonstrated an efficient ytterbium laser based on T-DCF as the active medium, producing an output power of 750 W with a slope efficiency of 81.9% and near diffraction-limited beam quality ($M^2 = 1.7$).

#125834 - $15.00 USD Received 22 Mar 2010; revised 23 May 2010; accepted 24 May 2010; published 27 May 2010

Appendix 7

Publication 7

J. Kerttula, V. Filippov, Y. Chamorovskii, V. Ustimchik, K. Golant, and O. G. Okhotnikov, "Tapered fiber amplifier with high gain and output power", *Laser Physics*, vol. 22, no. 11, pp. 1734-1738, 2012.

Appendix 8

Publication 8

J. Kerttula, V. Filippov, Y. Chamorovskii, K. Golant, and O. G. Okhotnikov, "Actively Q-switched 1.6-mJ tapered double-clad ytterbium-doped fiber laser", *Optics Express*, vol. 18, no. 18, pp. 18543–18549, 2010.

Actively Q-switched 1.6-mJ tapered double-clad ytterbium-doped fiber laser

Juho Kerttula,[1,*] Valery Filippov,[1] Yuri Chamorovskii,[2] Konstantin Golant,[2] and Oleg G. Okhotnikov,[1]

[1]*Optoelectronics Research Centre, Tampere University of Technology, P.O. Box 692, 33101 Tampere, Finland*
[2]*Institute of Radio and Electronics of the Russian Academy of Sciences, Mokhovaya 11, bld.7, 125009 Moscow, Russia*
**juho.kerttula@tut.fi*

Abstract: We have demonstrated an actively Q-switched tapered double-clad fiber laser capable of single-shot generation of 1.6-mJ, 64-ns pulses. The active medium based on tapered double-clad fiber is shown to exhibit a reduced level of amplified spontaneous emission which allows for high-energy pulse extraction at extremely low repetition rates.

OCIS codes: (060.2280) Fiber design and fabrication; (060.2320) Fiber optics amplifiers and oscillators; (060.3510) Lasers, fiber

References and links

1. O. Schmidt, J. Rothhardt, F. Röser, S. Linke, T. Schreiber, K. Rademaker, J. Limpert, S. Ermeneux, P. Yvernault, F. Salin, and A. Tünnermann, "Millijoule pulse energy Q-switched short-length fiber laser," Opt. Lett. **32**(11), 1551–1553 (2007).
2. F. Di Teodoro, and C. Brooks, "Multi-MW peak power, single transverse mode operation of a 100 micron core diameter, Yb-doped photonic crystal rod amplifier", Fiber Lasers IV: Technology, Systems, and Applications, Proc. of SPIE **vol. 6453**, 645318, (2007).
3. L. Michaille, D. M. Taylor, C. R. Bennett, T. J. Shepherd, and B. G. Ward, "Characteristics of a Q-switched multicore photonic crystal fiber laser with a very large mode field area," Opt. Lett. **33**(1), 71–73 (2008).
4. J. A. Alvarez-Chavez, H. L. Offerhaus, J. Nilsson, P. W. Turner, W. A. Clarkson, and D. J. Richardson, "High-energy, high-power ytterbium-doped Q-switched fiber laser," Opt. Lett. **25**(1), 37–39 (2000).
5. C.C., "*Renaud,* H.L. *Offerhaus,* J.A. *Alvarez-Chavez,* J. *Nilsson,* W.A. *Clarkson,* P.W. *Turner,* D.J. *Richardson and* A.B. *Grudinin,* "Characteristics of Q-switched cladding-pumped ytterbium-doped fiber lasers with different high-energy fiber designs," IEEE J. Quantum Electron. **37**(2), 199–206 (2001).
6. J. A. Alvarez-Chavez, A. B. Grudinin, J. Nilsson, P. W. Turner, and W. A. Clarkson, "Mode selection in high power cladding pumped fiber lasers with tapered section", *Conf. Lasers and Electro-Optics, OSA Technical Digest*, pp. 247 - 248, 1999.
7. V. Filippov, Y. Chamorovskii, J. Kerttula, A. Kholodkov, and O. G. Okhotnikov, "Single-mode 212 W tapered fiber laser pumped by a low-brightness source," Opt. Lett. **33**(13), 1416–1418 (2008).
8. V. Filippov, Y. Chamorovskii, J. Kerttula, A. Kholodkov, and O. G. Okhotnikov, "600 W power scalable single transverse mode tapered double-clad fiber laser," Opt. Express **17**(3), 1203–1214 (2009).
9. V. Filippov, Y. Chamorovskii, J. Kerttula, K. Golant, and O. G. Okhotnikov, "750 W double-clad ytterbium tapered fiber laser with nearly theoretical limited efficiency," Fiber Lasers VII: Technology, Systems and Applications, Proc. of SPIE **vol. 7580**, 758017 (2010).
10. V. Filippov, Y. Chamorovskii, J. Kerttula, K. Golant, M. Pessa, and O. G. Okhotnikov, "Double clad tapered fiber for high power applications," Opt. Express **16**(3), 1929–1944 (2008), http://www.opticsinfobase.org/abstract.cfm?URI=oe-16-3-1929.
11. K. M. Golant, "Surface plasma chemical vapor deposition: 20 years of application in glass synthesis for lightguides (a review)", XXI International Congress on Glass, Strasbourg, Proc. on CD ROM,paper L13 (2007).

#129597 - $15.00 USD Received 4 Jun 2010; revised 28 Jul 2010; accepted 29 Jul 2010; published 16 Aug 2010

12. S. Maryashin, A. Unt, and V. P. Gapontsev, "10-mJ pulse energy and 200 W average power Yb-doped fiber laser" Fiber Laser III: Technology, Systems and Applications, Proc. of SPIE **vol. 6102**, 6102O–1 (2006).
13. *Rare-earth-doped fiber lasers and amplifiers* Second edition, Michel J. F. Digonnet, ed., (Marcel Dekker, Inc., 2001).
14. J. R. Marciante, and J. D. Zuegel, "High-gain, polarization-preserving, Yb-doped fiber amplifier for low-duty-cycle pulse amplification," Appl. Opt. **45**(26), 6798–6804 (2006), http://www.opticsinfobase.org/ao/abstract.cfm?URI=ao-45-26-6798.
15. J. Nilsson, R. Paschotta, J. E. Caplen, and D. C. Hanna, "Yb($^{3+}$)-ring-doped fiber for high-energy pulse amplification," Opt. Lett. **22**(14), 1092–1094 (1997), http://www.opticsinfobase.org/ol/abstract.cfm?URI=ol-22-14-1092.
16. M. E. Fermann, "Single-mode excitation of multimode fibers with ultrashort pulses," Opt. Lett. **23**(1), 52–54 (1998), http://www.opticsinfobase.org/ol/abstract.cfm?URI=ol-23-1-52.
17. K. Shiraki, M. Ohashi, and M. Tateda, "Suppression of stimulated Brillouin scattering in a fiber by changing the core radius," Electron. Lett. **31**(8), 668–669 (1995).
18. A. Liu, "Suppressing stimulated Brillouin scattering in fiber amplifiers using nonuniform fiber and temperature gradient," Opt. Express **15**(3), 977–984 (2007), http://www.opticsinfobase.org/oe/abstract.cfm?URI=oe-15-3-977.

1. Introduction

Gain media based on double-clad fiber (DCF) offer a technological platform for high brightness, highly efficient laser sources. Operating such a laser in the pulsed regime, and particularly in an actively Q-switched state, is beneficial for a wide range of applications, such as marking, machining, and range finding. Currently, there are two main approaches for high-energy Q-switching: utilization of short, rod-type photonic crystal fibers (PCF) with one or multiple cores [1–3] or the use of large mode area (LMA) double-clad fibers [4,5]. Either LMA fibers with a low numerical aperture (NA) or multimode fibers with a short tapered section are the main approaches used so far to achieve high-brightness lasing with large mode volume [5,6].

The fundamental mechanism limiting the pulse energy especially at repetition rates below 1 kHz is the high level of amplified spontaneous emission (ASE) accumulated during the long time slot between the pulses. ASE prevents efficient energy storage in the fiber cavity and becomes progressively stronger with decreasing repetition rate. A practical solution to this problem would allow for multi-mJ pulses with sub-100-ns duration at low duty cycles needed for industrial and LIDAR applications. Actively Q-switched fiber lasers reported to date are either long-cavity lasers producing pulse widths in the range from 100 ns to few μs with duty cycles of 10^{-4} – 10^{-3} [4], or alternatively lasers using short rod-like fibers with few-ns pulses and duty cycles of the order of 10^{-5} [1].

Recently we have proposed tapered double-clad fiber (T-DCF) as a promising gain medium for high-power lasers and amplifiers [7–10]. The advantages of the T-DCF approach in the actively Q-switched scheme are demonstrated in this study by generation of 1.6-mJ, 64-ns pulses at very low repetition rates, up to single-shot operation.

2. Experimental setup and results

The experimental setup of the Q-switched fiber laser used in this study is schematically shown in Fig. 1. The active fiber was end-pumped by a fiber-coupled diode bar at 915 nm through the wide fiber end via a collimating/focusing lens pair and a 1-μm dichroic splitter. The laser cavity is terminated by Fresnel reflection from the wide fiber end and a broadband (BB) high-reflection (HR) mirror at the narrow end of the fiber, which was angle-cleaved (AC) to suppress spurious lasing. Active Q-switching was achieved by an acousto-optic modulator (AOM) placed between the narrow fiber end and the HR mirror that reflected the 1st diffraction order back to the cavity. A 1-μm edge filter was placed between the fiber and the AOM to filter out unabsorbed pump, reducing thermal load on the modulator. Laser radiation monitored from the wide end of the fiber was analyzed using a pyroelectric energy sensor (up to 25 kHz, 500 ns), a fast photodetector, and a thermal power meter.

The composition of the T-DCF used in this experiment was similar to composition which we have exploited earlier for the design of the CW high power Yb fiber laser [7–10]. The T-DCF was drawn from a preform fabricated by the SPCVD method [11]. The preform consists

#129597 - $15.00 USD Received 4 Jun 2010; revised 28 Jul 2010; accepted 29 Jul 2010; published 16 Aug 2010

of an Yb-doped aluminosilicate core, a pure-silica inner cladding, and a fluorine-doped silica outer cladding. Yb ion concentration corresponds to an in-core absorption of 1000 dB/m at 975 nm wavelength. Fiber core and cladding have numerical apertures of 0.11 and 0.22, respectively.

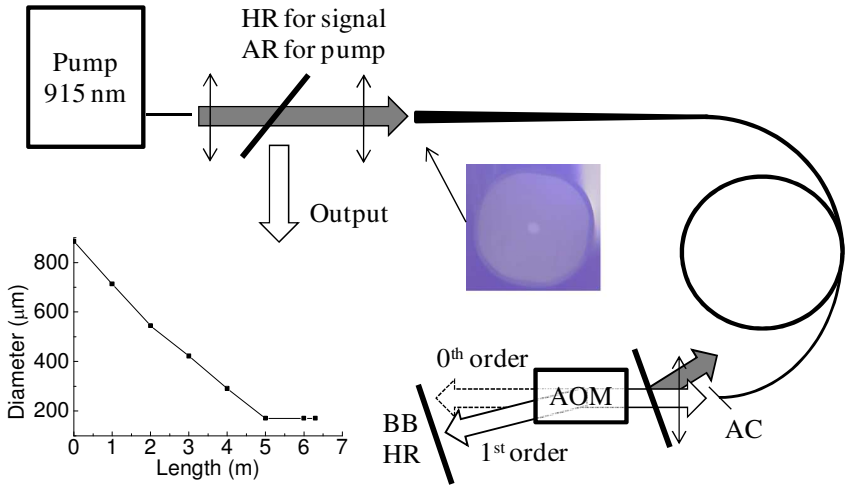

Fig. 1. Schematic of the Q-switched laser setup, a micrograph of the wide fiber end, and the longitudinal profile of the T-DCF.

The longitudinal profile of the active T-DCF with total length of 6.3 m is shown as an inset in Fig. 1. The cladding diameter of the slightly non-circular T-DCF varied from 880 μm to 940 μm at the wide end. The tapering ratio of the T-DCF is 5.5 with the core/cladding diameter ratio kept at 1:10, i.e. the core diameter was 83 μm and 15 μm at the wide and narrow ends of the taper, respectively. The double-clad pump absorption has been measured for radiation launched into the T-DCF from the narrow side to avoid pump power loss via vignetting [8]. The measured pump absorption was 10.1 dB (1.6 dB/m) at 915 nm. The T-DCF was coiled with 35 cm diameter and placed on a water-cooled aluminium plate. The T-DCF was first characterized in quasi-CW regime (high duty cycle) up to 6 W average power at 1070 nm. The measured slope efficiency with respect to launched pump was 43%, limited by coupling loss and the diffraction efficiency of the AOM.

#129597 - $15.00 USD Received 4 Jun 2010; revised 28 Jul 2010; accepted 29 Jul 2010; published 16 Aug 2010

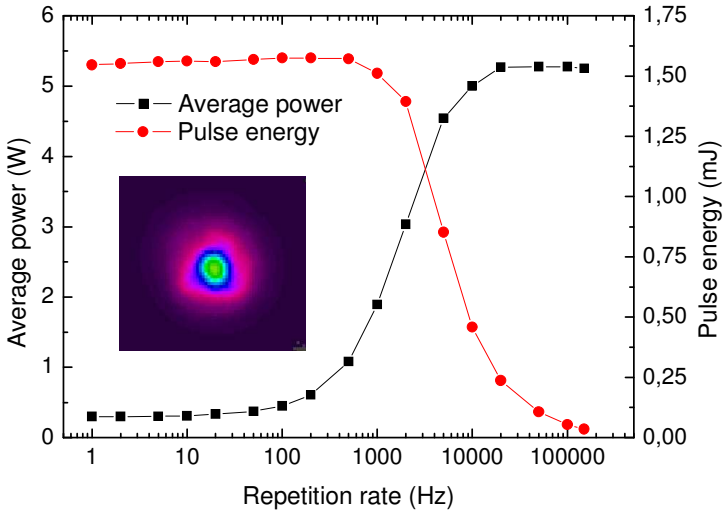

Fig. 2. Pulse energy and average power (including ASE) versus repetition rate at a constant pump power. The output beam profile with $M^2 = 2.7$ is shown as an inset.

In the Q-switched regime, the laser was operated at various repetition rates and pump powers. Figure 2 shows the pulse energy and average power as a function of repetition rate in the range of 1 Hz – 150 kHz. The ASE fraction of the total output power was below 9% at 1 kHz.

Figure 3 shows the pulse energy and peak power as a function of absorbed pump power at a constant repetition rate of 5 Hz. Figures 2 and 3 show that the pulse energy decreases with increasing repetition rate due to the decrease in the energy storage for small pulse periods and increases with pump power limited by the onset of stimulated Brillouin scattering (SBS). The average power increases with both pump power and repetition rate, as expected from general theory of Q-switched lasers. The pulse width decreases with increasing pump power and increases with the repetition rate. These effects can be attributed to incomplete inversion between pulses. Indeed, low pump power and/or short low-Q time reduce the energy storage in the fiber resulting in low gain and longer pulse build-up time.

#129597 - $15.00 USD Received 4 Jun 2010; revised 28 Jul 2010; accepted 29 Jul 2010; published 16 Aug 2010

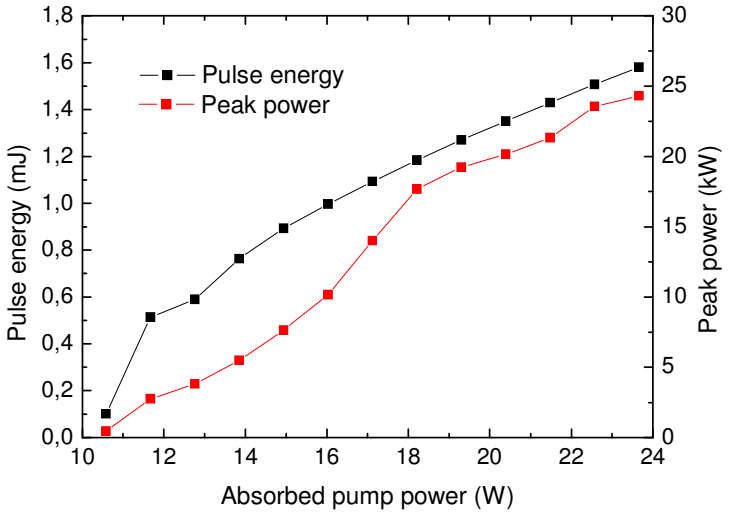

Fig. 3. Pulse energy and peak power versus absorbed pump power at a constant repetition rate of 5 Hz.

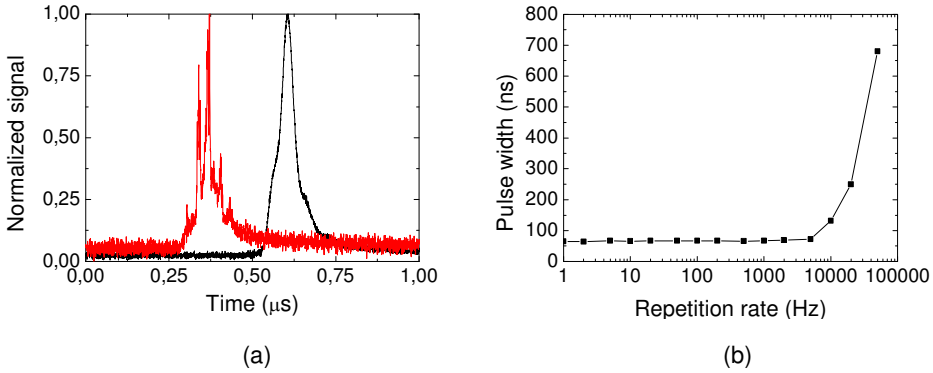

Fig. 4. (a) 1.6-mJ pulse before (black) and after (red) the onset of SBS-induced pulse breakdown; (b) pulse width versus repetition rate at constant pump power.

A pulse energy as high as 1.58 mJ corresponding to a peak power of 24.3 kW was achieved. Above this value, irregular backward-propagating pulses and pulse breakdown were observed, as illustrated in Fig. 4a. Figure 4b shows the dependence of pulse width on the repetition rate. Independent of pump power, single-shot operation was also achieved by manually triggering the AOM control pulse, without notable changes in pulse energy or pulse shape.

Figure 5 shows the optical spectra of the laser at a repetition rate of 500 Hz for 0.1 mJ and 1.6 mJ pulse energy, and the ASE spectrum peaking at 1035 nm when the cavity was blocked. At repetition rates below a few kHz, ASE grows rapidly relative to the signal with decreasing repetition rate, constituting an increasing fraction of the output power.

Finally, we measured the output beam quality of the laser by the clip level method. M^2 determined at the narrow and wide taper ends resulted in $M^2 = 1.8$ and $M^2 = 2.7$, respectively.

#129597 - $15.00 USD Received 4 Jun 2010; revised 28 Jul 2010; accepted 29 Jul 2010; published 16 Aug 2010

It is interesting to note that the spatial distribution of ASE observed below the lasing threshold from the wide end of the taper with a core diameter of 83 µm had an $M^2 = 4.2$.

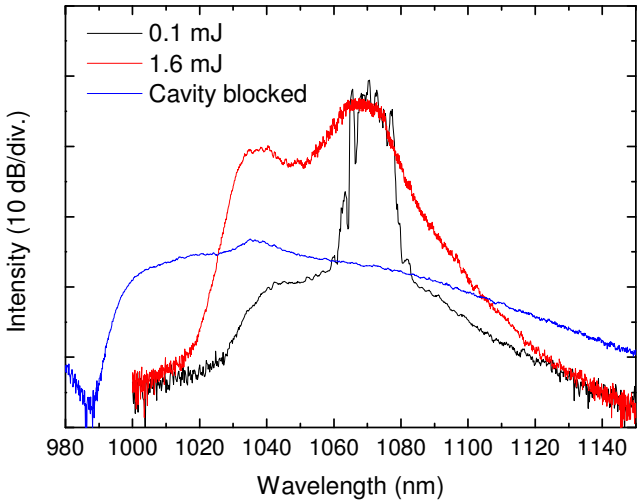

Fig. 5. Optical spectra of the Q-switched T-DCF laser at 500 Hz repetition rate with 0.1 mJ (black) and 1.6 mJ pulse energy (red, FWHM = 14 nm), and without lasing when the cavity is blocked (blue).

3. Discussion

Tapered double-clad fiber is demonstrated to offer attractive features for energetic pulse generation, namely the large mode volume and intrinsic mechanisms for ASE and SBS suppression. The very large doped core area at the wide taper end (5410 μm^2) is useful for both efficient energy storage and for decreasing the power density at the fiber end face. Because of the reduced thermal load at the wide fiber end, optical damage has never been observed within this study. The tapered fiber with an average core area of ~3000 μm^2 allows values of extractable energy of ~3 mJ and saturation energy of 0.3 mJ to be estimated [5,12].

The detrimental effect of amplified spontaneous emission depleting the inversion limits the potential of pulse energy scaling and inhibits pulse operation with low duty cycle. Few techniques have been considered to alleviate ASE impact. They include doping the fiber with a saturable absorber to avoid significant ASE growth, using optical isolators to suppress backward ASE, and spectral filtering of broadband ASE radiation [13,14]. ASE suppression has been observed in a fiber with ring doping exhibiting a small signal gain, however this approach requires long-length gain fiber which would inevitably increase the pulse width and impede operation at low duty cycles [15].

An intrinsic attribute of the tapered fiber, essential for Q-switched operation, is the built-in mechanism of ASE filtering. ASE propagating in a T-DCF from the wide to the narrow end experiences vignetting, i.e. part of the spontaneous emission leaks out of the core thus mitigating the detrimental effect of inversion depletion. This effect becomes more pronounced with increasing tapering ratio [8–10]. Since the intensity of spontaneous emission is proportional to the number of propagating modes, counter-propagating ASE in a taper (from narrow to wide end) is also weaker compared to a cylindrical DCF with similar average core size due to mode selection in the small-core section of the tapered fiber [5]. ASE generated in the small-core section of the fiber and propagated towards the wide end is comprised primarily of low-order modes [5,16]. An estimation for the number of propagating modes N based on the ASE beam quality factor of $M^2 = 4.2$ measured from the wide fiber end yields N

#129597 - $15.00 USD Received 4 Jun 2010; revised 28 Jul 2010; accepted 29 Jul 2010; published 16 Aug 2010

~$(M^2)^2$ ~18. However, according to an estimation based on the V-parameter of the wide fiber end, the number of modes is N ~$V^2/2$ ~430. A comparison of these values indicates an efficient mechanism of mode selection in the T-DCF resulting in a significant reduction of counter-propagating ASE modes, and thus contributing to ASE suppression.

Since most of the ASE is generated in the large-core section of the taper with large gain volume, the ASE spectrum peaks around 1035 nm, while the signal spectrum peaks at a longer wavelength of 1065 nm. This specific feature, intrinsic to the tapered structure, provides another opportunity for ASE suppression through spectral filtering. This observation is not typical for Q-switched fiber sources based on uniform fibers.

Finally, the variation of fiber diameter is a well-known technique for SBS suppression [10,17,18]. Using tapered waveguide structures is advantageous in terms of Brillouin gain reduction and is another attractive feature provided by the T-DCF.

4. Conclusion

We present the first actively Q-switched laser using a tapered double-clad fiber. The large mode volume, efficient energy storage, and intrinsic mechanisms of ASE and SBS suppression of the T-DCF enabled low-duty-cycle operation with the highest measured pulse energy of 1.6 mJ for a 64-ns pulse. Vignetting of the co-propagating ASE and a reduced number of spatial modes for the counter-propagating ASE result in an inherently low ASE background, which in turn allows for robust operation at very low repetition rates (up to single-shot generation) without degradation of the pulse energy, or shape, or stability of the train. For repetition rates above ~1 kHz, the pulse energy is limited by insufficient energy storage between pulses which is a general characteristic of Q-switched lasers, while at low repetition rates the energy is eventually limited by the onset of SBS, though its threshold is notably higher than in uniform cylindrical fibers. The results show the potential of tapered double-clad fibers for high-energy, low-duty-cycle pulse generation and amplification.

Acknowledgements

This research was supported in part by the Finnish Funding Agency for Technology and Innovation (LAMP project), the Graduate School in Electronics, Telecommunications and Automation (GETA), the Walter Ahlström Foundation, the Ulla Tuominen Foundation, and the KAUTE Foundation.

#129597 - $15.00 USD Received 4 Jun 2010; revised 28 Jul 2010; accepted 29 Jul 2010; published 16 Aug 2010

Appendix 9

Publication 9

J. Kerttula, V. Filippov, Y. Chamorovskii, K. Golant, and O. G. Okhotnikov, ”250 μJ Broadband Supercontinuum Generated Using a Q-switched Tapered Fiber Laser”, *IEEE Photonics Technology Letters*, vol. 29, no. 6, pp. 380–382, 2011.

250 µJ Broadband Supercontinuum Generated Using a Q-switched Tapered Fiber Laser

Juho Kerttula, Valery Filippov, Yuri Chamorovskii, Konstantin Golant, and Oleg G. Okhotnikov

***Abstract*—We demonstrate supercontinuum generation in a photonic crystal fiber pumped with 50-ns pulses from a Q-switched tapered fiber laser. The continuum spans from 600 nm to beyond 1600 nm with pulse energy up to 250 µJ at the repetition rate of 1 kHz. To the best of our knowledge, this represents the highest pulse energy of a broadband supercontinuum demonstrated to date.**

***Index Terms*—Optical fiber lasers, Q-switched lasers, Supercontinuum generation, Tapered double-clad fiber**

I. Introduction

SIGNIFICANT achievements in supercontinuum (SC) generation demonstrated during the last decade were possible exclusively after the invention of high-nonlinearity photonic crystal fibers (PCFs) [1], [2]. Though continuous wave (CW) pumping has been demonstrated [3], [4], the most common approaches for supercontinuum generation exploit short pulse pumping with high peak powers enabling efficient SC generation with a short length of PCF [5]. Ultrafast supercontinuum sources, however, are typically high repetition rate systems with relatively low pulse energy. Some applications would benefit from highly energetic pulses with large spectral coverage, which allow high pulse energy to be maintained after spectral slicing.

In the nanosecond pump regime either actively or passively Q-switched sources have been used for SC generation with the highest reported pulse energy of 23 µJ [6]. It should be noted that the process of supercontinuum development depends critically on the temporal characteristics of pump signal. Particularly, for Q-switched pulses with nanosecond-scale duration, effects of self-phase modulation (SPM) are negligible and the supercontinuum develops mainly from noise-seeded four-wave mixing (modulational instability, MI) and stimulated Raman scattering (SRS). The MI leads to formation of solitons that experience self-frequency shift (SFS) and generate dispersive waves (DWs) resulting in broadening of the spectrum, which is effectively averaged out by noise-induced jitter [7], [8]. Nanosecond regime broadband supercontinua have been reported using various approaches with pulse widths ranging from sub-ns to 100 ns and pulse energies typically not exceeding 10 µJ [9], [10]. A supercontinuum with 10-ns, 40-µJ pulses has been demonstrated by pumping with an 8-km long cavity mode-locked MOPA system [11].

In this study, we use a Q-switched ytterbium fiber laser based on tapered double-clad fiber (T-DCF) [12], as the pump source for SC generation. Recently, we have demonstrated kW-level CW power [13] and over 2 mJ of Q-switched pulse energy [14] using this technology, which illustrates the high potential of these sources for nonlinear optics research.

II. Experimental Setup and Results

Fig. 1 shows the experimental setup for SC generation using actively Q-switched tapered fiber laser as a pump source. The general design and characteristics of tapered fiber lasers are described in [13], [15]. The 30-m Yb-doped active fiber used in this work was linearly tapered from a cladding diameter of 420 µm down to 170 µm. The core/cladding diameter ratio of the tapered fiber is 1:25, and cladding and core numerical apertures are 0.4 and 0.11, respectively. At the repetition rate of 1 kHz, the laser produced up to 830 µJ pulse energy with an average output power of 1.0 W, limited by stimulated Brillouin scattering [15].

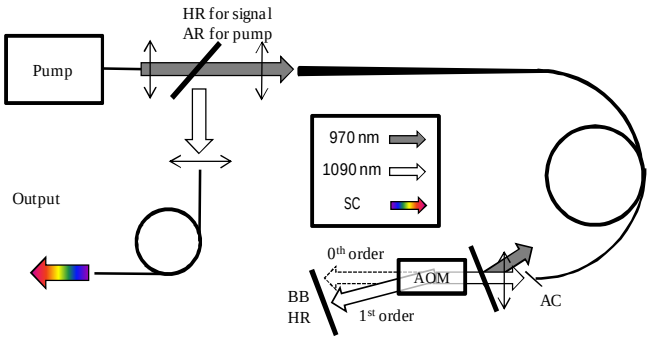

Fig. 1. Experimental setup used for SC generation. HR – High reflection, AR – Anti-reflection, AC – angle cleave, BB - broadband

Manuscript received November 20, 2010. This work has been supported in part by the Graduate School in Electronics, Telecommunication, and Automation (GETA), the Walter Ahlström Foundation, and the KAUTE-foundation.

J. Kerttula, V. Filippov, and O.G. Okhotnikov are with the Optoelectronics Research Centre, Tampere University of Technology, Korkeakoulunkatu 3, 33720 Tampere, Finland. Corresponding author's phone: +358 40 198 1063; fax: +358 3115 3400; e-mail: juho.kerttula@tut.fi.

Y. Chamorovskii and K. Golant are with the Institute of Radio and Electronics of the Russian Academy of Sciences, Mokhovaya 11, bld.7, 125009 Moscow, Russia.

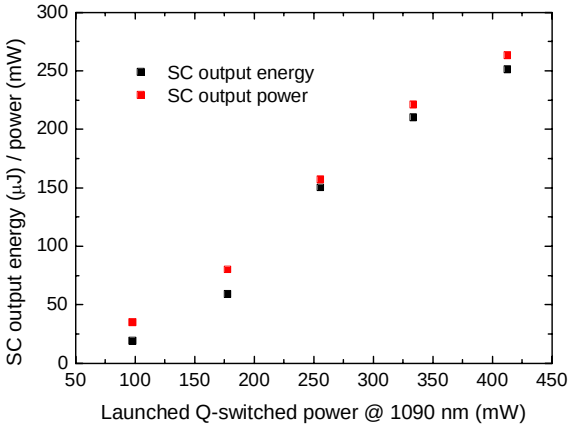

Fig. 2. Average supercontinuum output power and pulse energy at the repetition rate of 1 kHz as a function of launched Q-switched laser power at 1090 nm.

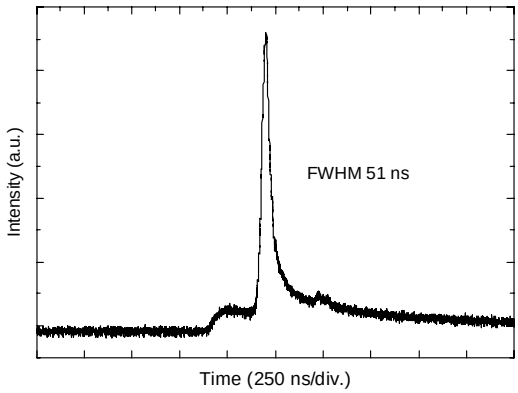

Fig. 4. Pump pulse shape at the repetition rate of 1 kHz measured at the highest pulse energy.

The laser parameter important for this work is the high beam quality (M^2 = 1.3), which allowed coupling of the radiation into single-mode fiber with efficiency of 51%. 9 m of commercially available photonic crystal fiber (NKT Photonics SC-5.0-1040) with core diameter of 5 μm, cladding diameter of 125 μm, and zero-dispersion wavelength of 1040 nm was used as a nonlinear medium. This length of the PCF was found to provide optimal blue shifting in the SC spectrum. The fiber has a hole diameter of 2.5 μm, and a hole-to-hole pitch of 5 μm. The collimated output beam of the tapered fiber laser was launched into the PCF with an aspheric lens with a focal length of f = 4.5 mm.

The SC average power and pulse energy at the output of the PCF are shown in Fig. 2 as a function of launched Q-switched power at 1090 nm. The slope efficiency of the Q-switched laser is 28 %, determined by the low diffraction efficiency of the acousto-optic modulator.

The highest measured SC average output power and pulse energy were 263 mW and 251 μJ, respectively, at the repetition rate of 1 kHz used throughout these experiments. The conversion efficiency of Q-switched radiation to SC is 63%.

Pulse trains at the input and output of the PCF at the repetition rate of 1 kHz demonstrate identical temporal behavior, as shown in Fig. 3. A 51-ns Q-switched pump pulse with estimated peak power of 3.2 kW is shown in Fig. 4. The pulse width increases with increasing repetition rate, and decreases with increasing pump power. The asymmetric pulse shape, typical for Q-switching, is attributed to reduced gain at the trailing edge of the pulse.

Maximum output power in this regime was limited by the catastrophic optical damage on the input facet of the PCF. In the ns-pulse regime, the damage is mainly thermal, and the

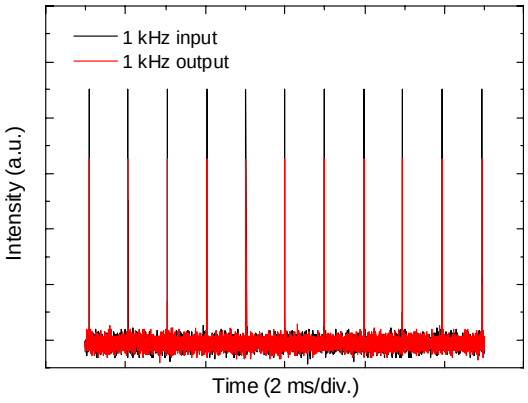

Fig. 3. Pulse trains of the pump laser and supercontinuum radiation at a repetition rate of 1 kHz.

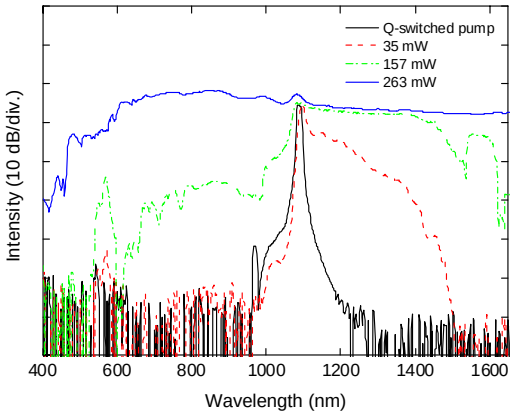

Fig. 5. The Q-switched pump laser spectrum and the supercontinuum spectra at three values of average output power. The spectra were recorded with a resolution of 10 nm.

threshold fluence depends on pulse width τ as $\tau^{1/2}$ [16], As elaborated in [17], the maximum sustainable peak power can be estimated as $P_{max} = XA_{eff}/\tau^{1/2}$, where X = 1.5 kW $ns^{1/2}/\mu m^2$, A_{eff} is the effective mode area in μm, and τ is the pulse duration in ns. For A_{eff} = 18.1 μm^2 and τ = 51 ns, this yields P_{max} = 3.8 kW, which agrees reasonably well with the damage threshold observed within this study, albeit the actual threshold is affected by several technical details. Damage at the output end of the PCF was also occasionally observed, most likely due to facet imperfections, e.g. cleave and contamination defects.

Fig. 5 shows the evolution of the SC spectrum with increasing pump power, typical for nanosecond pumping in the anomalous dispersion regime [7], [8]. The black curve in the figure corresponds to the Q-switched laser spectrum, showing the fundamental wavelength of 1090 nm and low-intensity residual pump at 970 nm. For the highest output power, the supercontinuum spans more than 1000 nm bandwidth from 600 nm to beyond 1600 nm within 5 dB intensity variation.

III. Conclusion

In conclusion, we have demonstrated high-energy, broadband supercontinuum generation using a sub-100-ns Q-switched tapered ytterbium fiber laser. The highest measured pulse energy of 251 μJ with spectral bandwidth over 1000 nm was limited by the optical damage on the facets of photonic crystal fiber used as a nonlinear medium. The smooth supercontinuum spectrum reveals excellent spectral flatness with intensity excursions less than 5 dB. It is understood, however, that the spectral features caused by pulse-to-pulse fluctuations are smoothed to a certain extent due to measurements using integration and averaging.

Acknowledgment

The authors would like to acknowledge the support of A. Grudinin from Fianium Ltd., UK. This work has been financially supported in part by the Graduate School in Electronics, Telecommunication, and Automation (GETA), the Walter Ahlström Foundation, the Ulla Tuominen Foundation, and the KAUTE Foundation.

References

[1] P. St.J. Russell, "Photonic-Crystal Fibers," *J. Lightwave Technol.*, vol. 24, pp. 4729-4749, Dec. 2006.

[2] J. M. Dudley and J. R. Taylor, "Ten years of nonlinear optics in photonic crystal fibre," Nature Photonics, vol. 3, pp. 85 – 90, Feb. 2009.

[3] A. Mussot, M. Beaugeois, M. Bouazaoui, and T. Sylvestre, "Tailoring CW supercontinuum generation in microstructured fibers with two-zero dispersion wavelengths," *Opt. Express*, vol. 15, pp. 11553-11563, Aug. 2007.

[4] J. C. Travers, A. B. Rulkov, B. A. Cumberland, S. V. Popov, and J. R. Taylor, "Visible supercontinuum generation in photonic crystal fibers with a 400W continuous wave fiber laser," *Opt. Express*, vol. 16, pp. 14435-14447, Aug. 2008.

[5] K. K. Chen, S. Alam, J. H. V. Price, J. R. Hayes, D. Lin, A. Malinowski, C. Codemard, D. Ghosh, M. Pal, S. K. Bhadra, and D. J. Richardson, "Picosecond fiber MOPA pumped supercontinuum source with 39 W output power," *Optics Express*, vol. 18, pp. 5426-5432, Mar. 2010.

[6] J. Cascante-Vindas, A. Diez, S. Torres-Peiro, J. Cruz, and M. Andres, "Enhanced supercontinuum generation in the nanosecond pump regime using specialty microstructured fibers," *in Transparent Optical Networks, 2009. ICTON '09. 11th International Conference on*, pp. 1-4, 2009.

[7] J. M. Dudley, G. Genty, and S. Coen, "Supercontinuum generation in photonic crystal fiber," *Rev. Mod. Phys*., vol. 78, p. 1135, Oct. 2006.

[8] J. M. Dudley, G. Genty, F. Dias, B.Kibler, N. Akhmediev, *Optics Express*, vol. 17, pp. 21497-21508, Nov. 2009.

[9] J. Cascante-Vindas, A. Díez, J. L. Cruz, and M. V. Andrés, "Supercontinuum Q-switched Yb fiber laser using an intracavity microstructured fiber," *Opt. Lett.*, vol. 34, pp. 3628-3630 Nov. 2009.

[10] J. M. Stone and J. C. Knight, "Visibly "white" light generation in uniform photonic crystal fiber using a microchip laser," *Opt. Express* vol. 16, pp. 2670-2675 Feb. 2008.

[11] S. Kobtsev, S. Kukarin, Y. Fedotov, and S. Smirnov, "All-fiber supercontinuum generator with high-energy pulses," *Lasers and Electro-Optics 2009 and the European Quantum Electronics Conf., CLEO Europe - EQEC 2009. European Conference on*, pp.1-1, 2009.

[12] V. Filippov, Y. Chamorovskii, J. Kerttula, K. Golant, M. Pessa, and O. G. Okhotnikov, "Double clad tapered fiber for high power applications", *Opt. Express*, vol. 16, pp. 1929-1944, Jan. 2008.

[13] V. Filippov, Y. Chamorovskii, J. Kerttula, A. Kholodkov, and O. G. Okhotnikov, "Highly efficient 750 W tapered double-clad ytterbium fiber laser", *Opt. Express*, vol. 18, pp. 12499-12512 May 2010.

[14] J. Kerttula, V. Filippov, Y. Chamorovskii, K. Golant, and O. G. Okhotnikov, "2-mJ actively Q-switched ytterbium tapered fiber laser operating in the single-shot regime", *4th EPS-QEOD Europhoton Conf*, Tue1, 2010.

[15] J. Kerttula, V. Filippov, Y. Chamorovskii, K. Golant, and O. G. Okhotnikov, "Actively Q-switched 1.6-mJ tapered double-clad ytterbium-doped fiber laser", *Opt. Express*, vol. 18, pp. 18543-18549, Aug. 2010.

[16] B. C. Stuart, M. D. Feit, A. M. Rubenchik, B. W. Shore, and M. D. Perry, "Laser-Induced Damage in Dielectrics with Nanosecond to Subpicosecond Pulses", *Phys. Rev. Lett.*, vol. 74, pp. 2248–2251, Mar. 1995.

[17] D. J. Richardson, J. Nilsson, and W. A. Clarkson, "High power fiber lasers: current status and future perspectives", J. Opt. Soc. Am. B, vol. 27, pp. B63-B92, Oct. 2010.

Tampereen teknillinen yliopisto
PL 527
33101 Tampere

Tampere University of Technology
P.O.B. 527
FI-33101 Tampere, Finland

ISBN 978-952-15-3085-2
ISSN 1459-2045